University of Alberta

A New Approach to Improving Cable Shovel Dipper Design for Cutting Soft Rock and Soils

by

Ning Shi

A thesis submitted to the Faculty of Graduate Studies and Research in partial fulfillment of the requirements for the degree of Doctor of Philosophy

in

Mining Engineering

Department of Civil and Environmental Engineering

Edmonton, Alberta

Spring, 2007

Library and
Archives Canada

Published Heritage
Branch

395 Wellington Street
Ottawa ON K1A 0N4
Canada

Bibliothèque et
Archives Canada

Direction du
Patrimoine de l'édition

395, rue Wellington
Ottawa ON K1A 0N4
Canada

Your file Votre référence
ISBN: 978-0-494-29743-8
Our file Notre référence
ISBN: 978-0-494-29743-8

NOTICE:
The author has granted a non-exclusive license allowing Library and Archives Canada to reproduce, publish, archive, preserve, conserve, communicate to the public by telecommunication or on the Internet, loan, distribute and sell theses worldwide, for commercial or non-commercial purposes, in microform, paper, electronic and/or any other formats.

The author retains copyright ownership and moral rights in this thesis. Neither the thesis nor substantial extracts from it may be printed or otherwise reproduced without the author's permission.

AVIS:
L'auteur a accordé une licence non exclusive permettant à la Bibliothèque et Archives Canada de reproduire, publier, archiver, sauvegarder, conserver, transmettre au public par télécommunication ou par l'Internet, prêter, distribuer et vendre des thèses partout dans le monde, à des fins commerciales ou autres, sur support microforme, papier, électronique et/ou autres formats.

L'auteur conserve la propriété du droit d'auteur et des droits moraux qui protège cette thèse. Ni la thèse ni des extraits substantiels de celle-ci ne doivent être imprimés ou autrement reproduits sans son autorisation.

In compliance with the Canadian Privacy Act some supporting forms may have been removed from this thesis.

While these forms may be included in the document page count, their removal does not represent any loss of content from the thesis.

Conformément à la loi canadienne sur la protection de la vie privée, quelques formulaires secondaires ont été enlevés de cette thèse.

Bien que ces formulaires aient inclus dans la pagination, il n'y aura aucun contenu manquant.

Canada

Abstract

The design of dippers for cable shovels has essentially remained unchanged for the last 100 years. In the past 10 years, shovel manufacturers have started taking another look at dipper design, resulting in changes that address some of the wear conditions and material-retention problems responsible for most of the maintenance and operational costs. However, with the exception of added lateral curvatures to the front and corners of the dipper, most of the basic features including geometry and functionality remain essentially unchanged.

This research examines the criteria for a better cutting dipper design and suggests an alternative design approach for use in ground conditions where cutting of virgin ground rather than scooping of blasted material is required. The criteria include the dipper capacity, digging force, trajectory, wear and damage, which, as indicators of dipper performance, can be thought of in terms of three basic considerations: power (energy consumption), volume delivered (production) and lifespan (wear and strength). The approach basically consists of 3D solid modeling and the simulation of a shovel's duty cycle, in which shovel kinematics, and ground-dipper interactions are primary considerations. The research aims at an improved geometry which will improve performance considerably without changing any configuration of the current shovel design.

A 3 yd^3 prototype dipper was fabricated to match a Dominion 500 cable

shovel for field testing. This proposed design and the original configuration, that came with the Dominion shovel were tested in the field. The test results gave some indication that performance improvements are possible for the scale dipper geometry tested.

The shovel size-performance relation was reviewed and analyzed. It was found that various shovel and dipper sizes share the same or similar configurations, which exhibit similar performance patterns in similar mining conditions. This sets the path for future researchers to scale proposed geometric designs from a prototype size eventually to ultra class sizes.

Acknowledgements

I wish to first of all acknowledge Dr. Tim Joseph, my supervisor, for his great support during the course of this research.

Dr. Joseph and I would like to thank JPi geo-industry engineering consultants (JPi) for permission to use the 2000-3 JPi dipper design concepts as the backbone of this thesis work. JPi provided not only financial support for the student and project, but also covered the cost of all field work and fabrication of test models. JPi's fabrication and test partners, Brospec 2001 Engineering (the Golosky Group), Leo Robert Enterprises, Coneco Equipment, Graham Brothers' Construction and REN Consulting, have contributed both in-kind fabrication and much support during the course of this work. Particular thanks go to Doug Golosky, Marlene Martz, Leo Robert, and Roger Nicolas.

Suncor Energy played host to the JPi dipper test in May 2005 that was used to acquire verifying data for this work.

Finally, the author would like to thank his family---Jingtao, Aurora, and his mother--- for their patience, love and support.

Table of Contents

Chapter 1 Introduction 1

1.1 Significance of the problem 1

1.1.1 Cable Shovel performance 2

1.1.2 Shovel dipper design potential 5

1.2 Cable shovel dipper 6

1.2.1 Cable shovel dipper components 6

1.2.2 Performance indicators 8

1.2.3 Dipper design focus 9

1.2.4 Dipper design approach 9

1.3 Dipper-ground interactions 10

1.4 Research objectives 12

1.5 Hypotheses 13

Chapter 2 Background 15

2.1 Research on shovel dipper design 15

2.2 Current dipper design review 18

2.3 Other Ground Engaging Tool (G.E.T.) 22

2.4 Previous work related to dipper design 26

2.4.1 Digging kinematics 26

2.4.2 Digging forces 28

2.4.3 Dipper - ground interactions 31

2.5 Soft rock and oil sand 38

2.5.1 Soft rock in comparison to hard rock 38

2.5.2 Oil sand 41

2.6 Summary 44

Chapter 3 Digging Kinematics 47

3.1 Cable shovel geometric model 47

3.1.1 Assumptions 47

3.1.2 Shovel position in cylindrical coordinates 48

3.2 Cable shovel kinematic model 49

3.2.1 Dipper motion geometry 49

3.2.2 Derivation of the dipper motion function 52

3.3 Digging spatial characteristics 56

3.3.1 Shovel duty cycles 56

3.3.2 Digging motion range 57

3.3.3 Minimum tuck profile 59

3.3.4 Shovel advancing steps 63

3.4 Determine trajectories 65

3.5 Summary 68

Chapter 4 Shovel-Ground Interaction 70

4.1 Dipper-ground interactions 70

4.1.1 Dipper-ground geometry 70

4.1.2 Ground properties 71

4.1.3 Dipper-ground interaction 72

4.1.4 Digging forces 77

4.2 Digging simulation 80

4.3 Shovel simulation software 86

4.4 Simulation outputs 88

Chapter 5 Cable Shovel Dipper Design 91

5.1 Design criteria and focus 91

5.2 Variation of the front wall 93

5.2.1 Trajectory and front profile correlation 93

5.2.2 Sensitivity analysis 99

5.3 Additional Geometry Considerations 105

5.3.1 Back wall 106

5.3.2 Side walls 109

5.4 Cold weather digging 111

5.5 Three-dimensional dipper models 112

5.5.1 A generic dipper model 112

5.5.2 Current ultra class dipper models 113

5.5.3 JPi concept dipper models 115

Chapter 6 1/20th Scale Prototype Field Tests 119

6.1 Dominion 500 shovel 119

6.2 3 yd^3 dipper design 121

6.2.1 Dipper design 121

6.2.2 Door design 122

6.2.3 Dipper and door virtual assembling 123

6.2.4 Prototype dipper fabrication 125

6.3 Field test 126

6.3.1 Sensor placement 126

6.3.2 Sensor and instrumentation detail 128

6.3.3 Test sequences 131

6.3.4 Test site and face conditions 133

6.3.5 Testing with the original dipper 135

6.3.6 Testing with the prototype dipper 136

6.4 Data analysis 137

6.4.1 Transformation 137

6.4.2 Visualization of data 147

6.4.3 Test analysis 149

6.5 Conclusions 158

Chapter 7 Correlating to the bigger size 159

7.1 Objective 159

7.2 Shovel analogy 161

7.3 Performance analogy 163

7.3.1 Hoist performance 163

7.3.2 Crowd performance 170

7.4 Normalized performance 171

7.5 Conclusions 174

Chapter 8 Conclusions 176

8.1 Main conclusion 176

8.1.1 Dipper-ground matching 176

8.1.2 Less interference 177

8.1.3 Prototype field test result 177

8.1.4 Scaling performance trends 178

8.2 Research contributions 178

8.2.1 Shovel simulation formulation and software 178

8.2.2 A curved dipper concept 179

8.2.3 A dipper design approach 179

8.3 Future work recommendations 180

8.3.1 Future shape concept 180

8.3.2 Structural considerations 181

List of References 182

Appendix A 191

MatLab codes for shovel kinematic models 191

Appendix B 204

Shovel Action Simulation Software 204

Appendix C 210

Dominion 450/500 Shovel and Dipper Specifications 210

Appendix D 213

1/20th Prototype Dipper and Door Specifications 213

Appendix E 219

Hensley Tooth and Adaptor Specifications 219

Appendix F 221

New dipper Test Location 221

Appendix G 222

New dipper Project Field Test Visual Report 222

Appendix H 224

JPi (2001) New Dipper Concept 224

Appendix I 225

Visible Weakness of Current Dipper Designs 225

Appendix J 228

P&H 4100 Hoist Motor Armature Current Record 228

List of Tables

Table 1-1: Main parts of a cable shovel 3

Table 1-2: Shovel Performance Indicators 5

Table 2-1: Suggested minimum tooth angle and rake angle 17

Table 2-2: Properties of some typical soft mined materials (Singh, 1995), (Dusseault and Morgenstern, 1978) * 34

Table 4-1: Oil sand properties (Morgenstern and Scott, 1997) (Collins, 2005) 71

Table 6-1: The Prototype Dipper's Specifications 125

Table 6-2: Parameters of the Showa NE-MA-5-350 Strain gauge 128

Table 6-3: Parameters of the AccuStar® Electronic inclinometer 129

Table 6-4: Physical properties of the oil sand in situ (Suncor, 2005) 134

Table 6-5: Dipper test results summary 157

Table 7-1: Summary of available shovel performance data 160

Table 7-2: Hoist force in relation to the weight of dipper, handle and material 166

Table 7-3: Different sized shovels' specification and performance 168

Table 7-4: Shovel performance data normalizing factor 173

List of Figures

Figure 1-1: Schematics of the P&H4100 BOSS cable shovel (Courtesy of JPi geo-industry engineering consultants) 2

Figure 1-2: A two-dimensional illustration of typical cable shovel dippers 7

Figure 1-3: Definition of the rake angles, α: rake angle, α_1: tooth angle 7

Figure 1-4: A three-dimensional illustration of typical cable shovel dipper 8

Figure 1-5: Diagram of the dipper-ground trajectory and interaction 11

Figure 2-1: A generic dipper concept 18

Figure 2-2: A high attack angle decease sdigging performance 19

Figure 2-3: Face interference leads to heel wear and damage. 19

Figure 2-4: P&H Optima® Plus dipper (P&H, 2001C) 20

Figure 2-5: Bucyrus Fastfil dipper (Bucyrus, 2003) 21

Figure 2-6: ACARP Concept dipper (ACARP, 2002) 22

Figure 2-7: Various hydraulic shovel and loader buckets 24

Figure 2-8: Dragline bucket (Howarth et al.,1987) 25

Figure 2-9: Simplified shovel geometry (Daneshmund and Hendricks, 1993) 28

Figure 2-10: Dipper-handle free body diagram and the acting forces 30

Figure 2-11: a modified dipper-handle free body diagram 31

Figure 2-12: Fundamental Earth-moving actions (Blouin, 2001) 32

Figure 2-13 : A 2D scheme for soil cutting 35

Figure 2-14: 3D scheme of soil-cutting model (Hettiaratchi and Reece, 1967) 37

Figure 2-15: Un-blasted soft material face 39

Figure 2-16: Blasted rock face 40

Figure 2-17: In-situ structure of oil sands (Dusseault and Morgenstern, 1977) 42

Figure 2-18: Failure envelope of recompacted rich oil sand undrained triaxial tests 43

Figure 3-1: Schematic of shovel and working face 48

Figure 3-2: Representations of cylindrical coordinates 49

Figure 3-3: Shovel dipper geometry in x-y pane 50

Figure 3-4: Shovel dipper geometry in x-z plane 51

Figure 3-5: Local dipper coordinate transformation to the digging plane 51

Figure 3-6: Geometric derivation of the dipper motion function 52

Figure 3-7: Shovel-truck digging/loading methods 56

Figure 3-8: 3D digging volume for a shovel move 57

Figure 3-9: P&H 4100 digging envelope (P&H, 2001C) 58

Figure 3-10: P&H 4100 shovel digging motion ranges created by collision detection 59

Figure 3-11: Basic collision detection techniques 60

Figure 3-12: Dipper-track interference and the minimum tuck position 61

Figure 3-13: Shovel crawler 3 views and diagonal profile (A-A) 62

Figure 3-14: P&H 4100 shovel's minimum tuck position projected on the ground: Positions 1 and 2 are the same as that in Figure 3-13 62

Figure 3-15: Shovel's range diagram and repositioning increment 64

Figure 3-16: Cutting trajectories in two-dimensional sequences 68

Figure 4-1: Geometrical relationship of the dipper-ground interaction 70

Figure 4-2: Static equilibrium approx. of a failure surface, after Singh (1995). 72

Figure 4-3: An example of determing the angle of failure plane. 74

Figure 4-4: Simplified model: a flat blade moving through soil.................... 75

Figure 4-5: Static equilibrium as an approximation for the failure surface. .. 75

Figure 4-6: Handle-dipper digging forces 78

Figure 4-7: A simplified equilibrium model for the dipper system................ 79

Figure 4-8: Step-wise digging simulation 83

Figure 4-9: Data flow for the digging simulation 85

Figure 4-10: Shovel simulation software 87

Figure 4-11: Digging angle variation 88

Figure 4-12: Crowd, hoist and dipper tip velocity 89

Figure 4-13: Simulation output: digging forces generated for cutting oil sand 90

Figure 5-1: A selected digging trajectory as a reference to design dipper front 94

Figure 5-2: A relationship between the tooth angle and productivity 96

Figure 5-3: A relationship between the tooth angle and the wear (ACARP, 2002) 97

Figure 5-4: Two-dimensional dipper profile design....................................... 97

Figure 5-5: Possible variations of a front wall profile 98

Figure 5-6: Variation of the start point and the profile.................................. 99

Figure 5-7: Comparison of attack angles referenced to the original configuration

.... 100

Figure 5-8: Theoretical heel-ground clearance plots for different profile ... 101

Figure 5-9: Dipper-crawler interference 102

Figure 5-10: Reduced dipper-crawler interference 103

Figure 5-11: Equivalent tool shape for the round shape tool (McKeys, 1985) 103

Figure 5-12: Effective attack angles and digging depths for a curved front 104

Figure 5-13: Simulated digging force plots for original vs proposed configurations 105

Figure 5-14: The void space and the skewed back wall geometry change .. 107

Figure 5-15: The void space and the skewed back wall geometry change .. 108

Figure 5-16: The void space and the skewness of the back wall 108

Figure 5-17: Trapezoidal angles applied to oil sand dippers........................ 110

Figure 5-18: Increased capacity due to trapezoidal side walls......................111

Figure 5-19: A generic three-dimensional dipper model.............................. 113

Figure 5-20: A three-dimensional model of the FastFil ® (Bucyrus, 2003) 114

Figure 5-21: A three-dimensional model of P&H Optima plus® (P&H, 2001C) 114

Figure 5-22: The first trial of the new concept dipper 116

Figure 5-23: A curved and skewed dipper model.. 117

Figure 5-24: A curved, skewed and trapezoidal dipper model..................... 117

Figure 5-25: A curved, skewed, trapezoidal and flared dipper model 118

Figure 6-1: Dominion 500 shovel during transportation 119

Figure 6-2: Two dimension model of Dominion 500 shovel (units in feet). 120

Figure 6-3: Comparison of the geometrical configuration between JPi and original dippers 121

Figure 6-4: Testing dipper design based upon steel-plate (Dimension in inches) 122

Figure 6-5: A door for the testing dipper (Dimension in inches) 123

Figure 6-6: Test dipper and matching door prior to physical assembly 124

Figure 6-7: An interactive rendered model using Solidworks Assembly..... 124

Figure 6-8: The 3 yd^3 dipper being built in the workshop 125

Figure 6-9: Dipper teeth adpater (Hensley, 2003).. 126

Figure 6-10: Field test sensors and arrangement (dimension in inches)...... 127

Figure 6-11: DAQ system configuration... 130

Figure 6-12: Test wiring and cable protection 131

Figure 6-13: Dipper test: π/8 angle increment 132

Figure 6-14: Dominion 500 field test digging and dumping plan................ 133

Figure 6-15: Oil sand face condition at Suncor Energy test site.................. 134

Figure 6-16: The Dominion shovel in the oil sand operation 135

Figure 6-17: The concept JPi prototype dipper on a Dominion 500 shovel 137

Figure 6-18: Handle sticks and cross-sectional shape 139

Figure 6-19: Bail strain gauge position and cross-sectional shape 140

Figure 6-20: Hoist and crowd force strains calibration position.................. 140

Figure 6-21: Hoist and crowd strain calibration model 141

Figure 6-22: Handle and cable orientation referenced to a neutral orientation. 144

Figure 6-23: Determination of the dipper-handle position from the inclinometer measurements 145

Figure 6-24: Dipper test result visualization modeling software for the new dipper configuration 148

Figure 6-25: Static test without load in the dipper 150

Figure 6-26: Static test without load (first two cycles) and with incremental load in the dipper (third cycle) 151

Figure 6-27: Comparison between the original dipper and the new dipper. 153

Figure 6-28: Pitch brace used by both the original and concept dippers 153

Figure 6-29: Hoist and crowd force plots for the original AMSCO 2yd^3 dipper 154

Figure 6-30: Hoist and crowd force plots for the JPi concept dipper 155

Figure 7-1: Process of scaling 160

Figure 7-2: Geometrical analogy of P&H 4100 BOSS and Dominion 500, actual scale. 162

Figure 7-3: A segment of the digging cycle for the Dominion 500 shovel .. 165

Figure 7-4: A segment of the digging cycle for a P&H 2300 shovel (Hendricks and Scoble, 1990) 165

Figure 7-5: A segment of the digging cycle for the P&H 4100 shovel (Joseph and Hansen, 2002) 166

Figure 7-6: P&H 2300, P&H 4100 shovel loaded and suspended position. 167

Figure 7-7: Dipper capacity versus the suspended load and the peak force 169

Figure 7-8: Different shovels' peak hoist force increment rate.................... 170

Figure 7-9: A segment of the crowd force plot for Dominion 500 shovel ... 171

Figure 7-10: A segment of the crowd motor current plot for the P&H2300 shovel (Hendricks and Scoble, 1990) 171

Figure 7-11: various shovel hoist performance plots 173

Figure 7-12: Dominion 500, P&H 2300 and 4100 shovel normalized hoist performance index plots 174

Figure 8-1: The dipper design approach 180

Figure 8-2: A double curved dipper model (courtesy JPi) 181

List of Symbols

$2D$	Two-dimensional
$3D$	Three-dimensional
A	Cross-sectional area of the handle sticks or bail bracket
A_{bail}	Cross-sectional area of the bail bracket.
A_{handle}	Cross-sectional area of the handle sticks.
a_x, a_y	Dipper acceleration's x and y components, respectively
c	Soil cohesion
d	Cutting depth.
E	Young's modulus of the handle or bail material.
E_{bail}	Young's modulus of the bail material.
E_{handle}	Young's modulus of the handle material.
F	Crowding or hoisting force
F_h	Hoist force.
F_s	Supporting force normal to the handle.
f_x	x component of each force
$(F_h)_{reference}$	Hoist force at the reference position.
$(F_l)_{reference}$	Crowd force at the reference position.
F_x, F_y	Functions of h and l to determine the dipper position x and y, respectively
f_y	y component of each force.
G	Weight of the handle, dipper and material.

GF	Gauge Factor
g	Acceleration due to gravity
h	Cable release length measured from the tangent point on the sheave to the bail point
$h(t)$	Cable release length at time t.
h'	Effective cable release length, from the sheave shaft point to the bail point
h_0	Hoist cable release length at the digging start point.
h_i	i^{th} h discretion.
h_n	Hoist cable release length at the digging end point.
H_p	Peak hoist force
H_s	Suspended load
i	Sequence index
IR	Increment rate
l	Handle extension length
$l(t)$	Handle crowd length at time t
l'	Effective handle extension length measured from the saddle shaft to the bail point
l_0	Handle crowd length at the digging start point.
L_f	Failure surface length.
l_G	Arm length of the weight referencing the bail point.
l_i	i^{th} l discretion.
l_n	Handle crowd length at the digging end point.
l_P	Arm length of the supporting force referencing the bail point.

l_R	Arm length of the total resistance referencing the bail point.
L_t	Soil-tool contact length.
M	Distance from saddle shaft to the sheave shaft.
N_c	Soil cutting force cohesive factor
N_q	Soil cutting force surcharge factor
N_{sc}	Soil side cutting force cohesion factor.
$N_{s\gamma}$	Soil side cutting force frictional factor.
N_γ	Soil cutting force gravitational factor
P	Total tool cutting force
$\theta_{profile}$	Angle of the polar coordinates
q	Surcharge pressure acting on the soil surface
R	Total resistance.
r_1	Distance from saddle shaft (point) to the handle direction (line) passing the bail point
r_2	Sheave radius
R_f	failure surface resistance.
R_g	Gauge resistance
R_L	Line resistance
$r_{profile}$	Radius of the polar coordinates.
t	Time
V_{EX}	Excitation voltage
v_h	Hoisting speed.
v_l	Crowding speed.

Vr	Reference potential
V_{signal}	Signal voltage
v_x, v_y	Dipper velocity's x and y components, respectively
W	Weight of the soil wedge.
w	Tool width
w'	Effective width of the side zone.
x, y	Coordinates of any point on the dipper or handle in the digging plane
x', y'	Coordinates of the bail point in the dipper local coordinates
x_0, y_0	Coordinates of the bail point in the digging plane
x_i^0, y_i^0	Coordinates of the trajectory followed by the bail point.
$x_{profile}$	Cartesian x coordinate of the spiral
x_{saddle}, y_{saddle}	Coordinates of the saddle shaft point in the digging plane.
$x_{sheave}, y_{sheavee}$	Coordinates of the sheave wheel center in the digging plane.
$y_{profile}$	Cartesian y coordinate of the spiral
α	Dipper rake angle
β	Handle angle referenced to the horizontal
β_1	Effective handle angle, from the saddle shaft to the bail point referenced to the horizontal
β_2	Difference between boom angle and effective handle angle
$\beta_{MEASUREMENT}$	The read-out of the inclinometer on the handle
$\beta_{NEUTRAL}$	Orientation where the inclinometer on handle is zero
γ	Soil density

$\Delta\beta$	Difference between handle angle and effective handle angle
ε	Measured strain
ε_{bail}	Strain on bail bracket.
ε_{handle}	Strain on handle sticks.
$\eta_{MEASUREMENT}$	The read-out of the inclinometer on the bail
$\eta_{NEUTRAL}$	Orientation where the inclinometer on the bail is zero
η	The cable direction
κ	Rupture surface inclination
λ	Boom angle
ξ	Blade direction, an angle from the horizontal
ρ	The instantaneous attack angle.
σ	The normal pressure acting on the internal shear surface and
φ	Internal friction angle
χ	Slope of ground surface

Chapter 1

Introduction

1.1 Significance of the problem

Electric cable shovels are the most extensively used high volume excavators in open pit mining. Previous work to improve the production capability of these units focused on updating their mechanical and electrical components and optimizing utilization and operational approaches. Little work has been done to improve dippers and their ground interactions. With the trend towards higher production forcing the development of ever bigger, faster and smarter cable shovels, the need exists to move beyond the aging geometry of the dippers, which have been relatively unchanged for the past 100 years.

In the Athabasca oil sand deposits of Northern Alberta, Canada, mine operators employ the biggest cable shovels with dipper capacities upwards of 44 m^3. However, the wear and impact associated to ground-equipment interference problems plague these monster class shovel dippers, and have continually done so for the past decade. The manufacturers' variations have concentrated on internal wear and material retention issues, but have not considered the actual kinematics and major external problems, such as dipper-crawler collision and poor dipper-ground interaction. These problems will result in a relatively shorter dipper life, shorter maintenance period, higher digging energy requirement and lower productivity. A simple dipper design improvement relying heavily on geometric change may result in greater performance improvements with relatively little cost.

1.1.1 Cable Shovel performance

Cable shovels built by Bucyrus and P&H are proving successful in tar sands environments, although there are also plenty of large hydraulic machines operating there as well (Wolf, 2001). Compared to other loading/digging machines, they are of high production and low cost (HPLC). Shovel performance is one of the key criteria dominating oil sand operations in the Athabasca deposit. Figure 1-1 illustrates the model with the largest population in Northern Alberta, the P&H 4100 TS/BOSS shovel, which was specifically designed for oil sand operations.

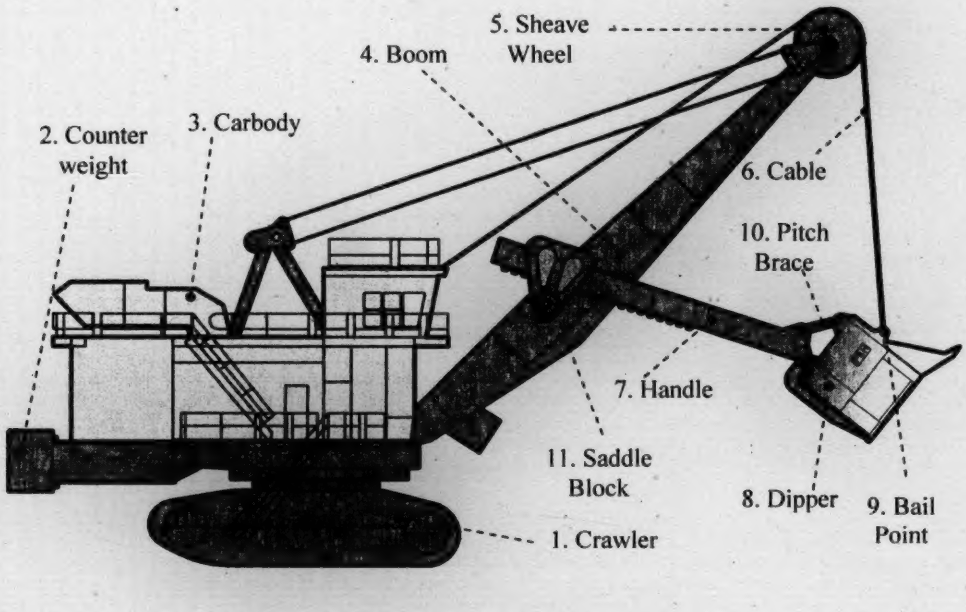

Figure 1-1: Schematics of the P&H4100 BOSS cable shovel (Courtesy of JPi geo-industry engineering consultants)

The common nomenclature of the cable shovel shown in Figure 1-1 is summarized in Table 1-1.

Table 1-1: Main parts of a cable shovel

Part	Action	Description
1. Crawler	Propel	The track is propelled back or forth to relocate the shovel.
2. Carbody	Swing	The rotating of carbody allows swinging the boom, handle and dipper to dumping spots or back to face.
3. Counter Weight	-	Attached to the rear end of the carbody to balance the weight of boom, handle dipper and material.
4. Boom	-	Attached to the front end of the carbody and erected at around 45 degrees to which the handle and cable are attached. It remains stationary to the shovel carbody during the operation.
5. Sheave Wheel	-	Support and deliver the cable.
6. Cable	Hoist	Hoist or lower the dipper.
7. Handle	Crowd	Retract and extend the dipper in and out.
8. Dipper	Dig/Dump	Dig the face and dump the load.
9. Bail Point	-	The connection point between the cable and dipper.
10. Pitch Brace	-	A pair of steel bar to connect the dipper and the handle.
11. Saddle Block	-	A pair of sleeves shafted on boom to hold the handles.

Typical shovel operations include:

- Digging: to break the face and fill the material into the dipper by the motion produced by cable hoisting and handle crowding,
- Propelling: to reposition the shovel close to the face or travel in the pit,
- Dumping: to unload the dipper, being triggered by latch releasing,
- Swinging: to swivel the upper works, allowing positioning the handle and dipper for digging or dumping.

Such a shovel accounts not only for a huge proportion of an open pit mine's capital investment, but also for a major portion of the operating costs. The shovel's productivity directly influences mining production rates. Therefore, mines often assign more trucks than the theoretical truck number calculated with the production matching (over-truck) to maximize the shovels' efficiency.

From operational experiences, a shovel's key performance indicators (KPI) such as productivity, cost, operational flexibility, reliability, and availability have been used to evaluate a shovel's performance (P&H, 2001A). Table 1-2 shows some of these principal indicators and their relation to dipper performance..

Most of shovel performance indicators described in Table 1-2 are related to dipper performance. The definition of a 'good' dipper design is one with high payload, short cycle time, high fill factor, low maintenance and operating cost, low digging resistance and low down-time. Currently, manufacturers pay more attention to improving a shovel's electric/electronic performance rather than optimizing dipper shape configuration.

Table 1-2: Shovel Performance Indicators

General Indicators	Indicators	Description	Dipper related?
Production	Payload	Material loaded in dipper	Y
	Cycle Time	The time to complete a dig-dump cycle	Y
	Fill Factor	The ratio of loaded volume over nominal dipper capacity	Y
Cost	Capital	Shovel purchasing cost	N
	Maintenance	Maintenance Cost	Y
	Operation	Operating Cost	Y
Operation	Digging Resistance	The resistant forces from face overcome by hoist and crowd forces	Y
	Downtime	Machine failure time	Y
	Travel Speed	The speed at which the shovel moves	N

1.1.2 Shovel dipper design potential

A potential improved dipper design would approach better performance evaluated via a set of appropriate performance indicators. To increase production at an identical or lower cost, reducing the resistant digging force is a priority.

An improved dipper design should yield the following benefits (P&H, 2001B) (ACARP, 2002):

(1) Reduced digging resistance

Improved attack angles along trajectories resulting in lower digging resistance.

(2) Smooth digging process

A resistance plot that is smooth and flat, with fewer spikes, resulting in structural longevity.

(3) Better fill performance

The filling is faster and the fill factor (filled volume divided by nominal capacity) is higher.

(4) Better dump performance

The dumping is smooth and has less harsh impact on the truck body.

(5) Less energy required

A reduced energy requirement for operation of the shovel in terms of both continuous output and instantaneous power surges.

(6) Less dipper wear

Less wear due to less stressful ground-tool contact, resulting in longer dipper life, less maintenance and replacing time.

1.2 Cable shovel dipper

1.2.1 Cable shovel dipper components

As illustrated in Figure 1-2, the cable shovel dipper consists of

(1) Teeth and lip system,
(2) Front wall, including wear protection rib and heel,
(3) Side wall,
(4) Back Wall,
(5) Bottom Door and
(6) Attachment and Connection.

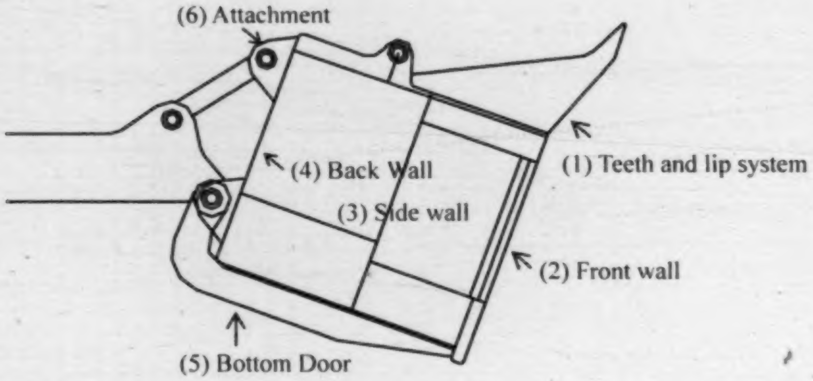

Figure 1-2: A two-dimensional illustration of typical cable shovel dippers

Figure 1-3 illustrates two frequently used terminologies for shovel ground engaging tools (G.E.T.). The tooth angle is denoted by α_1, rake angle is denoted by α and defined as the angle formed between the level ground line from the leading edge of the dipper tip to the point at which an individual rack pinion tooth contacts the dipper handle rack. As the rake angle is adjusted up or down, the tooth angle adjusts with it (P&H, 2001B).

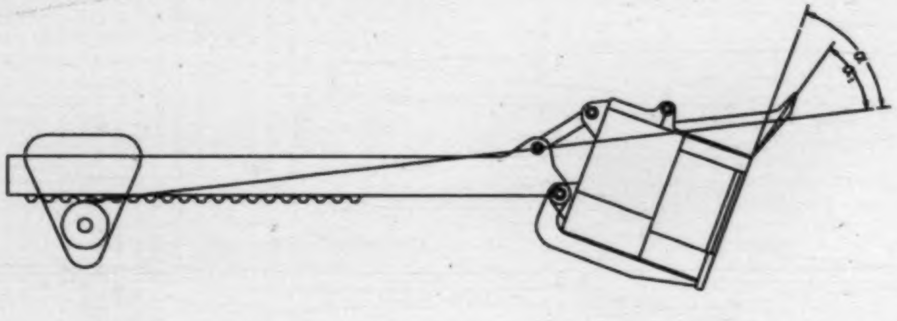

Figure 1-3: Definition of the rake angles, α: rake angle, α_1: tooth angle

Figure 1-4 illustrates a traditional generic dipper. The three dimensions of a dipper are width: from side to side; height: from the front wall to back wall; depth: from the ingress to the egress (the front and back walls are also known as the bottom and top walls).

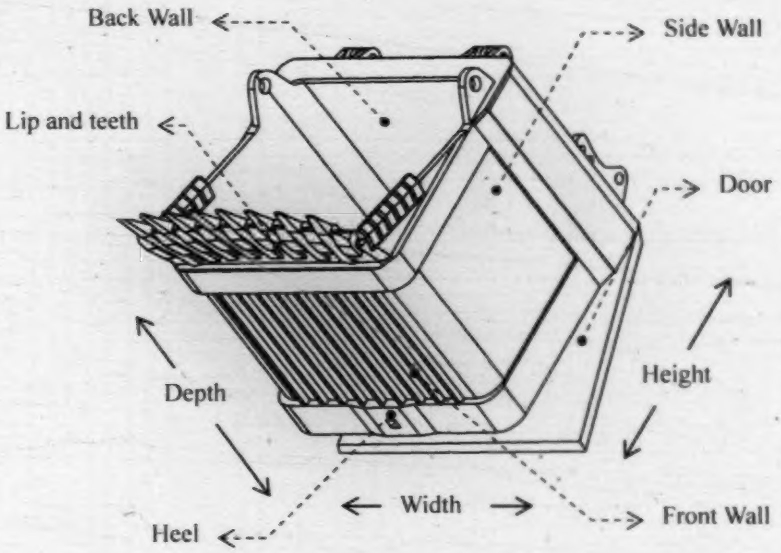

Figure 1-4: A three-dimensional illustration of typical cable shovel dipper

1.2.2 Performance indicators

The Australian Coal Association Research Program (ACARP) (2002) summarized the performance indicators (PI) for the analysis of physical dipper models:

(1) Production,
(2) Payload,
(3) Fill time,
(4) Cycle time,
(5) Fill energy and
(6) Digging resistive forces.

In this present study, the payload, fill time and digging resistive forces will be adopted in the performance evaluation.

1.2.3 Dipper design focus

To clarify the dipper design objectives, it is assumed that the shovel's geometry and structure remain unchanged. This study and the subsequent study could focus on redesigning the following constituents:

(1) Three-dimensional geometry
(2) Rake angle and tooth angle
(3) Front wall profile, either straight or curved from top to bottom
(4) Dipper back wall and attachment arrangement with respect to handle end connection points

Although the shovel design itself has advanced over the past 100 years, little work has been done on the ground-engaging-tools. In this present study, geometry, and front wall profile were primary concerned for a novel design which potentially greatly improve the shovel's performance, even if the original shovel configuration is retained.

1.2.4 Dipper design approach

In recent years, computer simulation techniques have dominated the industry's approach to system and product designs. These have many obvious economic and logistical advantages over physical modeling approaches; however, verification is still a field application. The sheer size of a full-scale physical prototype and the expense of building one force many shovel manufacturers to rely on the feedback of customers, often on an as-built basis, where failure has dire consequences on the manufacturer-operator relationship. Consequently, physical models are frequently much smaller than the full proposed design, and scaling then becomes an issue in the prediction of the full-scale-version's performance. Another problem involves simulation within the walls of an experimental facility versus the undisturbed virgin ground conditions of the field. Predicting the performance without some scaled field testing is virtually impossible; predicting the effects of scaling is difficult, and, perhaps most of all difficult is the need for both the manufacturer and the operator to take a leap of faith before any new design can make the transition to manufacture and utilization.

An integrated methodology is anticipated for industries to implement a total solution such that advanced computer techniques; simulation, optimization, modeling and field testing are seamlessly incorporated, allowing for the creation of an innovative ultra class dipper design in a cost-effective and reliable manner.

1.3 Dipper-ground interactions

Digging behavior as an interaction between the shovel and the ground is affected by both machine characteristics, such as geometric configuration, drive power and tool shape, and ground properties such as density, void ratio, moisture content and strength. The interactions between these characteristics and properties affect the machine's performance.

During a shovel digging cycle, the teeth and lip break the ground, filling the bucket while the dipper moves along an operator-controlled trajectory. Consequently, the bank face takes on a new profile similar to the above trajectory. Two principal actuating forces and one normal support force from the saddle block are exerted on the handle and dipper (See Figure 1-5), the sum of those components is equal to the sum of the handle and dipper's weight and the digging resistance.

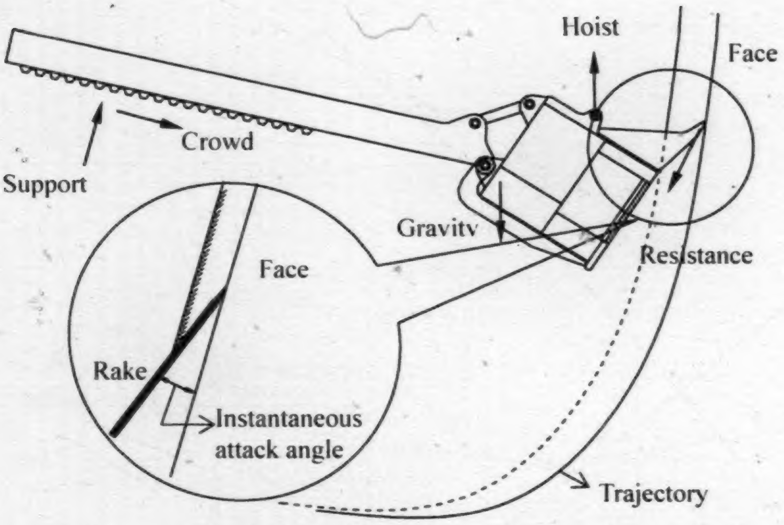

(a) Digging trajectory and dipper-ground interaction

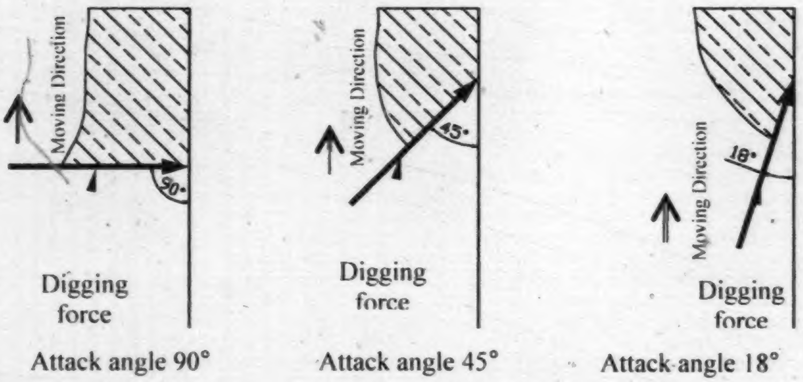

(b) Variation of the attack angle when the blade moves vertically

Figure 1-5: Diagram of the dipper-ground trajectory and interaction

A simplified digging model is shown in the circle in Figure 1-5 in terms of a straight rake intersecting the ground at a given attack angle. The digging force or resistance is a function of the material, digging depth and the attack angle. The smaller the attack angle the lower the digging resistance. Although this diagram is not an accurate model to predict digging forces, the diagram does show a relationship between attack angle and the digging force required. Generally, from 90° to 0°, for a given rake length, the digging effort will decrease while the attack angle decreases. However, it is not feasible in reality to always achieve the lowest attack angle due to invoking severe wear on the rake front. In chapter 5 the discussion will analyze the relationship between the dipper geometry and digging trajectory.

1.4 Research objectives

The objectives of this research are to

(1) Propose an amalgamation of several established design tools to develop an alternative dipper design approach, integrating 3D solid modeling, kinematics simulation, computer-aided analyses, physical modeling and field testing;

Very little work on the shovel dipper design approach was revealed from literature searches. Shovel manufacturers tend to keep their design approaches and methodology as part of their confidential intellectual property. Other researchers have shown little interest in this field due to the small machine population and the difficulty of gaining permission to perform field tests.

Due to the sheer expense of fabricating an ultra or even intermediate class dipper, a model on such a scale is not feasible for an academic research program. As a result, the performance of a developed scale model was compared to reported larger sizes from the literature and access to ultra class operating mining shovels.

(2) Suggest a design with a novel geometric shape for an ultra class shovel,

which has the potential to reduce digging resistance and energy requirements without affecting the main attached shovel structure and the corresponding drive systems.

As an example of output, a proposed dipper design for an ultra class shovel in an oil sands operation is developed utilizing the above approach. The design focuses on shape reconfiguration for an improved operational performance.

1.5 Hypotheses

To narrow the focus of the research, two hypotheses were made before any proposed work was carried out:

(1) A dipper shape configuration affects efficiency dramatically. An improved dipper profile can reduce digging resistance, wear, cycle time and energy and decrease maintenance periods, and with a reduction in wall thicknesses can increase payload and production.

Undoubtedly, the variation of the dipper shape will change the way the dipper interacts with the ground. As a result, the ground digging resistance, the wear and damage on the dipper body may increase or decrease depending on how the new shape is correlated to the ground profile and material properties. For a given set of ground conditions and shovel, there theoretically exists an optimum shape configuration that provides the best overall performance. However, not only is the approach to an improved shape very difficult, but also the methodology to evaluate the improvement an even bigger challenge. Once a feasible design approach and evaluating methodology can be established, current dipper designs could be improved for better performance.

(3) A scaled physical model would perform in the same way as a proposed

ultra class scale.

As a part of the methodology to develop a design concept, physical prototypes are used to evaluate performance at a scaled size. If the result from a scaled evaluation is favorable, the application to the full size dipper can still not be made without an in-depth analysis as to the validity of scaling up. If this hypothesis is shown to be potentially valid, the cost of building full size dipper design prototypes could be saved.

Chapter 2

Background

2.1 Research on shovel dipper design

Little work on the cable shovel dipper design has been reported in the literature due mainly to corporate manufacturer intellectual property issues. Compared to other high populated machine, the cable shovel dipper attracts very little attention from both researchers and manufacturers.

Whittingham (1971) built a laboratory model to test the pitch variation (changing the length of the pitch brace) for dipper teeth relative to the movable surface. He proposed a cable-controlled variable pitch dipper with 108° range. This design prevented dipper heeling which results from a conflict between the dipper heel and ground and provides a longer cleanup radius for a given shovel advance, so that a shorter swing angle and increased production were achieved. Shovel advance refers to the shovel's incremental movement for the dipper to reach the face.

ACARP(2002) made a series of physical dipper models to investigate the relationship between some key design factors: length:width:height ratios, bail (bailless) positions, tooth angle and arrangement, and the shovel's performance in term of payload, fill time, energy required, tooth force.

The key findings of this work provide a series of key dipper design principles, which are subject to a provisional patent held by GBI Consulting Pty Ltd.

(1) When looking into the mouth of the dipper, the height / width ratio will depend on what is being dug, such that:

- Coal - 1.0
- Soft Digging - 0.75
- Blocky Digging - 0.6

If a range of ground materials are being dug, a mine either needs multiple dippers or utilizes a height / width ratio of 0.65 - 0.70

(2) The dipper needs to be designed in such a way so as to minimize the void volume at the corners of the open mouth with the back wall as a percentage of apparent material volume.

- The dipper needs to be as shallow (distance from teeth end to door) as possible.
- The height from teeth to door should be at least twice as long as the height at the rear of the dipper.

(3) The length and orientation of the dipper back need to be designed in such a way as to minimize the void space when the spoil flowing into the dipper.

(4) Rounded (high radius) corners should be utilized wherever possible. The shape of the back needs to be rounded to account for the shape of

spoil flowing into the dipper.

(5) A minimum rake angle of 75° is recommended. Higher angles provide improved productivity but will also increase heel wear. This angle can be increased if the design allows the heel to be further from the face.

(6) The tooth angle and rake angle need to be balanced to maximize productivity and minimize heel wear. More work is needed in this area on a site by site basis but as a starting point a rake angle of 80° and tooth angle of 65° are recommended.

(7) The hoist rope connection needs to be as far back as possible; at least in line with the rear of the dipper.

P&H (2001B) suggested starting points for adjusting the tooth angle and rake angle (see Table 2-1).

Table 2-1: Suggested minimum tooth angle and rake angle

	Hard Rock digging	Medium Digging
Tooth Angle	46°-48 °	48 °-50 °
Rake Angle	57 ° -59 °	59 ° -61 °

Although little literature is available on the front wall profile, the compromise between digging performance and heel life was mentioned in all above research. For example, the variable pitch dipper (Whittingham, 1971) tried to increase the rake angle for better digging and decrease the rake angle for heel protection. ACARP (2002) research suggested a 75 ° degree rake angle for an acceptable productivity and 80 ° for a balance between the productivity and the heel wear based on the field experiment.

2.2 Current dipper design review

Dipper profiles have had a box shape until recently. As summarized by ACARP (2002), Whittingham (1971), P&H (2001B), traditional dipper design has some generic drawbacks (see Figure 2-1):

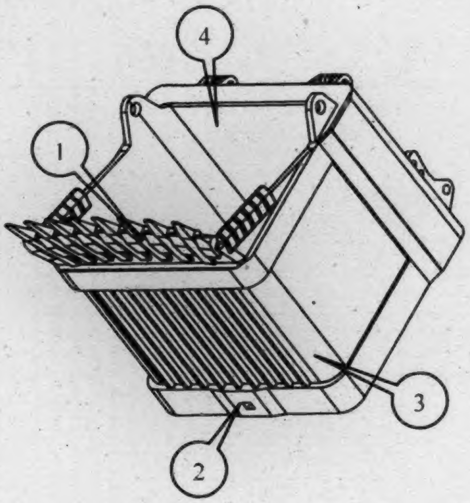

Figure 2-1: A generic dipper concept

(1) Tooth angle and rake angle: With a straight front wall, the compromised tooth and rake angle result in a high attack angle during the tucking or initial digging (see Figure 2-2).

(2) Heel: With a straight front wall, the heel is vulnerable to the ground wear and damage, it is not cost-effective to increase the tooth angle and rake angle as desired for a reduced digging resistance because of rapid increase of wear and damage on the front (see Figure 2-3).

(3) Corner: For a flat front wall, the corner wear is significant as the corner keeps touching the side material when the dipper penetrates in the face made of non-blasted material.

(4) Back wall: The cubic shape of the traditional design may lead to void space around the top area of the back wall.

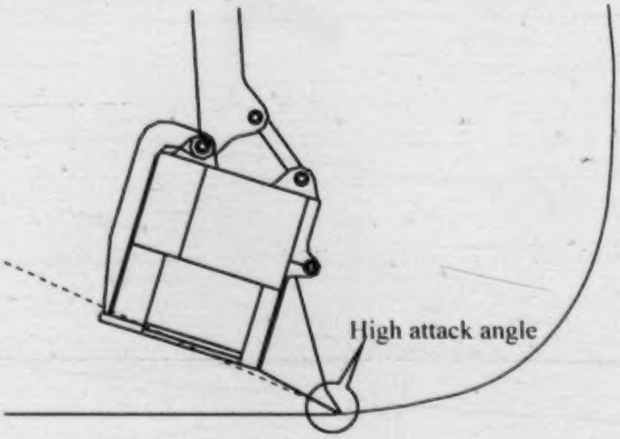

Figure 2-2: A high attack angle deceases digging performance

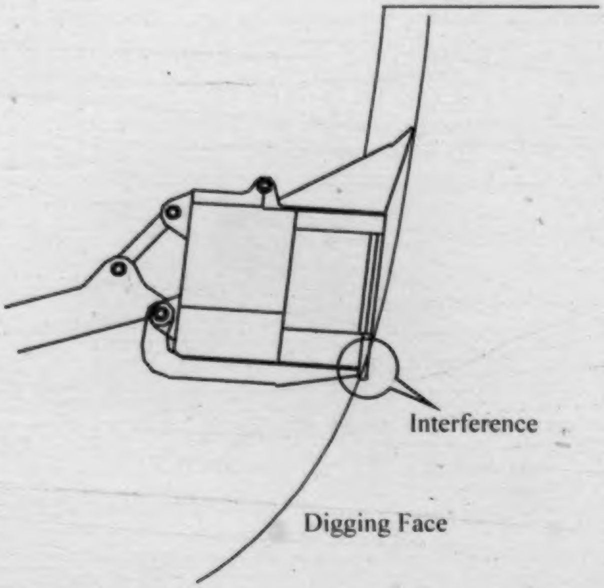

Figure 2-3: Face interference leads to heel wear and damage.

P&H MinePro Services launched the P&H Optima® plus dipper line for both P&H shovels and other non-P&H shovels in 2000 (see Figure 2-4). This design was introduced to attempt to provide a better balance for digging and loading. had an improved geometry for fast filling and easy, even-pass, resulting in increased production (P&H, 2001C). The dipper kit for P&H 4100 XPB allows expanding or reducing their payload capacity from 63 cu yd to 80 cu yd. (Coal age, 2001). P&H (2001C) claimed this dipper has three outstanding design features:

(1) A curved side-to-side front profile reduces ground engaging impact and avoids corner wear.

(2) A smaller height-to-width ratio improves material filling.

(3) A shortened latch keeper reduces latch wear and damage, decrease the down time.

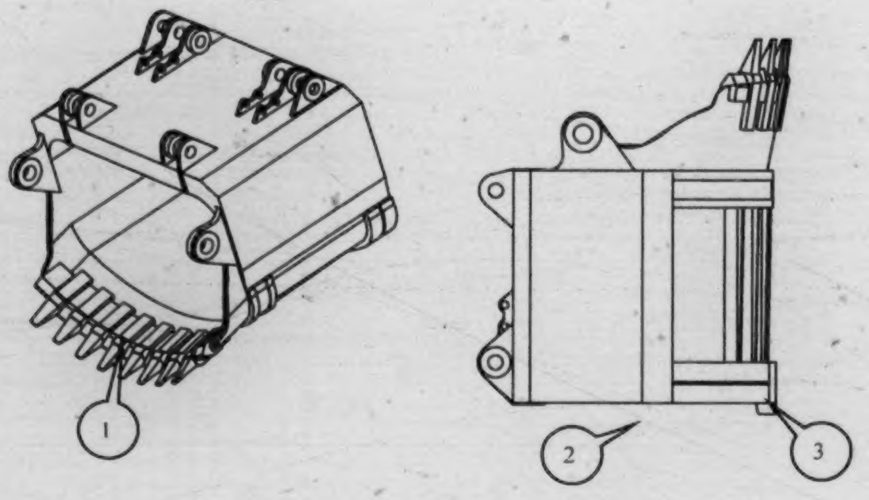

Figure 2-4: P&H Optima® Plus dipper (P&H, 2001C)

Bucyrus International at the same time developed the FastFil^{a} series of dippers (see Figure 2-5) for their shovels, which improved the fill factor (ratio of the filled volume to dipper capacity) (Bucyrus, 2003). The FastFil^{a} series essentially has a similar specification to that of P&H, but has the following features:

(1) A higher tooth angle in addition to the laterally curved lip and front wall.

(2) A trapezoidal back to reduce void space.

(3) A shortened back wall to reduce dipper weight and reduce void space.

(4) Bailless design, the dipper is not held by a bail frame but a pair of wheels through which the hoist cables are attached.

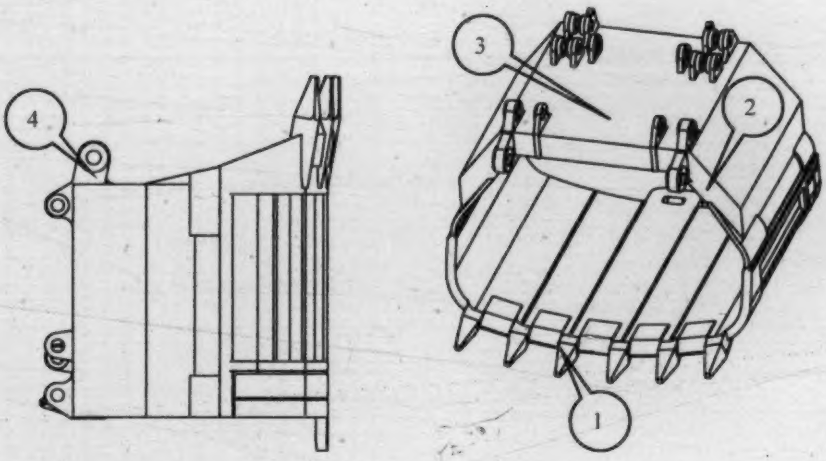

Figure 2-5: Bucyrus Fastfil dipper (Bucyrus, 2003)

ACARP also developed a conceptual design based on their experimental results (see Figure 2-6). This design is very similar to Bucyrus's Fastfil dippers, except for a flat front wall. No literature reveals the relationship between these two designs.

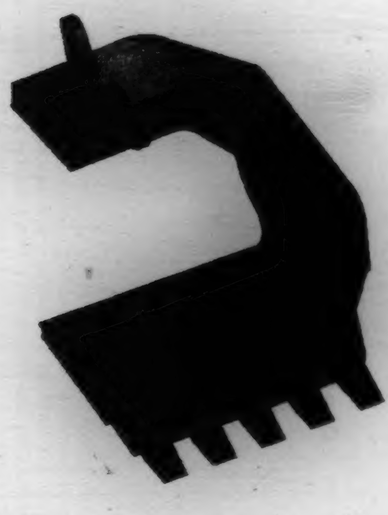

Figure 2-6: ACARP Concept dipper (ACARP, 2002)

ESCO, a Portland, Oregon-based tool company (originally AMSCO of Manitoba, Canada), developed the Maxi-Pro series shovel dippers, which featured a curved lip (side to side) and high wear protection (ESCO, 2002) (no figure available).

Based on above review, it is anticipated a dipper front wall that can not only achieve a high digging performance but also a long heel life. All previous dippers have straight front walls (from the teeth to the door latch). Therefore, a curved one may have great potential to satisfy both criteria (high performance and long heel life).

2.3 Other Ground Engaging Tool (G.E.T.)

Relatively more information has been published for the hydraulic excavator and loader G.E.T. than for the cable shovel dipper.

Unlike the dipper for an electrical cable shovel, the G.E.T for a hydraulic shovel or front end wheel loader is normally known as the 'bucket'.

The buckets for hydraulic shovel, backhoe and front end loader perform in a similar way to cable shovel dippers. Hydraulic front shovels and backhoes are often assigned to harder material digging jobs so that their buckets are normally compact, solid built and of high height:width ratio. By comparison, the front end loader bucket is of low height:width ratio and less solid built. (see Figure 2-7).

For hydraulic excavators, various bucket designs are in wide use. In general, manufacturers offer digging buckets for (Caterpillar, 2005)

- General purpose

They are designed to improve performance in moderate-to-easy to penetrate soils that are not highly abrasive. These buckets take advantage of the easier to load soil by using a larger tip radius to get more capacity for each bucket width.

- Heavy duty

These buckets are designed to work in all but the most abrasive work conditions. They are more durable than the general purpose buckets. For a given width they have a smaller tip radius. This insures good loadability in difficult to penetrate soils. They have thicker base edges and larger teeth than the general purpose buckets.

- Heavy duty rock

These buckets are designed for the most severe rock conditions. They offer the same capacity, tip radius, and teeth as the heavy duty buckets, but material thickness has been increased and wear plates are larger than the heavy duty buckets.

- Cleaning

This is a wide, shallow bucket designed for cleaning ditches and slope work. It is also good for grading in light materials. They may not have teeth or side shrouds.

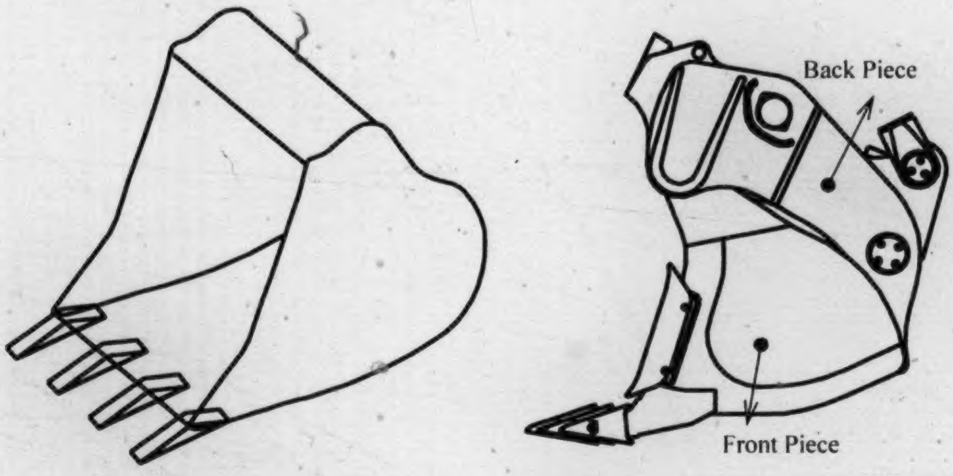

(a) Hydraulic backhoe bucket

(b) Hydraulic front shovel bucket

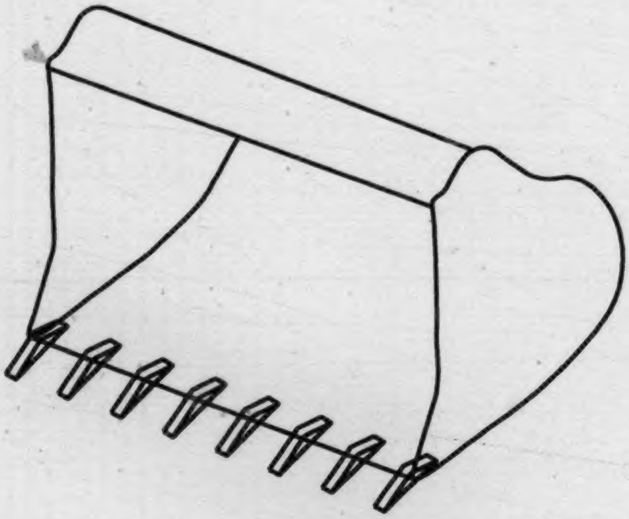

(c) Front end loader bucket

Figure 2-7: Various hydraulic shovel and loader buckets

Kuhn and Wardecki (1983) described typical hydraulic shovel buckets and worked out a comparison of various bucket configurations with various rock masses. One of his conclusions was to emphasize the importance of the selection of the right bucket for a given set of ground mass properties.

Howarth et al. (1987) described dragline bucket filling characteristics by carrying out field and laboratory studies of the relationship between the drag and carry angles (see Figure 2-8). Favorable angle combinations which result in minimum volume lost and volume waste (space not utilized) were found for different materials.

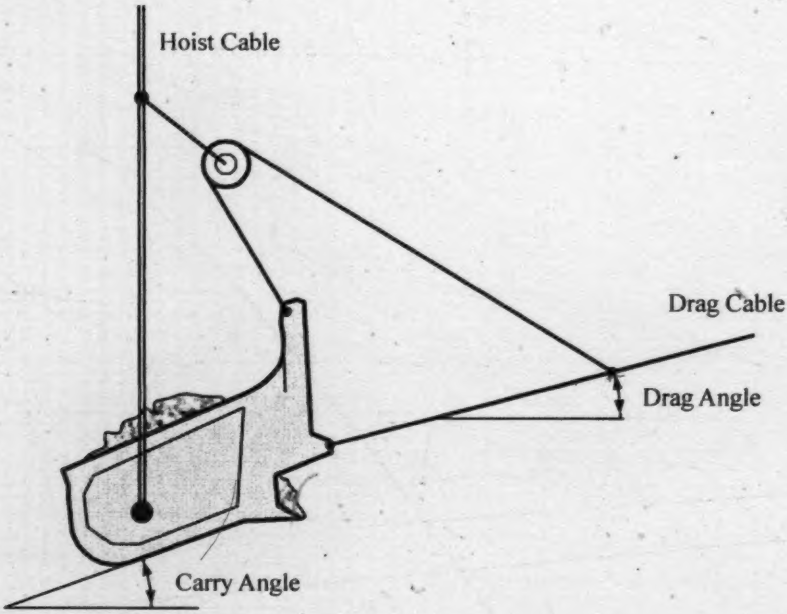

Figure 2-8: Dragline bucket (Howarth et al.,1987)

Rowlands and Just (1992) described the performance characteristics of dragline buckets by building three experimental rigs, one at a 1:32 scale, one at a 1:12.5 scale and one at a 1:6 scale.

These arrangements yielded valuable data resulting in an improved understanding of dragline bucket-filling behavior and allowing for an improved bucket whose top matches the shape of the ground material at an angle of repose. They also compared the test data to the performance data from a full scale bucket in operation. One important conclusion that is meaningful for this study is that the scaled test version of the bucket can be very helpful for a full scale new design.

2.4 Previous work related to dipper design

2.4.1 Digging kinematics

Several researchers have worked out models for cable shovel kinematics and dynamics relationships. Daneshmund and Hendricks (1993) developed a simplified generic kinematic model for shovels. In their work, the position of the dipper was determined by the geometry shown in Figure 2-9, in which *M* is the length of the shovel boom from the crowd arm attachment to its end; *h* is the length of hoist rope, and *l* is the crowd arm extension.

In the model, the handle was considered as a beam that was assumed to be extended and retracted though a pivot point on the boom. The sheave wheel radius was neglected and assumed to be a point.

Utilizing this model, the shovel dipper kinematics was summarized with the following equations:

$$x = F_x(h,l) = x_0 + \frac{M^2 + l^2 - h^2}{2M}\cos\lambda + \left(l^2 - \frac{\left(M^2 + l^2 - h^2\right)^2}{4M^2}\right)^{\frac{1}{2}}\sin\lambda \tag{2.1}$$

$$y = F_y(h,l) = y_0 + \frac{M^2 + l^2 - h^2}{2M}\sin\lambda - \left(l^2 - \frac{\left(M^2 + l^2 - h^2\right)^2}{4M^2}\right)^{\frac{1}{2}}\cos\lambda \tag{2.2}$$

$$v_x = \frac{dx}{dt} = \frac{\partial F_x}{\partial h}\frac{dh}{dt} + \frac{\partial F_x}{\partial l}\frac{dl}{dt} \tag{2.3}$$

$$v_y = \frac{dy}{dt} = \frac{\partial F_y}{\partial h}\frac{dh}{dt} + \frac{\partial F_y}{\partial l}\frac{dl}{dt} \tag{2.4}$$

$$a_x = \frac{dv_x}{dt} = \frac{\partial v_x}{\partial h}\frac{dh}{dt} + \frac{\partial v_x}{\partial l}\frac{dl}{dt} \tag{2.5}$$

$$a_y = \frac{dv_y}{dt} = \frac{\partial v_y}{\partial h}\frac{dh}{dt} + \frac{\partial v_y}{\partial l}\frac{dl}{dt}. \tag{2.6}$$

Where:

a_x, a_y	Dipper acceleration's x and y components, respectively
F_x, F_y	Functions of h and l to determine the dipper position x and y, respectively
h	Hoist cable release length
l	Handle extension length
t	Time

v_x, v_y	Dipper velocity's x and y components, respectively
x, y	Dipper position in the digging plane coordinates
x_0, y_0	Saddle block shaft position.
λ	Boom angle.

The above model is summarized as follows:

- The handle and dipper position is a function of the handle extension and the hoist cable release length.
- The dipper velocity and acceleration are a function of the crowd and hoist velocity and acceleration.

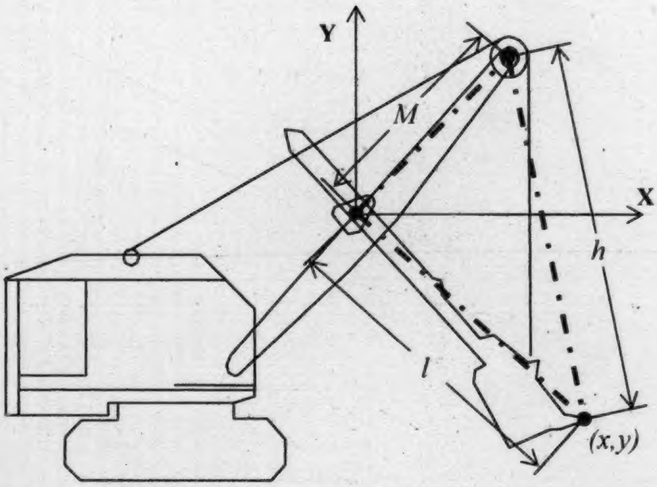

Figure 2-9: Simplified shovel geometry (Daneshmund and Hendricks, 1993)

2.4.2 Digging forces

For the purpose of dipper investigation, the handle-dipper forces equilibrium is of primary concern in considering shovel digging behavior. To generalize the problem, the forces illustrated in Figure 2-10, in which F_s is the support force perpendicular to the handle from the saddle block, F_p is the crowding force generated at the crowding motor, F_h is the hoisting force generated at the hoist motor, G_d is the gravity force of the dipper plus the handle acting at its composite centroid, G_o is the gravity force of the material in the dipper acting at its centroid, F_{cx} and F_{cy} are the cutting resistance forces generated at the working face in the X and Y directions, F_{fe} is the frictional force acting on the external front dipper wall, N_e is the normal force acting on external front dipper wall, F_{fi} is the frictional force acting on the internal front dipper wall and N_i is the normal force due to the material moving in the dipper acting on the internal front dipper wall.

Member (1986) outlined the forces acting on the front attachment shovel. He used the equilibrium of forces to determine the shovel's digging forces. He considered the bucket dynamics in several key positions:

(1) When digging activity is just about to start, until the dipper stick is in the vertical position;
(2) When digging is well in progress, until the dipper stick is at about 45 degrees to the vertical;
(3) When digging is about to be completed, until the dipper stick is approaching the horizontal;
(4) Free in the face, until the stick at a set angle to the boom.

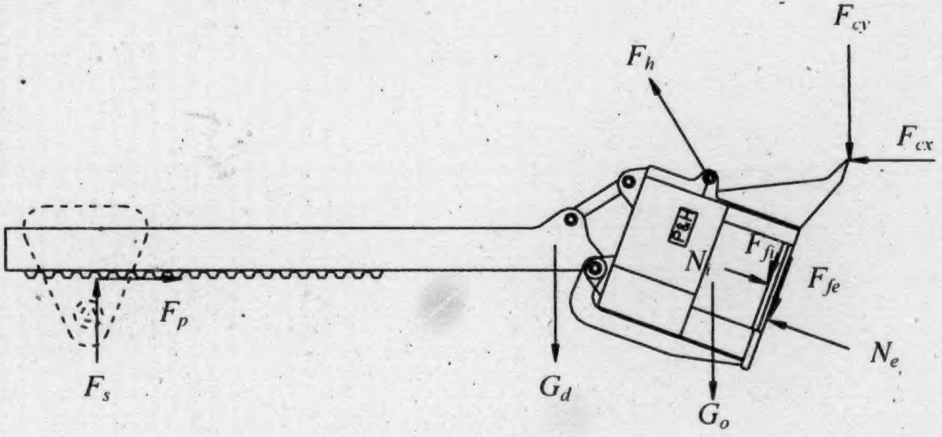

Figure 2-10: Dipper-handle free body diagram and the acting forces

Henami (1992) did more extensive work with hydraulic loaders; he devised kinematic and dynamic models for a load-haul-dump unit (LHD) used in underground mines.

In Figure 2-10, the weight of the dipper and handle G_h and G_d are constant and that of the ground mass in the dipper G_o increases during digging. The centroid of the mass in the bucket obviously varies too but keeps within a small range. Regarding the handle, dipper and mass in the bucket as a single body with weight G, in this study, the changing position of the centroid for the body was neglected due to its insignificant influence on the force equilibrium.

The frictional force and normal force acting on the outside of the front wall result from flowing material moved with the digging action. For non-blasted material, the amount of the falling, flowing material is a minor contribution to the force equilibrium. Nevertheless, the amount and moving direction of the falling material are unpredictable.

The resistive forces F_{cx}, F_{cy}, N_i, F_{fi} are the components of total digging resistance R, the opposite of the digging effort described by the dipper-ground interaction model in later discussion.

Therefore, the hoist force, crowd force, handle support force, gravity and a combination of the resistive forces are considered in a model shown in Figure 2-11.

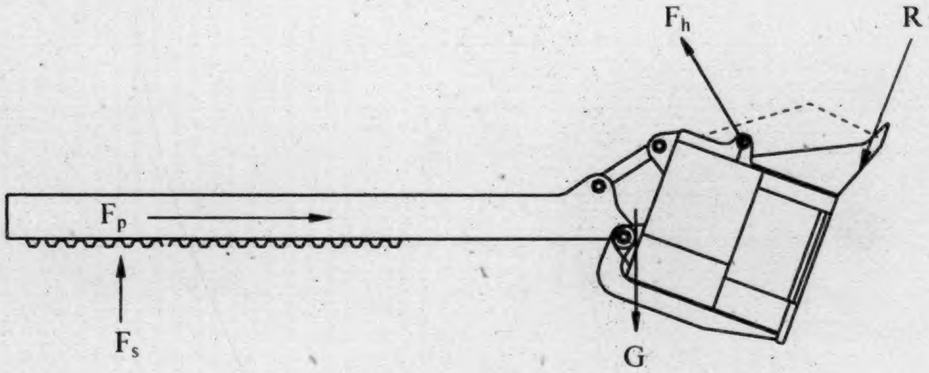

Figure 2-11: a modified dipper-handle free body diagram

2.4.3 Dipper - ground interactions

The shovel's digging process consumes a large amount of energy in operation, resulting in machine wear and adverse impact on the moving structure. Extensive field research has been done on ground-tool interactions. Model-based analysis of the dynamics of earthmoving can be applied to equipment design, system identification, performance monitoring, simulation, and control. Knowledge of the forces encountered by a tool in earthmoving operations can be useful for tool and machine design. The interactions between a tool and a medium can be divided into three actions: penetration, cutting and loading (see Figure 2-12) (Blouin, 2001).

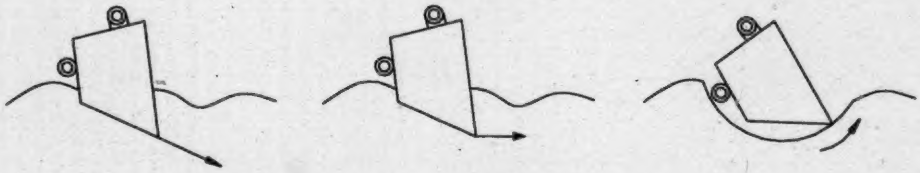

a) Penetration b) Cutting c) Loading

Figure 2-12: Fundamental Earth-moving actions (Blouin, 2001)

Penetration, the simplest activity of soil breakage, is to penetrate the blade in to the soil along the blade direction. Cutting is to break the soil via moving the bucket through the soil. Although penetration and cutting are distinct actions, the resistive forces observed while cutting were found to be of the same nature as those encountered during penetration (Zelenin et al., 1985). Loading is to fill the broken soil into the bucket (Blouin, 2001).

The cutting action was of greatest concern in this study as it accounts for the largest portion of the shovel digging behavior.

During the last four decades, the methodologies used in modeling soil cutting have progressed from an experimental approach, to 2D/3D analytical methods, to finite element methods and recently, discrete element methods. The theory involved covers Terzaghi's (1943) passive earth pressure theory, elastro-plastic mechanics, and plastic flow, rheology and particle mechanics.

The magnitude of forces required to cause soil failure is a function of the shear strength of the medium and the dimensions of the ruptured surface. (Blouin, 2001).

With respect to the digging process, the ground model describes how the ground will fail and yield. The most common soil failure model is the shear stress and shear strength theory.

In 1776 Coulomb noted that there exist two mechanical processes that determine the shearing strength of a material. One process (friction) is proportional to the pressure acting perpendicular to the shearing surface. The other process (cohesion) seems to be independent of normal pressure. Coulomb modeled the shear strength, τ of a soil as the sum of these two components:

$$\tau = C + \sigma \tan\varphi \tag{2.7}$$

where

C cohesion,

σ the normal pressure acting on the internal shear surface and

φ internal friction angle

Table 2-2 shows typical values of cohesion (C), and angle of internal friction (φ) for some commonly mined soft materials.

Osman (1964) analyzed a wide cutting blade scenario via checking two theories for passive pressure, (a) Coulomb's solution for granular material and (b) Ohde's (1938) logarithmic spiral method (see Figure 2-13). The boundary condition at failure in Coulomb's theory was assumed to be a plane surface from the blade tip to the free surface. The inclination of the plane was governed by the minimum force. The material failure boundary in Ohde's theory was composed of a logarithmic spiral and a plane surface identical to that postulated for long retaining walls.

Table 2-2: Properties of some typical soft mined materials (Singh, 1995), (Dusseault and Morgenstern, 1978) *

Material	Cohesion(kPa)	Friction Angle(degree)
Lean Clay	17.2	17.2
Heavy Clay	68.9	34
Dry Sand	1.0	28
Sandy Loam	1.7	29
Coal	0	30
Oil sand*	0	20-60

Osman concluded that Coulomb's wedge solution holds good for smooth blades of small attack angles working in cohesionless materials. The dipper soon becomes very smooth after launching into operation due to high abrasiveness of the oil sand. Not like the actions of ripping and tillage, the digging in oil sand is mainly an action of the cutting or peeling that carries relatively small attack angles. Dusseault and Morgenstern (1978) concluded that the oil sand is cohesionless. Therefore, the oil sand digging scenario matches this conditions that Osman proposed based on the facts of the shovel digging action and oil sand properties.

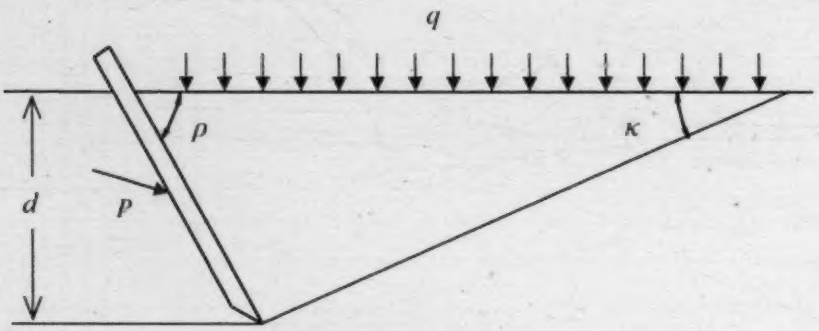

(a) Plane rupture surface

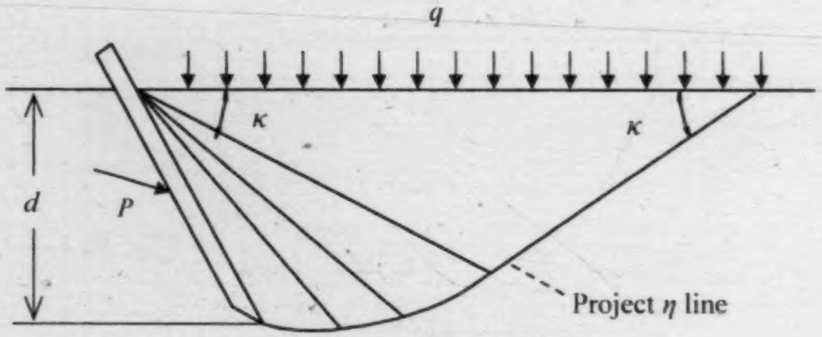

(b) Logarithmic spiral rupture surface

Figure 2-13 : A 2D scheme for soil cutting

Reece (1965) recognized that the mechanics of earthmoving are similar in many respects to the bearing capacity of shallow foundations on soil as described by Terzaghi (1943). He proposed the following equation for universal ground-breaking force estimation.

$$P = \left(rgd^2 N_r + cdN_c + c_a dN_a + qdN_q\right)w, \qquad (2.8)$$

where

c	Soil cohesion
c_a	Soil-tool adhesion
d	Tool working depth
g	Acceleration due to gravity
N_a	Soil cutting force adhesive factor
N_c	Soil cutting force cohesive factor
N_q	Soil cutting force surcharge factor
N_γ	Soil cutting force gravitational factor
P	Total tool cutting force
q	Surcharge pressure acting on the soil surface
w	Tool width
γ	Soil density
κ	Rupture surface inclination
ρ	Rake attack angle

N_a, N_c, N_q and N_r depend not only on the soil friction strength, but also on the tool geometry and tool to soil strength properties.

As the tool surface is normally very smooth in contrast to the soil so that the adhesion is not significant, the component $c_a dN_a$ in Equation 2.8 is often neglected.

Based on Osman's work, Hettiaratchi and Reece (1974) developed charts to determine factors N, N_c, N_q. This method is not convent for iterative simulation.

Both graphical and analytical methods were used to determine the factors for the trial wedge model. One of those was to determine the factors by seeking the minimum digging effort. This method will be discussed and developed further later in chapter 4.

Hettiaratchi and Reece (1967) also proposed a three-dimensional model as shown in Figure 2-14.

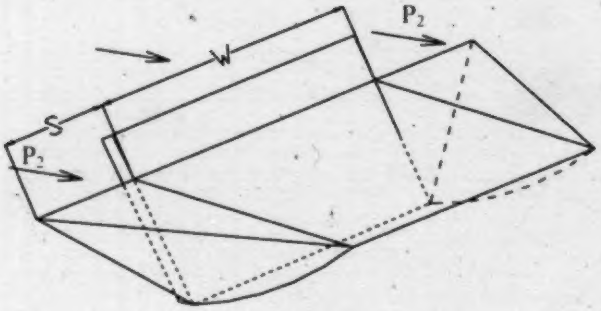

Figure 2-14: 3D scheme of soil-cutting model (Hettiaratchi and Reece, 1967)

In the three-dimensional model, the composite cutting force, P, is the sum of the component P_1 for cutting the middle zone, and twice that of P_2 for cutting the two side zones:

$$P = P_1 + 2P_2 \tag{2.9}$$

The two-dimensional methods previously mentioned are appropriate for calculating P_1 and equation 2.9 was proposed for calculating the cutting forces for the side zones.

$$P_2 = \left\lfloor \gamma g \left(d + q / \{rg\}\right)^2 w' N_{s\gamma} + c w' d' N_{sc} \right\rfloor K_b, \tag{2.10}$$

where

d Tool working depth.

K_b $= \dfrac{\tan^{-1} \kappa \sin \rho \cot \kappa}{\left(\dfrac{\pi}{2} - \kappa\right)}$

N_{sc} Soil side cutting force cohesion factor.

$N_{s\gamma}$ Soil side cutting force frictional factor.

w' Effective width of the side zone.

$$w' = \frac{d}{\frac{1}{2}\tan\kappa \sin\left(\alpha + \frac{1}{2}\left[\delta + \varphi + \frac{\pi}{2} + \sin^{-1}\left(\frac{\sin\delta}{\sin\varphi}\right)\right]\right)\sin^{-1}\frac{1}{2}\left[\delta + \varphi + \frac{\pi}{2} + \sin^{-1}\left(\frac{\sin\delta}{\sin\varphi}\right)\right]}$$

The N factors in above equation can be analytically determined using the N factors for a two dimensional soil cutting model (McKyes, 1985).

In the general case, the two dimensional analysis developed above is insufficient. However, McKyes (1985) notes that in the case a tool has side-walls (as with excavator buckets) the walls help push the soil into the bucket and constrain the failure to a volume directly ahead of the bucket. This suggests that in this case a two dimensional analysis will suffice if a typical excavator bucket is used.

2.5 Soft rock and oil sand

2.5.1 Soft rock in comparison to hard rock

There are no set guidelines in specifying between soft and hard rock. Miners use mass strength, block size, weathering and fracture density to derive an index for determining whether blasting is needed. In the shovel digging context, the relatively soft ground material that need not be blasted before digging is normally regarded as soft rock or soil.

Ideally un-blasted soft bank face material that consists of fine and even size material takes a similar profile as the dipper moves through it along a set digging trajectory. The dipper will often need to move along an extended path to peel off the material from the face. In this action only a small amount of loose material flows down on the bank toe (see Figure 2-15).

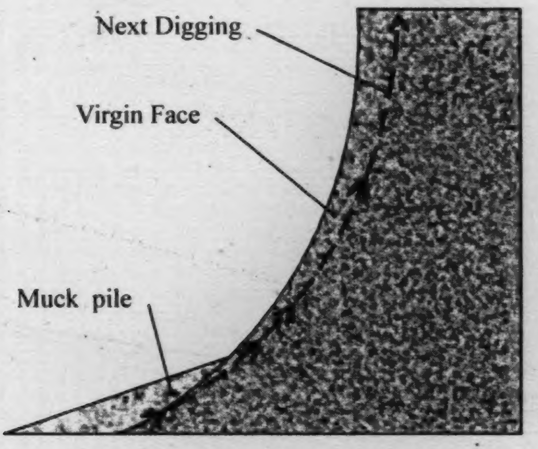

Figure 2-15: Un-blasted soft material face

In contrast to an un-blasted soft material face, a blasted face which consists of uneven blocks of rock requires a different mode of excavation. The dipper will normally move a very short distance (approximately 2~3 times of the dipper depth). A large amount of fragmented rock falls down at the face toe and accumulates in a rock pile. The digging action is more like scooping loose material. While the rock pile is cleaned, more rock falls down with or without minor digging in the face itself (see Figure 2-16).

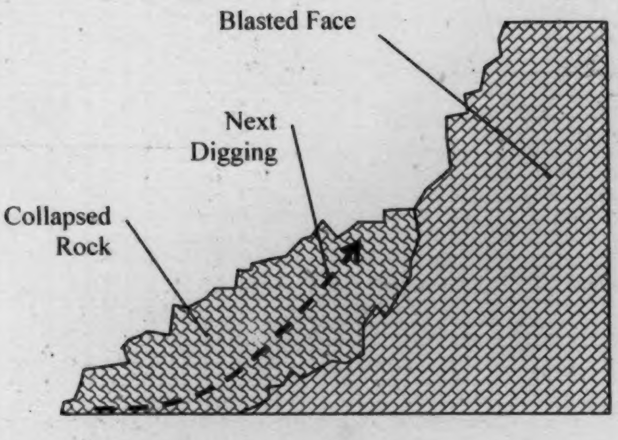

Figure 2-16: Blasted rock face

Another significant difference between the two types of digging is the influence of volume expansion, which is often indicated with the swell factor (SF).

The swell factor is defined as

$$SF = \frac{Bank \quad Material \quad Density}{Loose \quad Material \quad Density}, \tag{2.11}$$

The un-blasted material will swell dramatically while it moves into the dipper after being broken from the face.

In contrast to un-blasted material, blasted rock swells to some degree within the bank after blasting. This leads to different filling behavior from the soft un-blasted material.

In this research, soft rock and soil conditions are assumed, where the muck pile at the face toe is small compared to the dipper capacity. The loading action is fulfilled by cutting through the virgin face.

2.5.2 Oil sand

Alberta's oil sand deposits are some of the biggest oil sand reserves in the world and represent a major source of oil. Canada's crude bitumen exists entirely in sedimentary formations in three regions: the Athabasca, Cold Lake, and Peace River oil sand areas (National Energy Board, 2000).

The oil sand deposits are composed primarily of quartz sand, silt and clay, water and bitumen, along with minor amounts of other minerals, including titanium, zirconium, tourmaline and pyrite. Although there can be considerable variation, a typical composition is:

- 75 to 80 percent inorganic material, with this inorganic portion composed of 90 percent quartz sand.
- 3 to 5 percent water.
- 10 to 12 percent bitumen, with bitumen saturation varying between zero and 18 percent by weight.

The bulk density of uniformly graded rich oil sand ranges from 2.05 to 2.18 g/cm^3.

A key aspect of the oil sand reservoirs is the presence of bound formation water, which surrounds the individual sand grains as layer. The bitumen is trapped within the pore space of the rock itself. This is similar to most conventional oil reservoirs, and the reservoir rock is said to be "water-wet", that is, each sand grain is surrounded by an envelope or film of water about 10 nanometres thick. The presence of the water layer around the grains enables the bitumen to be recovered more easily since the bonding forces between the bitumen and water are much weaker than those between the water and the sand grains (National Energy Board, 2003).

Figure 2-17 shows the in-situ structure of oil sands (Dusseault and Morgenstern, 1977). The pore liquids are saturated with gas containing 75% to 90% methane and 10% to 25% carbon dioxide under in situ conditions (Kosar, 1989).. The porosities of the high-grade oil sand are around 25 to 35%. This high porosity shows a lack of cementation and hence cohesion in the oil sands.

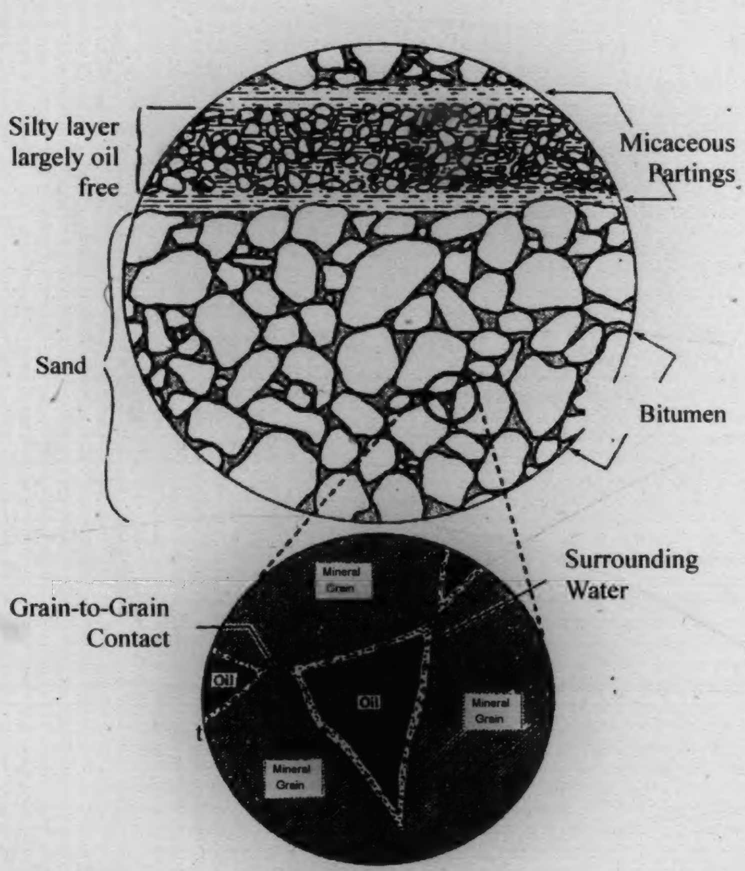

Figure 2-17: In-situ structure of oil sands (Dusseault and Morgenstern, 1977)

In-situ, the pore fluid, particularly the bitumen, contains significant quantities of dissolved gases which, upon release of confining pressure, come out of solution. The relatively low permeability of the oil-rich sand does not permit rapid dissipation of evolved gas and the net outward pressure results in gross fabric disruption by expansion. Once the structure is broken, the trapped gas will escape rapidly, resulting in a speeding swelling. This will be considered in chapter 5 where expansion causes capacity issues for dipper designs.

As it is near impossible to sample in-situ oil sand without disturbing the material with release of gases and expansion of the structure, Dusseault and Morgenstern (1977) conducted drained and undrained triaxial tests on recompacted rich oil sand with 13.5% bitumen content. The triaxial tests were run at around 4°C. The results showed a Mohr-Coulomb failure envelope for undrained rich oil sand which can be described as follows (see Equation 2.12, Figure 2-18).

$$\tau_f = 1.13\sigma_n^{0.83} \tag{2.12}$$

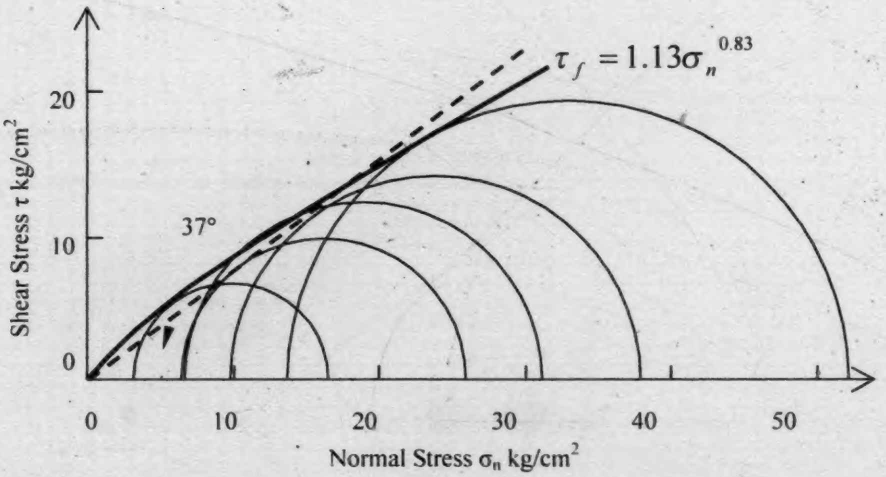

Figure 2-18: Failure envelope of recompacted rich oil sand undrained triaxial tests (Dusseault and Morgenstern, 1977)

Dusseault and Morgenstern (1978) suggest zero cohesion for densely recompacted oil sand. However, in-situ oil sand often shows very high slope angles. A Mohr-Coulomb plot of triaxial test data from the Canadian oil sands shows a surprisingly high tangent angle of friction at low confining stresses (Dusseault, 2001).

Typically, in-situ undisturbed oil sand will have a friction angle of 50° to 60°; it is reasonable to use a friction angle of 50° for undisturbed oil sands (Collins, 2005), (Morgenstern and Scott, 1997).

2.6 Summary

Very little literature directly pertaining to shovel dipper design has been reported. Nevertheless, all published previous work noticed the conflict between rake angle and dipper life (wear). Side-to-side curvatures have been adopted in the most recent dipper designs (to 2006), however, no tooth-to-heel curvature concept has been proposed. The tooth-to-heel curve concept may potentially solve the conflict between digging performance and dipper life. This research therefore focuses on development of a design concept incorporating this front wall curvature.

Only ACARP (2002) published a dipper design approach that is 100% physical test based. There are no combinations of analytical or simulation methodologies reported as manufacturers are over concerned over intelligent property protection, and other researchers show little interest due to the development expense involved.

In addition to an experimental dipper design approach, the research here is an analytical study of a proposed dipper design, based on the shovel kinematics, dipper geometry, ground conditions and dipper-ground interaction. To reach the objective of the study, an approach that integrates the kinematic analysis, digging simulation and prototype test will be proposed.

Since the target material for the proposed dipper is oil sand, the properties of oil sand were reviewed. As a kind of soft rock or soil, oil sand in Northern Alberta has different behavior to that of the blasted rock mining context. In-situ, the pore fluid, particularly bitumen, contains significant quantities of dissolved gases which, upon release of lateral ground confining pressures during excavation, come out of solution. The relatively low permeability of the oil-rich sand does not permit instantaneous rapid dissipation of the evolved gas and the net outward pressure results in gross fabric disruption by expansion once it resides in the dipper body.

Some literature on shovel digging kinematics and ground - tool interactions were reviewed. Previous shovel kinematic models were over simplified with respect to geometry and action. This research will devise a model that fully represents the shovel's geometry and action.

Although, there are advanced methodologies that can be used for ground breaking analysis, the trial wedge which is based on shear strength and shear stress theory is suitable for oil sand digging analysis. This method will be discussed and developed further later in chapter 4. It is simple and hence fast to run and widely accepted as accurate for oil sand modeling purposes. There are some modifications that will need to be applied to the model to be applicable for cable shovel digging actions as this machine's digging behavior is beyond the previous trial wedge ground breaking model.

To validate the concept of a curved (teeth to heel) front wall that will increase rake angle whilst decreasing heel wear or damage, a digging simulation approach that incorporates digging kinematics, ground conditions, dipper-ground interactions and force equilibrium will be proposed in subsequent chapters. Previous research with respect to the above is lacking in the literature and hence provides the scope for this work.

Chapter 3

Digging Kinematics

3.1 Cable shovel geometric model

3.1.1 Assumptions

Only two main manufacturers, Bucyrus International (formerly Bucyrus Erie) and P&H Mining Equipment (Harnischfeger Corporation), remain in the cable shovel market around the world. Each has kept to its own classical mechanical shovel configuration although dimensions and electronics have advanced in recent years. As the P&H 4100 BOSS shovel is extensively used in Northern Alberta oil sand operations, this configuration was used as a basis for dipper modeling. As such it was assumed that:

(1) The shovel main structure and associated components are rigid.

(2) The shovel's main structure remains stationary during digging operations, while the dipper and handle assembly is allowed to move through the face defining the shape of the dipper front; the crux of this research.

(3) The shovel operates in homogeneous isotropic oil sand ground material.

(4) The working mining face dimensions are appropriate for oil sand geotechnical stability and the shovel operating geometry (see Figure 3-1).

From these assumptions, the shovel action was modeled based purely on geometrical restrictions. A geometrical shovel model was input into an analytical shovel kinematic model written in MatLab (see Appendix A.1).

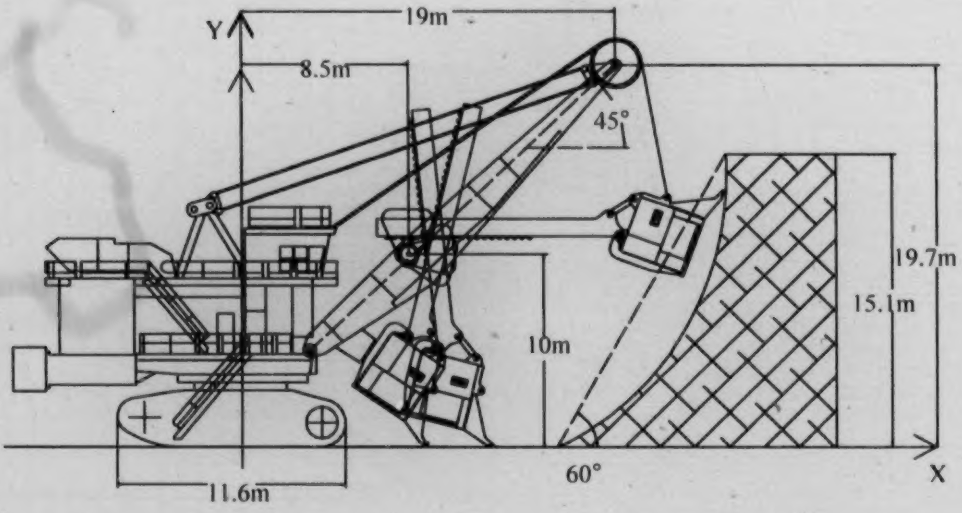

Figure 3-1: Schematic of shovel and working face

3.1.2 Shovel position in cylindrical coordinates

Normal cylindrical coordinates use (r, θ, z) to represent a point in 3D space (see Figure 3-2 (a)).

To make a smooth transition from the two-dimensional shovel model developed by early researchers and from range diagrams freely available to the mining industry from the manufacturer of the shovel via equipment specification sheets, a special coordinate system was established (Figure 3-2 (b)) where x, y and θ are employed as the notation system. For this study, the cylindrical coordinates are denoted as (x, y, θ).

In this coordinate system, the notations for a two-dimensional kinematic model are unchanged in the x-y plane. With the introduction of the third coordinate θ that is the shovel's upper body swing angle, a three-dimensional representation of the shovel motion was effected.

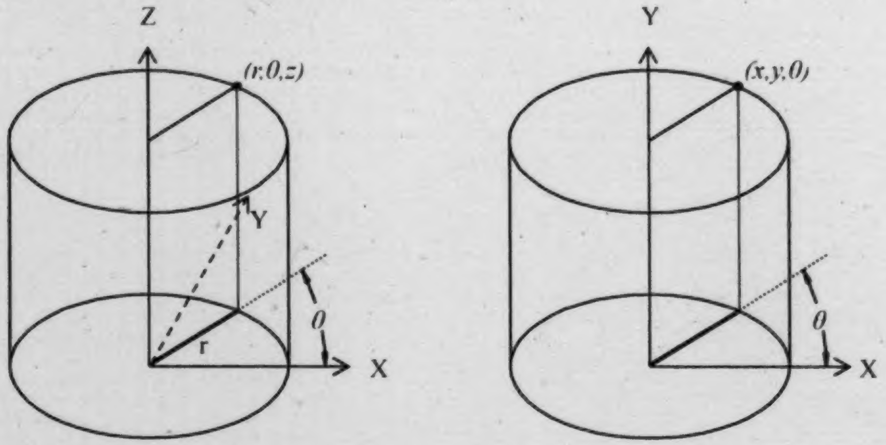

(a) Normal cylindrical coordinates (b) Self-defined cylindrical coordinates

Figure 3-2: Representations of cylindrical coordinates

In the numerical model and evaluation, the full mechanism of the hoist and crowd system was modeled without simplification. For example, the geometric relations at the saddle block and sheave point were more accurately modeled rather than simplified as points as had been done in earlier research.

3.2 Cable shovel kinematic model

3.2.1 Dipper motion geometry

The coordinate origin was defined as the shovel's revolving center projected onto the horizontal ground surface (see Figure 3-1). In the digging plane (X-Y plane), as shown in Figure 3-3, the rotation center of the saddle block, O, and the rotation center of the sheave point, P', are fixed but vary in the third dimension as the swing angle θ changes, Figure 3-4.

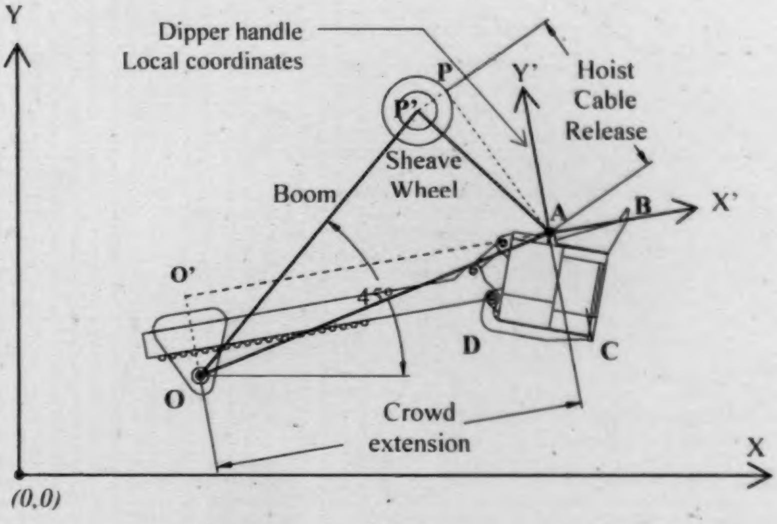

Figure 3-3: Shovel dipper geometry in x-y pane

The handle is connected to the boom via the saddle block so that the distance (OA) from the bail point A to the shipper shaft, point O, is not equal to the crowd extension O'A, OA can be calculated via triangle OAO', where OO' is fixed during a given unit digging operation.

The rope is tensioned or released via the sheave wheel so that the point of tangency (P) is not fixed, and the location P can be determined via triangle APP', where PP' is fixed during a given unit digging operation.

The position of the dipper is represented by point A (the bail point), as the geometry of the dipper relative to this point remains unchanged during operation. Two given variables, crowd extension length and hoist cable release length, allow the dipper's position in the digging plane to be determined at any time.

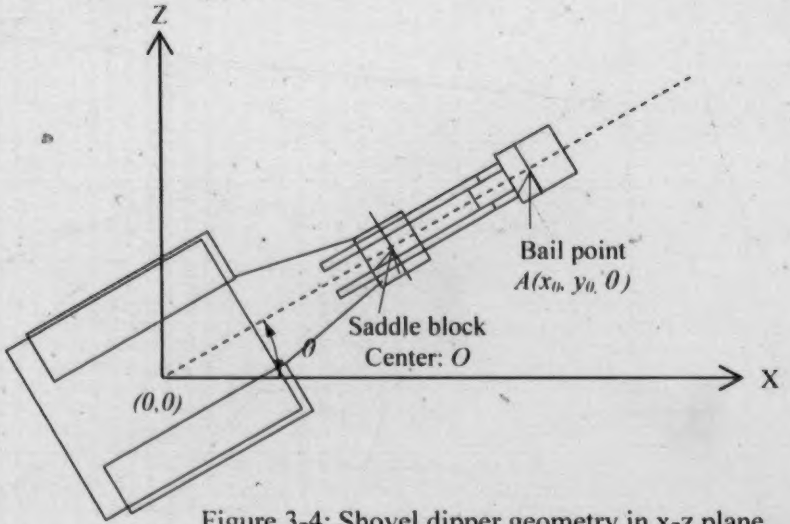

Figure 3-4: Shovel dipper geometry in x-z plane

As shown in Figure 3-5, given the coordinates of point A, the coordinates of any point on the dipper or handle in the digging plane can be determined from the local coordinates.

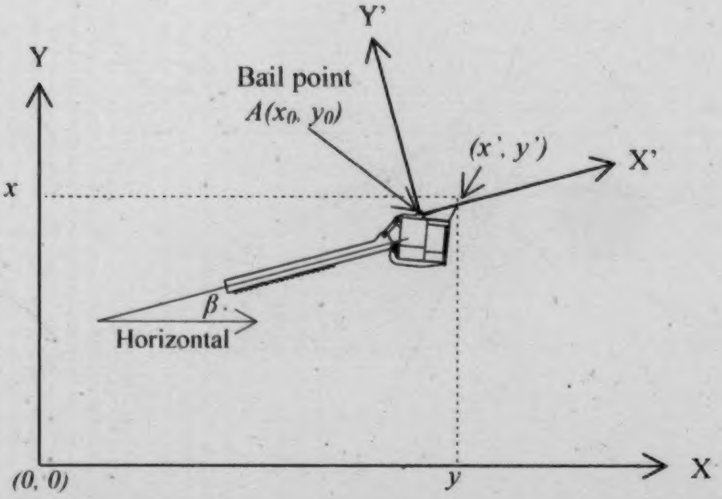

Figure 3-5: Local dipper coordinate transformation to the digging plane

3.2.2 Derivation of the dipper motion function

Figure 3-6 illustrates a geometric representation of the shovel's digging motion. The dipper position (the bail point) can be determined at any time by using the triangle side lengths printed in bold lines in the figure.

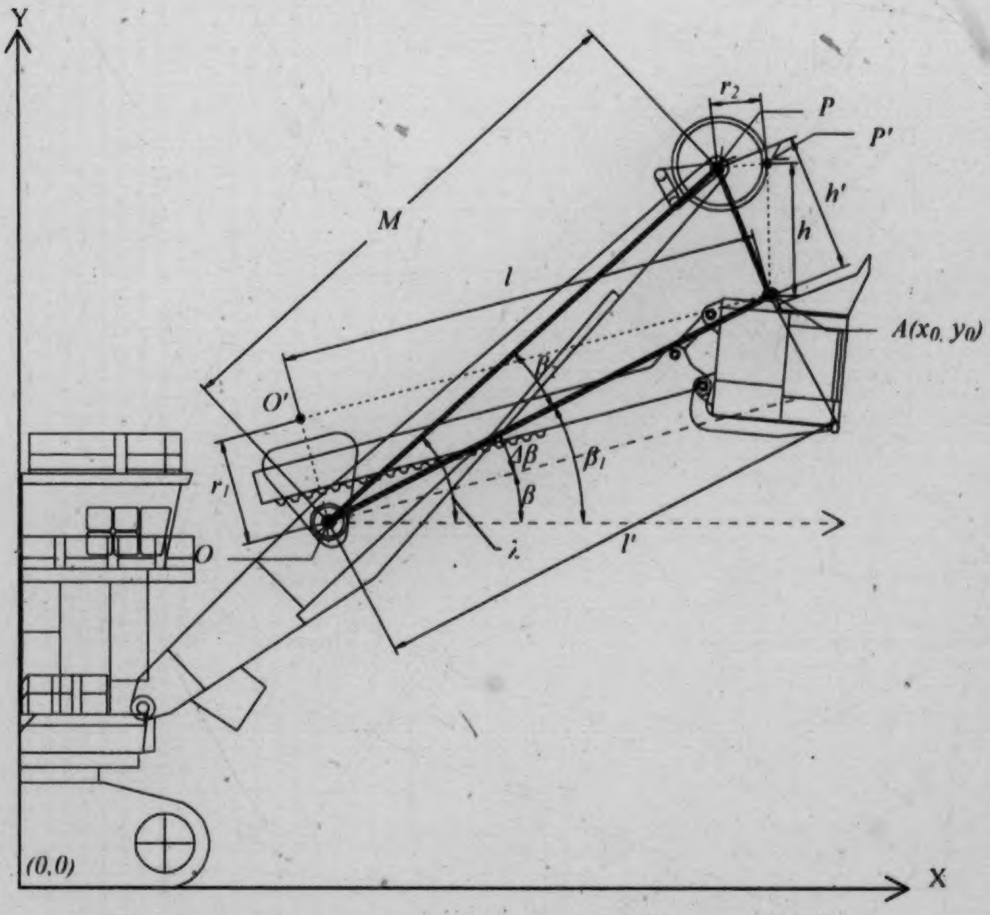

Figure 3-6: Geometric derivation of the dipper motion function

Given the input of crowd extension length, l, and cable release length, h, two motion edges of the triangle, h’ and l’, can be determined; thus, angle β_1 and the location of the dipper point A can be determined at any instant.

The boom angle is a constant and defined as in Equation 3.1:

$$\lambda = \tan^{-1}\left(\frac{y_{saddle} - y_{sheave}}{x_{saddle} - x_{sheave}}\right) \tag{3.1}$$

The effective cable release, h' and effective crowd extension, l' are

$$h' = \sqrt{h^2 + r_2^{\,2}} \tag{3.2}$$

and

$$l' = \sqrt{l^2 + r_1^{\,2}} \tag{3.3}$$

In triangle OAP,

$$\beta_2 = \cos^{-1}\left(\frac{l'^2 + M^2 - h'^2}{2Ml'}\right). \tag{3.4}$$

Thus,

$$\beta_1 = \lambda - \beta_2 \tag{3.5}$$

In triangle OAO',

$$\angle OAO' = \Delta\beta = \tan^{-1}\left(\frac{r_1}{l}\right) \tag{3.6}$$

and the handle angle is

$$\beta = \beta_1 - \Delta\beta \tag{3.7}$$

The dipper bail point position is given by the coordinates

$$\begin{aligned} x_0 &= x_{saddle} + l'\cos\beta_1 \\ y_0 &= y_{saddle} + l'\sin\beta_1 \end{aligned} \tag{3.8}$$

After substituting l' and β_1 within equations 3.2 through 3.6,

$$x_0 = x_{saddle} + \sqrt{l^2+r_1^2}\left(\cos\lambda\left(\frac{l^2+r_1^2+M^2-h^2-r_2^2}{2\times M\times\sqrt{l^2+r_1^2}}\right)+\sin\lambda\sqrt{1-\left(\frac{l^2+r_1^2+M^2-h^2-r_2^2}{2\times M\times\sqrt{l^2+r_1^2}}\right)^2}\right) \tag{3.9}$$

$$y_0 = y_{saddle} + \sqrt{l^2+r_1^2}\left(\sin\lambda\left(\frac{l^2+r_1^2+M^2-h^2-r_2^2}{2\times M\times\sqrt{l^2+r_1^2}}\right)-\cos\lambda\sqrt{1-\left(\frac{l^2+r_1^2+M^2-h^2-r_2^2}{2\times M\times\sqrt{l^2+r_1^2}}\right)^2}\right) \tag{3.10}$$

As shown in Figure 3-5, the coordinates of any point on the dipper or handle can be determined by using the following matrix equation:

$$\begin{bmatrix} x \\ y \end{bmatrix} = \begin{bmatrix} \cos\beta & \sin\beta \\ -\sin\beta & \cos\beta \end{bmatrix}\begin{bmatrix} x' \\ y' \end{bmatrix} + \begin{bmatrix} x_0 \\ y_0 \end{bmatrix} \tag{3.11}$$

where

h Cable release length measured from the tangent point on the

	sheave to the bail point
h'	Effective cable release length, from the sheave shaft point to the bail point
l	Handle extension length
l'	Effective handle extension length measured from the saddle shaft to the bail point
M	Distance from saddle shaft to the sheave shaft.
r_1	Distance from saddle shaft (point) to the handle direction (line) passing the bail point
r_2	Sheave radius
x, y	Coordinates of any point on the dipper or handle in the digging plane
x', y'	Coordinates of the bail point in the dipper local coordinates
x_0, y_0	Coordinates of the bail point in the digging plane
x_{saddle}, y_{saddle}	Coordinates of the saddle shaft point in the digging plane.
$x_{sheave}, y_{sheavee}$	Coordinates of the sheave wheel center in the digging plane.
β	Handle angle referenced to the horizontal
β_1	Effective handle angle, from the saddle shaft to the bail point referenced to the horizontal
β_2	Difference between boom angle and effective handle angle
$\Delta\beta$	Difference between handle angle and effective handle angle
λ	Boom angle

These motion equations were modeled with a program written in MatLab (see Appendix A.2)

3.3 Digging spatial characteristics

3.3.1 Shovel duty cycles

Three common shovel-truck digging/loading methods are normally used in open pit operations (see Figure 3-7): Single truck back-up, double truck back-up, single truck drive-by. After a number of digging and loading cycles, the shovel will have to advance closer to the face (see Figure 3-7 (d)). No matter which loading method is employed in a mining operation, the single volume for each shovel advance is of a similar shape as shown in Figure 3-8. This volume is formed by the surface of the previous cut and the shovel's incremental reach range after the advance.

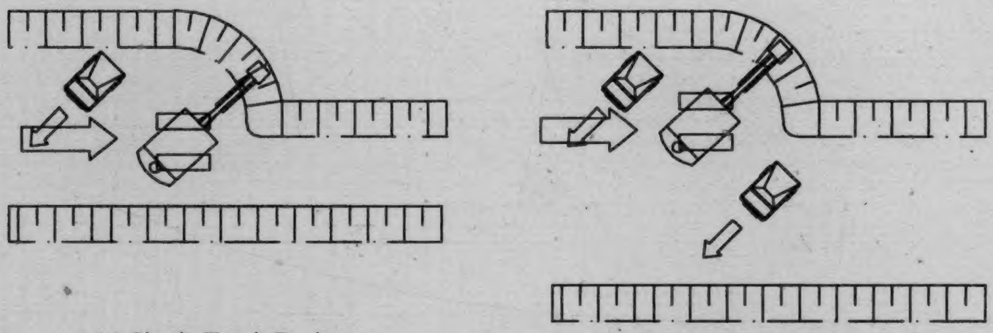

(a) Single Truck Backup

(b) Double Truck Backup

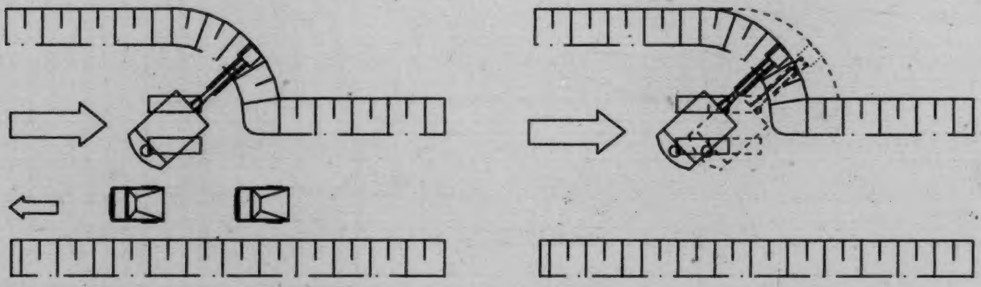

(c) Single Truck Drive-by

(d) Shovel Repositioning

Figure 3-7: Shovel-truck digging/loading methods

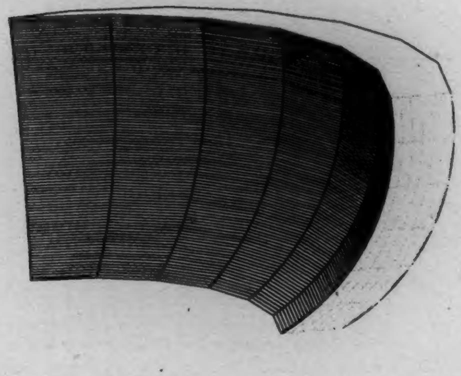

Figure 3-8: 3D digging volume for a shovel move

3.3.2 Digging motion range

Most manufacturers suggest a range of digging motions for a given shovel model in the specification sheet, which is effectively a range diagram of the dipper's cutting tip. However, the mathematical method used to find this range is not published. It is unknown whether manufacturers measure these ranges from their shovels or calculate/simulate via a computer. In this research, a MatLab program was applied to establish range parameters (see Appendix A.3).

Here in evaluating the shovel's digging motion range the dipper profile was represented with a polygon as was the shovel boom, body and crawlers. Using the following boundary criteria, a motion range was discerned for the P&H 4100 model shovel targeted:

- The handle can be extended or retracted, being constrained solely by the rack teeth extent on the handle;
- The cable can be pulled until the bail collides with the point sheave;
- The cable can exert only a pulling force;
- The boom is protected from the dipper by the bumper blocks on the

boom when the dipper is in the tuck position;

- The dipper and the handle are not allowed to collide with the boom, body, crawler and sheave.

Figure 3-9 illustrates the motion range for a P&H 4100 model provided by P&H (2001C). The MatLab program developed to establish the P&H 4100 shovel's motion range, output an envelope for the dipper tip, Figure 3-10. A comparison shows that the simulation derived here matches the manufacturer's solution. Moreover, the simulation result here provides a full motion envelope instead of only part of the motion range reported by the manufacturer.

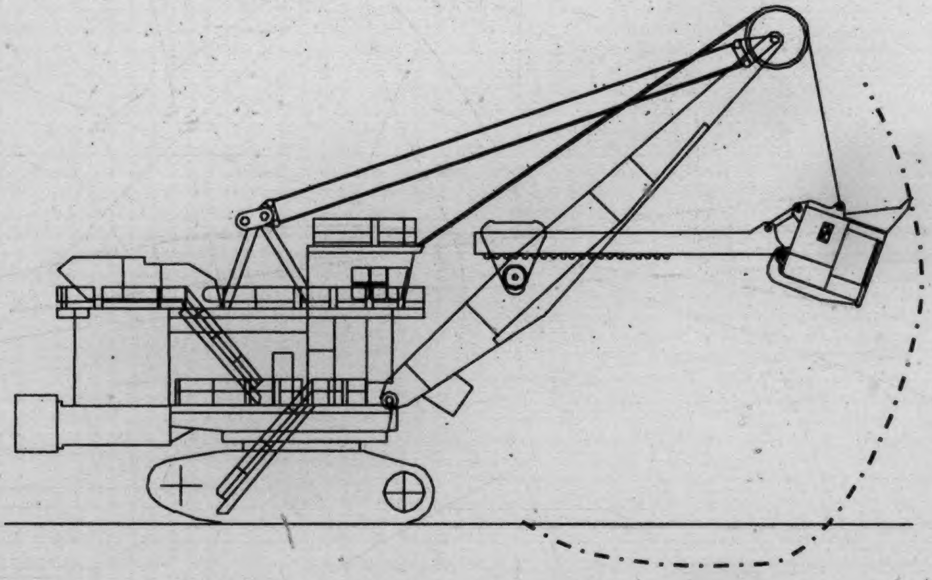

Figure 3-9: P&H 4100 digging envelope (P&H, 2001C)

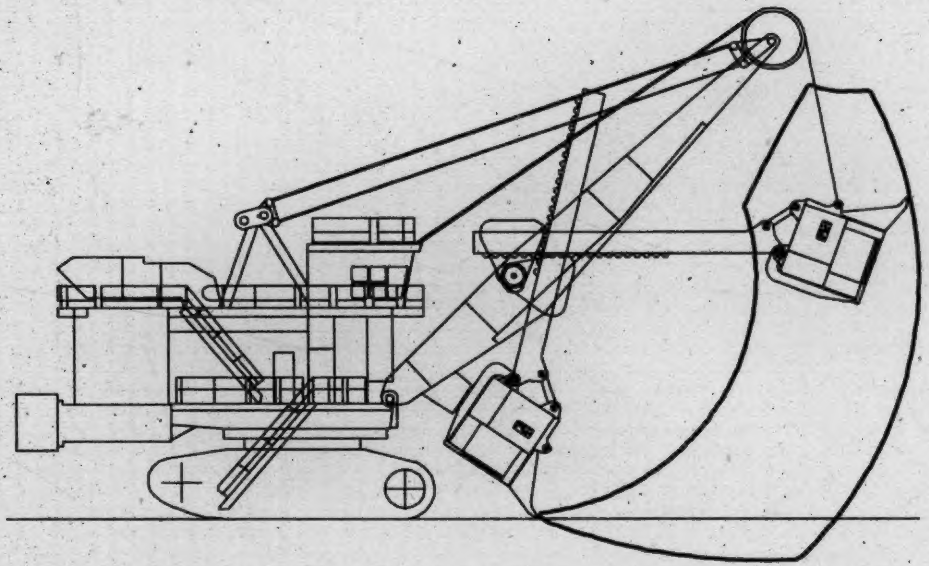

Figure 3-10: P&H 4100 shovel digging motion ranges created by collision detection

It should be borne in mind that the full range of motion shown in Figure 3-10 reveals that multiple sweeps and hence dipper loadings from the same shovel position are obviously possible, confirmed by common operational mining practices in the field.

3.3.3 Minimum tuck profile

The digging motion range diagram established above depicts an envelope that constrains the dipper's motion in the vertical plane. To evaluate the dipper's motion in a horizontal plane close to the ground, a minimum tuck profile was evaluated via collision-detection techniques in MatLab (see Appendix A.4).

The problem of collision detection between moving objects is fundamental to simulations in the physical world. This problem has been studied in a number of different research communities, including robotics, computer graphics, computer-aided design, and computational geometry. The basic idea of collision detection is to disassemble the geometrical surface into smaller shapes (mesh) and detect whether the side of one triangle passes through the area of another triangle.

As shown in Figure 3-11 (a), in a two dimensional case, the detecting program written for this research checks whether any vertex of a triangle on the surface of the dipper is located within the area of another triangle on the surface of another object while the dipper moves.

Draw a free line cross vertex Q of the second triangle, if there are two intersections between the free line and sides of the first triangle, for example Q' and Q'', and $|Q'Q''| = |Q'Q| + |QQ''|$, the vertex Q is located within the area of triangle ABC. Thus, two triangles (objects) collide.

In a three dimensional case (b), determine the intersection of a side of the second triangle, for example, intersection X between plane ABC and line OP. Using above two dimensional method to check whether X is located within triangle ABC. If so, two triangles (objects) collide (see Figure 3-11 (b)).

MatLab has built in a function to check whether a point is located within a polygon and make this detection easier.

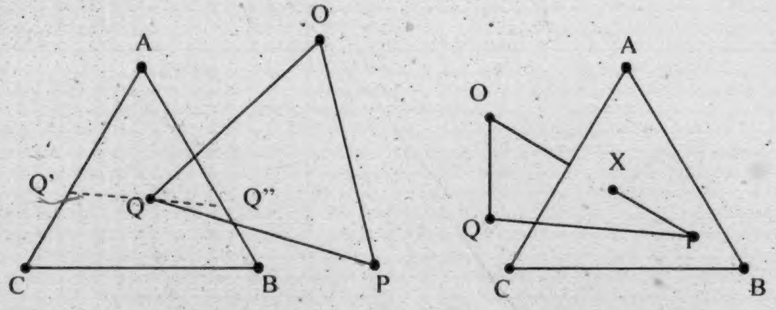

(a) Two dimensional collision detection

(b) Three dimensional collision detection

Figure 3-11: Basic collision detection techniques

The minimum tuck position while the upper body is parallel to the tracks allows the dipper to be drawn between the tracks, whereas when the shovel body is oriented in the diagonal direction the dipper is able to interfere with the track position (see Figure 3-12).

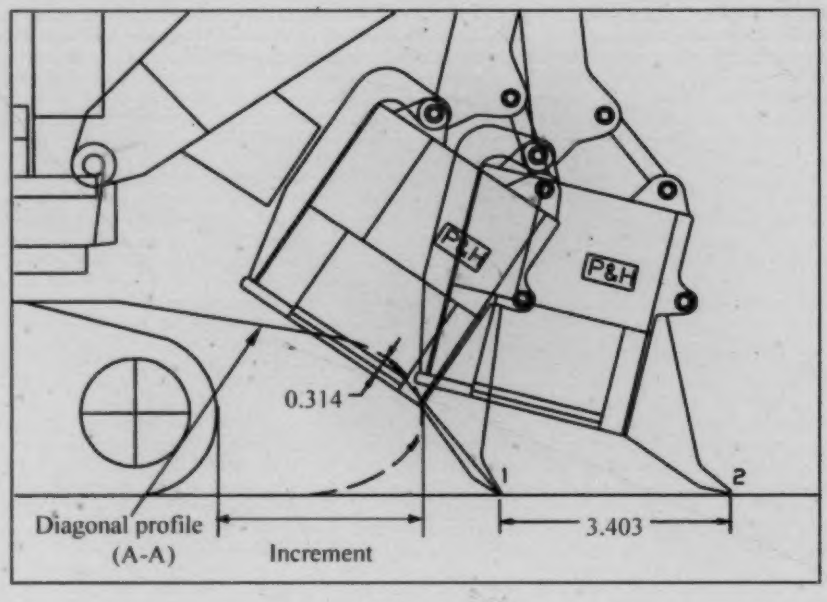

Figure 3-12: Dipper-track interference and the minimum tuck position

In Figure 3-12, position 1 represents the upper body when parallel to the track centerline; position 2 represents the upper body when parallel to the diagonal (A-A) (see Figure 3-13 for corresponding track profiles).

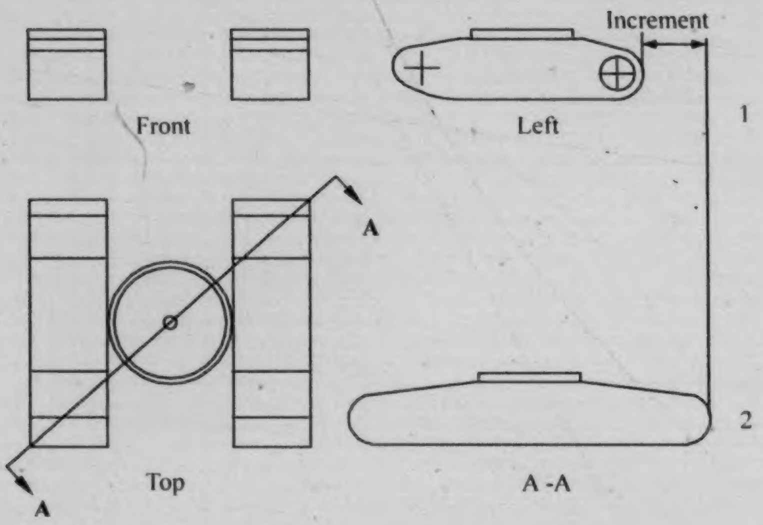

Figure 3-13: Shovel crawler 3 views and diagonal profile (A-A)

A collision trace profile marked on the bearing ground surface is shown in Figure 3-14 illustrating for any point on the profile the closest point that the dipper teeth can touch while the shovel's upper body is slewed at a given angle, *θ*.

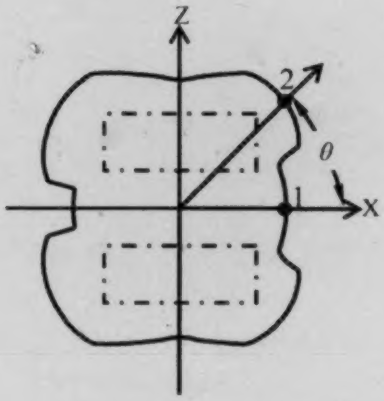

Figure 3-14: P&H 4100 shovel's minimum tuck position projected on the ground: Positions 1 and 2 are the same as that in Figure 3-13

3.3.4 Shovel advancing steps

As shown in Figure 3-7 (d), the shovel regularly advances to the face after a number of digging cycles. The distance of the advance depends on the shovel geometry, shovel motion range, minimum tuck profile and mining face dimensions (15 metres high, with a 60° face angle are common for oil sand). Combining the dipper's motion range, minimum tuck profile and face geometry, the shovel's advancing step was identified.

The generated digging envelope, minimum tuck position profile, shovel configuration, and the working bank dimensions were transferred to AutoCAD to simulate the shovel advancing.

As shown in Figure 3-15, the shovel's advancing step can be graphically derived by using geometrical constraints. Here, it was found that the incremental distance for the P&H 4100 shovel advancing step is 3.77 metres, again keeping in mind that multiple sweeps of the face and slewing positions for one shovel location are possible between advances.

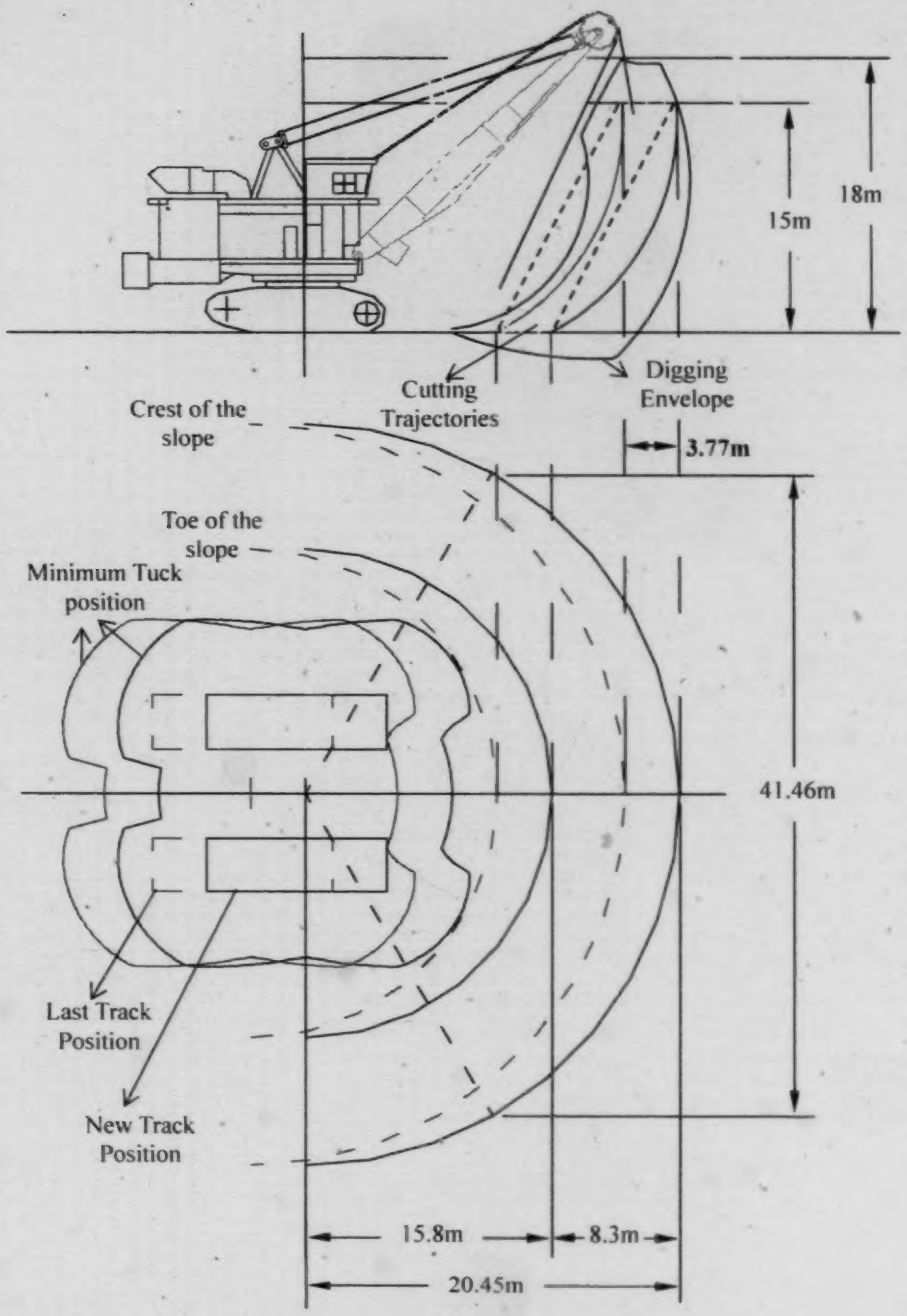

Figure 3-15: Shovel's range diagram and repositioning increment

3.4 Determine trajectories

As determined above, for a P&H 4100 shovel operating in a 15m, 60° mining face, the maximum advancing step is 3.77 m. As a result, an overall sum of incremental cutting depths between shovel advances is 3.77m (see Figure 3-16).

Figure 3-16 shows the trajectories for cuts 1 through 4 required to advance the mining face by 3.77 m.

The following criteria determine the shape and depth of each trajectory, where the material in the dipper is loose compared to the material in the face being in-situ.

- Strip volume = dipper capacity/swell factor
- Each cutting starts at the toe and ends at the crest.

For each cut, it is assumed that both crowding and hoisting motions are maintained at a constant speed during the digging action. In the real world. the driving motors first overcome the inertia of the components from zero speed through to a constant operational speed. The time the driving motors spend on accelerating is very short and considered here as negligible for the analytical model devised here for the digging simulation.

Thus, for each cut, the hoist cable release length, h, and the handle crowd length l was described as follows:

$$h(t) = h_0 + v_h t \tag{3.12}$$

$$l(t) = l_0 + v_l t \tag{3.13}$$

Where

h_0 hoist cable release length at the digging start point.

$h(t)$	handle crowd length at time t.
l_0	handle crowd length at the digging start point.
$l(t)$	hoist cable release length at time t
v_l	crowding speed.
v_h	hoisting speed.
t	time starting from the tuck moment.

Discretizing t, h and l as n of t_i, h_i and l_i

$$t_0 = 0$$

$$h_i = h_0 + v_h \cdot t_i = h_0 + \frac{(h_n - h_0)}{t_n} t_i$$

$$h_i = h_0 + (h_n - h_0) \cdot i / n, (i = 0, n) \tag{3.14}$$

$$l_i = l_0 + v_l \cdot t_i = l_0 + \frac{(l_n - l_0)}{t_n} t_i$$

$$l_i = l_0 + (l_n - l_0) \cdot i / n, (i = 0, n) \tag{3.15}$$

Where

h_i	i^{th} h discretion.
h_n	hoist cable release length at the digging end point.
i	Sequence index

l_i	i^{th} l discretion.
l_n	handle crowd length at the digging end point.

Substituting h_i and l_i, in Equations 3.9 and 3.10, a bail point trajectory is obtained.

$$x_{i}^{0} = F_x(h_i, l_i) \tag{3.16}$$

$$y_{i}^{0} = F_y(h_i, l_i) \tag{3.17}$$

Where

x_i^0, y_i^0	coordinates of the trajectory followed by the bail point.
F_x, F_y	dipper motion functions (Equations 3.9 and 3.10).

The dipper tip trajectory (x_i, y_i) was obtained from Equation 3.11. The sum of the dipper tip points resulted in the establishment of the digging trajectory.

Given constant crowding and hoisting speeds, a start point (x_0, y_0) and an end point (x_n, y_n), the trajectory generating MatLab program (see Appendix A.5) outputs a digging trajectory including the data of x_i, y_i, l_i, h_i, β_i that will later be used for further dipper-ground interaction study.

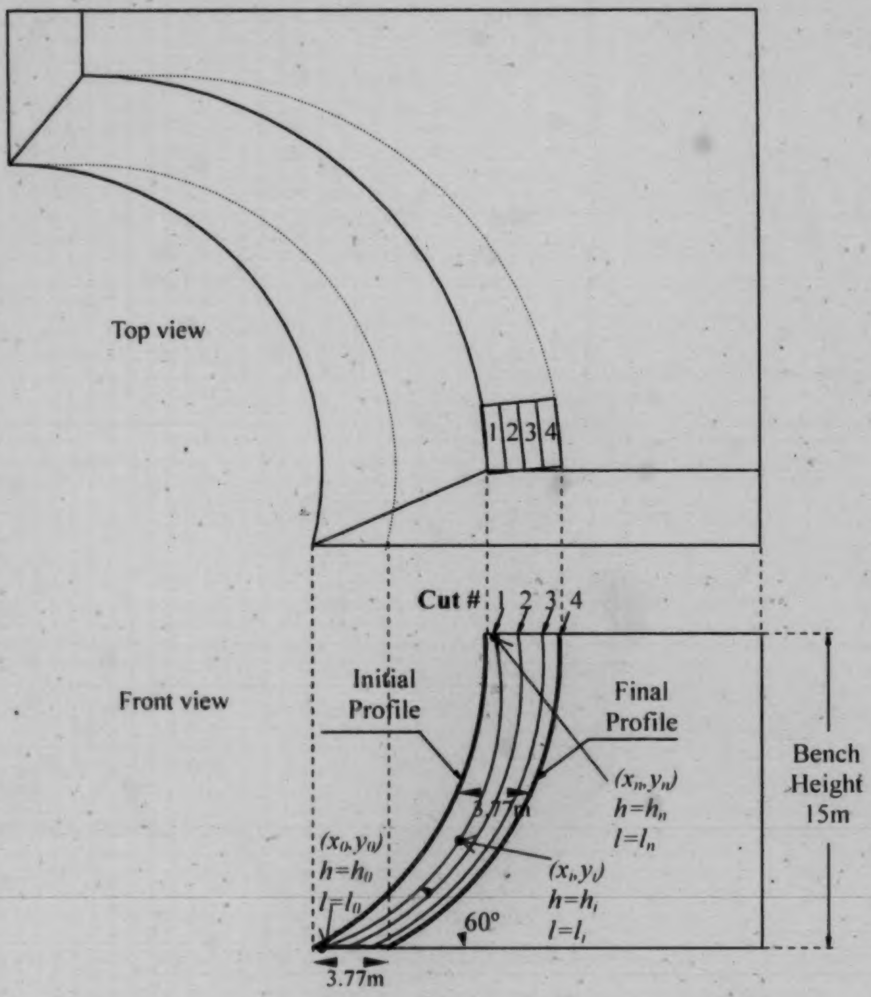

Figure 3-16: Cutting trajectories in two-dimensional sequences

3.5 Summary

The motion functions based on the P&H 4100 model shovel were first derived. Given a handle crowd length and hoist cable release length, the position of the bail point was determined by using the functions, allowing the position of any point on the dipper or handle including tooth tip to be determined using a transform matrix.

Based on shovel digging motion functions, the shovel geometrical constraints and the mining face dimensions were investigated. In addition, the collision detection method was applied to find the shovel motion range in both vertical and horizontal plan. Utilizing both ranges, a maximum shovel advancing step was determined based on the geometrical constraints and an idealized operation pattern.

After obtaining the geometrical relationship and the digging motions, the digging trajectories were generated for the P&H 4100 model shovel working in a typical oil sand mining face.

The geometrical relationship between the shovel dipper and the ground is an important factor in any dipper-ground interaction analysis. The generated digging trajectories provide all the required geometrical information for the digging simulation which consisted of a series of instantaneous dipper-ground interaction snapshots.

Previous simplified shovel motion functions output inaccurate dipper motion tracks. No literature revealed the relationship between the shovel motion functions, face geometry and shovel geometry. In short, all the work in this chapter pertained to developing the modeling tools necessary for generating the accurate digging trajectories for current dipper geometry and the later study of dipper-ground interactions for a dipper of alternative geometry.

Chapter 4

Shovel-Ground Interaction

4.1 Dipper-ground interactions

4.1.1 Dipper-ground geometry

Every two adjacent trajectories in the same shovel slew orientation that were represented in Figure 3-16 form a single digging strip (see Figure 4-1).

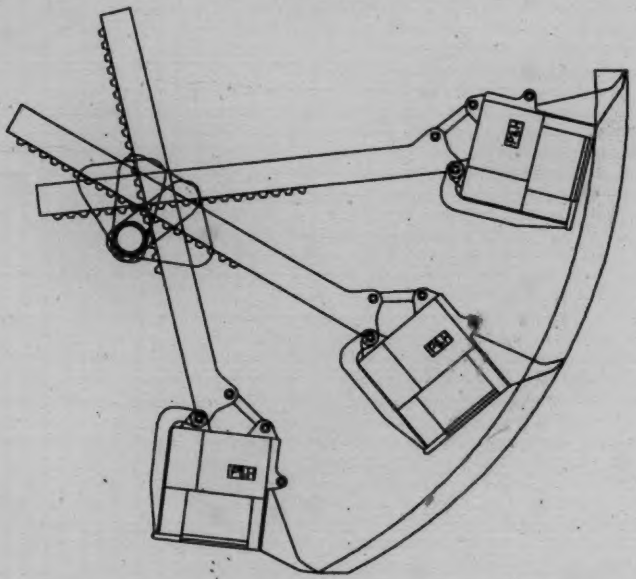

Figure 4-1: Geometrical relationship of the dipper-ground interaction

4.1.2 Ground properties

Since this research focused on the dipper performance for oil sand ground condition, the oil sand material properties described in Table 4-1 were applied to a dipper-ground interaction model devised to account for the generated digging forces.

Table 4-1: Oil sand properties (Morgenstern and Scott, 1997) (Collins, 2005)

Properties	Parameters in the model
Cohesion (C)	0 kPa
Friction Angle (φ)	50°
Adhesion (C_a) *	0 kPa
Tool-oil sand friction angle (δ)**	37°
In-situ density (γ)	2000kg/m^3

* The adhesion between the oil sand and the tool (C_a) is normally smaller than the cohesion (C) so that in this case it was taken as 0.

** The tool-oil sand friction angle is of the steel with the disturbed oil sand. It was thought reasonable to use Dusseault and Morgenstern's (1977) determination of peak friction angle for compacted oil sand to represent hard digging conditions in this unconsolidated material.

4.1.3 Dipper-ground interaction

Singh (1995) applied an approximate equilibrium wedge model to the mechanics of a flat blade penetrating soil (see Figure 4-2).

The blade resists the soil with a force equal to the sum of the perpendicular force that the blade provides the (soil-tool) frictional force and the (soil-tool) adhesion. Similarly the soil resists shearing by a force equal to the (soil-soil) frictional force and the cohesion along the entire failure surface.

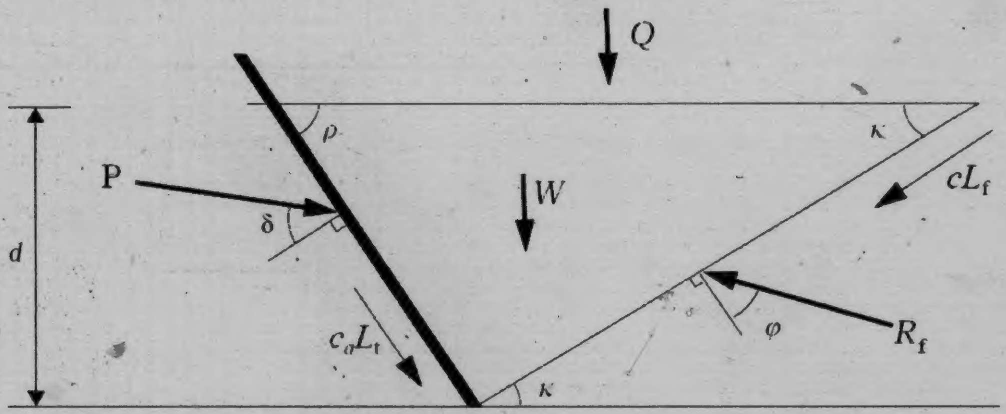

Figure 4-2: Static equilibrium approx. of a failure surface, after Singh (1995).

The force equilibrium equations for this model (neglecting adhesion) are:

$$\sum f_x = P\sin(\rho+\delta) + C_aL_t\cos\rho - R_f\sin(\kappa+\varphi) - CL_f\cos\kappa = 0 \qquad (4.1)$$

$$\sum f_y = P\cos(\rho+\delta) - C_aL_t\sin\rho + R_f\cos(\kappa+\varphi) - CL_f\sin\kappa + W + Q = 0 \qquad (4.2)$$

Solving for P,

$$P = \frac{W + Q + Cd\left[1 + \cot\kappa(\kappa + \varphi)\right] + Cad\left[1 - \cot\rho(\kappa + \varphi)\right]}{\cos(\rho + \delta) + \sin(\rho + \delta)\cot(\kappa + \varphi)} \qquad (4.3)$$

where

d	cutting depth.
L_f	failure surface length.
L_t	soil-tool contact length.
P	the digging effort..
Q	surcharge pressure.
R_f	failure surface resistance.
W	weight of the soil wedge.
κ	failure surface angle.
ρ	the instantaneous attack angle.

The shape of the resulting failure surface is such that the force required to produce failure is minimal. While the failure surface angle κ varies from 0° to 90°, the digging effort P also varies, where the most likely value of κ is found for a minimum value of P.

Figure 4-3 illustrates an example of a straight blade cutting though the soil. In this example, the soil would fail at a 38°plane where 4.1 kN would be required to cut the soil.

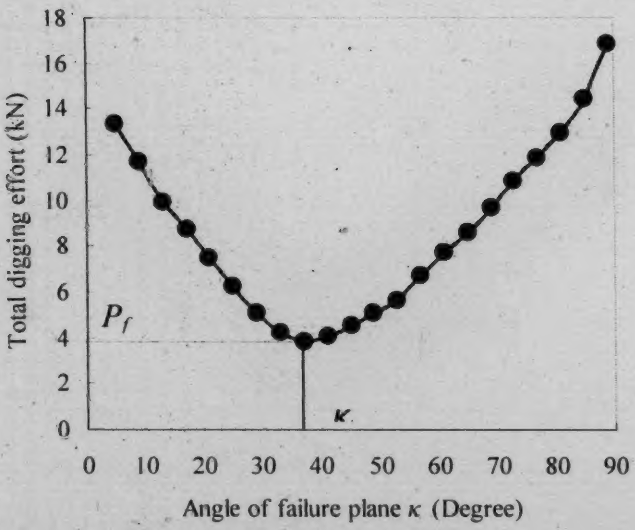

Figure 4-3: An example of determing the angle of failure plane.

Coulomb's shear strength relation simplifies the ground surface to be horizontal and utilizes a surcharge pressure q to simulate an irregular or sloping surface. In any case the surcharge is simplified as being evenly distributed. This approach does not work well for this study as the dipper motion and the mining face profile vary from one digging cycle to another.

As shown in Figure 4-4, the major difference to previous models was that the mining face is never horizontal. A modified model was developed in this research to evaluate the instantaneous ground digging effort, Figure 4-5. This model did not neglect the adhesion between the tool and soil.

Figure 4-4 illustrates the base geometrical relationship between the shovel handle, front wall (blade) and the face orientation. Figure 4-5 illustrates the modified trial wedge model developed here with the required parameters defined in Equations 4.4 through 4.10.

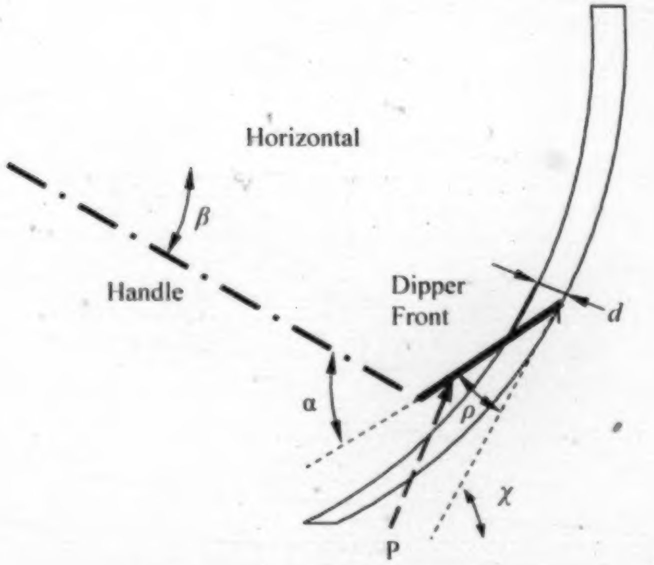

Figure 4-4: Simplified model: a flat blade moving through soil.

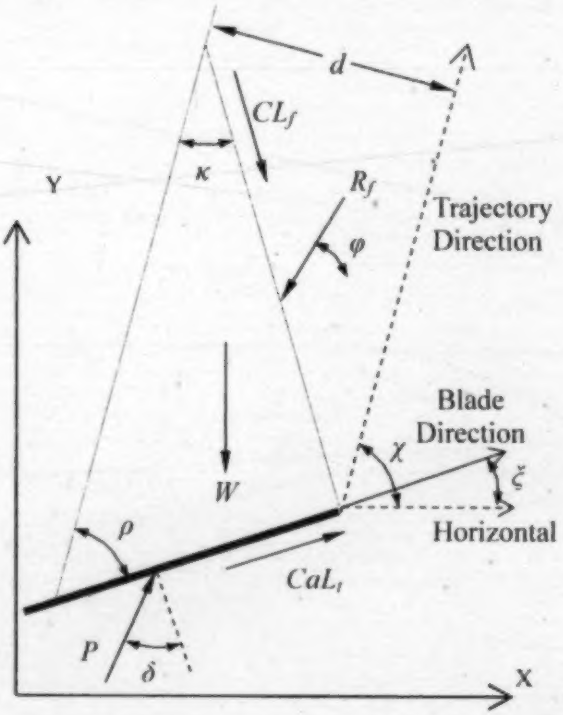

Figure 4-5: Static equilibrium as an approximation for the failure surface.

Weight of the wedge:

$$W = \frac{1}{2}\gamma g d^2(\cot\rho + \cot\kappa) \tag{4.4}$$

Blade length penetrating the ground:

$$L_t = \frac{d}{\sin\rho} \tag{4.5}$$

Ground failure surface length:

$$L_f = \frac{d}{\sin\kappa} \tag{4.6}$$

Force equilibrium:

$$\sum f_x = 0 \tag{4.7}$$

$$P\sin(\rho + \delta - \chi) + C_a L_t \cos(\rho - \kappa) - R\sin(\kappa + \varphi + \chi) - CL_f \cos(\kappa + \chi) = 0$$

$$\sum f_y = 0 \tag{4.8}$$

$$P\cos(\rho + \delta - \chi) - C_a L_t \sin(\rho - \kappa) + R\cos(\kappa + \varphi + \chi) - CL_f \sin(\kappa + \chi) - W = 0$$

Solving for P,

$$P = \frac{W + (1) + (2)}{\cos(\rho + \delta - \chi) + \sin(\rho + \delta - \chi)\cot(\kappa + \varphi + \chi)} \tag{4.9}$$

Where

$$(1) \quad = \frac{Cd\left[\sin(\kappa + \chi) + \cos(\kappa + \chi)\cot(\kappa + \varphi + \chi)\right]}{\sin\kappa}$$

$$(2) \quad = \frac{C_a d\left[\sin(\rho-\chi)-\cos(\rho-\chi)\cot(\kappa+\varphi+\chi)\right]}{\sin\rho}$$

Given the blade width is w, the digging effort is:

$$P = \frac{\left[W + (1) + (2)\right]w}{\cos(\rho+\delta-\chi)+\sin(\rho+\delta-\chi)\cot(\kappa+\varphi+\chi)} \tag{4.10}$$

Where

f_x	x component of each force
f_y	y component of each force
α	dipper rake angle
ξ	blade direction, an angle from the horizontal
χ	slope of ground surface

Varying the value of κ between 0 and 90 degrees, the most likely value of the angle of failure plane, κ, is found at the minimum value of P (see Figure 4-3).

4.1.4 Digging forces

With the prediction of the total digging effort P, we now have an estimate of the total digging resistance, R.

$$R = -P \tag{4.11}$$

Figure 4-6 shows the forces acting on the dipper and handle. Note that as the material flows in the dipper, the center of gravity of the dipper-load must change.

In contrast to the overall weight of the dipper and handle, the weight of the flowing material is small. Therefore, the displacement of the centre of gravity was considered negligible in this analysis. The centre of gravity for the dipper shape was also applied to the loaded material in the dipper.

As shown in Figure 4-6, the digging resistance, R, is depicted at the top of the teeth. This does not mean the model only considered the force to be applied at the teeth. From the digging model described by Equation 4.11, the digging effort P accounted for the force to break the ground and the friction force generated between the tool and the ground. To be more realistic, the point of action for the sum of the resisting forces will change within the top portion of the front wall of the dipper. However, as the variation of the point of action is small, for this research it was assumed that the sum of the resistance forces, R, acts at the tip of the teeth.

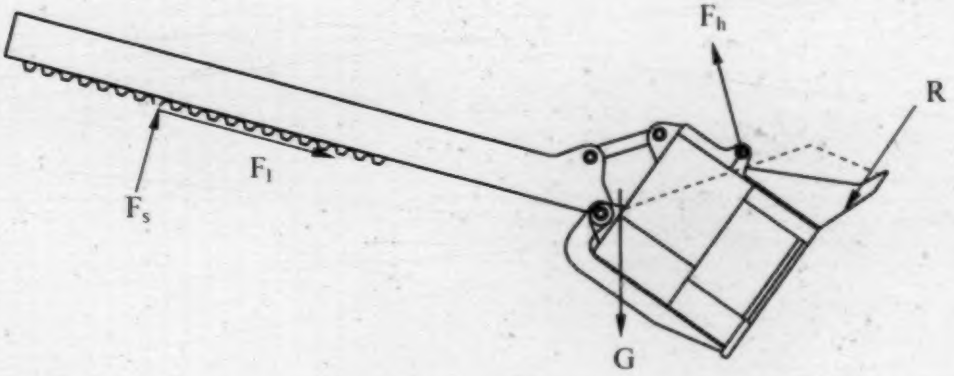

Figure 4-6: Handle-dipper digging forces

Figure 4-7 shows the resulting equilibrium model from which both crowd and hoist forces were determined.

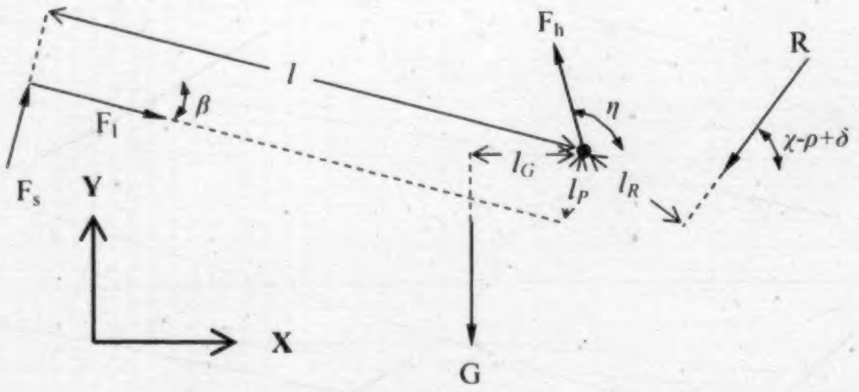

Figure 4-7: A simplified equilibrium model for the dipper system

Where

F_h	hoist force.
F_l	crowd force.
F_s	supporting force normal to the handle.
G	weight of the handle, dipper and material.
l	handle crowd extension length
l_G	distance from the force G to the bail point.
l_P	distance from the crowd force F_l to the bail point.
l_R	distance from the total resistance R to bail point.
R	total resistance.

From the force and moment equilibrium for this model, we obtain:

$$\sum f_x = 0$$

$$F_h \cos\eta - R\cos(\chi - \rho + \delta) + F_l \cos\beta + F_s \sin\beta = 0 \tag{4.12}$$

$$\sum f_y = 0$$

$$F_h \sin\eta - R\sin(\chi - \rho + \delta) + F_l \sin\beta + F_s \cos\beta - G = 0 \tag{4.13}$$

$$\sum Moment = 0$$

$$F_l l_P + G l_G - R l_R - F_s l = 0 \tag{4.14}$$

Solving for *F*

Solving for F_l, F_s and F_h:

$$F_s = \frac{[R\sin(\chi - \rho + \delta - \eta)]l_P + (G l_G - R l_R)\sin(\beta - \eta)}{l\sin(\beta - \eta) + l_P\cos(\beta + \eta)} \tag{4.15}$$

$$F_l = \frac{[R\sin(\chi - \rho + \delta - \eta) + G\cos\eta]l}{l\sin(\beta - \eta) + l_P\cos(\beta + \eta)} + \frac{(G l_G - R l_R)\sin(\beta - \eta)l}{l \cdot l_P \sin(\beta - \eta) + l_P^{2}\cos(\beta + \eta)} - \frac{(G l_G - R l_R)}{l_P} \tag{4.16}$$

$$F_h = \frac{R\cos(\chi - \rho + \delta) - F_l\cos\beta - F_s\sin\beta}{\cos\eta} \tag{4.17}$$

The result of F_s and F_l out of Equations 4.15 and 4.16 can be applied into Equation 4.17.

4.2 Digging simulation

Simulation techniques have been widely used in system and product designs. These approaches have many advantages over physical modeling. Although a physical prototype model is an essential step for a final product, simulation can still be very helpful in understanding the performance of an object in a feasibility study. In this research, the physical modeling approach has its limitations as well: due to the sheer size and expense of an ultra class dipper, a prototype can only be a fraction of the size of the final product, so that the performance, as may be measured by a physical test, can not be expected to be identical to the performance of an actual full scale dipper. Therefore, particularly where cost is a concern, simulation modeling provides a good design approach for preliminary phases in endeavours such as dipper design.

To this end, during simulation the system considered:

(1) The geometrical position of the dipper defined within the x-y coordinates and the corresponding attack angle, rake angle, handle angle.

(2) The geometry of the face (ground), before and after the digging.

(3) The geotechnical properties of the face material being excavated. The objective being to evaluate the resistance forces on the ground engaging tools. From one simulation iteration to another, the dipper trajectory output allowing definition of a new face profile was used as the input for estimating the face resistance in the next iterative cycle.

(4) The required hoisting and crowding forces necessary with respect to an iterated face resistance prediction.

The outputs from the simulation were set as the critical parameters in improving shovel dipper design.

- Digging resistance: the sum of all the forces from the ground reaction that need to be balanced by the hoist and crowd forces.

- Required crowding and hoisting forces.

In the simulation, the digging process was discretized in a series of n steps. For each step, the trajectory data such as handle extension length, handle angle, tooth tip x and y co-ordinates were retrieved. From these, the digging performance indicators such as digging resistance, crowd and hoist forces were determined via the simulation models (see Figure 4-8).

For example, a trajectory information generated in Chapter 3 was stored in a format of n (number of time steps) rows and five columns (l_i, h_i, β_i, x_i and y_i). Each row represented the geometrical information at a given digging position for a given time step. The additional required input for the dipper-ground interaction model was the dipper-ground geometrical information and the ground material properties, such as cohesion, adhesion and friction angle.

The dipper-ground interaction model output the digging effort comprising the digging resistance, the weight of the dipper, material and the handle. With the digging effort estimated by the dipper-ground interaction model, the crowd and hoist forces were determined.

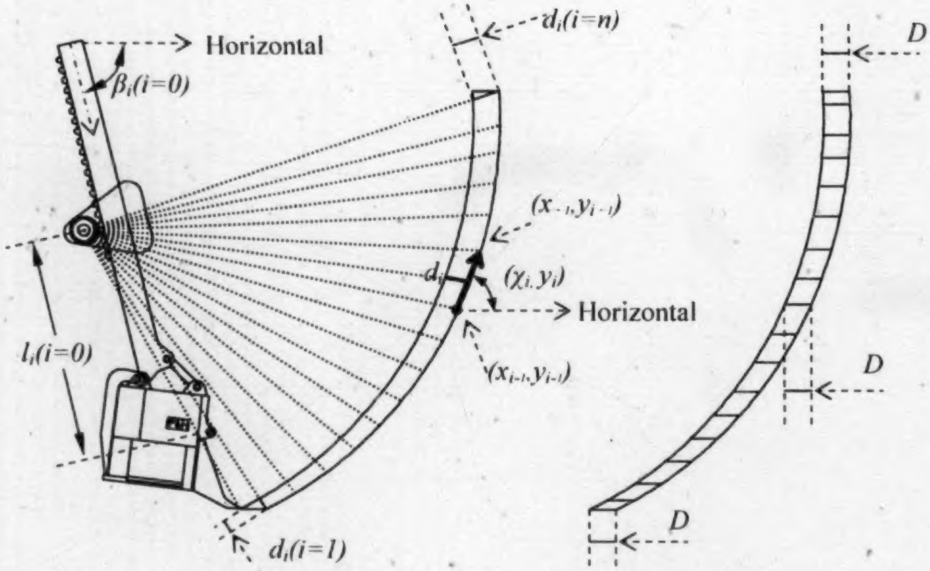

Cutting depth

Horizontal depth

Figure 4-8: Step-wise digging simulation

The digging simulation procedure is as follows (see Figure 4-9):

(1) i=0

(2) i=i+1

(3) $\xi_i = \beta_i + \alpha : \chi_i = \tan^{-1}\left(\dfrac{y_{i+1} - y_{i-1}}{x_{i+1} - x_{i-1}}\right) : \rho_i = \chi_i - (\beta_i + \alpha_i)$ (see Figure 4-4 and Figure 4-5)

(4) $d_i = \sqrt{\left(x_i - x_i^p\right)^2 + \left(y_i - y_i^p\right)^2}$ (see Figure 4-8)

(5) Varying κ to seek κ_f (see Figure 4-3)

a. *j=0*

```
    b.  $j=j+1$
    c.  $\kappa_j = j/m*90^o$
    d.  Calculate: $P_j$ using equation 4.11
    e.  if $j=m$ then goto (5) else goto a
(6) $P=minimum(P_j(\kappa_{j,}\ j=1\ to\ m))$
(7) $G=dipper\ weight + handle\ weight + Ore\ weight$ where: $Ore\ weight=i/n*Payload$
(8) Using Equations 4.16 and 4.17 to calculate $F_l$, $F_h$.
(9) if i>=n then go to (10) else go to (2)
(10) Output the result and end.
```

Where i is the indexing of the simulation time steps; n is the number of the simulation steps; j is the indexing of the trial calculations for a minimum P; m is the number of the trial calculations for κ at which the ground will fail ; and the previous trajectory is (x_i^p, y_i^p).

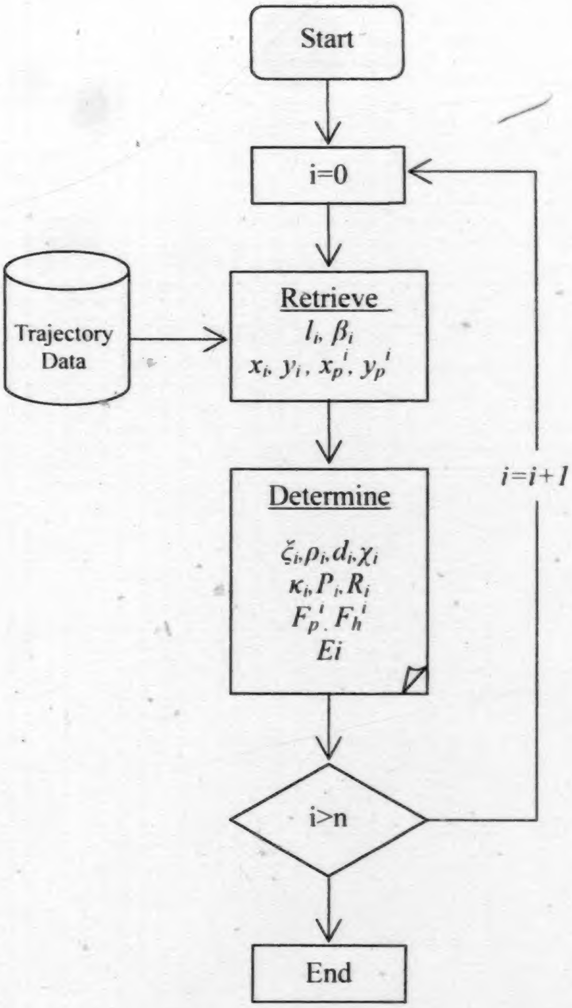

Figure 4-9: Data flow for the digging simulation

Here the above model was established with a few subroutines and spreadsheet formulas in Excel and VBA that would iteratively allow successive digging trajectories and reaction forces to be determined, establishing the front wall shape for the dipper to be defined for less face reaction and machine interference (see Appendix B).

4.3 Shovel simulation software

The above discussion outlined a procedure for shovel digging simulation. However, without a proper interface, the mere program code for these formulations and simulation can not provide explicit inputs and outputs for researchers to use. The MatLab programs developed in the previous chapter, although comprising mathematical functions that are very powerful which can export static vector graphics, were in a form difficult to create a user-friendly and interactive interface. For this purpose, some of the kinematic simulation code was transplanted into Microsoft Excel VBA to enhance the interactive nature of the shovel digging simulation program.

Figure 4-10 illustrates the interface of the software. The kinematic functions, shovel digging simulation and ground properties and reaction were developed as modules using VBA. The base shovel geometrical information and graphical representation were stored in the Excel sheet directly.

Input cells defined the shovel geometric configuration and the ground materials properties. Button and slider controls were used to control the shovel manually or start the simulation. Dropdown lists were used to select the predefine actions.

The software was designed to be straight forward and easy to use. One of the most important outputs, the digging force plot, was directly output to the screen updated simultaneously when starting a new duty cycle simulation.

Some simulation outputs, such as the trajectory, dipper velocity and dipper-ground geometry were stored in the Excel sheet and made accessible once a given simulation was completed.

Any given dipper configuration was imported into the software manually. Since the shovel digging simulation software was based on a two dimensional model, the two dimensional dipper profile and a width of the dipper were required by the software to run an iteration.

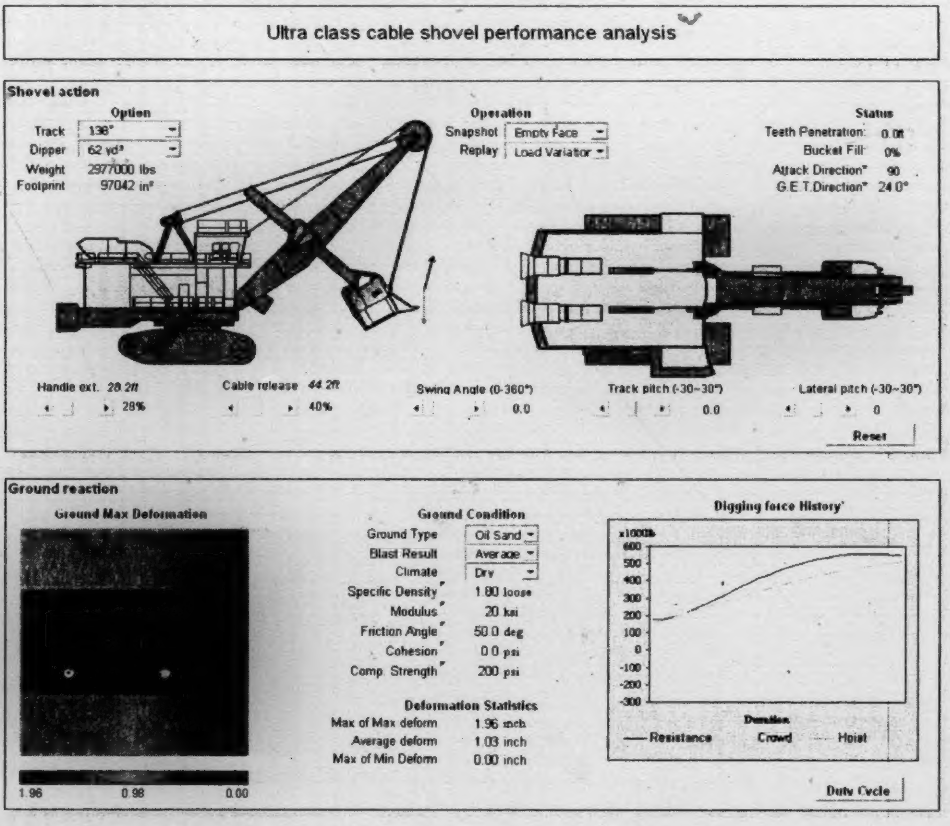

Track 138°
Dipper 62 yd³
Weight 2977000 lbs
Footprint 97042 in²
Snapshot Empty Face
Replay Load Variation
Teeth Penetration: 0.0ft
Bucket Fill: 0%
Attack Direction° 90
G.E.T.Direction° 24.0°
Handle ext. 28.2ft 28%
Cable release 44.2ft 40%
Swing Angle (0-360°) 0.0
Track pitch (-30~30°) 0.0
Lateral pitch (-30~30°) 0
Ground Type Oil Sand
Blast Result Average
Climate Dry
Specific Density 1.80 loose
Modulus 20 ksi
Friction Angle 50.0 deg
Cohesion 0.0 psi
Comp. Strength 200 psi
Max of Max deform 1.96 inch
Average deform 1.03 inch
Max of Min Deform 0.00 inch

Figure 4-10: Shovel simulation software

Once a dipper design was imported into the software, the digging forces were used to evaluate the dipper performance, compared to the benchmark created by running the original dipper configuration. Machine inference was checked via simulating the dipper in the position of concern (e.g. tucked and over a track corner).

4.4 Simulation outputs

As an example of the simulation output, the curves of the blade (rake) direction ξ_i, attack angle ρ_i and ground slope χ_i against time *i*Δt (i=0 to n)* were plotted (see Figure 4-11).

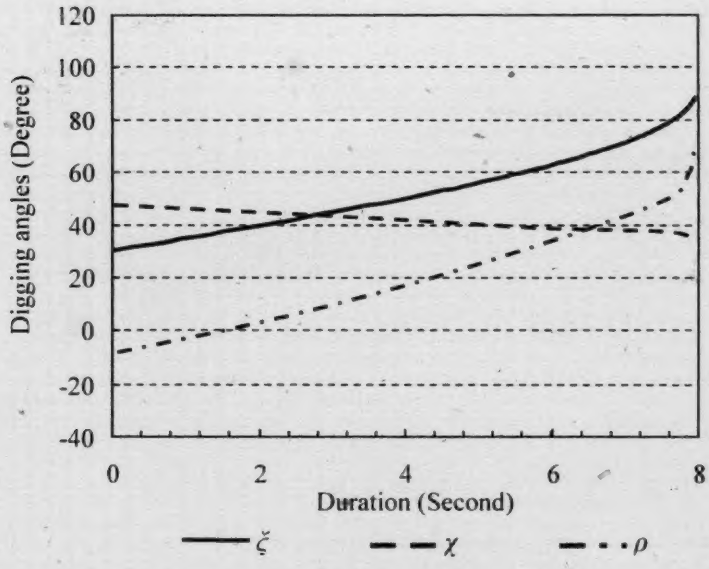

Figure 4-11: Digging angle variation

Given a constant hoist and crowd speed and ignoring the dynamic response of the system, the dipper tip velocity was estimated via equation 4.18. For a typical oil sand, the P&H 4100 shovel normally operates at a crowd speed of about 0.5m/s speed. To obtain a trajectory prescribed in Chapter 3, a hoist speed of about 1.7m/s is required (see Figure 4-12).

$$v_i = \frac{\sqrt{(y_i - y_{i-1})^2 + (y_x - x_{i-1})^2}}{\Delta t} \tag{4.18}$$

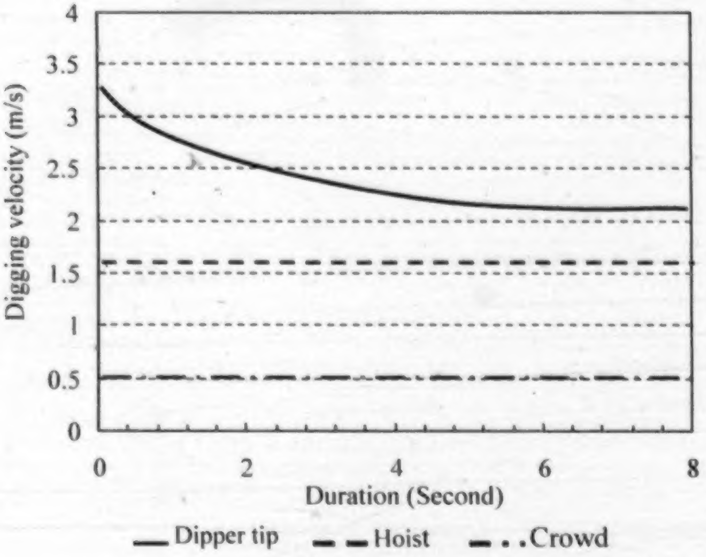

Figure 4-12: Crowd, hoist and dipper tip velocity

Figure 4-13 shows the digging force plots from the simulation prescribed in Figure 4-9. For the hoisting force, tension is positive. For the crowding force, compression is positive.

Using the trial wedge cutting model, the total digging effort is obtained given the handle orientation and the digging depth. Thus, the crow and hoist forces are obtained using the free body diagram of the handle and dipper.

The resistance illustrated in

Figure 4-13 is not merely the digging resistance from the face, but the combination of the digging resistance and the weight of the handle, dipper and material that the hoist and crowd forces must overcome.

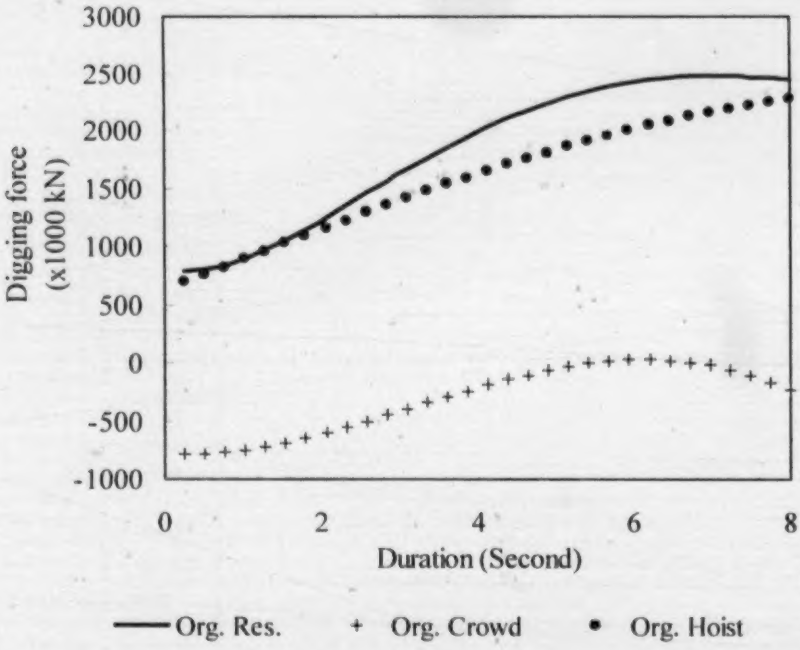

Figure 4-13: Simulation output: digging forces generated for cutting oil sand

The output of the simulations can be used to evaluate the new dipper performance, compared to the benchmark created by running the original dipper configuration. In Chapter 5, the result from the simulation will be used to evaluate the performance of a traditional dipper and a curved front dipper design.

Chapter 5

Cable Shovel Dipper Design

5.1 Design criteria and focus

Since the objective of this research is to suggest an alternative front wall shape to potentially improve the dipper design for an existing ultra class cable shovel, any suggested changes should have a minimum if no influence on the shovel operation. Based on this consideration, the following criteria were set before any further research work proceeded:

- Consistent capacity: the dipper capacity should remain roughly identical to the original configuration so that any new design will match the original truck fleet for which the given mining operation originally purchased the shovel.
- Consistent weight: the new dipper weight should be roughly identical to the original design so that the shovel balance is maintained without adjusting the counterweight.
- Back attachment: the new dipper should fit the original handle attachment with minor or no modification.
- Cutting tip: the tooth tip should be close to the relative original position to minimize its influence.

In chapter 1, the main elements of a dipper design were identified as

- Three-dimensional geometry and ratios of height to width to depth,
- Dipper and teeth angles,
- Front and side wall profiles, (linear or curved), mouth to door, or side to side,
- Dipper attachment arrangement referring to the handle's connection points,
- And bail position.

To create a new design to potentially perform better in oil sand, two key design features were investigated, while all other original constituents kept unchanged or adopted previous research outcomes.

- Front wall tooth-to-heel profile, favoring a curved one.

  Since the longitudinal (tooth-to-heel) profile of the dipper was identified in this research as the most likely factor to affect digging forces, the study concentrated on the effect of a single curved front wall profile. Side to side curvatures and lip/teeth arrangements were not investigated, but kept the same as the original configuration, so as to concentrate on the effect of varying the front wall shape to closely match the trajectory output from the previous digging simulations.

- Back wall skewness.

  Given the effect of curving the front wall generated a tighter egress (smaller open area) from the dipper compared to the mouth, it became evident that to maintain a minimum of compounding shape factors that would confuse a comparison of original to proposed front geometries there was a need to revise the orientation of the dipper back to maintain unrestricted material egress during dumping. This was a concern over operational considerations for the physical field test than the outcome of the simulation analysis and as such regardless of the back configuration, the front wall curvature as indicated by simulation was kept constant once established. Another operational purpose of the back wall skew was to reduce the void space when loading.

5.2 Variation of the front wall

5.2.1 Trajectory and front profile correlation

As both dippers and handles are symmetrical for either the P&H double-stick or the Bucyrus single-stick original configurations and due to the dipper's geometric characteristics, it is rational to develop and analyze a concept profile in two dimensions first.

As discussed previously, a curved profile has the potential to improve the conflict between dipper digging performance and heel wear. However, what kind of curve should be proposed is the question. The analysis in chapter 3 shows trajectory shape but did not give a mathematical formula. Those trajectories will now be generalized as a mathematical form and a corresponding dipper front wall shape proposed in a similar form.

In chapter 3, the procedure to generate trajectories suggested four digging trajectories were required to complete a volumetric sweep before advancing the shovel. The actual shovel operations, however, have many possible trajectories enclosed within the reach envelope of the shovel. To remain representative, a trajectory at the mid location of all possible trajectories was selected as a reference to establish the shape of the dipper front profile (see Figure 5-1).

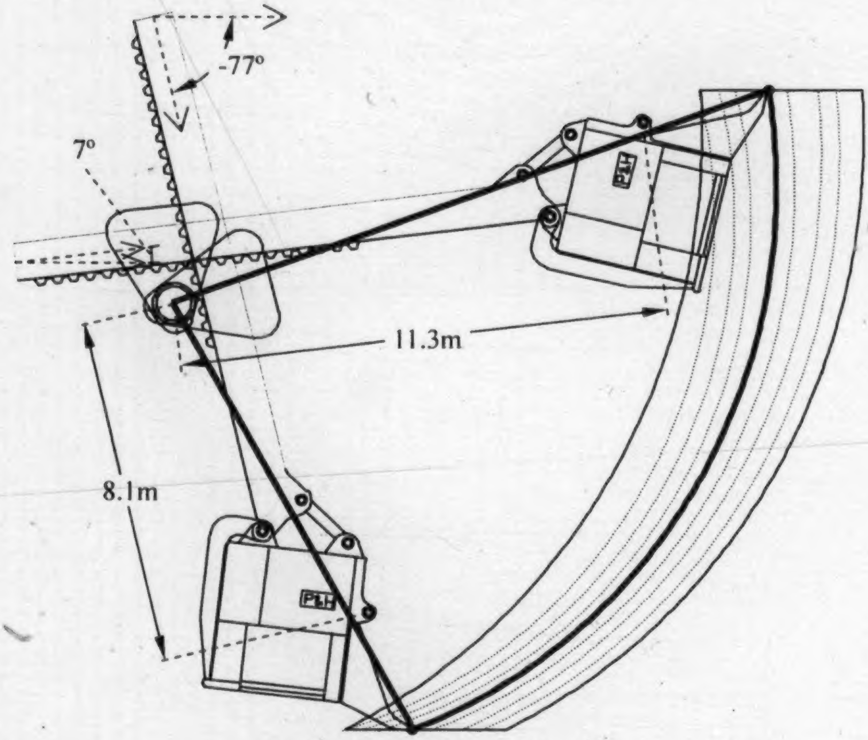

Figure 5-1: A selected digging trajectory as a reference to design dipper front

The assumptions with which these trajectories were generated were:

- Constant crowding speed
- Constant hoisting speed

To obtain the trajectory shown in Figure 5-1, the two speeds were kept as a constant ratio.

Basically, for these trajectories, the digging radius (from the tooth tip to saddle shaft) increased as the dipper was hoisted. Although this is not any standard form of the mathematic spiral, it may be generally referred to as "spiral".

It may be described as a logarithmic spiral which has constant growth of radius due to the constant crowd speed.

Mathematically, these curves can be expressed by:

$$r_{\text{profile}} = a \cdot e^{b \cdot \theta_{\text{profile}}} \tag{5.1}$$

or

$$\begin{aligned} x_{\text{profile}} &= a \cdot \cos(\theta_{\text{profile}}) \cdot e^{b \cdot \theta_{\text{profile}}} \\ y_{\text{profile}} &= a \cdot \sin(\theta_{\text{profile}}) \cdot e^{b \cdot \theta_{\text{profile}}} \end{aligned} \tag{5.2}$$

where

$x_{profile}$	Cartesian x coordinate of the spiral
$y_{profile}$	Cartesian y coordinate of the spiral
$r_{profile}$	Radius of the polar coordinates.
θ_{profile}	Angle of the polar coordinates

To generate a spiral dipper front, the shaft of the saddle block was set up at the rotation center of the spiral. Then the handle extension length was set a $9.7=((11.3+8.1)/2)$ metres which is at the middle point of the handle extension/retracting range for the specific trajectory shown in Figure 5-1, for the P&H 4100 model shovel.

To further narrow the variables affecting the front profile, some previous dipper design criteria were adopted:

- Lip angle: Keep tooth tip position unchanged, lip height unchanged and utilize 10 ° lip down pitch angle according to ACARP (2002). Hence, the end point of the curved segment was found.
- Effective rake angle for cutting: ACARP (2002) found the

productivity , the digging volume (Bank cubic meter) per unit time (hour), increase significantly while the tooth angle passes over 60°. When the tooth angle is approaching 70 °, which is identical to 80° of rake angle given a 10° lip angle (see Figure 5-2), the productivity increases in-significant. Bucyrus has adopted the outcome of the research in their recent dipper products, using a 70° tooth angle. Although this is only available performance data with respect to the rake angles, in this research, it assumes to be valid.

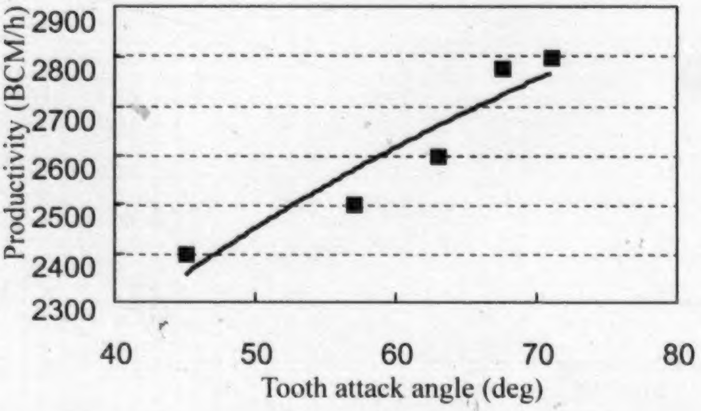

Figure 5-2: A relationship between the tooth angle and productivity (ACARP, 2002)

- Effective rake angle for heel wear: ACARP (2002) found that there is no significant heel wear until the tooth angle reaches 60° (see Figure 5-3). The 60° of tooth angle is identical to 70° of rake angle given a 10° lip angle. Figure 5-3 indicates a significant increase of the dipper wear that means a significant decrease in the productivity due to the longer machine down-time. It is therefore a compromise between the productivity and wear like most engineering decision. This is also applicable to select a tooth angle.

Considering that the oil sand is more abrasive than clay and other soft weathered rock, the 60° (or less) of the effective tooth angle would potentially be suitable for a dipper specifically for oil sand .

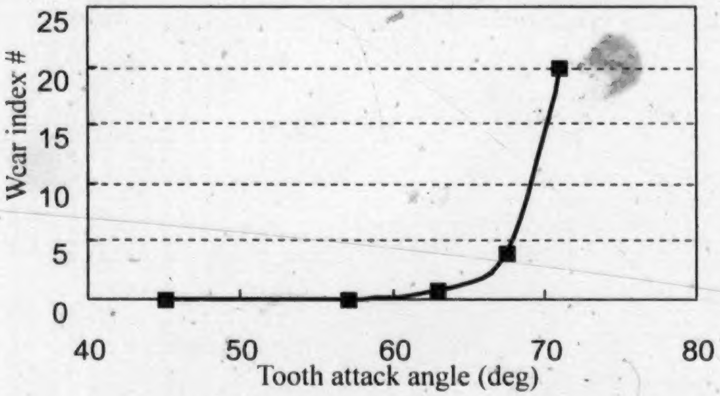

Figure 5-3: A relationship between the tooth angle and the wear (ACARP, 2002)

The logarithmic spiral front does not include the lip system, the design of the lip and teeth are outside the scope of this investigation and discussion (see Figure 5-4).

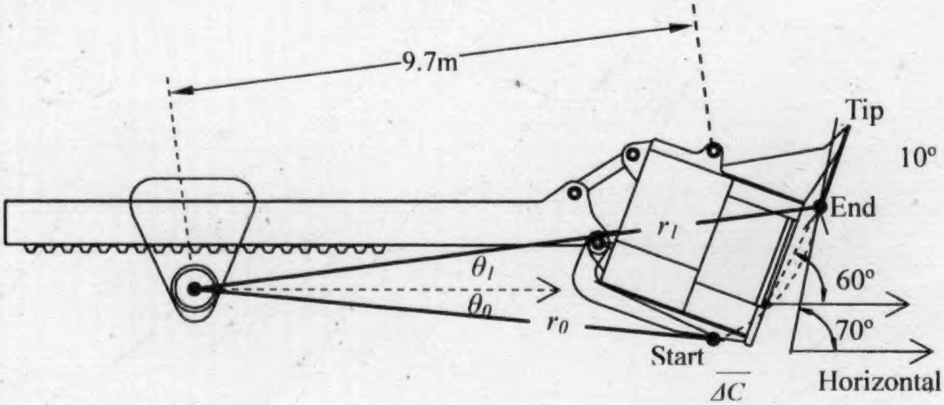

Figure 5-4: Two-dimensional dipper profile design

So far, the start point becomes the only variable element for the proposed spiral front wall. Once a start point is located by r_0 and θ_0 and the end point is located by r_1 and θ_1 a logarithmic spiral dipper front wall may then be obtained from:

$$r_0 = a \cdot e^{b \cdot \theta_0}$$

$$r_1 = a \cdot e^{b \cdot \theta_1} .$$

Solving for *a* and *b*

$$a = \frac{r_0}{e^{\theta_0 \frac{\ln r_1 - \ln r_0}{\theta_1 - \theta_0}}} \tag{5.3}$$

$$b = \frac{\ln r_1 - \ln r_0}{\theta_1 - \theta_0} \tag{5.4}$$

With the variation of a and b in the above equations, a set of curves were compared and analyzed, as shown in Figure 5-5.

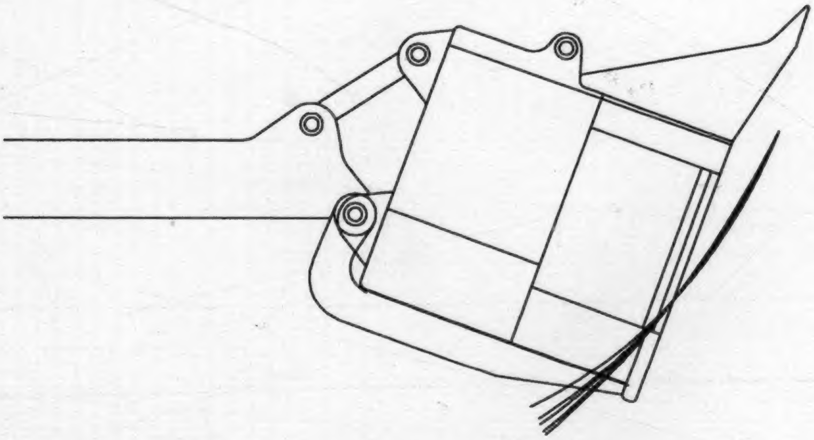

Figure 5-5: Possible variations of a front wall profile

5.2.2 Sensitivity analysis

In order to find a relationship between the dipper performance and the spiral parameter proposed previously, three new profiles and the original dipper front were evaluated (see Figure 5-6).

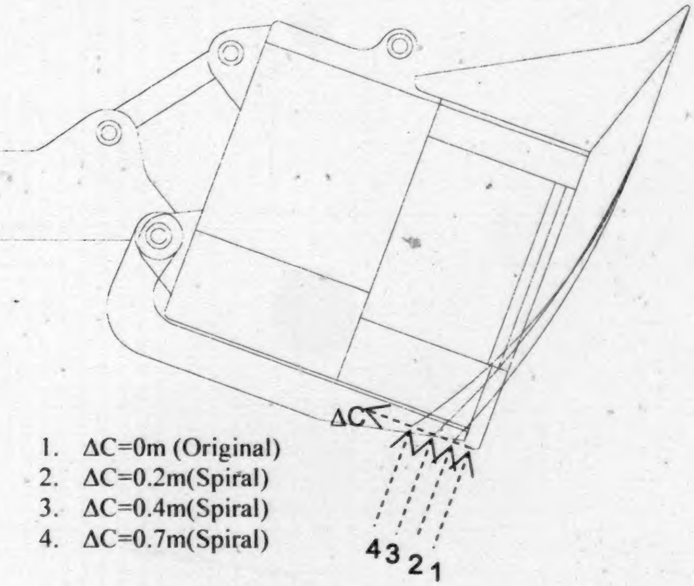

Figure 5-6: Variation of the start point and the profile

To make the problem clearer, the different curvature start points were represented by a variable, ΔC, the distance from a new start point to the original heel along a line parallel to the door floor (see Figure 5-6: V). To evaluate each configuration with following performance criteria were used:

(1) Attack angle

Normally the smaller the attack angle, the lower the cutting resistance. Therefore attack angle could be a measurement to estimate the dipper digging resistance. Figure 5-7 illustrates the simulation output for the variation of the attack angle during the digging with respect to each design configuration.

From Figure 5-7, it was found that even the first configuration step change ($\Delta C=0.2$m) resulted in a significant improvement of attack angle. Beyond $\Delta C>0.4$m, the attack angle kept decreasing but was not significant. The curves for $\Delta C=0.4$m and $\Delta C=0.7$m are very close during the whole digging process. In this scope, $\Delta C>0.4$m, the improvement on the attack angle can hardly pay back the over-modification (compared to the original) that may lead to many other issues. Therefore, $\Delta C=0.4$m can be a compromise between the improvement of the attack angles and the impact to the original shovel structure.

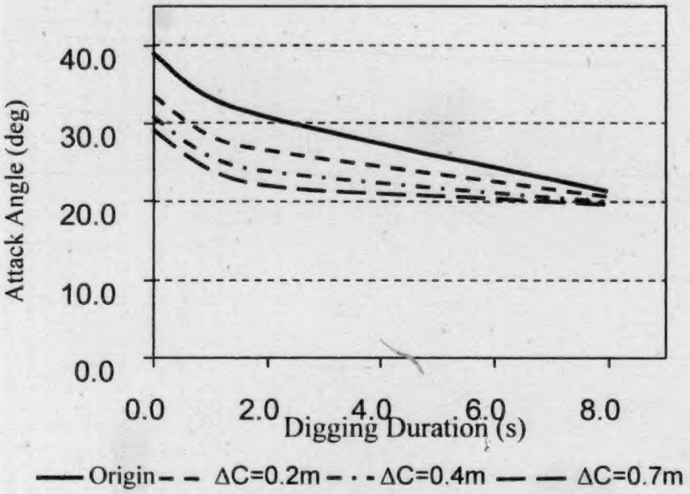

Figure 5-7: Comparison of attack angles referenced to the original configuration

(2) Heel-ground clearance

The heel-ground clearance is well known in the mining industry to be very closely related to heel wear, damage and significanyt shovel downtime.

A mining face can never be expected to be perfect, homogenous and isotropic and there exists unpredictable falls of ground and deformation at the face. As a result the heel will undoubtedly make contact with the ground. Despite this, relative heel-ground distance (clearance) to the original configuration represents a good measure to evaluate heel life as greater clearance intuitively means less chance of ground contact. Figure 5-8 shows the simulation output reflecting that the proposed configurations all provide greater heel – ground clearance compared to the original configuration with increasing ΔC.

All curves in Figure 5-8 provide positive clearance during the digging process. Theoretically, there won't be any collision between the heel and the ground. However, in a real case, the post-digging ground profile will not fully follow the digging trajectory due to in-homogeneousness and anisotropy of the ground. There may also fall some material from face during the digging process. Therefore, the heel will touch the ground material more or less depending on the heel-ground clearance. Less clearance will lead to higher possibility of the interaction between heel and the ground material. However, it is impossible for this study to predict the relationship quantitively.

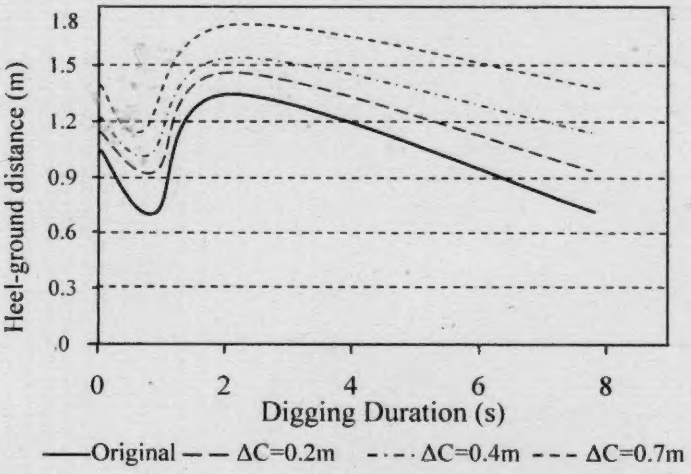

Figure 5-8: Theoretical heel-ground clearance plots for different profile

(3) Dipper-crawler interference

As shown in Figure 5-9, the spiral front will reduce the dipper-crawler interference.

Less dipper-crawler interference means the dipper can move closer to the shovel tracks. Thus, the shovel can move closer to the face and can clean the face toe. The closer the shovel advance to the face, the longer advance distance the shovel obtain. The longer distance the shovel advances, the less frequent the shovel is required to advance. The less frequent the shovel advance (traveling), the higher utilization (productivity) the shovel obtain.

With variation of heel retraction, expressed as ΔC, an inferred relationship from the simulation results showed an improvement on dipper-crawler interference is obtained (see Figure 5-10).

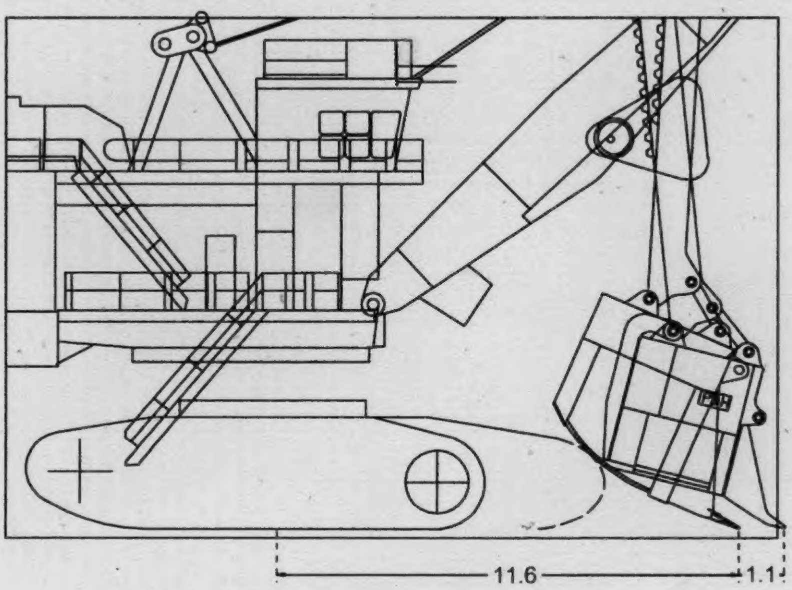

Figure 5-9: Dipper-crawler interference

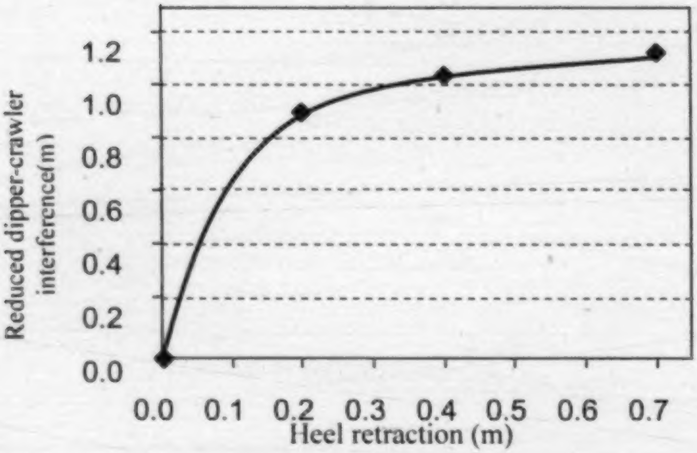

Figure 5-10: Reduced dipper-crawler interference

(4) Digging forces

From the digging simulation, digging force plots for both original and proposed profiles were obtained. As the proposed profile has a higher (effective) rake angle, it has the potential for improved digging performance in terms of digging forces.

McKeys (1985) concluded that the round shape soil digging tool performs in a very similar way as does a straight tool illustrated in Figure 5-11.

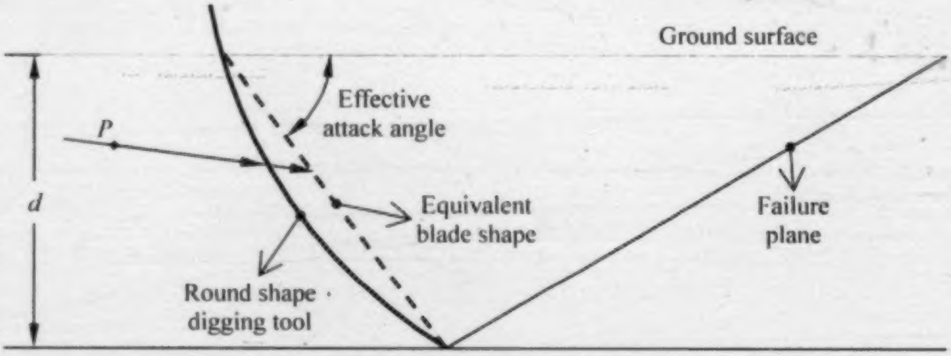

Figure 5-11: Equivalent tool shape for the round shape tool (McKeys, 1985)

During the shovel digging process, for a curved front dipper, as the digging depth increases, the equivalent digging blade varies in length and orientation. By using McKeys' method, the modified trial wedge model that was developed for a straight tool can be applied to the proposed curved front dipper (see Figure 5-12).

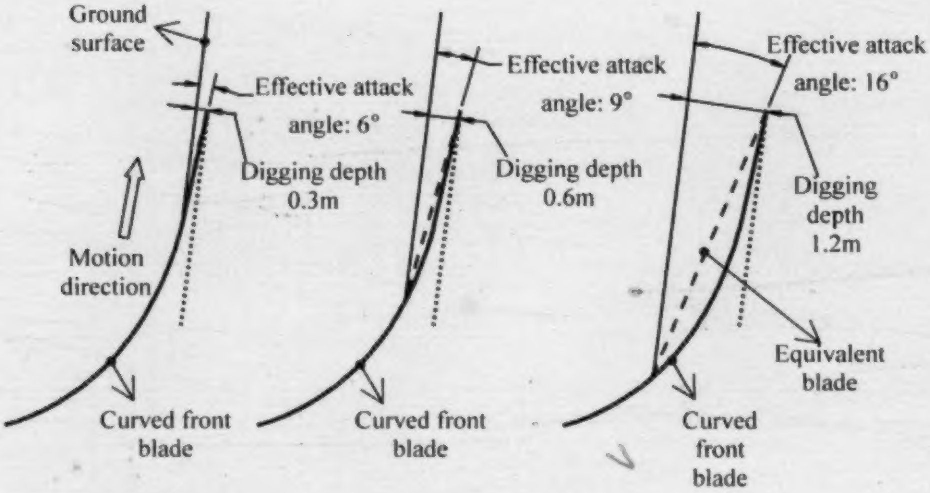

Figure 5-12: Effective attack angles and digging depths for a curved front

For example, applying the profile 3 from Figure 5-6: V in a dipper design, the effective rake for the curved profile is about 80°. Comparing to a original P&H design with 65° rake angle, the new design has a peak hoist load at 2100kN that is 200 kN lower that the original design at 2300 kN (see Figure 5-13).

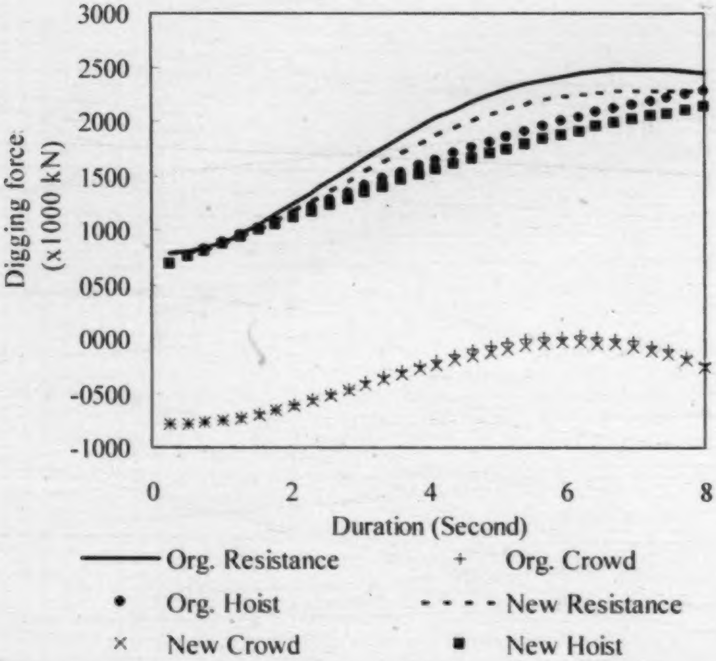

Figure 5-13: Simulated digging force plots for original vs proposed configurations

In Figure 5-13, the hoist force keeps increasing due to the growing cutting depth during the simulation. As a result, the highest hoist load happens at the greatest cutting depth. Although this is a little different from the real case, the simulations show a change from a flat front profile to one that has a spiral curvature. The output shows that the latter configuration will potentially yield performance and maintenance improvements over the original.

5.3 Additional Geometry Considerations

In introducing a curved dipper front, issues of flow through the shape due to the expansion and flow properties of excavated oil sand well known in the Northern Alberta mining industry were qualitatively identified by experienced operators at mine sites. These issues, although not the focus of this thesis work were necessary to address in order to facilitate an operable field scale test dipper. The field test scale dipper was designed to allow an evaluation of the curved front shape without the impact of other geometric concerns. In order to ensure that the proposed shape would not be hindered by capacity or flow, the project sponsor, JPi asked for two geometric considerations to be made related to the back (a skew) and side walls (a trapezoid), allowing the front curvature to be tested unhindered by these other effects and at the same time effect an improved flow of material from the design compared to the original configuration. It should be recognized that the basis for these design inclusions outlined in 5.3.1 and 5.3.2 were more qualitative from field experience by the sponsor and not based on engineering and mathematical principles as with the front curvature above. The two sections that follow attempt to simply justify the reasoning behind the capacity considerations made by the sponsor.

5.3.1 Back wall

As mentioned before, a consequence of the proposed change to the front wall is the dipper's ingress area becomes larger that the egress. Moreover, the generated mismatch between the front and back walls leads to a void space (black area in Figure 5-15 (a)) inside the dipper.

A skewed back wall may solve both problems for the same fragmented material considered at its natural angle of repose. Firstly, the degree of skewing was determined such that the ingress and egress cross sectional areas were matched. Secondly, this simple geometric change also results in Figure 5-15 (b) where the void space (black area) is now smaller than that in Figure 5-15 (a).

Given free flowing face cut material, a slope at the natural angle of repose of the material is created as a cap to the material that has already flowed into the dipper. When the toe the slope is established in contact with the back wall, a void space is introduced.

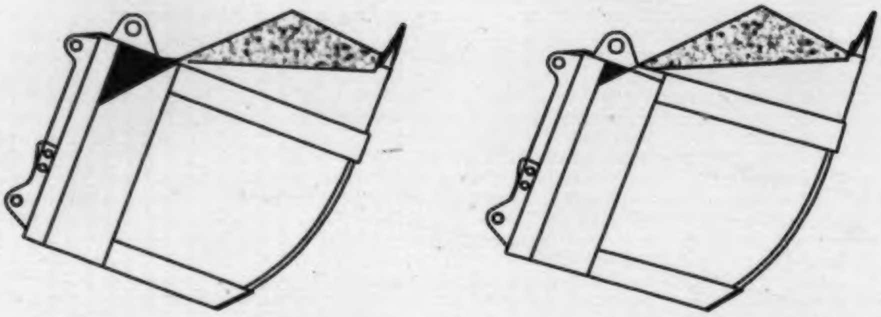

(a) Curved front profile with original back (b) Curved front profile with skewed back

Figure 5-14: The void space and the skewed back wall geometry change

The slope of the stack pile is controlled solely by the material angle of repose from front to back and relatively flat from side to side parallel to the lip. Not like the hydraulic shovel buckets, cable shovel dippers use the stroke volume as the nominal capacities (light, medium and dark gray areas respectively).

The geometrical area shown in the dipper side profile can be used to estimate the void space ratio. The void space ratio is defined as follow

Void space ratio =Void space/Dipper nominal capacity

As shown in Figure 5-15, when no skewness on the back wall, the ratio of the big shadowed area (triangle) to the light gray area is 5%; when 5°skewness , the ratio of the small shadowed area (triangle) to the medium gray area is 1.8% ; when 10°skewness, there is no void space in the dipper.

Given that the stack pile slope is 2:1 (SAE standard for excavator bucket capacity), the relationship between the void space ratio (the void space versus dipper nominal capacity) and the degree of the skewness was represented in

Figure 5-16, in which the void space approaches zero as the back wall skew angle approaches 9°.

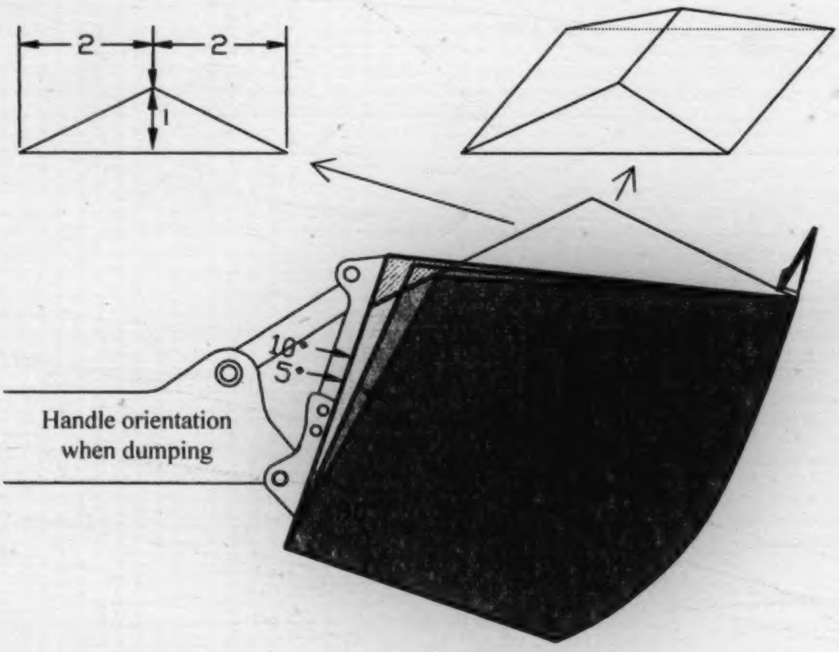

Figure 5-15: The void space and the skewed back wall geometry change

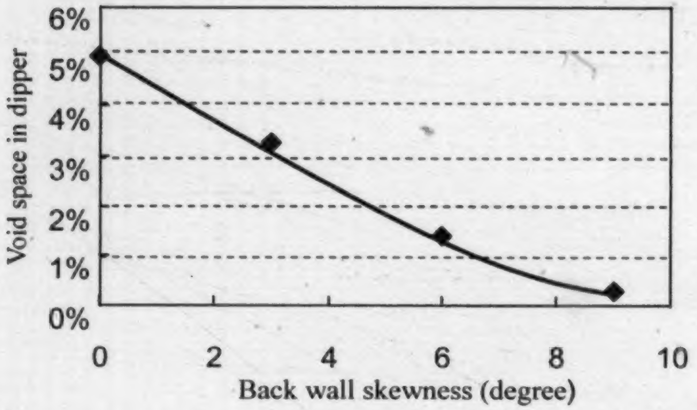

Figure 5-16: The void space and the skewness of the back wall

5.3.2 Side walls

In situ material, when mined, will swell from 10 to 60%, depending on the type of material and fracture frequency. In hard rock operations, the swell factor is commonly between 30% to 50%, meaning that one in-situ unit will swell to a volume of 1.3 to 1.5 units. In soft rock and soil operations, the swell factor is commonly between 10 to 30% (Hartman, 1992). For oil sand, the swell factor is about 1.3 (Morgenstern and Scott, 1997).

Unlike blasted hard rock face material which expanded during blasting, virgin oil sand face expands on excavation and dipper filling. Peculiar to oil sand is the unique expansion effect due to oil sand gas relief often causing oil sand to become a solid lump (loafing) in the dipper on release.

For normal unconsolidated sandstone material, the swell factor is normally 25% for heaped volume versus bank volume. The frequent used swell factor for oil sand is normally 30%. Hence the swelling factor due to the gas relief for oil sand is about 5%. Gas relief is a time dependent function such that it is estimated by oil sand mining operators that about 50% of the gas relief occurs during the dipper loading/dumping cycle. If the dipper can provide enough space in the rear or side geometry, approaching say an additional 3% buy volume, it will prevent the in-dipper oil sand from loafing. This technique has been proven out by field application to hydraulic shovel buckets currently in oil sand operation (Joseph, 2001).

Figure 5-17 demonstrates the concept of introducing trapezoidal side walls where the wings provide greater space for expanding material.

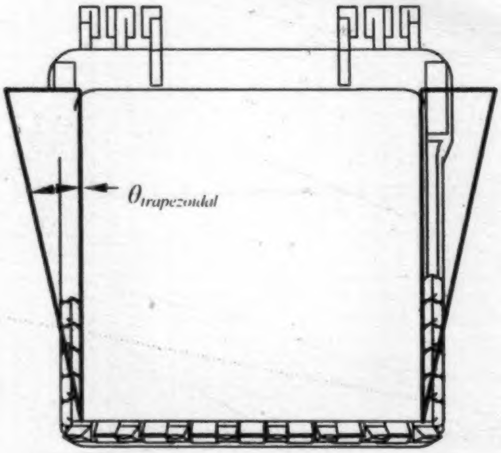

Figure 5-17: Trapezoidal angles applied to oil sand dippers

Figure 5-18 shows the relationship between the angle of the trapezoidal side walls and the increased dipper capacity. In contrast to the original right angled dipper design, the trapezoidal design increases capacity. Unlike the concept of reducing void space above, this configuration provided for greater space for the oil sand to occupy on expansion. In this context it is assumed that the dipper would fill, constrained by the ingress and then the extra space would allow the oil sand to expand in volume to prevent it from becoming a loaf. The result of this analysis showed that for an additional trapezoidal angle of 5^{o}, there would be a 3% increase in overall volume, sufficient to address the concern.

The swelling occurs along the whole cycle of the oil sand processing. The first swelling occurs while the oil sand breaks out of the working face; then the relief of the gas leads to the volume to expand. During the transportation, sizing, crushing, and slurrying, the volume of the oil sand keeps increasing. However, it is only the in-bucket expansion due to the gas relief that results in the loafing effect.

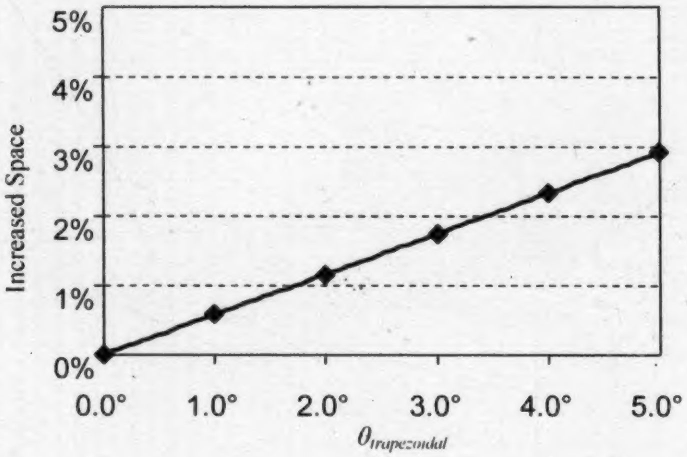

Figure 5-18: Increased capacity due to trapezoidal side walls

5.4 Cold weather digging

The climate of the Athabasca region is continental sub-Arctic with cold winters and warm summers. The mean annual temperature in Fort McMurray is 0°C (Morgenstern and Scott, 1997). Winter temperatures drop as low as -45°C and weeks of -30 to -40°C are not uncommon. From November through April, temperatures seldom rise above freezing. Plant productivity is maintained throughout the winter months, although periods of extended cold take their toll on men and machines, affecting mine output (Morgenstern and Scott, 1997).

If the shovel keeps digging in the same face during the winter season, the face material will not freeze. In this case, the shovel would operate similar to that under summer conditions. The worst scenario is a non-active face that has not been disturbed by any machine in winter.

In summary, there is minimal concern for oil sand digging during winter, especially utilizing an ultra class shovel.

5.5 Three-dimensional dipper models

Major equipment manufacturers have recently adopted three-dimensional design and modeling tools for both parts and assembly design. Software such as Solidworks, is widely used by mining equipment manufacturers. In this research, Solidworks was adopted as a three-dimensional design and modeling tool.

5.5.1 A generic dipper model

A generic dipper was first modeled to learn the methodology of 3D modeling and design. The generic design that was most frequently utilized in the past one hundred years to about 2001 is a box shape (see Figure 5-19). Each wall of the dipper is basically a straight or flat piece of cast/fabricated steel; a curved shape has been applied at the corners to facilitate smoother stress transitions. The digging analysis performed earlier showed that the straight design was less suitable for digging un-blasted material due to its large contact area during the digging process. This design introduces a conflict between the dipper and the shovel tracks. As well, an improper geometry ratio was prone to result in a void space during filling. Both end users and manufacturers have recognized these issues and have made some effort to redesign the unit in the past 5 years since 2001.

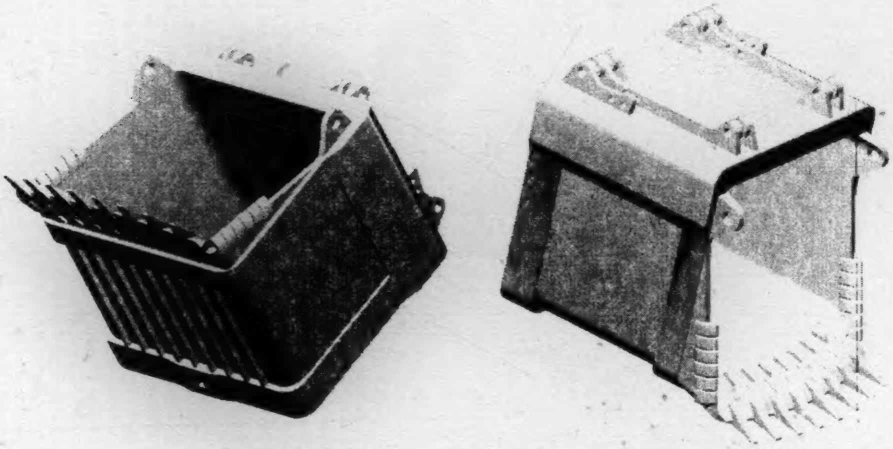

Figure 5-19: A generic three-dimensional dipper model

5.5.2 Current ultra class dipper models

To further analyze the features of current dippers, the two latest dipper designs from major shovel manufacturers were modeled and reviewed. The Bucyrus FastFil® was modeled (see Figure 5-20). This dipper, with a 46 yard^3 capacity, has been used with the Bucyrus 495BII HF shovel at oil sand sites. The OEM identified this design's three principal features: a curved front wall from side to side (laterally), a shortened back wall, and a trapezoidal mouth shape. The first feature has been well accepted by shovel operators as it qualitatively improves digging performance. The objective of the trapezoidal concept is to reduce the void space inside the dipper during the loading. This concept might work in the case of blasted rock, but in oil sand, it might not work as well due to the expansion effect resulting from oil sand gas relief.

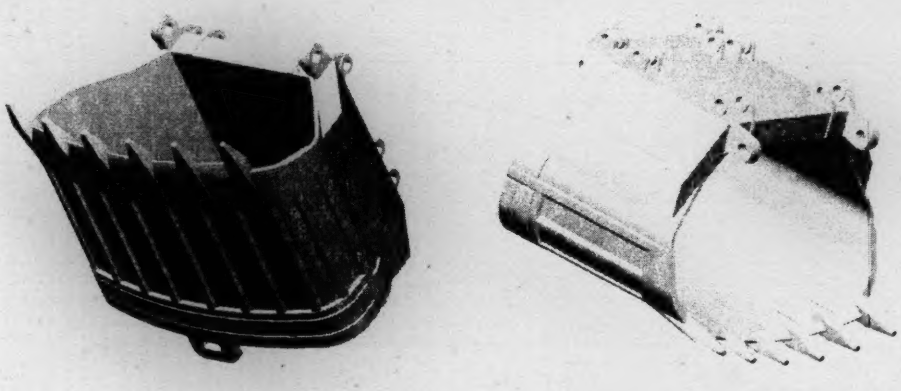

Figure 5-20: A three-dimensional model of the FastFil ®
(Bucyrus, 2003)

Similarly, P&H has developed the Optima Plus ® for their 4100 BOSS shovels at oil sand sites. As shown Figure 5-21, the dipper features a curved front wall and a shallow height. As with Bucyrus's lateral curve design, P&H's curved design works well in the oil sand digging. A wider but shallower profile is presumed by the OEM to perform better with oil sand, as it may need shorter time and less energy to fill, however, as with other recent developments there has not been any literature that proves this; the wider dipper may potentially result in high digging resistance and impacts on the handle and frame.

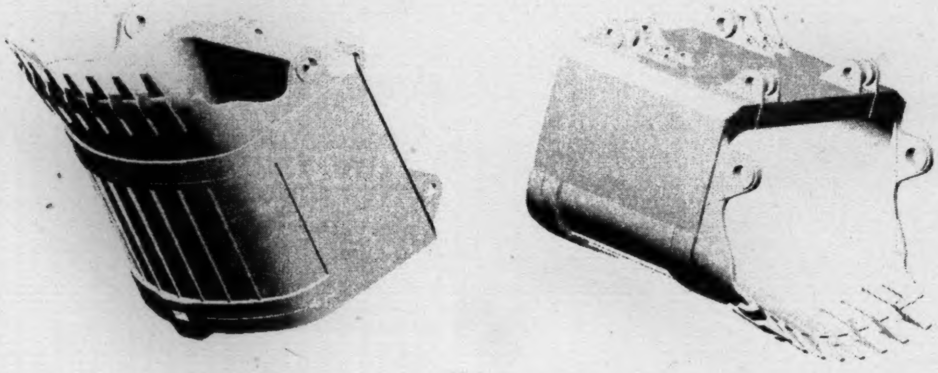

Figure 5-21: A three-dimensional model of P&H Optima plus® (P&H, 2001C)

The models of these two dippers differ not only in their geometry but also in the number of teeth. The Bucyrus's FastFil® has six teeth while the P&H's® Optima Plus has eight. Currently, ESCO provides both P&H and Bucyrus the teeth and adapters. So far, no research has attempted to correlate dipper production to the number of teeth, and the end users (mines) have not compared the two dippers side by side. In this research, the number of the teeth is not considered, but the relative scale ratio of tooth size and spacing to lip size from the original to proposed curved configuration was essentially kept constant in an attempt to remove this as a factor in evaluating the curved front performance.

Despite the above differences, the two current main production dippers of P&H and Bucyrus have some common problems, among which dipper-ground interactions and dipper-shoe interference are two of the most important.. In addition to the dipper's performance benchmark, which includes variables such as digging resistance and energy consumed, the heel life or heel damage is a very important factor that contributes to a dipper high maintenance schedule. Moreover, during a dipper's operation, a median cannot be found where the shovel's production and the dipper's heel life are both improved. With a smaller attack angle the digging force decreases while the heel interference with ground or shovel shoes increases. Based on this fact, some very recent but unproven concept base dipper profiles developed by the project sponsor, JPi geo-industry engineering consultants, particularly for front profile and material flow were developed, the front shape engineering and concept proving of which was the focus of this thesis. These entire composite designs are outside the scope of this work but are worth mentioning their development existence.

5.5.3 JPi concept dipper models

The first objective of a new concept dipper design adopted by JPi was to minimize the influence on the original shovel, so that a new design could be easily applied to an original shovel. As shown in Figure 5-22, the first version of the new dipper had a totally different front element but kept all other elements in a generic dipper unchanged (Joseph and Hansen, 2001). For example, the means of attaching a new dipper to a P&H 4100BOSS shovel remained exactly the same as that of attaching a traditional generic dipper. Even the door for an original P&H 4100 dipper was reused in the design.

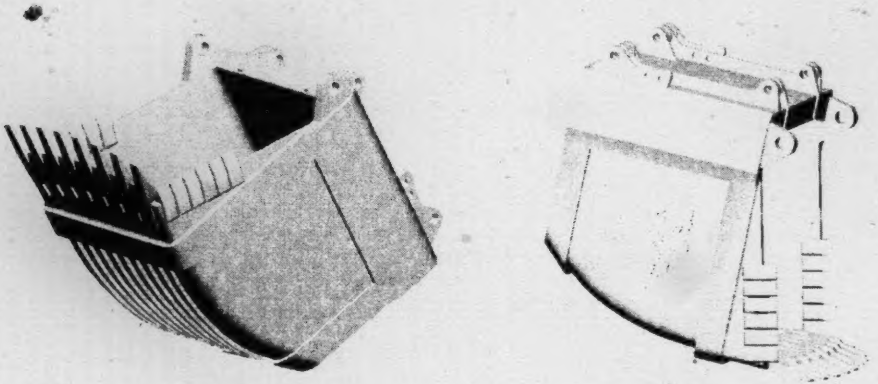

Figure 5-22: The first trial of the new concept dipper

This concept design was introduced to the mining industry for comments through three-dimensional print models (Shi and Joseph, 2004). Feedback was encouraged from all parts of the industry including shovel operators, mine management and manufacturing engineers.

Most comments were summarized in three points:

- The curved front could potentially improve digging-performance, and a prototype test would be a must.
- The retracted heel design would improve the dipper's life and decrease maintenance intervals.

- The smaller egress might result in blockage during dumping cycles.

As shown in Figure 5-23, a concept of the skewed back wall was shortly after introduced with the curved front wall. The skewed back wall led to a match of the dipper ingress and egress area such that any blocking problems could be eliminated.

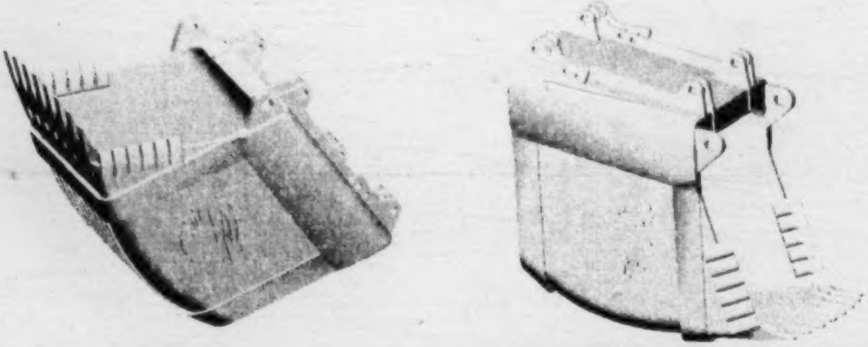

Figure 5-23: A curved and skewed dipper model

The trapezoidal profile was then introduced, Figure 5-24 to provide the excavated oil sand room for expansion such that the loafing phenomenon would be alleviated.

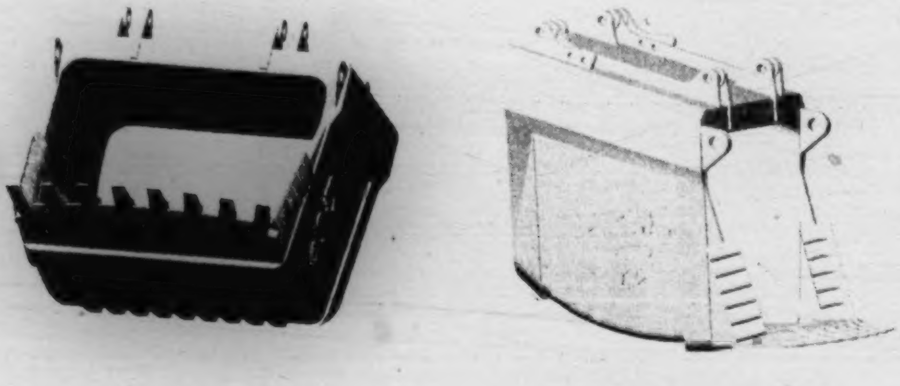

Figure 5-24: A curved, skewed and trapezoidal dipper model

A later development previously unmentioned but considered by the sponsor is shown in Figure 5-25. The flare in the dipper design results in a tilt angle of both side walls; from the ingress to the egress, the side walls tilt outward of about 1 or 2 degrees, was similar to the tilt angle suggested for hydraulic shovel buckets (JPi, 2001). The intention here was to generate still more room for oil sand expansion in the dipper shape.

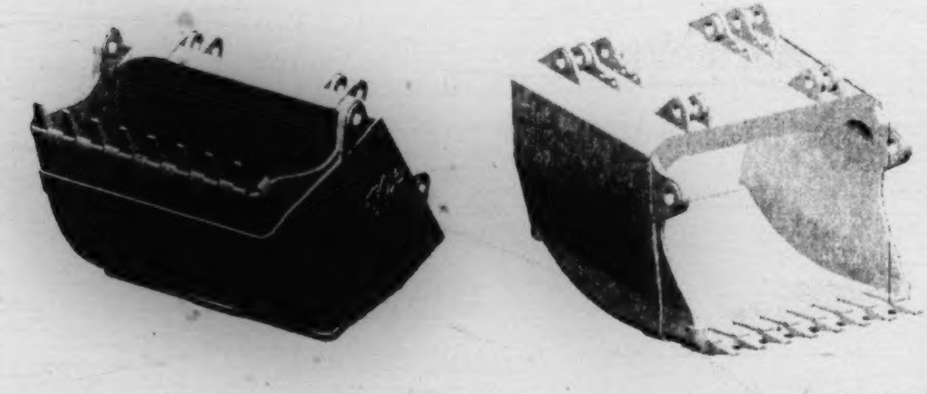

Figure 5-25: A curved, skewed, trapezoidal and flared dipper model

Chapter 6

1/20th Scale Prototype Field Tests

6.1 Dominion 500 shovel

To further demonstrate the new concept's viability, a 3 yd^3, 1/20th scale model of an ultra class scale dipper was fabricated to match a Dominion 500 cable shovel ,Appendix C, which still had its original AMSCO 2 yd^3 dipper, Figure 6-1. In the shovel and dipper manufacturing and mining industries, capacities of shovel dippers are cited in yd^3 as a standard rather than m^3. The sponsor, JPi and its fabrication partners absorbed the entire cost of fabricating the dipper, and the refurbishing cost of the 1949 shovel.

Figure 6-1: Dominion 500 shovel during transportation

The 3 yd^3 fabrication targeted testing of the curved front, although a skew, flare and trapezoidal geometry change were also included by the sponsor, who also wanted to see the test proceed with unrestricted material flow when dumping. Only the curved front feature was investigated as the focus of this thesis. In this respect, the rest of dipper shape was considered merely a holding structure for the front curvature, to compare with the performance of the flat front used in the original 2 yd^3 AMSCO dipper of the Dominion 500 shovel.

The Dominion 500 was identified as having the same operating action and geometric orientation as the P&H 4100 modern ultra class shovels at 1/20 of the dipper scale, Figure 6-2, (Dominion, 1957).

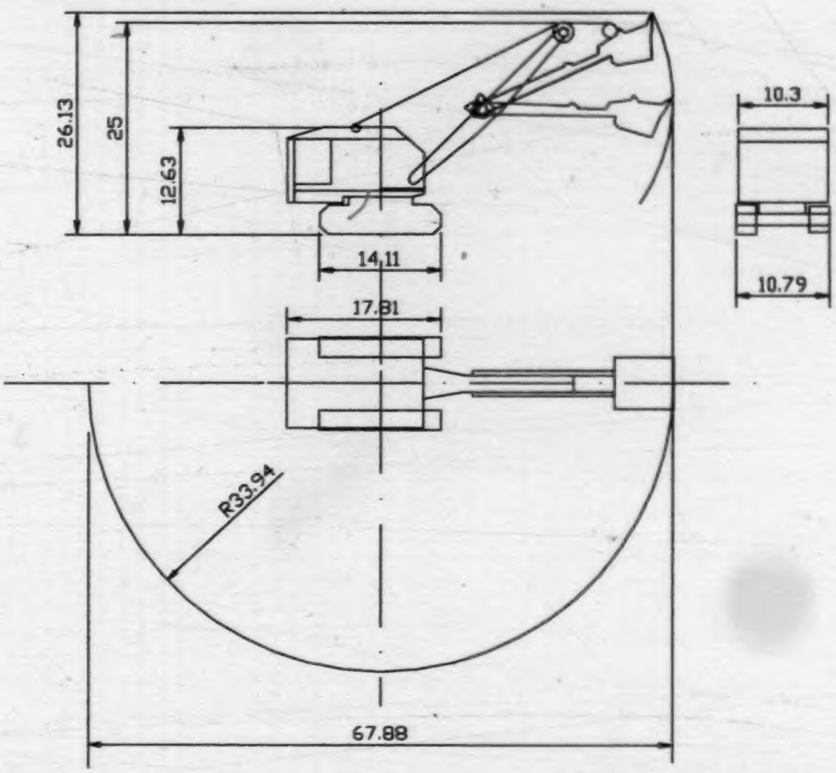

Figure 6-2: Two dimension model of Dominion 500 shovel (units in feet)

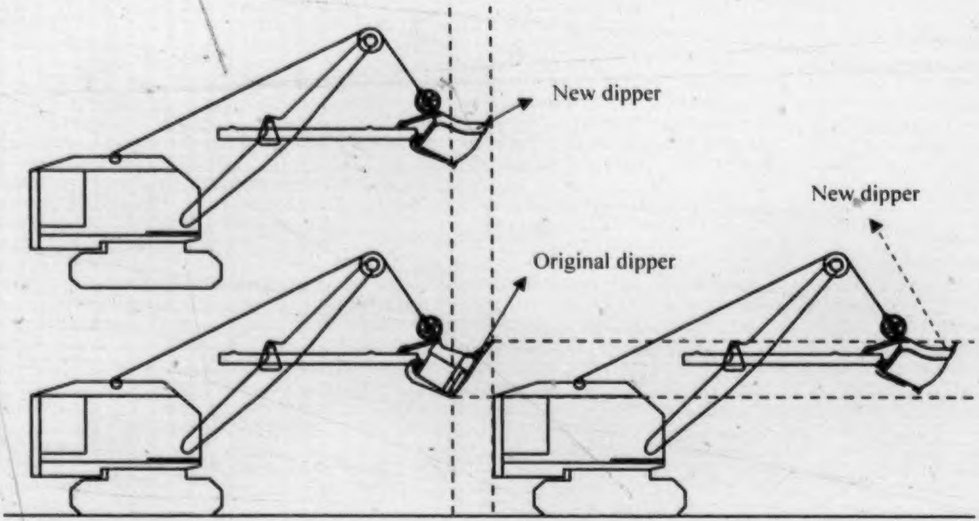

Figure 6-3: Comparison of the geometrical configuration between JPi and original dippers

6.2 3 yd^3 dipper design

6.2.1 Dipper design

Given the front curvature concept design from the modeling exercises performed earlier and with the sponsor's addition of the geometric flow oriented changes, a prototype was blueprinted by the sponsor. Due to the use of lighter materials and rolled fabrication rather than casting processes, the dipper capacity was increased to 3 yd^3 (see Appendix D), or 50% more than the original AMSCO dipper capacity of 2 yd^3, for the same overall weight as exhibited by the 2yd^3 original.

Figure 6-4 shows the design of the dipper that was fabricated. The back attachments were identical to the original dipper to facilitate use with the Dominion 500 shovel with no changes to the shovel's operating configuration.

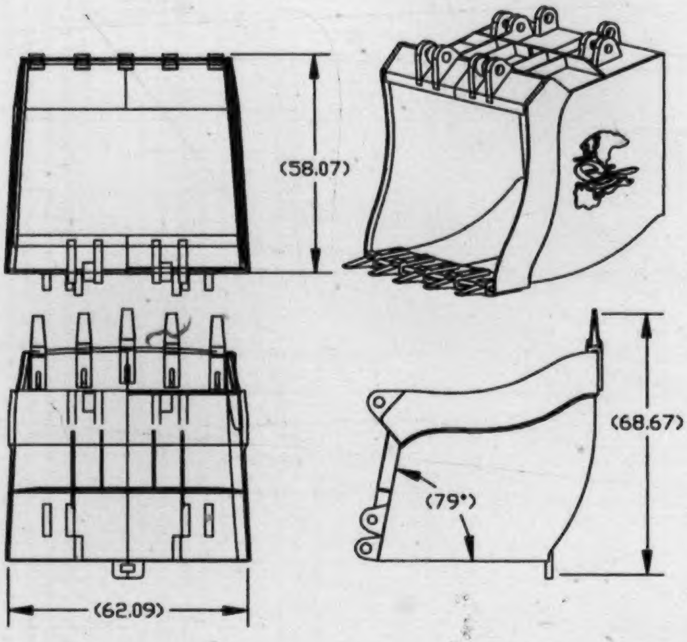

Figure 6-4: Testing dipper design based upon steel-plate (Dimension in inches)

6.2.2 Door design

As shown in Figure 6-5, a specific door to match the dipper was also fabricated. The door adopted the same mechanism as that of the original dipper for the Dominion 500, which is also similar to those used in modern ultra class shovels, but here one that would not impede the operating action of the existing test shovel.

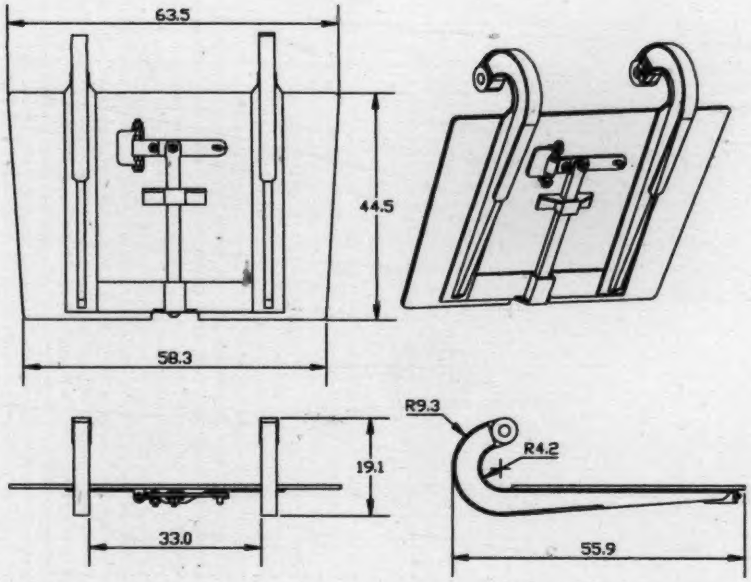

Figure 6-5: A door for the testing dipper (Dimension in inches)

6.2.3 Dipper and door virtual assembling

To validate the design for the fabrication, a virtual assembly in SolidWorks of the dipper body, and door parts was done before the physical work was performed. Figure 6-6 shows the completely assembled dipper.

Starting with static virtual assembly, some design features were validated for the fabrication:

- Dimension matching between parts
- Static geometric relationships
- Material weight estimations.

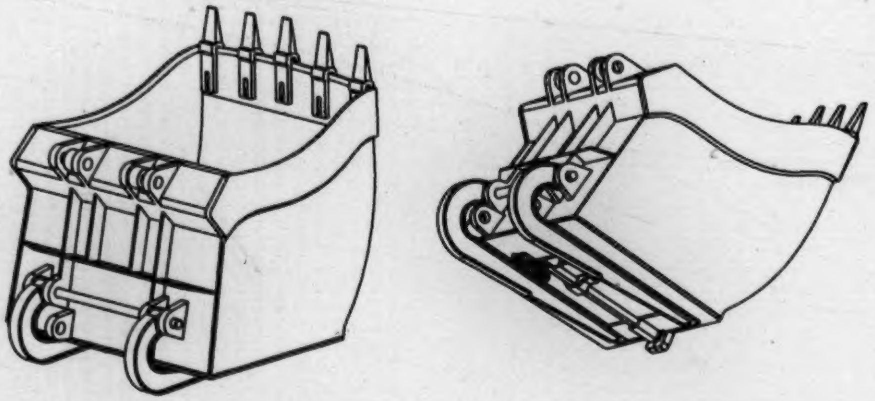

Figure 6-6: Test dipper and matching door prior to physical assembly

An interactive rendered model was set up by using Solidworks Assembly. Two snapshots are presented in Figure 6-7, showing the door both opened and closed to reveal the dimensional match. By using the interactive model, the dipper door and latch bar motion were mimicked for operational confidence.

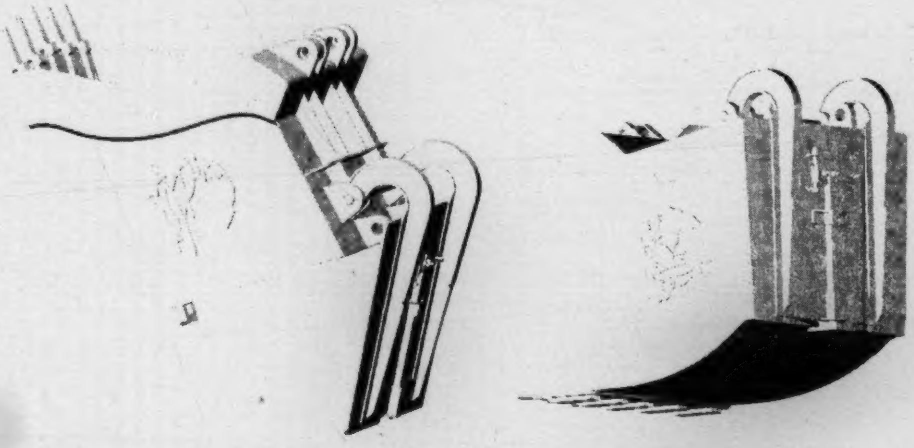

Figure 6-7: An interactive rendered model using Solidworks Assembly

6.2.4 Prototype dipper fabrication

Figure 6-8 shows the dipper being fabricated. Table 6-1 provides a summary of the dipper's specifications.

Figure 6-8: The 3 yd^3 dipper being built in the workshop

Table 6-1: The Prototype Dipper's Specifications

Weight (including door)	6800 lb
Nominal capacity	2.98 yard^3
Maximum width	62 in
Maximum height	58 in
Maximum depth	68 in

As shown in Figure 6-9, Hensley teeth were attached to the lip system (see Appendix E), such that the number and spacing were commensurate with the lip coverage for an ultra class P&H 4100 Dipper.

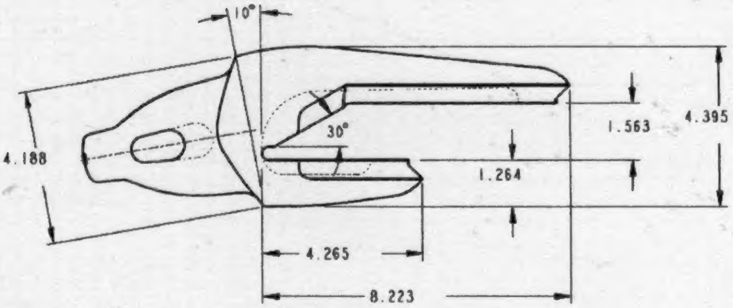

(Units in inches)

Figure 6-9: Dipper teeth adpater (Hensley, 2003)

6.3 Field test

6.3.1 Sensor placement

Two types of sensors were employed in the field test: strain gauges and inclinometers. The sensor arrangement is illustrated in Figure 6-10.

Two inclinometers were used to measure the orientations of the handle and the hoist cable from which the dipper (tip) position can be determined at any instant. One inclinometer was attached to the bail that has the same orientation as the cable. The other was attached to the side of the handle. A pair of uni-axial strain gauges was mounted on the top and bottom of the handle respectively close to its front end where the gauges would not be damaged by the saddle block action and falling material. Another pair of strain gauges were mounted on the neck of bail that is the longitudinally uniform portion. In this study, as only the crowd force and the hoist force as relative measures were targeted, it was assumed that the stress within the handle cross section is uni-axial and symmetrical and the stress within the bail neck cross section is uniform. The original dipper was tested first then the new dipper replaced the original dipper and was tested.

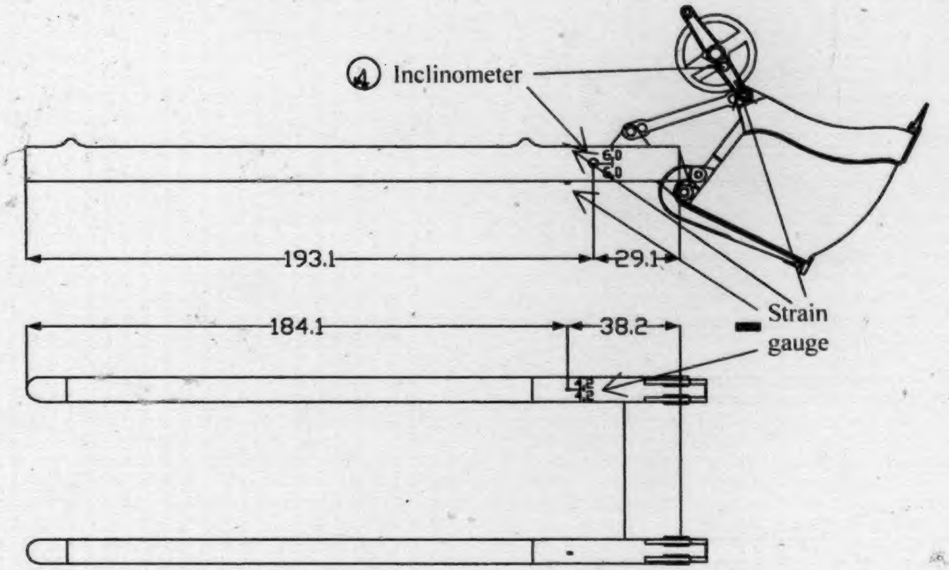

(a) Sensor arrangement and locations

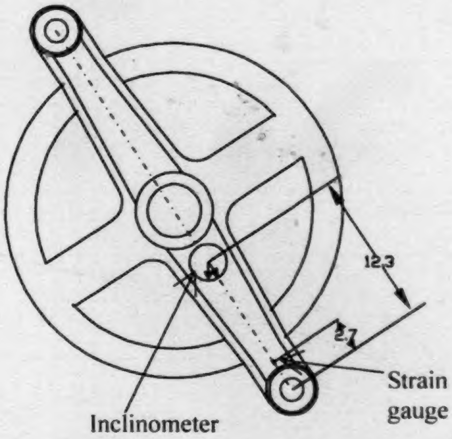

(b) Location of sensors on the bail

Figure 6-10: Field test sensors and arrangement (dimension in inches)

6.3.2 Sensor and instrumentation detail

6.3.2.1 Sensors

The Strain-stress field in the handle stick and the bail bracket were assumed to be simply uni-axial. The measurement results were used obtain an idea of the relative loading magnetite during digging operation versus free suspended load when not engaged in the face. Uni-axial gauges were adopted to measure the crowding force on the handle and the hoisting force on the bail. As both the preparation of the gauges had to be done in the field, the 5mm strain gauge that is relatively easy to operate was select and mounted on the handle and the bail.

In the test, the NE-FA-5-120-11 strain gauge (Showa Measuring Instruments, Japan) was employed for all strain measurements, and the AccuStar® Electronic inclinometer (Sherborne Schaevitz, United Kingdom) was used for measuring the handle and bail inclination. The basic parameters of those sensors are shown in Table 6-2 and Table 6-3.

Table 6-2: Parameters of the Showa NE-MA-5-350 Strain gauge

Gauge Length	5mm
Gauge Resistance	120 ohm
Gauge Resistance Tolerance	+/-0.5%
Gauge Factor	2.14 (Nominal)
Gauge Factor Tolerance	+/-1%

Table 6-3: Parameters of the AccuStar® Electronic inclinometer

Total Range	+/-60 degree
Linear Range	+/-45 degree
Threshold	0.001degree
Scale Factor	60 mV/degree +-10%
Voltage Supply	+/-12V

Four strand cables, three of which were used, served as the signal leads to the data acquisition terminals. This configuration reduced the lead wire resistance effect to a minimum. The two inclinometers were connected by two separate cables attached to the handle and bail.

6.3.2.2 Data acquisition

National Instrument SCXI-1000 chassis (NI, 2005) with three sets of SCXI-1314 (NI, 2005) and SCXI-1520 (NI, 2005) were employed as the data-acquisition system. Each strain gauge module, SCXI-1520 with a SCXI-1314 mounting terminal block, had eight channels such that a total of 24 channels were available with the DAQ system. Two of them were rewired and re-configured to be compatible with the inclinometer transducers while all other channels were by default in a quarter bridge strain gauge signal configuration. The local mine safety code required that no one but the shovel operator was allowed on the board during operation; therefore, a 802.11g wireless network was employed to remotely control the DAQ host computer which was located in the shovel maintenance house.

As illustrated in Figure 6-11, the strain gauges and inclinometers were connected to the DAQ chassis via the lead wire (represented by the dash line); the DAQ unit scanned the data into each channel and sent the resulting data package to the host computer at a rate of 10-100 Hz. The host computer ran as a blind server while another remote computer provided the interface to fully control the DAQ software and the data recording. The laptop communicated with the host computer via remote connection protocol carried on 802.11g.

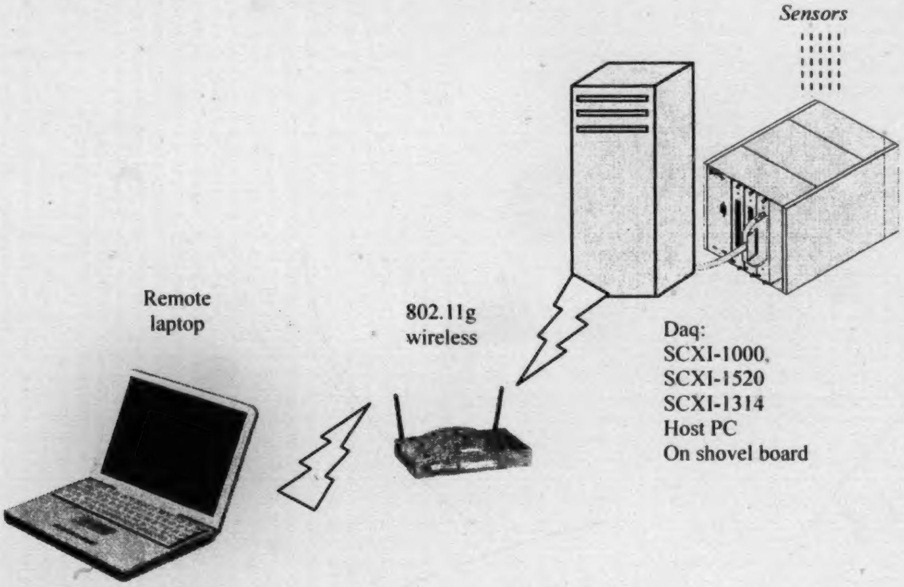

Figure 6-11: DAQ system configuration

6.3.2.3 Wiring and protection

The strain gauges were connected to the strain DAQ system by using a quarter bridge configuration with a dummy gauge installed on the wiring end terminal for each channel to compensate for temperature fluctuations. The Excitation voltage was 2.5V, with a voltage gain of 1000, and the signal filter was set to 20 Hz.

For the inclinometers connected to DAQ system, the gain factor was set to 1, with no filter and no excitation voltage (0V). The wiring terminals which incorporated the dummy strain gauge were disconnected and rewired to fit the inclinometers' voltage signal.

In the test, one of challenges while collecting data was protecting both the sensors and the cables as all sensors were attached to the shovel's moving and ground engaging parts. The sensor and attached cables could be easily destroyed during operation if they were not protected properly. For example, as shown in Figure 6-12, a set of welded steel tubes and plates was utilized as shielding for strain gauges mounted on the dipper body. These gauges as yet unmentioned were installed for data gathering which will be used in another project, targeted at the structural integrity of the test dipper, but outside the auspice of this thesis. This latter data is the property of the sponsor.

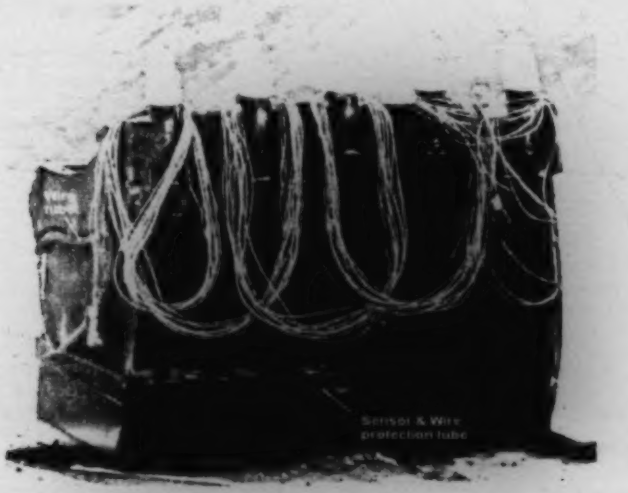

Figure 6-12: Test wiring and cable protection

6.3.3 Test sequences

Four types of shovel operation were employed during the test. The first two were performed to discern the hoist and crowd forces during static snapshots of in and out of face activity with no dynamic material reaction from the face. This knowledge would be helpful during the interpretation and analysis of the dynamic data.

(1) Duty cycle static loading without face activity

Here, the dipper was incrementally raised and held in an equilibrium position with no dipper load from the tucked to the maximum horizontal stick position at full extent in π/8 angle increments to evaluate the empty dipper's static empty loads by position (see Figure 6-13).

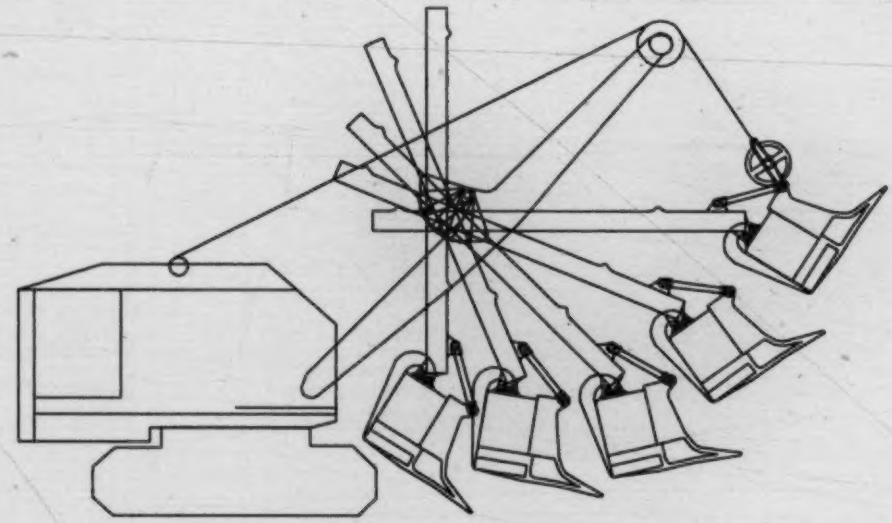

Figure 6-13: Dipper test: π/8 angle increment

(2) Duty cycle static loading with face activity

The dipper was incrementally raised and held in an equilibrium position with a proportional dipper load from the tuck to the maximum horizontal stick position at full extent, in π/8 angle increments. No dynamic face activity at measurement.

(3) Duty cycle dynamic loading with face activity

The dipper made complete duty cycles, making digging passes through to full load and dumping release to a side pile. The objective was to evaluate the integral effect of both the dead weight, payload and the dynamic face activity (see Figure 6-14).

(4) Dipper motion ranges

The dipper was pushed as close as possible to the ground and as close as possible to the shovel tracks to evaluate the degree of dipper interference with the ground or tracks.

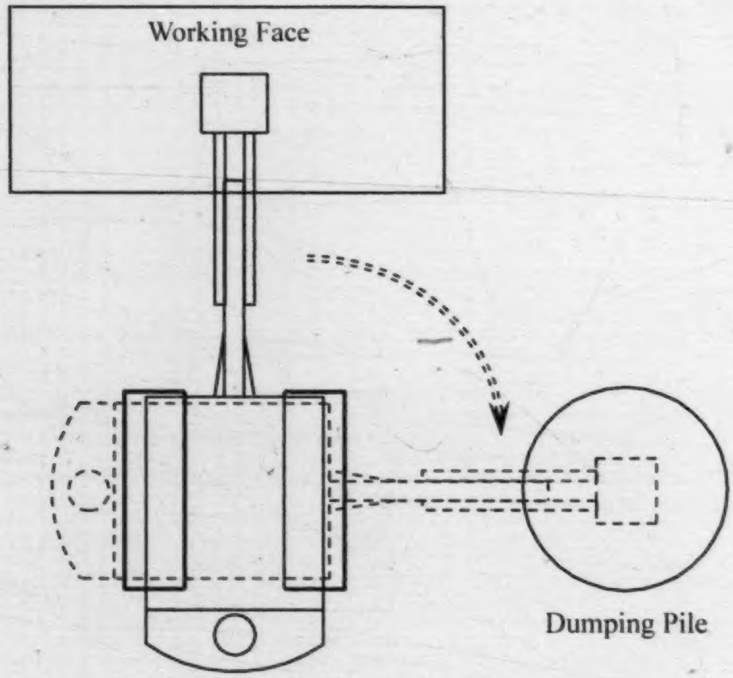

Figure 6-14: Dominion 500 field test digging and dumping plan

6.3.4 Test site and face conditions

The test site was located in an inactive pit at Suncor Energy, Fort McMurray, Appendix F. The face material comprised oil sand with a varying bitumen content of 7% to 12%. The floor consisted of mainly limestone and a small amount of the clay. The face height was about 10 m. Generally, the face was typical of the oil sand mining conditions that ultra class mining shovels deal with every day. Figure 6-15 shows the mining face at the time of testing.

The physical properties of the oil sand are summarized in Table 6-4 (Suncor, 2005).

Figure 6-15: Oil sand face condition at Suncor Energy test site

Table 6-4: Physical properties of the oil sand in situ (Suncor, 2005)

Specific density	1.9~2.1
Bitumen content	7%-12%
Water content	5%-8%
Friction angle of the material	22°-60 °

6.3.5 Testing with the original dipper

The test was initially conducted with the original AMSCO 2 yd^3 dipper in accordance with the guidelines described above. The static test followed the procedure outlined above while the dynamic test was evaluated by using real shovel digging passes, with which the operator was well experienced. The operator had over 40 years of experience of operating shovels or draglines, 10 years of which were with similar oil sand conditions. His qualitative feedback regarding the digging conditions revealed that the oil sand face was not as easy to dig as it looked, so that a greater degree of hoist force was needed to cut through the virgin face than had been expected. But this was the same experience for the original and test dipper. Figure 6-16 illustrates the shovel in operation.

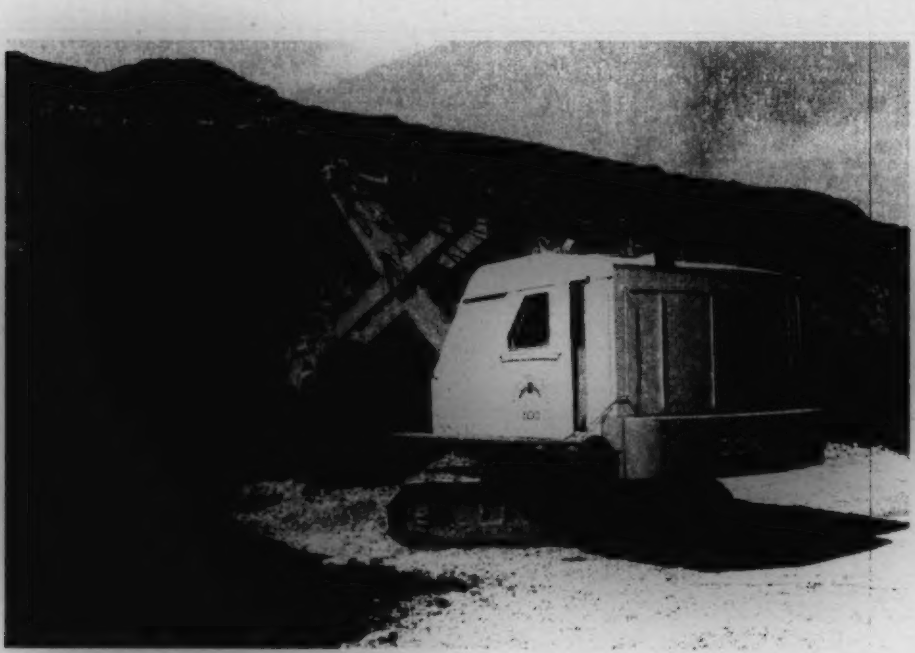

Figure 6-16: The Dominion shovel in the oil sand operation

6.3.6 Testing with the prototype dipper

The operator's qualitative feedback regarding the new dipper's performance indicated that he thought the new unit required less hoist force than the original dipper but required an increase in the crowd force. This gave pre-analysis indication of what should be looked for when looking at the hoist and crowd data. A decrease in the hoist force had been expected for this dipper design, due to the directional change invoked by the curved design directing the front in the direction of motion through the face material. But the increase in crowd force needed some analysis and explanation.

Qualitative observations of the tests found that the dipper generally ran more smoothly than the original dipper. The new dipper more easily scooped and cleaned the material around the shovel tracks; the digging in the face appeared consistent at any orientation.

The dump flow out of the dipper, an additional concern by the sponsor which was addressed by the skew, trapezoidal and flare geometry changes has a flowing characteristic and certainly did not release material as a solid lump. In this latter concern, which was only evaluated qualitatively, the sponsor gained the information they needed to progress with the design.

Figure 6-17 illustrates the new dipper attached to the Dominion shovel. The JPi instrument truck beside served as the control cab for manipulating all the data recording remotely.

Figure 6-17: The concept JPi prototype dipper on a Dominion 500 shovel

6.4 Data analysis

Data from strain gauges on the handle and the bail, inclinometers on the handle and the bail were analyzed.

6.4.1 Transformation

6.4.1.1 Strain and stress

(1) Signal to strain

The output signals from the DAQ were in units of voltage that were transformed into micro strain via a LabView program using Equation 6.1. In this case, the lead wire resistance was assumed to be zero as the three-wire configuration canceled most of its influence.

$$\varepsilon = \frac{-4V_r}{GF \cdot (1 + 4V_r)} \times \left(1 + \frac{R_L}{R_g}\right) \tag{6.1}$$

$$V_r = \left(\frac{V_{signal}}{V_{EX}}\right)_{STRAINED} - \left(\frac{V_{signal}}{V_{EX}}\right)_{UNSTRAINED} \tag{6.2}$$

where

ε	Measured strain
GF	Gauge Factor
R_g	Gauge resistance
R_L	Line resistance
V_{EX}	Excitation voltage
V_{signal}	Signal voltage
Vr	Reference potential

(2) Strain to stress

The generic expression for tension or compressive stress on the handle and bail is given as

$$\sigma = E \cdot \varepsilon, \tag{6.3}$$

where

E	Young's modulus of the handle or bail material.
σ	Stress in the handle or bail.

In the handle, the strain/stress on the top and the bottom of the structure would be different if a bending moment occurred along the sticks. Since the objective of this research was not to perform a stress field or structural analysis of the loaded shovel components, but merely to gain a relative change form the original to the prototype dipper configuration in terms of crowd and hoist forces to operate the two, the effective strain in the stick cross-section was taken as the average of the strain on the top, ε_1, and the strain on the bottom, ε_2, as shown in Figure 6-18:

$$\varepsilon = \frac{\varepsilon_1 + \varepsilon_2}{2} \quad . \tag{6.4}$$

(3) Stress to force

As show in Figure 6-18 and Figure 6-19, the force passing through the sticks and bail sheave bracket was

$$F = \sigma \cdot A$$

$$F = E \cdot A \cdot \varepsilon \tag{6.5}$$

where

A	Cross-sectional area of the handle sticks or bail bracket
F	Crowding or hoisting force

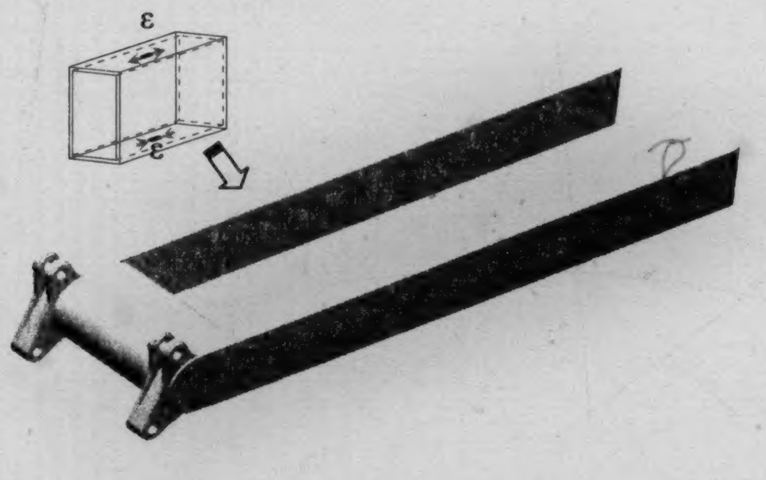

Figure 6-18: Handle sticks and cross-sectional shape

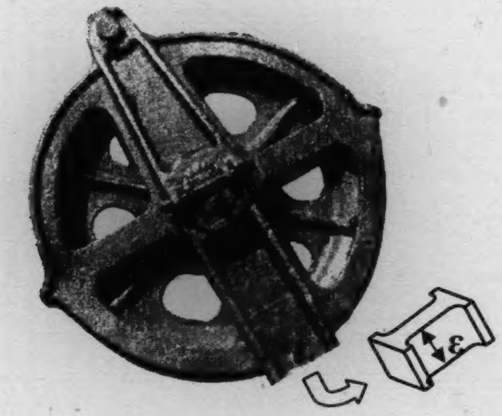

Figure 6-19: Bail strain gauge position and cross-sectional shape

(4) Calibration

When the handle is oriented at the horizontal and the dipper is free of the mining face, Figure 6-20, the model shown Figure 4-7 becomes the one shown in Figure 6-21.

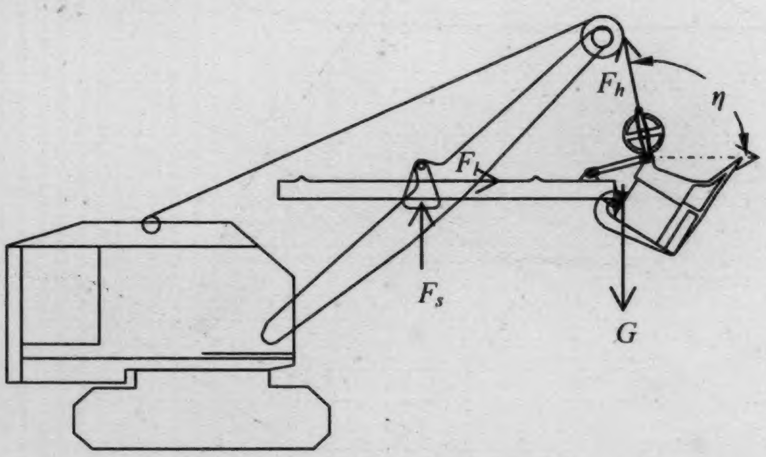

Figure 6-20: Hoist and crowd force strains calibration position

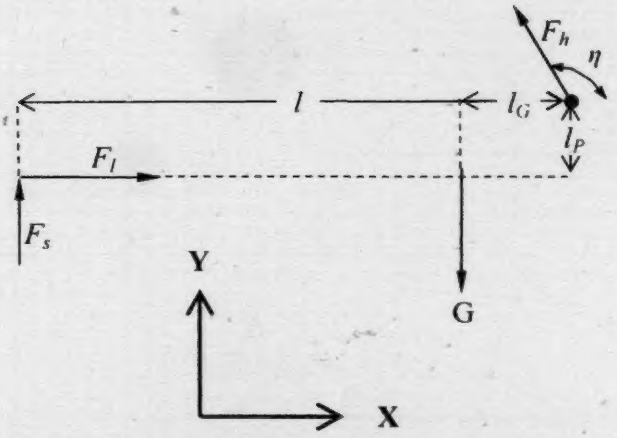

Figure 6-21: Hoist and crowd strain calibration model

$$\Sigma f_x = 0$$

$$F_h \sin(\eta - \frac{\pi}{2}) = F_l \tag{6.6}$$

$$\Sigma f_y = 0$$

$$F_h \cos(\eta - \frac{\pi}{2}) + F_s = G \tag{6.7}$$

$$\Sigma Moment = 0$$

$$Gl_G + F_l l_p = F_s l \tag{6.8}$$

Solving the above equations for F_h and F_l.

$$F_h = G \frac{(l - l_G)}{(l \sin\eta - l_p \cos\eta)} \tag{6.9}$$

$$F_l = -G \cos\eta \frac{(l - l_G)}{(l \sin\eta - l_p \cos\eta)} \tag{6.10}$$

In the static test without face activity, the handle would be held horizontally without load in the dipper, G is the sum of the weight of the handle and dipper, and the handle extension length would be given by the two inclinometers' measurements. Thus, both hoist and crowd forces can be determined via the above equations.

At any instant, the reference bail strain, $\varepsilon_{r\text{-}bail}$, and reference handle strain, $\varepsilon_{r\text{-}handle}$ would be given by

$$(F_h)_{reference} = E_{bail} A_{bail} \varepsilon_{r-bail}$$

$$(F_l)_{reference} = E_{handle} A_{handle} \varepsilon_{r-handle}$$

Rearrange these two equations,

$$E_{bail} A_{bail} = \frac{(F_h)_{reference}}{\varepsilon_{r-bail}} \tag{6.11}$$

$$E_{handle} A_{handle} = \frac{(F_l)_{reference}}{\varepsilon_{r-handle}} \tag{6.12}$$

Thus, in any other case, the hoist force and the crowd force can be determined by using,

$$F_h = E_{bail} A_{bail} \varepsilon_{bail} \tag{6.13}$$

$$F_l = E_{handle} A_{handle} \varepsilon_{handle} \tag{6.14}$$

Where

A_{bail}	Cross-sectional area of the bail bracket.
A_{handle}	Cross-sectional area of the handle sticks.
E_{bail}	Young's modulus of the bail material.

E_{handle}	Young's modulus of the handle material.
ε_{bail}	Strain on bail bracket at the reference position.
ε_{bail}	Strain on bail bracket.
ε_{handle}	Strain on handle sticks at the reference position.
ε_{handle}	Strain on handle sticks.
$(F_h)_{reference}$	Hoist force at the reference position.
$(F_l)_{reference}$	Crowd force at the reference position.

6.4.1.2 Dipper position

The output of the inclinometers was the relative inclination referenced to a neutral direction where the attached inclinometer's center line pointed vertically downwards. The neutral directions for the handle and cable were selected at about the half of the handle and cable angle range to make full use of the measuring range for motion in either direction from neutral:

$$\beta = \beta_{NEUTRAL} + \beta_{MEAUSUREMENT} \tag{6.15}$$

$$\eta = \eta_{NEUTRAL} + \eta_{MEAUSUREMENT}, \tag{6.16}$$

where

β	The handle direction
η	The cable direction
$\beta_{NEUTRAL}$	Orientation where the inclinometer on handle is zero
$\beta_{MEASUREMENT}$	The read-out of the inclinometer on the handle
$\eta_{NEUTRAL}$	Orientation where the inclinometer on the bail is zero
$\eta_{MEASUREMENT}$	The read-out of the inclinometer on the bail

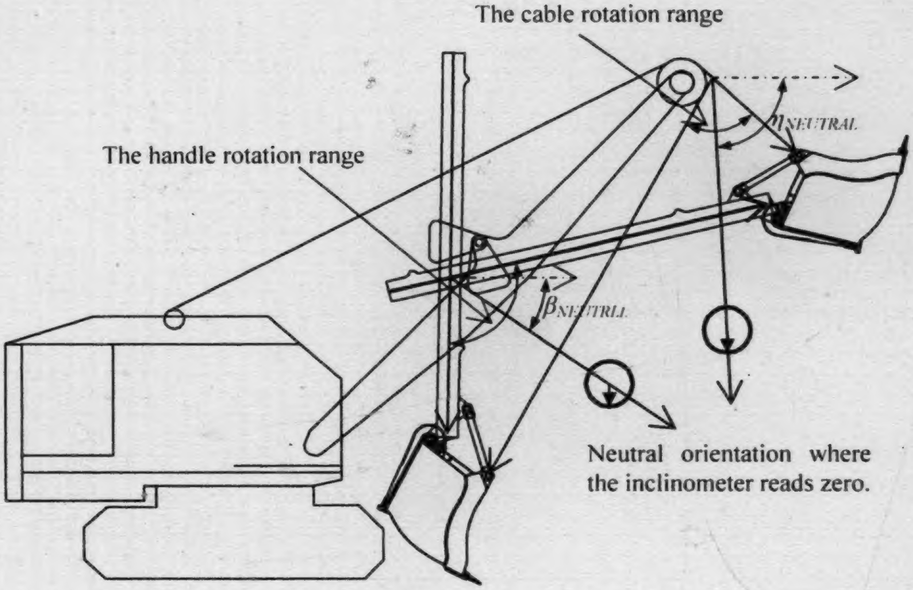
The cable rotation range
$\eta_{NEUTRAL}$
The handle rotation range
$\beta_{NEUTRAL}$
Neutral orientation where the inclinometer reads zero.

Figure 6-22: Handle and cable orientation referenced to a neutral orientation.

As discussed earlier, the bail point can be determined with the handle extension length h and the hoist cable release length l. Figure 6-23 (a) illustrates the Dominion 500 shovel's geometrical configuration. As shown in Figure 6-23(b), $\angle OO'O''=\pi+\beta-\eta$; $\angle OO''O'=\eta-\lambda$; $\angle O'OO''=\lambda-\beta$. Since M is a constant, OO' and $O'O''$ can be determined in $\angle OO'O''$. In $\angle O''P'P$, $O''P$ can be determined by using r_2 and $\angle OO''O'$. Similarly, in $\angle O'A'A$, $A'O'$ and AO' can be determined by using r_1 and $\angle OO'O''$.

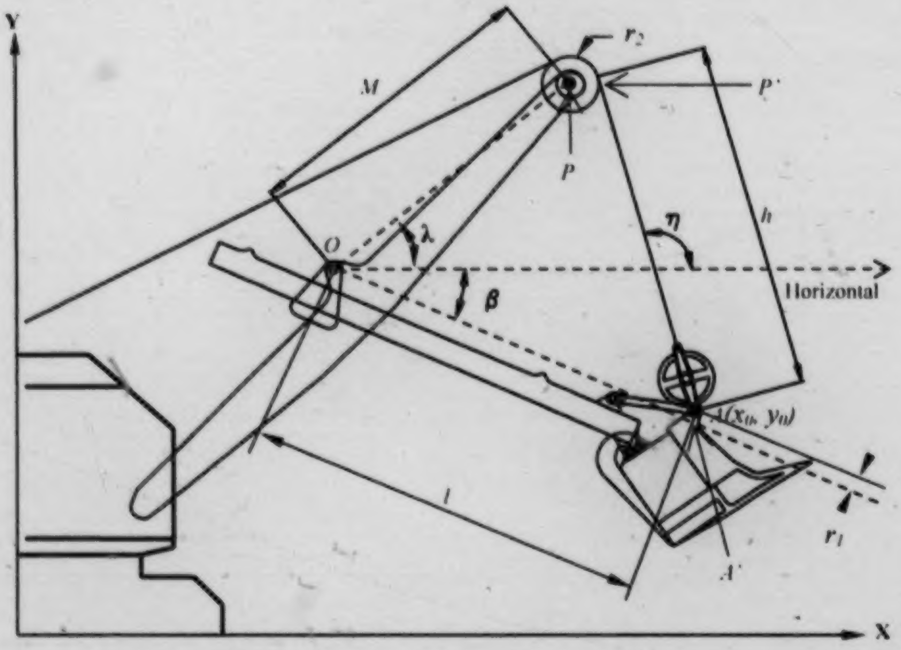

(a) Dominion 500 shovel boom, handle, dipper, cable geometrical relationship

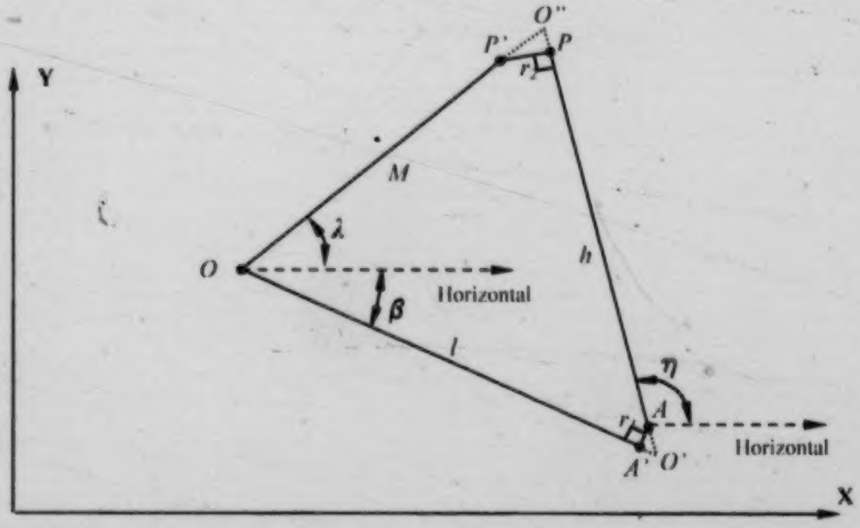

(b) Dominion 500 shovel boom, handle, dipper, cable geometrical model

Figure 6-23: Determination of the dipper-handle position from the inclinometer measurements

Given measurements β and η, the handle extension length l and the hoist cable release length h can be determined by using the following equations.

$$l = OO' - A'O'$$

$$l = \frac{M\sin(\eta - \lambda)}{\sin(\eta - \beta)} - \frac{r_1}{\tan(\beta - \eta)} \qquad (6.17)$$

$$h = O'O'' - O'A - O''P$$

$$h = \frac{M\sin(\lambda - \beta)}{\sin(\eta - \beta)} - \frac{r_1}{\tan(\eta - \beta)} - \frac{r_2}{\tan(\eta - \lambda)} \qquad (6.18)$$

where

h	Cable release length, from the tangent point on the sheave to the bail point
h'	Effective cable release length, from the sheave shaft point to the bail point
l	Handle extension length
M	Distance from the saddle shaft to the sheave shaft
r_1	Distance from saddle shaft (point) to the handle direction (line) passing the bail point
r_2	Sheave wheel radius
x_0, y_0	Coordinates of the bail point in the digging plane
β	Handle angle referenced to the horizontal
η	Cable angle
λ	Boom angle

Thus the coordinates of the bail point (A) can be determined by using Equations 3.9, 3.10 and 3.11.

6.4.2 Visualization of data

The recorded data were transferred into Microsoft Excel, compiled and input into specific visualization software developed with Microsoft Excel VBA, appendix G. Thus, the test data introduced into the visualization software could be retrieved and observed interactively.

In Figure 6-24, the top panel of three illustrates the instantaneous shovel working conditions translated from the sensors' readings. Because the crowd and hoist forces are related to the shovel action and the dipper position, the force plots alone are not sufficient to represent the relationship between the shovel action and the crowd and hoist force reaction at a given instant. In order to represent the relationship, a shovel action animation was programmed in Visual Basic to show the shovel's behavior with two synchronized pointers to indicate the crowd and hoist forces respectively. The instantaneous hoist force, crowd force, and their counterpart face resistance forces, which are the sum of the overall weight and the ground resistance, are illustrated by both graphic vectors and the numerical representation of the direction and scale. Correlating lines (magenta) on the crowd and hoist force plots in the next two panels provided a visual confirmation with the data itself. The second and the third panels present the crowd and hoist force plots for a given recording period, which can be selected by clicking the record name in the record list on the top left.

To allow the specific shovel action to be visualized, scroll bars were applied in the software to enable any instant of shovel activity to be observed. Both the shovel animation and the force charts were synchronized with the scroll bars and pointers. Moreover, for a selected record, three replay modes were provided in the software to demonstrate the continuous change at various face action speeds,

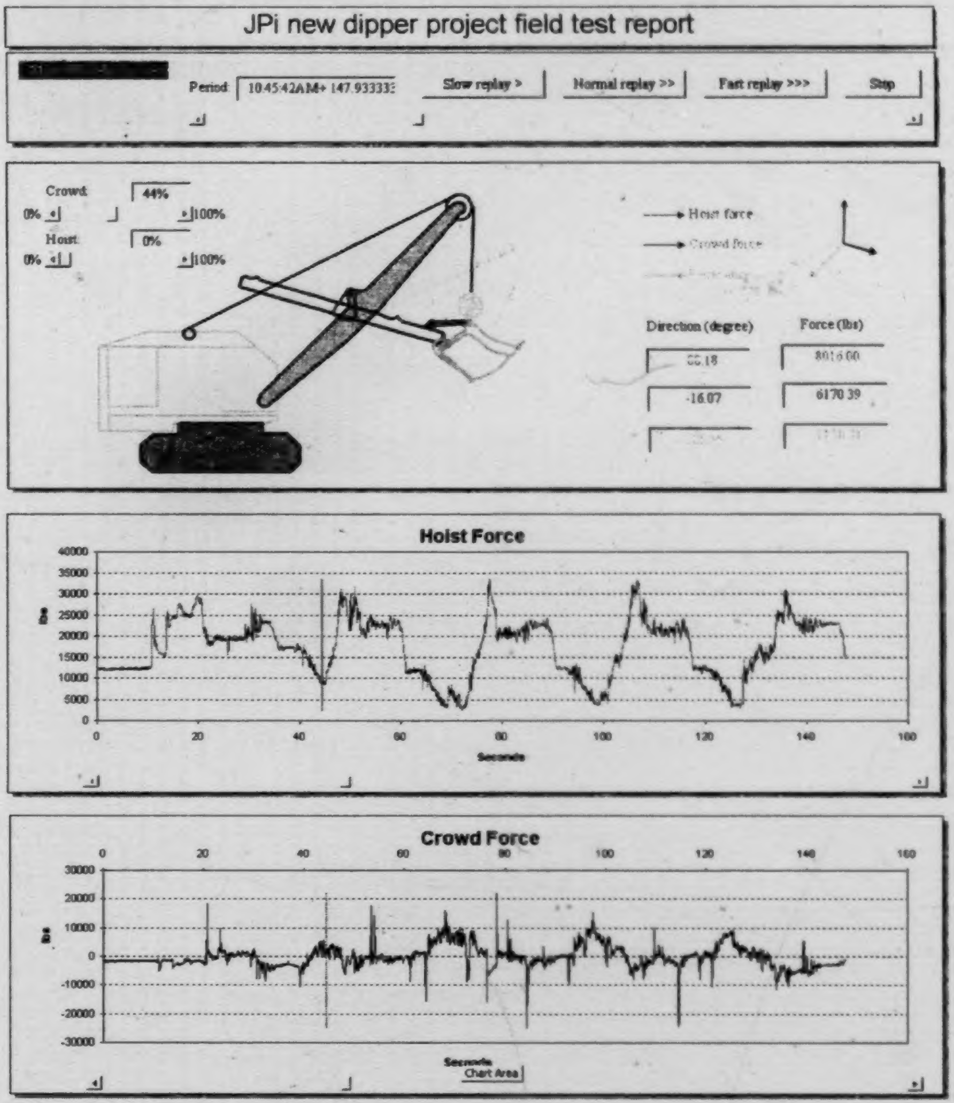

JPi new dipper project field test report

Period: 10:45:42AM+ 147.93333

Crowd: 44%

Hoist: 0%

Direction (degree)	Force (lbs)
66.18	8016.00
-16.07	6170.39
[illegible]	[illegible]

Figure 6-24: Dipper test result visualization modeling software for the new dipper configuration

6.4.3 Test analysis

6.4.3.1 Static test results

As outlined in Figure 6-13, static tests were performed in π/8 handle increments from the tuck position.. As both the original AMSCO dipper and the prototype were the same mass, about 3000kg each, and attached to the shovel handle identically, it is not surprising that the static test results were independent of the dipper front profile.

Figure 6-25 illustrates two cycles of the static test during which the dipper was increasingly raised and held at a range of positions from the tuck to the maximum horizontal stick position, in π/8 handle-angle increments.

The hoist force generally played a much more important role than crowding in implementing the digging actions. For example, in P&H 2800 XPB, there are two 2x533kw motors used for hoisting; there is only 1x300kw motor for crowding. The plots in Figure 6-25 show a similar scale.

The maximum empty suspended mass was found to be about 8,500kg for both configurations. This included the suspended mass contribution of the handle and bail. The horizontal empty suspended mass was found to be about 5000kg.

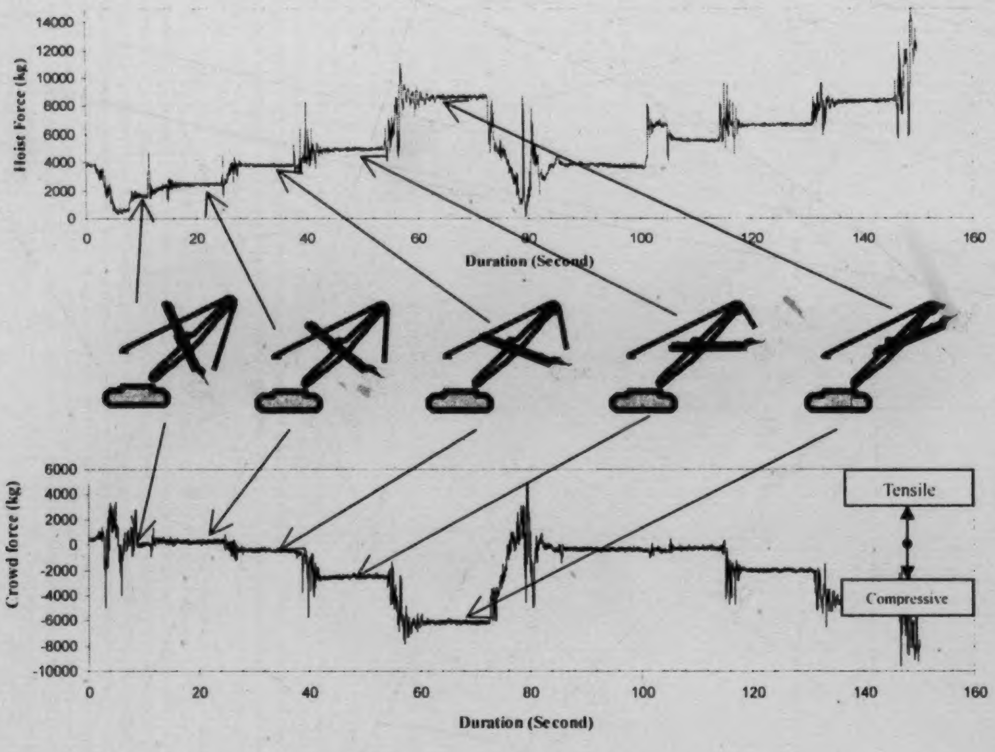

Figure 6-25: Static test without load in the dipper

Further static tests are shown in Figure 6-26; the first two cycles are still the static test without a load in the dipper, and the third is the static test with a proportional capacity load in the dipper, where the dipper was allowed to evenly take material during its sweep action up the face to the horizontal handle position. The increment in the hoist force between the two tests was about 5000 lb, which was directly proportional to the payload in the dipper. The frequent spikes in the crowd force plot are most likely signal noise and face impact forces during the dipper motion; this issue is beyond the scope of this research, but may be of interest for future work.

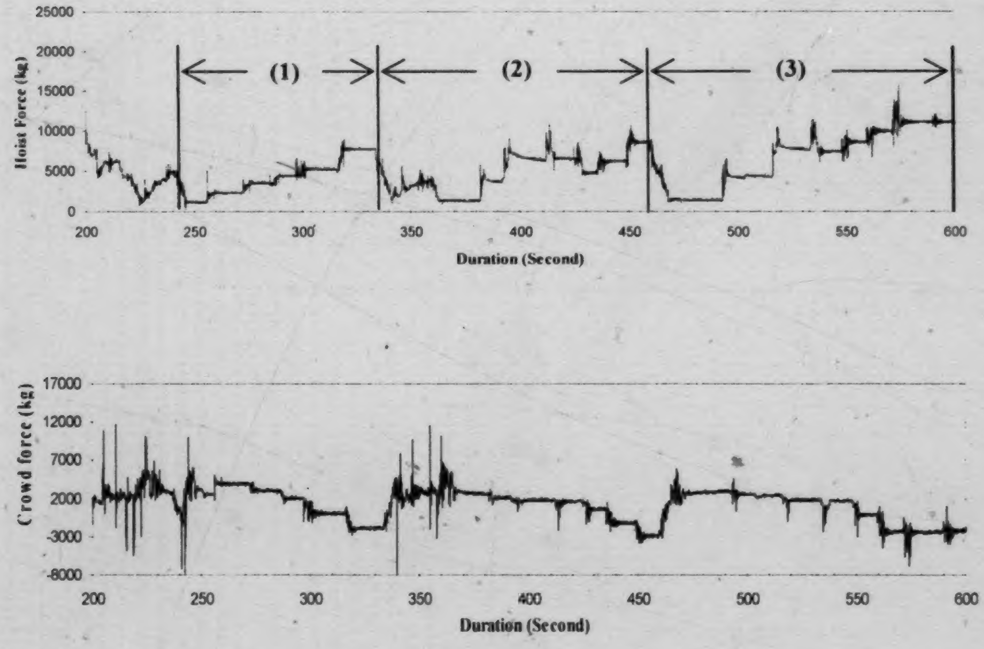

Figure 6-26: Static test without load (first two cycles) and with incremental load in the dipper (third cycle)

In interpreting the crowd force, 'positive' means a tensile force and 'negative' means a compressive force.

6.4.3.2 Comparison of the original to the proposed dipper shape

Some elementary comparisons between the original and concept dippers were made before the field test and some performance comparisons after the test.

(1) Weight and capacity

The original dipper, made of cast steel, had thick walls, while the concept dipper, made of fabricated steel, had thinner walls. Since it is the dipper teeth that break the ground, the thickness of the dipper wall has a minor influence on the hoist and the crowd forces. In this study, it was assumed that the difference in wall thickness would not impact digging resistance.

The original dipper had a nominal capacity of 1.53m^3 (2 yd^3) while the new dipper for the same configuration had a nominal capacity of 2.29 m^3 (3 yd^3) at about the same mass of 3000kg.

Generally, the hoist force required for the concept dipper should be greater than that for the original dipper; the difference should be around 0.76m^3 (1 yd^3) multiplied by the oil sand density.

(2) Geometrical configuration

Figure 6-27 shows that the new dipper had almost the same geometrical configuration as that of the original dipper. The dipper heel was located at about the same position in both configurations referencing to the attachment.

One noticeable difference is that the old dipper has longer teeth than the new one. This results in a difference in the tip point. Because the most important factor that influences the digging resistance is the tooth angle referenced to the handle, the difference in tooth length is not a high concern. Besides the capacity difference, the new dipper was pitched by using the end slots of the original pitch brace while the original dipper used one slot further in, so that the effective pitch brace was shorter, Figure 6-28.

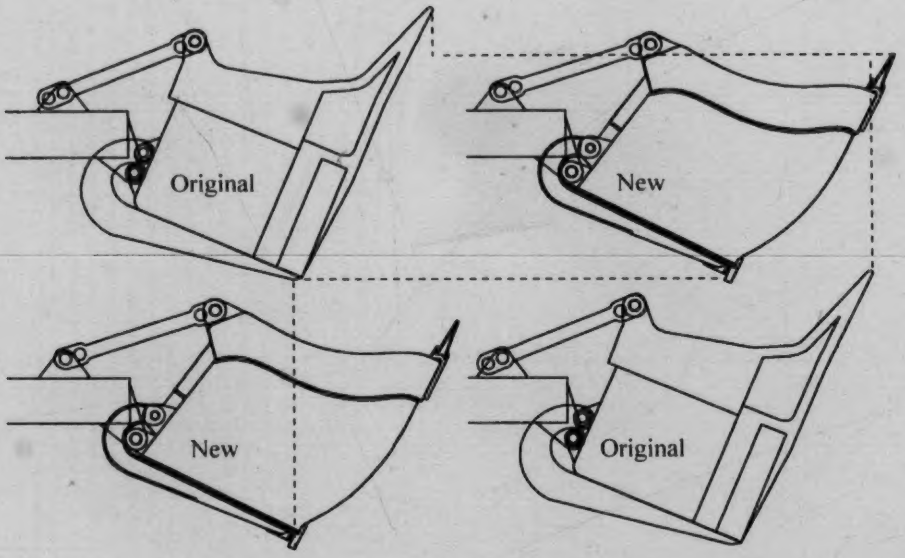

(a) Side view comparison

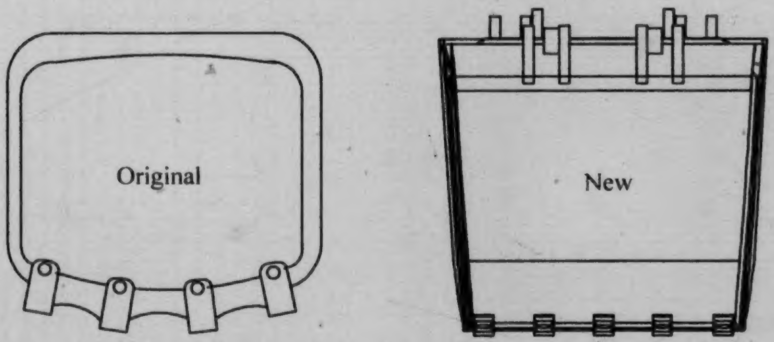

(b) Top view comparison

Figure 6-27: Comparison between the original dipper and the new dipper

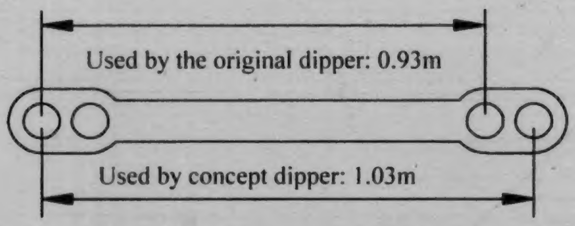
Used by the original dipper: 0.93m
Used by concept dipper: 1.03m

Figure 6-28: Pitch brace used by both the original and concept dippers

(3) Duty cycle key snapshots

As shown in Figure 6-29 and Figure 6-30, 8 key points of a shovel duty cycle were illustrated by the snapshots from the shovel animation. When the dipper is located at the tuck position, the dipper is held by the handle and supported by the ground, thus the hoist force is about to increase from zero and the crowd force reaches a positive peak. While the dipper is moving and filling , the hoist force increases and the crowd force becomes positive. The hoist force reaches a peak when the dipper is at $-\pi/8$ where the crowd force reaches a negative peak. Then the hoist force decreases to a relatively constant level until the dipper dumps its load; simultaneously the compressive crowd force decreases and then stays relatively constant.

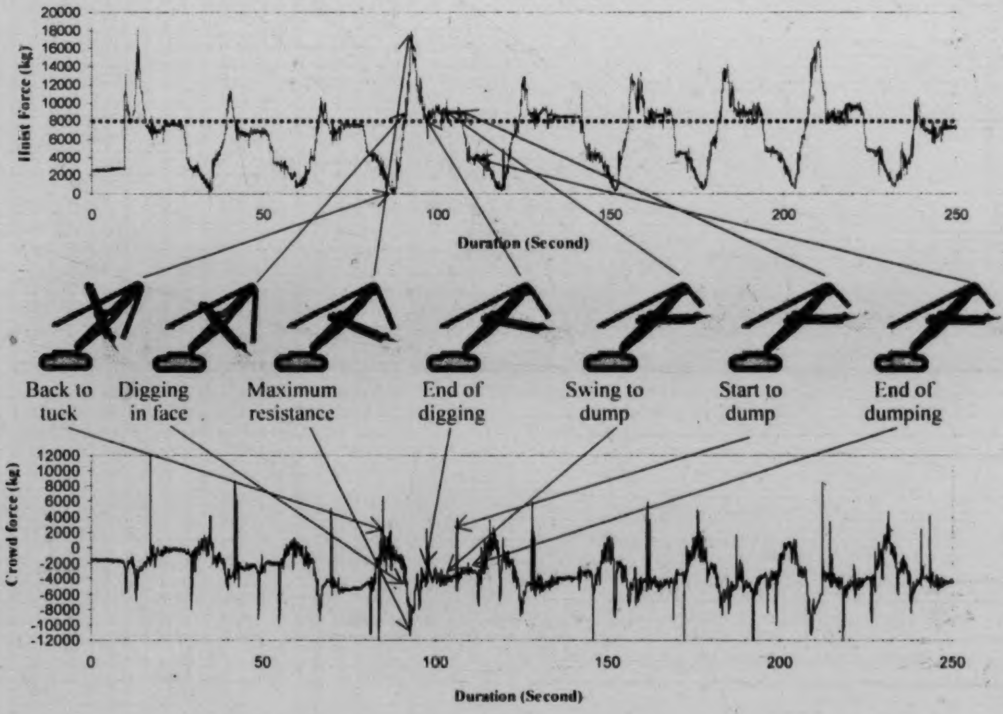

Figure 6-29: Hoist and crowd force plots for the original AMSCO 2yd^3 dipper

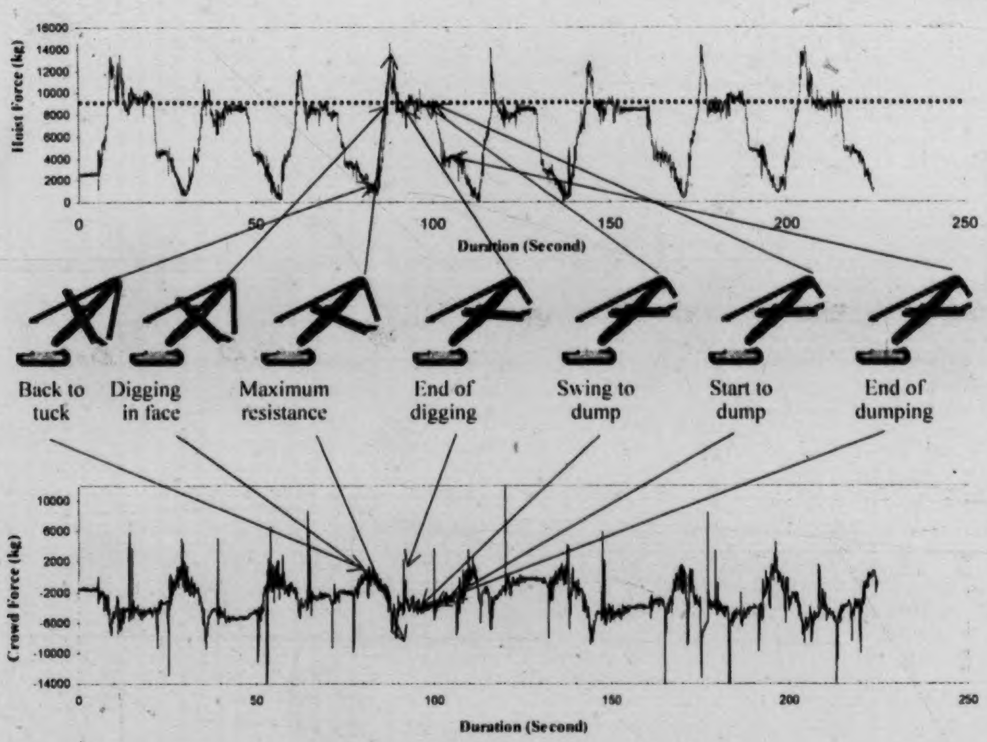

Figure 6-30: Hoist and crowd force plots for the JPi concept dipper

(4) Hoist force

As shown in Figure 6-29 and Figure 6-30, two sets of hoist force plots for the two dippers were compared. It can be concluded that

- The new dipper took a greater load without a significant increase in the face resistance forces. The average stabilized suspended mass (dashed lines) increased from 8,000kg to 9,100kg. The concept dipper has 0.76m^3 (1 yd^3) more capacity. If the extra capacity is filled with loose oil sand, the extra weight is 0.76m^3*2000kg/m^3/1.3=1176kg, where 2000kg/m^3 is the bank density and 1.3 is the swell factor. The difference of 1,100kg is about equal to the extra oil sand weight in the new dipper.
- The new dipper has a lower peak hoist force, which was the sum of the

weight and the maximum digging resistance in the face.

- The hoist force during the digging period did not vary between the two designs; however, the new dipper, being somewhat wider than the original dipper, seemed to have a qualitative smoother hoist force plot.
- Other parts of the plots corresponding to dumping, swinging and tucking are almost identical between the two dippers, which should be expected as the two dipper weights and modes of attachment were matched.

(5) Crowd force

As in Figure 6-29 and Figure 6-30, the two sets of crowd force plots for the two dippers were compared, concluding that

- The crowd force for the new dipper indicated more negative (compressive) values than that of the original dipper, so that the new dipper required more crowd effort to implement the digging action. The teeth on the concept dipper were oriented as an extension of the curvature, rather than providing more of a rake angle (an error in the fabrication process) so that the crowd force required was greater.
- There were less frequent impact peaks that occurred for the new dipper than the original. Since some of them may be due to the digging impact and some others seem to be signal noise for the original dipper in this study, it is unknown as to the exact cause and so no further comment or explanation is possible on these peaks here.

(6) Summary

A summary of the two tests is provided in Table 6-5.

Table 6-5: Dipper test results summary

Performance	Original Dipper	New dipper
Average stabilized suspended mass (empty dipper)	5,000kg	5,000kg
Average stabilized suspended mass (full payload)	8,000kg	9,100kg
Average Peak hoist equivalent mass	14,000kg	13.400kg
Average payload	3,000kg	4,100kg
Average cycle time	29 s	28 s

6.5 Conclusions

At this point, the results from the field test of the two dippers' performance show some advantage of the new concept design over the traditional.

Visually and qualitatively, an improved curved front, from lip to latch keeper results in a smoother interaction with the ground, matched to the shovel's range of motion.

In addition to having a higher capacity, the new concept dipper decreased the hoist force surge so that the digging actions became smoother. The cycle time remained essentially unchanged.

At a small size level, for the given test shovel, the Dominion 500, the new concept dipper appears to perform in a very similar way in which that the original dipper perform. Although the new dipper capacity increased by 50%, the hoist force didn't increase that much. On this aspect, the new dipper performs better.

Chapter 7

Correlating to the bigger size

7.1 Objective

If the test results from the scaled field test showed that the proposed dipper design performance was an improvement over the original design, can we conclude that a new concept ultra-class dipper would perform better than the traditional box shaped ultra-class shovel dipper still in many operations? Here, only ultra class box dippers pre 2001 models were considered as too many new variables are introduced with the post 2001 models of Bucyrus and P&H.

This question can not fully be answered without further analysis and a full ultra size prototype test. However, if a relationship between dipper performance and dipper size from the available data can be established, this would assist in designing a new concept ultra class sized dipper based on the performance and comparison of smaller versions of similar design.

The work shown in Figure 7-1 illustrates an approach to make use of the available shovel performance data to this end.

A literature and industry search for performance data representative of power draw from shovel monitoring systems or hoist and crowd forces from strain gauging. Table 7-1 provides a summary of the available and anticipated data.

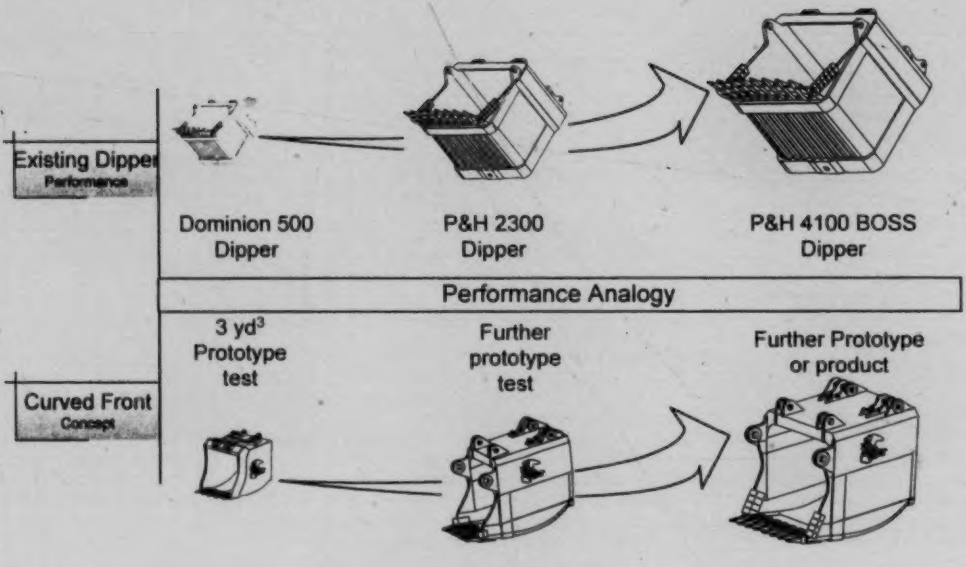

Figure 7-1: Process of scaling

Table 7-1: Summary of available shovel performance data

Status Dipper	Available now	Hoist/crowd force	Power draw	Source
Small size Traditional	Yes	Yes	No	Field test
Small size, Curved	Yes	Yes	No	Field test
Medium size, Traditional	Yes	No	Yes	Literature
Medium size, Curved	No	-	-	Further field test
Ultra class Traditional	Yes	No	Yes	Monitoring results
Ultra class, Curved	No	-	-	Further field test

7.2 Shovel analogy

If minor geometric differences are ignored, the first criteria that allows a relationship to be found between the performance and size of dippers is that the shovels must share the same structure, geometry, and mechanical configuration. Fortunately, over the last few decades, the shovel has not changed much. The only obvious difference is the two different crowding mechanisms: a rope drive from Bucyrus and a gear drive from P&H. As for the accompanying dippers from the two manufacturers, the only important improvement (or revision) is the side to side curvature. This is supposed to reduce the initial ground impact by engaging the teeth in sequence from the center to side. Data for these newer model dippers is not available and only the more traditional dipper shapes have data reported and available here.

All performance data used in this section came from P&H medium-sized or ultra-sized shovels. The performance data from the field test for the small size range were based on the Dominion 500 shovel. Therefore, an analysis is needed to show that the Dominion shovel has either the same or an acceptably similar configuration to the P&H shovel.

Figure 7-2 illustrates the comparison of the geometry configurations: The top right and bottom left projection of the Dominion 500 is scaled by 2.85 times to match the P&H4100.

The projection lines show that the Dominion shovel has a very similar configuration to that of the current P&H shovel, although the Dominion 500 is over 50 years old. The crowd mechanism, double stick and gear drive are also the same. The significant mechanical difference is that the P&H shovel crowd gear is located on the bottom of the handle while the Dominion shovel crowd gear is located on the top of the handle. The significant geometrical difference is that the Dominion shovel handle is proportionally longer than the P&H shovel handle.

From the Dominion 500 field test animation, it was found that except for the static test, the handle was seldom fully extended during the digging cycles. Therefore, the above difference did not appreciably affect the comparison between two shovels.

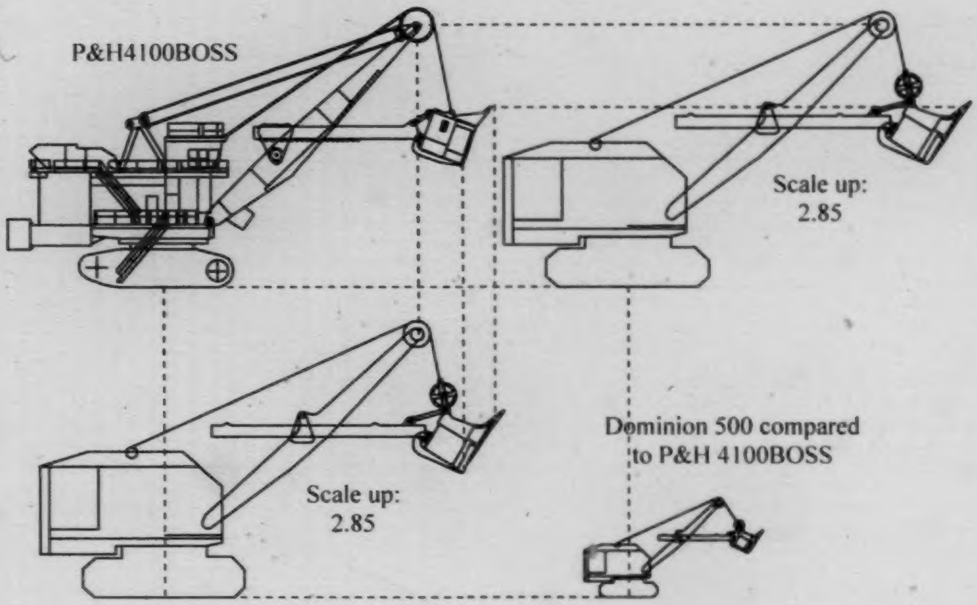

Figure 7-2: Geometrical analogy of P&H 4100 BOSS and Dominion 500, actual scale.

7.3 Performance analogy

7.3.1 Hoist performance

Figure 7-3 shows a segment of the shovel hoist force plot of the Dominion 500 shovel with the original dipper. Figure 7-4 shows a segment of hoist motor current plot for a P&H 2300 shovel (Hendricks and Scoble, 1990). Figure 7-5 shows a segment of hoist motor current plot of the P&H 4100 shovel (Joseph and Hansen, 2002).

Hendricks and Scoble (1989 and 1990) carried out an analysis of shovel performance monitoring. In this work, the electric motor power draws of the P&H 2300 mining shovel were recorded and analyzed. They concluded that the armature current of the motor is proportional to the output torque or force.

For all three performance plots, four phases and eight key points were identified and are marked as such on each.

I. Digging in the face
  (1) Tuck in the face toe
  (2) Peak force due to the dipper, handle and hoist drum inertia.
  (3) Peaking force due to the maximum ground digging resistance
  (4) Digging
II. Out of face and swing to dump
  (5) Hold the dipper and handle and swing to the dumping spot
  (6) Before dumping

III. Dumping

(7) After dumping

IV. Returning to the tuck position.

(8) Hold the dipper and handle, swing to the digging face and lower the dipper to the tuck position.

The significant difference between the hoist force plot and the hoist motor current plots are the current plot has higher magnitude surges when the dipper and handle change motion direction. For example, when the dipper has been lowered to the tuck position to commence a cycle, there is a surge on both types of plot. However, the current surge has a much higher magnitude in contrast to the force surge monitored on the bail. This is because the hoist motor has to resist the inertia of its own rotor, the transmission, the drive drum, the bail and the dipper while the hoist force monitored at the bail was influenced only by the inertia of the dipper and the handle.

From the plot for the P&H 4100 shovel combined with a video record, it was identified that the operator consistently lowered the dipper slightly after the dipper was pulled out of the face. As a result a clear flat segment that shows in other plots the loaded swing phase is not evident.

In a summary, although the hoist current and the hoist force monitored on the bail exhibit slightly different features, these plots show very similar patterns.

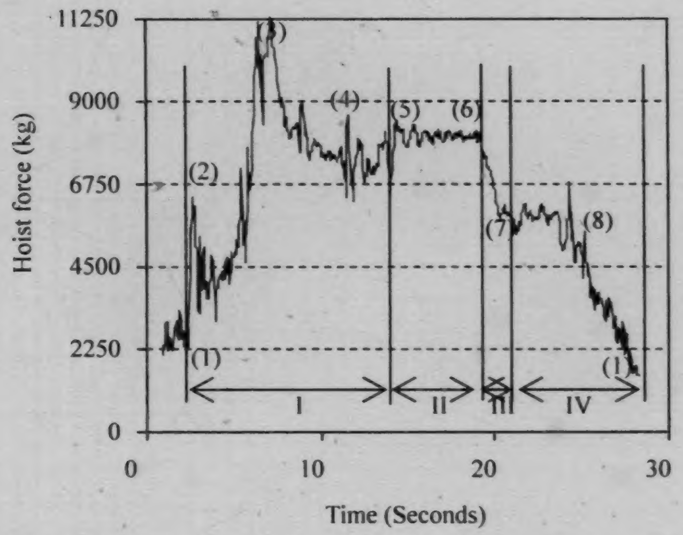

Figure 7-3: A segment of the digging cycle for the Dominion 500 shovel

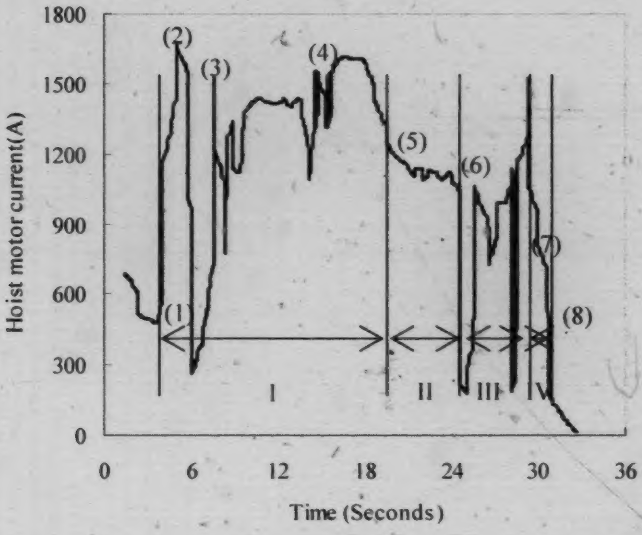

Figure 7-4: A segment of the digging cycle for a P&H 2300 shovel (Hendricks and Scoble, 1990)

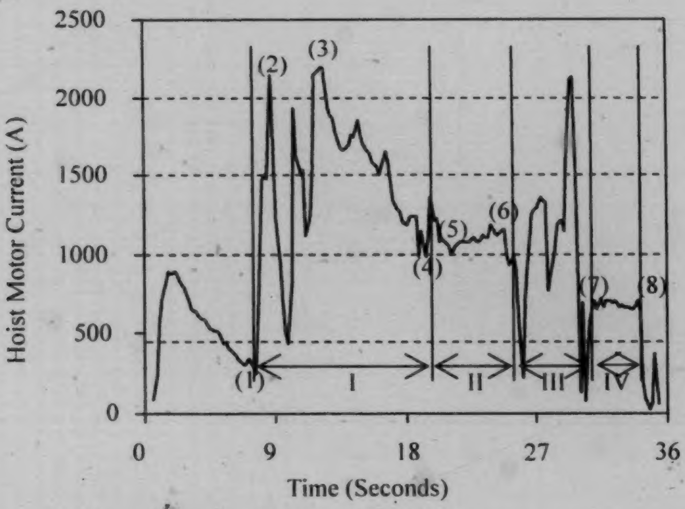

Figure 7-5: A segment of the digging cycle for the P&H 4100 shovel (Joseph and Hansen, 2002)

To compare these hoist performance plots it would be clearer to transform the motor currents to a force. The method that was used to calibrate the strain gauges was also used to transform the current to the force. Similarly, in Figure 7-4 and Figure 7-5, the phase II during which the dipper was fully loaded and the handle was held steadily at the horizontal was identified as a reference. In accordance with Equation 6.9, the ratio of F_h over G with respect to the cable angle η is described in Table 7-2.

Table 7-2: Hoist force in relation to the weight of dipper, handle and material

Cable direction (η)	P&H 2300: F_h/G	P&H 4100: F_h/G
90°	0.85	0.83
95°	0.85	0.83
100°	0.85	0.84
105°	0.87	0.85
110°	0.89	0.87
115°	0.92	0.90

When the handle of the P&H 2300 and 4100 held at the horizontal and fully extended and ready to dump (see Figure 7-6), the cable direction is about 105°. Over a number of the duty cycles, an average hoist motor current for free suspension and peak hoist motor current is obtained. By using the ratios shown in Table 7-2, the suspended load (hoist force) is obtained, thus the peak hoist force was obtained by scaling (see Table 7-3).

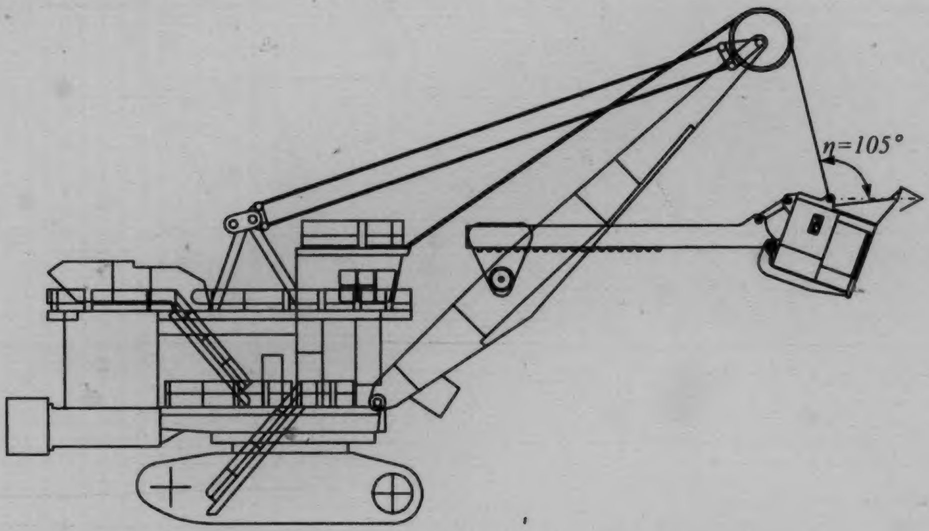

Figure 7-6: P&H 2300, P&H 4100 shovel loaded and suspended position

A summary of the three shovels' specifications and hoist performance are illustrated in Table 7-2. The dipper capacity and the weight of the dipper and handle were taken from the manufacturers' specification sheets, (P&H, 1990 and 2001C). It is assumed that the dippers were loaded at the nominal capacity and for a loose material density of 1700kg/m^3.

Table 7-3: Different sized shovels' specification and performance

(Dominion, 1957) (P&H, 1990 and 2001C)

Spec./Perform. \ Model	Dominion 500	P&H 2300	P&H 4100
Dipper capacity (m^3)	1.53 (2yd^3)	23 (30yd^3)	44 (57.5yd^3)
Dipper width (m)	1.2	2.9	3.6
Payload (kg) (1700kg/m^3)	2,600	39,000	75,000
Dipper handle weight (kg)	5,400	65,000	119,500
Suspended load (kg) (loaded)*	8,000	90,480	165,325
Peak hoist force (kg) (Digging)**	14000	125,280	285,560

* When the handle is held at the horizontal and the dipper is fully loaded and free of the ground.

** When maximum digging resistance occurs.

Using the data from Table 7-3, the relationships between dipper capacities, suspended load and peak forces were plotted in Figure 7-7. The two curves show that the hoist force is proportional to the dipper capacity. In other words, given a material, the hoist performance and the shovel size has a linear relationship.

Figure 7-8 illustrates the peak hoist force increment rate from the free suspended load (hoist force) of the three shovels. The definition of the increment rate in the figure is given by

$$IR = (H_p - H_s)/H_s * 100\% \qquad (7.1)$$

Where

IR increment rate

H_p peak hoist force

H_s suspended load

The P&H 2300 shovel exhibited a lower increment rate. This can be explained as the P&H 2300 shovel data used in the study were from a different mine site where the ground material was relatively easier to break.

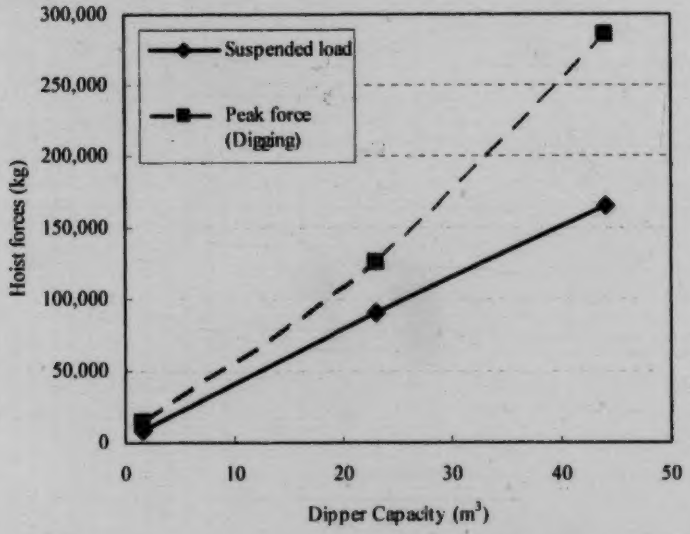

Figure 7-7: Dipper capacity versus the suspended load and the peak force

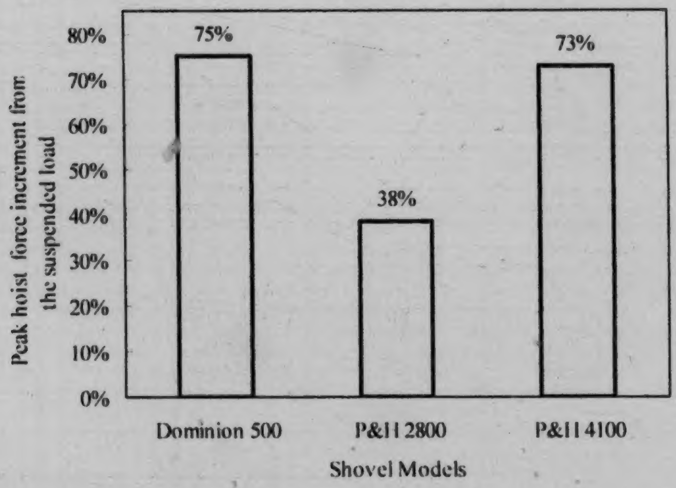

Figure 7-8: Different shovels' peak hoist force increment rate

7.3.2 Crowd performance

During the digging cycle, most of the energy was consumed in hoisting; only a small portion of the energy was consumed in crowding. Despite this, the crowding performance of each shovel should be reviewed.

Figure 7-9 illustrates a segment of the hoist force crowd for the Dominion 500 shovel. Here the tensile forces are positive and the compressive forces negative. Figure 7-10 illustrates a segment of the hoist motor current plot for the P&H 2300 shovel.

Generally, the two shovels were operated very similarly, with the crowd force and the crowd motor current plots exhibiting similar patterns. Like the hoist motor current plot, due to the inertia effect of the motor and transmission, the crowd motor current plot shows higher frequency and magnitude of fluctuation.

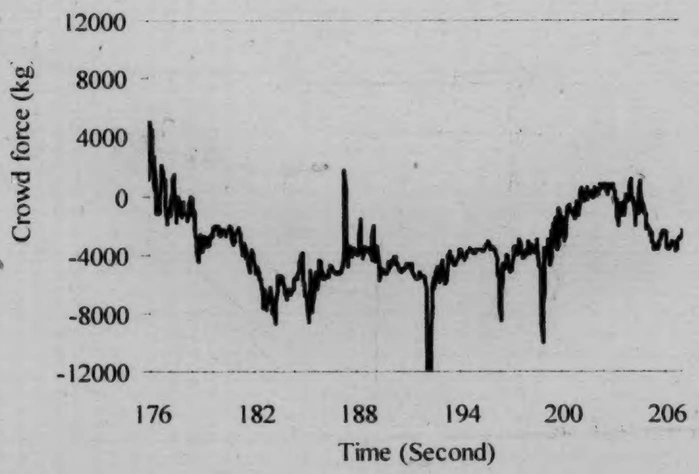

Figure 7-9: A segment of the crowd force plot for Dominion 500 shovel

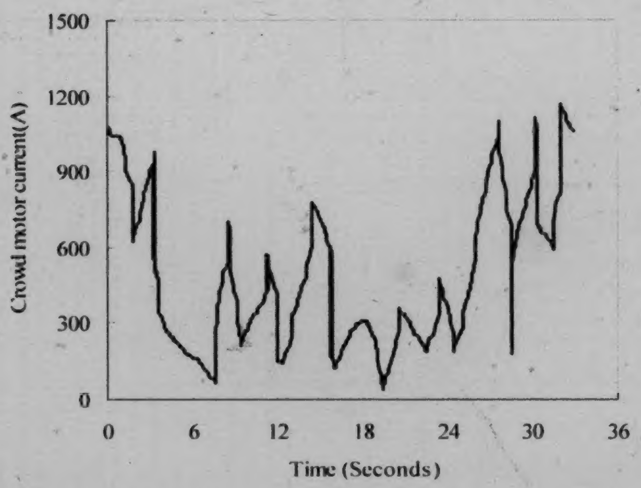

Figure 7-10: A segment of the crowd motor current plot for the P&H2300 shovel (Hendricks and Scoble, 1990)

7.4 Normalized performance

Figure 7-11 illustrates three hoist performance plots for three different shovels, the hoist force plot for the Dominion 500 shovel and the hoist motor current plots for the P&H 2300 and 4100 shovels. Although some shape similarity can be seen in the three separate plots, it is hard to identify common characteristics due to different units and scales.

In this evaluation, the three sets of hoist performance data that are of varying shovel size data source were normalized by using a normalizing factor that is the free suspended load expressed as hoist force or motor current. The average free suspended force or motor current for the different shovels are summarized in Table 7-4.

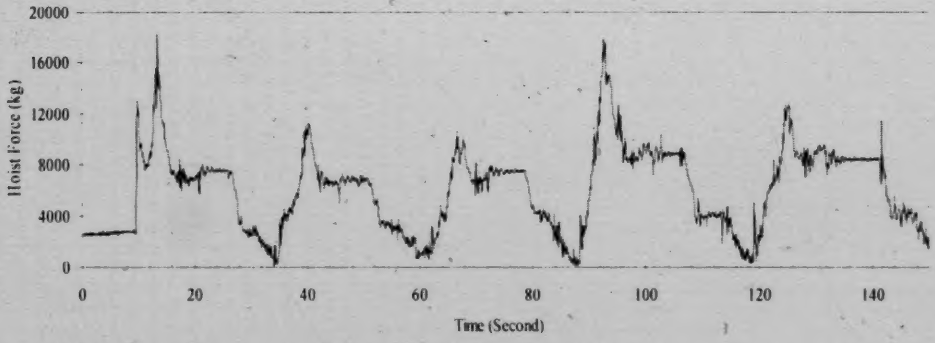

(a) Dominion 500 shovel hoist force plot

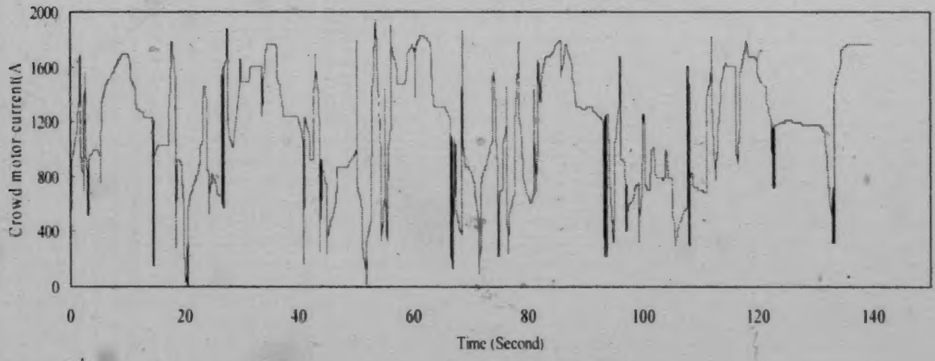

(b) P&H 2300 shovel hoist motor current plot

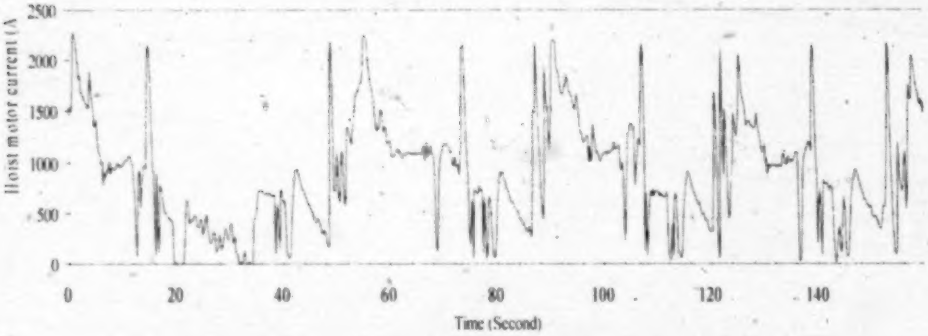

(c) P&H 4100 shovel hoist motor current plot

Figure 7-11: various shovel hoist performance plots

Table 7-4: Shovel performance data normalizing factor

Shovel performance Data	Normalizing factor	Units
Dominion 500 hoist force	8000	kg
P&H 2300 hoist motor current	1300	A
P&H 4100 hoist motor current	1100	A

The resulting normalized performance data obtained were plotted in Figure 7-12, enabling the three sets of data to be compared in the same chart.

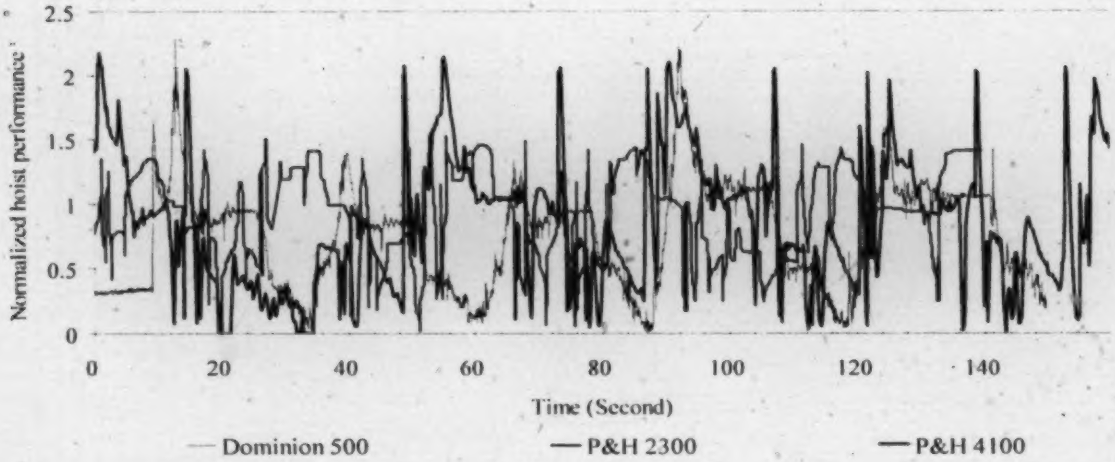

Figure 7-12: Dominion 500, P&H 2300 and 4100 shovel normalized hoist performance index plots

From Figure 7-12, it is obvious that the Dominion 500 and P&H 4100 shovels have very similar digging cycle shapes. Some cycles are almost identical. The P&H 2300 has smaller peak values than the other two shovels. This is likely also due to the different working geology conditions.

7.5 Conclusions

The review of several models of mining shovel, from small to ultra class size, has shown that shovels have not changed much with respect to geometric configuration and driving mechanisms. The literature on shovel performance shows that the performance indicators such as the hoist force or motor current maintain a proportional relationship as the unit size increases.

Based on above discussion, one encouraging message is that the performance of a revised dipper design for the same working geology may not be affected much by the size of the shovel and dipper. From the performance of the prototype dipper at 1/20 of the ultra class dipper size, a larger size of the same design has the potential for similar performance. Although only a physical test can ultimately prove this hypothesis, this analogy minimizes the initial risk of moving to an ultra class dipper.

Chapter 8

Conclusions

8.1 Main conclusion

8.1.1 Dipper-ground matching

This study proposed a curved front wall dipper. One of the outstanding features of the dipper is that the dipper would better match the range of the motions of a cable shovel. Mathematically, a logarithmatic spiral curve was adopted in the conceptual design for digging oil sand.

The typical cable shovel digging trajectories operating in cutting oil sand is approximated by a spiral curve. The logarithmatic curve used as the profile of the front wall of the dipper was derived from the dipper motion parameters and the original dipper configurations. One significant benefit of the curved shape is that the dipper retains a consistent position relative to the ground profile. This means less dynamic impact from digging actions. The curved shape maintains the dipper rake angle while keeping the heel out of the face. This leads to a reduced digging resistance without shortening the dipper's life.

8.1.2 Less interference

The curved front wall design reduced both the dipper-ground and dipper-track interference. An important feature of the curved front wall is that the heel is retracted naturedly without decreasing the rake angle.

Dipper-ground and dipper-track interference is a critical issue for the cable shovel to maintain high production and infrequent maintenance intervals. Both types of interference or collision will result in damage on the dipper heel, while dipper-ground inference increases digging resistance. The dipper-track interference will lead to an improved dipper tuck position preventing the shovel from colliding its tracks.

With the design, both types of collision problems appear to be improved. A closer tuck position and a greater heel-ground clearance are obtained.

8.1.3 Prototype field test result

A smaller scaled shovel (Dominion 500) was able to operate with a non-traditional dipper shape. The curved front wall dipper that increases capacity by 50% was successfully attached to and operated by the shovel. This enables a comparison of the two dippers in identical operating conditions.

The field test output showed that the new concept dipper did not introduce greater digging resistance in contrast to the original dipper, although the dipper capacity was increased by 50%. The test also showed smoother hoist force performance with the new dipper compared to the original.

The crowd force for the new dipper was larger than that for the original one. Although this was probably introduced by the wrong tooth direction, more study should be carried out to confirm the impact of the curved front to the crowding system.

8.1.4 Scaling performance trends

The sheer size and fabrication expense of an ultra class dipper dominates over validation of a new concept dipper through scaled prototype tests. By reviewing and analyzing performance data from a series of shovel sizes, the relationship between shovel size and shovel performance was inferred. This gives confidence in reducing the risk for a developer to scale a new design from a small prototype size to one that is larger.

8.2 Research contributions

8.2.1 Shovel simulation formulation and software

A kinematic shovel model that accurately represents shovel digging behavior has been developed in this thesis. The kinematic equations have been derived and are ready to use for further research. Based on the kinematic model, a dipper-ground interaction model was developed.

A series of simulation software were developed in this study; a group of MatLab programs for shovel kinematics, shovel digging simulation software and test data visualization software. The kinematic and the shovel digging simulation software were developed for analyzing shovel digging behavior in an un-blasted face. These tools will be useful for further research in dipper design.

8.2.2 A curved dipper concept

Based on the earlier work of the sponsor, JPi, a curved dipper concept was introduced and the prototype put to task in a field test. The design primarily included:

- A curved front wall using a logarithmatic spiral formula.
- A skewed back wall

8.2.3 A dipper design approach

The contribution of dippers to shovel production has historically not been fully investigated by shovel manufacturers or researchers. A specific model was developed based on an existing ultra-class shovel operating in oil sand conditions. The simulation work of this model led to a better understanding of the dipper's performance.

Three dimensional solid modeling techniques were adopted to draft the dipper for fabrication from the modeling output.

The prototype test procedures outlined in the study provide a logical methodology to set up a test, collect and process the data. It was shown that using two inclinometers to locate the dipper position was easier to implement than the traditional method that uses two displacement sensors for the handle extension length and the cable release length.

The dipper design approach is illustrated in Figure 8-1.

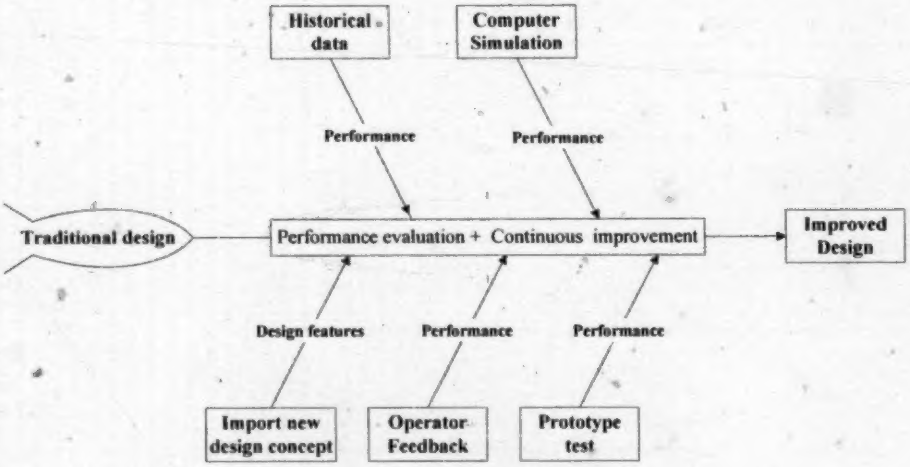

Figure 8-1: The dipper design approach

8.3 Future work recommendations

8.3.1 Future shape concept

Shovel manufacturers suggest that a side-to-side (laterally) curved dipper gradually engages the ground so that digging resistance increases more gradually than for a flat front dipper. Here the tooth-to-heel (longitudinally) curved dipper reduces the attack angle while continuing to protect the dipper heel. The potential of a combination of these two features in a double curved dipper concept has been suggested by the project sponsor with a combination of both lateral and longitudinal curves. This concept is reinforced by the common experience that a bowl-shaped hand yard shovel works better with clay and soil while a flat shovel works better with dry sand and gravel. As shown in Figure 8-2, a double curved front element has already been taken to the conceptual shape stage. This is outside the scope of this thesis. The biggest drawback of the concept is the complexity of fabrication, and for an ultra class dipper, the problem would be magnified during assembly. The dimensions of an ultra class dipper in this format are beyond the maximum casting capability of foundries so that the front wall would have to be cast in pieces and welded together. This would certainly require considerable structural integrity considerations.

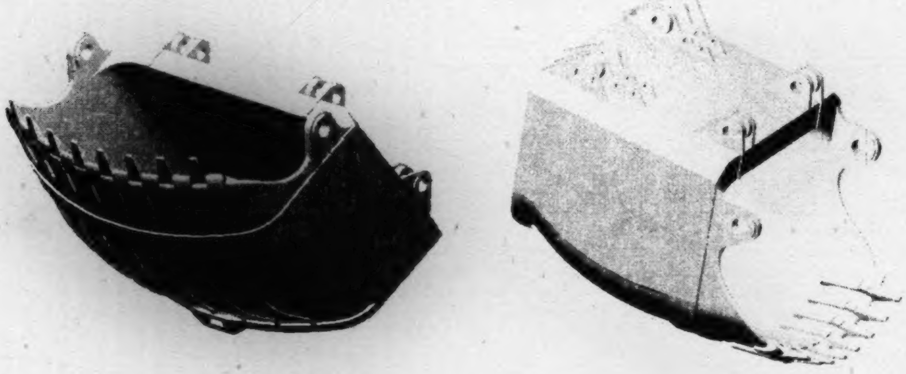

Figure 8-2: A double curved dipper model (courtesy JPi)

8.3.2 Structural considerations

This research did not cover the analysis of the material, strength, and thickness of the dipper body. Some in-depth work should be done to improve the suggested design based on the stress distribution while digging. Strain data was collected during the field test from gauges mounted on the body of the test dipper and is available as a starting point for the next research project that will follow this work. The three-dimensional solid model already available through this work makes this task easier with the application of appropriate boundary conditions. The field-test results and the FEA results could then be correlated accordingly to improve the design.

List of References

ACARP, 2002, Improved Understanding of Shovel Dippers and Processes, Australia Coal Association Research Program,

Blouin, S., 2001, Review of resistive force models for earthmoving processes, Journal of Aerospace Engineering, Vol. 14, No 3, pp.102-111, July

Boccafogli, A., Busatti, G., and Gherardi, F., 1995, Experimental evaluation of cutting dynamic models in soil bin facility, Journal of Terramechanics, Vol.29, No.1 , pp95-105.

Bucyrus, 2003, Bucyrus 495 BII HF cable shovel specifications sheets, Bucyrus International Inc.

Caterpillar, 2005, Cat Ground Engaging Tools Parts Sales Kit, 8th Edition,

Coal Age, Mar 1, 2001, PRIMEDIA Business Magazines & Media Inc.

Collins, P.M., 2005, Geomechanical Effects on the SAGD Process, SPE/PS-CIM/CHOA International Thermal Operations and Heavy Oil Symposium.

Coulomb, C.A., 1776, Essai sur une application des regles des maximis et minimis aquelques problems de statique relatifs a l'architecture, Memoires de Mathematique et de Physique, presentes a l'Acadamie royale des Sciences, par divers Savant, et lus dans les Assemblees, Paris, Vol. 7.

Daneshmend, L. and Hendricks, , 1993 C., Design of a mining shovel simulator, Innovative Mine Design for the 21st century, Bawden & Archilbald (eds), Balkema, Rotterdam

Dominion, 1957, Dominion 500 Shovel Manual, Dominion Inc, Montreal

Dusseault, M.B., 2001, "Comparing Venezuelan and Canadian Heavy Oil and Tar Sands", the Petroleum Society's Canadian International Petroleum Conference, Calgary AB, June 12-14, 2001

Dusseault, M.B., Morgenstern, N.R., 1977, Shear strength of Athabasca oil sands, Can. Geotechn. J. 15., pp. 216–238

Dusseault, M.B. and Morgenstern, N.R., 1978, "Characteristics of natural slopes in the Athabasca Oil Sand" , Canadian Geotechnical Journal, Vol. 15

Dusseault, M.B. and Morgenstern, N.R., 1979, Locked Sands, Quarterly Journal of Engineering Geology & Hydrogeology; May 1979; v. 12; no. 2; p. 117-131

ESCO , Maxi-Pro shovel dipper brochure, ESCO, 2002

Gill, W.R. and Vanden Berg, G.E, 1968, Agriculture Handbook, Number 316: Soil dynamics in tillage and traction, Agricultural Research Service, U.S. Department of Agriculture, Washington DC.

Godwin, R.J. and Spoor, G., , 1977. Soil failure with narrow tines on friction soils, Journal of Agriculture Engineering Research, Vol. 22, pp.213-218

Hadjigeorgiou, J. and Poulin, R. , 1998, Assessment of ease of excavation of Surface mines, Journal of Terramechanics, Vol.35, No.3 , pp. 137-153.

Hartman, H.L., 1992, SME Mining Engineering Handbook, 2 Vols., SME, 1992.

Henami, A. and Danesmend, L, 1992, Force analysis for automation of the loading operation in an L-H-D loader, Proceeding of the IEEE Conference on Robotics and Automation, Nice France, May.

Hendricks C. & Scoble MJ, 1990, Post-blast evaluation through shovel, erformance monitoring, Proc. of the Conf. on Explosive and Blasting Techniques, , Orlando, Florida, 227-243

Hendricks, C., Scoble, M.J., and Peck, J., 1989, Performance Monitoring of Electric Mining Shovels. Trans. Inst. Mining Metall. Section A: Mining Ind. 98, pp.151-159

Hendricks C. et al., 1988, Electric mining shovel diggability studies. In mine planning and equipment selection: proceedings of an international symposium, Calgary November 1988 Singhal R.K. ed. (Rotterdam: Balkerma), pp327-333.

Hendricks, C., Scoble, M.J. and Peck, J., 1989, Performance monitoring of electric mining shovels, Transaction of Institute of Mining and Metallurgy . Section A: Mining Ind. 98 (), pp.151-159

Hensley, 2003, K1150-20 tooth adapter specifications. Hensley industries, Inc.;

Hettiaratchi, D.R.P. &Reece, A.R, 1967, Symmetrical three-dimensional soil failure, J. Terramechanics, Vol.4, No. 3, pp. 45-67

Hettiaratchi, D.R.P. &Reece, A.R, 1974, The calculation of passive soil resistance, Geotechnique, Vol 24, No. 3 pp. 289-310

Howarth, D.F., Just, G.D. and Runge, G.A., 1987, Dragline bucket filing characteristics, Transaction of institute of Mining and metallurgy (Section A: Mining Industry), 96, October, pp. A189-192.

Jarzebowski,A., Maciejewski, J., Szyba, D., and Trempczyski, W. , 1994, Experimental and theoretical analysis of a cohesive soil shoving process (the optimization of the process), Proceeding of 6th European ISTVS conference, Wien , Austria, pp.731-740.

Joseph T.G. and Hansen G.W. 2002, Oil sand reaction to cable shovel motion, CIM bulletin, Vol 95 pp62-64

Joseph, T.G, Demoobed, A. and Shi, N., 2003, Shovel-ground duty cycle performance indicators, Preceding of CIM conference 2003, Oct, Saskatoon

Joseph, T.G. and Hansen, G., 2001, JPi concept dipper development blueprint, JPi, Internal Report

Joseph, T.G., 2001, Flared bucket design, Specification for O&K shovel brochure, JPi internal report.

JPi shovel performance analysis software, 2005, JPi geo-industry engineering consultants, Edmonton

Kosar, KM ,1989, Geotechnical properties of oil sands and related strata. Ph.D. Thesis, Department of Civil Engineering, University of Alberta, Canada

Kuhn, G. and Wardecki, N. , 1983, Anpassung der ladeschaufel von hydraulicbaggernan das felshaufwerk, BMT, No.10 October.pp.464-470.

Labutin. V.N., Mattis, A.R. and Kostrykin, V.N. , 1993, Study of loading bucket penetration into rock stockpile, Journal of Mining Science, No.5 pp.31-36.

Martin, J.W., 1982, Surface Mining Equipment, Martin Consultants, Inc.

McKyes, E. , 1985, Soil Cutting and Tillage, Elsevier.

Member, A.D., 1986, Analytical study of the forces acting on front attachment of shovel, Journal of MI, pp46-48, 1996.

Mine & Quarry Editor, 1987, Develompment of Hydraulic Excavators for Quarrying Applications: Part II, Mine & Quarry, Marchm pp.22-24.

Morgenstern, N.R., and Scott, J.D. ,1997,. "Oil Sand Geotechnique." Geotechnical News, Special Commemorative Edition, 15(4), 102-109.

Muro,. T., Fukagawa, R., and Watanade, H. , 1993, Experimental study on excavation forces of bucket shovel against soft rock mass, Proceeding of Civil Engineering Conference, Japan, No.462/VJ-18, pp.73-81.

Naational Energy Board, 2000, Canada's Oil Sands: A Supply and Market Outlook to 2015, Calgary AB, October 2000.

NI, SCXI-1000 Chassis, SCXI-1000 user manual, 2005, National Instrument

NI, SCXI-1314 mount terminal, SCXI-1314 user manual, 2005, National Instrument

NI, SCXI-1520 strain gauge module, SCXI-1520 user manual, 2005, National Instrument

Ohde, J., 1938, Theory of soil pressure with particular reference to its distribution, Bautechnic, 16, 1938.

Osman, M.S. . 1964, The mechanics of soil cutting blades, Journal of Agricultrure Engineering Research, Vol. 9, No. 4, pp.313-328

P&H MinePro Services, 1990, P&H2300XP electrical shovel specification sheet, Harnischfeger.

P&H MinePro Services, 2001A, Peak performance dippers practices, Harnischfeger,.

P&H MinePro Services, 2001B, Peak performance excavator selection, Harnischfeger,.

P&H MinePro Services, 2001C, P&H4100BOSS electrical shovel specification sheet, Harnischfeger.

Payne, P.C.J. , 1977, The relationship between the mechanical properties of soil and the performance of simple cultivate implements, Journal of Agriculture Engineering Research, Vol. 14 No.2, pp.43-58.

Ponamgi, M. K. , Manocha, D. and Lin, M. C., 1995, Incremental algorithms for collision detection between general solid models. Proceeding of. ACM Siggraph Symposium Solid Modeling, pp. 293-304.

Reece, A.R. , 1965, The fundamental equation of earth–moving mechanics, Symposium on Earth-moving machinery, Vol. 179, No. 3F, pp.16-22.

Rowlands, J.C. and Just G.D. , 1992, Performance characteristics of dragline buckets, Proceeding of the third large open pit mining conference, Mackay, pp.89-91.

Sherborne Schaevitz, AccuStar®, Electronic inclinometer user manual, United Kingdom

Shi, N. and Joseph, T.G. , 2004, Cable Shovel Simulation leading to A Novel Dipper Design, Proceeding of CIM conference 2004, Edmonton, May.

Showa, NE-FA-5-120-11 strain gauge Specification, Showa measuring instrument, Japan)

Singh, S, 1995, Synthesis of Tactical Plans for Robotic Excavation, Ph.D thesis, the Robotics Institute, Carnegie Mellon University

Singh, S. , 1997, The state of the art in automation of earthmoving, ASCE Journal of Aerospace Engineering, Vol. 10, No. 4, October.

Solidwork, Solidwork 2003 user manual, Solidwork, 2003.

Spektor, M. and Katz, M,, 1985, Experimental study if frontal resistance force in soil cutting, Journal of Terramechanics, Vol.22, No3, pp. 127-133, 1985.

Suncor Energy, Inc., 2005, JPi bucket test location data sheet.

Terzaghi, K. , 1943, The soil mechanics, Wiley, New York.

Whittingham, D.J. , 1971, Dipper design and attachment, Mining Congress Journal, September, pp.72-74.

Wolf, M. , 2001, Electric shovels, Toploaders, World Mining Equipment

Zelenin, A.N. and Balovnev, V.I. and Kerov, I.P. , 1985, Machines For Moving The Earth, American Publishing Co. Private Ltd., New Delhi, India

Appendix A

MatLab codes for shovel kinematic models

A.1 Shovel geometrical model and constants

%File Name: shovel_constant.m
%Use: be called by other kinematic simulation programs to set up shovel geometrical model and constants.
%Description: this program initializes the shovel geometrical parameters as MatLab variable.

```
%global constant
global ncount
global boom_angle
global pivot2sheave
global sheaveradius
global joint2handle
global pivot_x
global pivot_y
global sheave_x
global sheave_y
global min_angle
global max_angle
global min_handle
global max_handle
global min_hoist
global max_hoist
global saddle_gear_radius
global bench_height
global min_teeth_position
global min_cutting_handle
global soil_profile
global cutting_point
global dipper_heel
global door_end
global dipper_lu
global boom_font_angle
global boom_front_point
global track_front_length
global crawler_width
global track_width
global crawler_length
global dipper_width
global front_track_center
global front_track_radius
global front_track_slope_start
global front_track_slop_end
global track_height
global crawler_xy
global dipper_far_range
global relocation_step
global cutting_height
global dipper_volume
global loose_factor

ncount=100;
boom_angle=(42.7/180)*pi;
pivot2sheave=14.312;
sheaveradius=1.287;
joint2handle=2.77;
pivot_x=8.48;
pivot_y= 9.98;
sheave_x=18.998;
sheave_y=19.686;
min_angle=-(90+13)/180*pi;
max_angle=20/180*pi;
min_handle=6.359;
max_handle=13.159;
min_hoist=3.06;
max_hoist=19.171;
saddle_gear_radius=0.46;

bench_height=15;

bench_angle=50/180*pi;
min_tuck_position=9.414;
min_cutting_handle=6.647;
cutting_point=[2.868;0.385];
dipper_neck=[1.897;-1.068];
dipper_heel=[0.805;-4.04];
dipper_front_points=[dipper_heel,dipper_neck,cutting_point];
door_end=[-2.85;-2.903];
dipper_backtop=[-1.342;0.332];

boom_font_angle=49.2/180*pi;
boom_front_point=[9.777;8.526];

track_front_length=5.24;
crawler_width=12.78;
track_width=3.505;
crawler_length=11.58;
dipper_width=3.6;
front_track_center=[4.02;1.22];
front_track_radius=1.22;

front_track_slope_start=[2.496;2.86];
front_track_slope_end=[4.485;2.337];
```

```
track_height=3.03;

crawler_xy={'ARC',[4.4849;2.3371;6.39],[4.1287;0;6.39].[4.020;1.2091;6.39],1.22
'LINE',[4.1827453146371454;0.0;6.39],[-3.3832433291252602;0.0;6.39],[],0
'ARC',[-3.3832433291252602;0.0;6.39],[-5.2496;0.4477;6.39],[-3.3832;4.113805;6.39],4.113
8
'LINE'.[-5.2496;0.4477;6.39].[-5.8466032321804828;0.7516547126646161;6.39],[],0
'ARC',[-5.8466032321804828;0.7516547126646161;6.39].[-5.5799336245416367;2.4818284
553750072;6.39].[-5.4285426196615036;1.5728571359922849;6.39],0.9214923199999999
'LINE',[-5.5799336245416367;2.4818284553750072;6.39],[-3.481932493906982;2.8312547
712923539;6.39],[],0
'ARC',[-3.481932493906982;2.8312547712923539  ;6.39].[-2.8060797935492441;2.8871520
954766332;6.39].[-2.8060797935492441;-1.2266529045233661;6.39],4.1138050000000002
'LINE',[-2.8060797935492441;2.8871520954766332;6.39],[2.2867691741233811;2.8871520
954766332;6.39],[],0
'ARC',[2.2867691741233811;2.8871520954766332;6.39],[2.496021585090558;2.860097757
271935;6.39],[2.2867691741233811;2.0643910954766329;6.39],0.822761
'LINE',[2.496021585090558;2.860097757271935;6.39],[4.484905796073746;2.33706730363
24172;6.39],[],0};

% start_point=[15.8;0];
% end_point=[24.2;15];

dipper_far_range=[9.4155,9.6112,9.8105,10.01,10.217,10.425,10.638,10.854,11.075,11.299,1
1.528,11.761,11.998,12.24,12.487,12.738,12.995,13.257,13.524,13.795,14.074,14.359,14.648
,14.947,15.246,15.555,15.87,16.196,16.52,16.856.17.205,17.55,17.909,18.274,18.642,19.025
,19.413,19.805,20.1,20.347,20.587,20.822,21.051,21.274,21.492,21.703,21.907,22.106,22.29
8,22.484,22.663,22.835,23.001,23.16,23.311,23.456,23.594,23.725.23.849,23.965,24.074,24.
176,24.27,24.357,24.437,24.509,24.573,24.63,24.679,24.721.24.755,24.781,24.8,24.811,24.8
15,24.81,24.798,24.779,24.751,24.716,24.674,24.623,24.566.24.5,24.427,24.347,24.259,24.1
64,24.061,23.951,23.834,23.709,23.578,23.439,23.293,23.141,22.981,22.814,21.297,20.751;
0.0069432,-0.068329.-0.13976,-0.22696,-0.2904,-0.36948,-0.4443,-0.51473,-0.58061,-0.661
79,-0.71817,-0.78956,-0.85582,-0.91678,-0.99223,-1.0421,-1.106,-1.1639,-1.2156,-1.2608,-1.
3191,-1.3705,-1.4148,-1.471,-1.5004.-1.5411,-1.5737,-1.6168,-1.6325,-1.6579,-1.6924,-1.699
,-1.7139,-1.7186,-1.7129,-1.7139,-1.7036,-1.6819,-1.4998,-1.2451,-0.98519,-0.7201,-0.44997
,-0.17494,0.10486.0.38931,0.67826.0.97159,1.2692,1.5708,1.8764,2.1859,2.499,2.8156,3.13
55,3.4587,3.785.4.1142.4.4461,4.7806,5.1176,5.4569,5.7983,6.1416,6.4868,6.8336,7.1819,7.
5315,7.8822.8.234,8.5865,8.9397,9.2935,9.6475,10.002,10.356,10.71,11.063,11.417,11.769,1
2.121,12.471,12.821,13.169,13.516,13.86,14.204,14.545,14.884,15.22,15.555,15.886,16.215,
16.541,16.864,17.183.17.5,17.812,17.665,17.804]
max_bank_toe_radius=15.8;
 % bank_height=15;
relocation_step=3.5;
 cutting_height=15;
 dipper_volume=55;
loose_factor=1.15;
```

A.2 Dipper position determination

%File Name: dipper_position.m
%Use: to determine the position of a point on the dipper.
%Description: this program uses dipper motion equations 3.9, 3.10 and 3.11 derived in Chapter 3.
%Input: host cable length, handle crowd length and the point on the dipper.
%Output: dipper position, dipper and handle angle.

```
function [x,y,alpha,beta]=dipper_position(lc,lh,point)
echo off;
% retrieve the constant
shoveL_constant;
lc1=sqrt(lc.^2+joint2handle^2);
lh1=sqrt(lh.^2+sheaveradius^2);
alpha1=acos(min((lc1.^2+pivot2sheave^2-lh1.^2)./(2*pivot2sheave*lc1),1));
alpha1=boom_angle-alpha1;
theta=atan(joint2handle./lc);
alpha=alpha1-theta;
beta1=acos(min((lc1.^2+lh1.^2-pivot2sheave^2)./(2*lh1.*lc1),1));
beta1=pi-(beta1-alpha1);
theta=atan(sheaveradius./lh);
beta=beta1-theta;

x=lc1.*cos(alpha1)+pivot_x;
y=lc1.*sin(alpha1)+pivot_y;
if nargin==3
    [points_series,n]=transmit_all(x,y,alpha,point)
    x=points_series(1,:);
    y=points_series(2,:);
end
% error Out of Range
  i=find(lc< min_handle | lc>max_handle |lh< min_hoist| lh>max_hoist);
x(i)=-1000;
y(i)=-1000;
alpha(i)=-1000;
beta(i)=-1000;
return
```

A.3 Dipper motion range

%File Name:dipper_range.m
%Use: generating the dipper motion range in vertical plan.
%Description: the program uses the method described in Chapter 3.3.2 to find the motion

```
range .
%Input: reference point (dipper tip or any other point on dipper) and number of cycles
%Output: motion range coordinates.
function [x.y,lc,lh,alpha]=dipper_range(point,icount)
shovel_constant;
x=[];
y=[];
lh=[];
lc=[];
if nargin<1
    icount=ncount;
    point=cutting_point;
elseif nargin<2
    icount=ncount;
end
alpha=linspace(min_angle,max_angle,icount);
point(3)=1;
for i= 1 : icount
   lc(i)=min_handle;
   while lc<=max_handle
      [x(i),y(i).lh(i),beta]=dipper_angle_position(lc(i),alpha(i));
      trans_matrix=trans2D(x(i),y(i),alpha(i));
      dp_lu=trans_matrix*[dipper_backtop(1);dipper_backtop(2);1];
      r1=dp_lu-boom_front_point;
      [theta,r]=cart2pol(r1(1).r1(2));
      if x(i)<-100 | theta>boom_font_angle
           lc(i)=lc(i)+0.02;
      else
          break    ;
      end
   end
   if point(1:2) ~=0    % not joint point, transmit
      trans_matrix=trans2D(x(i),y(i),alpha(i));
       d=trans_matrix*point;
       x(i)= d(1)    ;
       y(i)= d(2);
    end
end
for j= icount:-1:1
   i=    2*icount-j+1;
   lc(i)=max_handle;
   while lc>=0
       [x(i),y(i),lh(i),beta]=dipper_angle_position(lc(i),alpha(j));
       if x(i)<-100 % | jp(:,3)>max_hoist+0.01    | (lc-min_handle>2 & jp(2)<1)
           lc(i)=lc(i)-0.02;
       else
          break    ;
       end
   end
   if point(1:2) ~=0    % not jopint points transmit
```

```
        trans_matrix=trans2D(x(i),y(i),alpha(j));
        d=trans_matrix*point;
        x(i)= d(1)   ;
        y(i)= d(2);
    end
end
x(2*icount+1)=x(1);
y(2*icount+1)=y(1);
return
```

A.4 Dipper minimum tuck profile

%File Name: dipper_tuck_position.m
%Use: generating the dipper minimum tuck profile on the bearing floor.
%Description: the program uses the method described in Chapter 3.3.3 to find dipper minimum tuck position.
%Input: swing angle, and dipper front wall profile in a series of points
%Output: tuck positions.

```
function [tuck_position,lc,handle_angle]=dipper_tuck_position(theta,dipper_front_points)
shovel_constant;
theta=abs(theta);
points=[];
ii=0
if size(dipper_front_points,2)<10;
    for i=2:size(dipper_front_points,2);
        n=fix(norm(dipper_front_points(:,i)-dipper_front_points(:,i-1))/0.05);
        points(1,ii+1:ii+n)=linspace(dipper_front_points(1,i-1),dipper_front_points(1,i),n);
        points(2,ii+1:ii+n)=linspace(dipper_front_points(2,i-1),dipper_front_points(2,i),n);
        ii=ii+n;
    end;
end;

for i=1:size(theta,2)
   tuck_position(i)=min_tuck_position;
   while tuck_position(i)>=min_tuck_position
     % Handle Position
     [jointx,jointy,lc(i),lh,handle_angle(i)]=handle_position(tuck_position(i),0,cutting_point);
     trans_matrix=trans2D(jointx,jointy,handle_angle(i));
     dipper_pts=trans_matrix*[points(1,:);points(2,:);repmat(1,1,size(points,2))];
     rx=sqrt(dipper_pts(1,:).^2+dipper_width^2/4);
     deta=atan(dipper_width/2./dipper_pts(1,:));
    theta1=theta(i)+deta;
    theta2=theta(i)-deta;
    pts_left=[rx.*cos(theta1);dipper_pts(2,:);rx.*sin(theta1)];
    pts_right=[rx.*cos(theta2);dipper_pts(2,:);rx.*sin(theta2)];
    interference=0;
    pts=[pts_left,pts_right];
    for j=1:size(pts,2)
          if   pts(3,j)<crawler_width/2   &   pts(3,j)>crawler_width/2 -track_width
                if isinshape(crawler_xy,pts(:,j)) ==1
                    interference=1;
                   break;
                end
         end
    end
    z=crawler_width/2;
    if interference==0
    for j=1:size(pts_left,2)

          if   abs(pts_left(3,j)-pts_right(3,j))>eps   &   (   pts_left(3,j)<crawler_width/2   &
pts_left(3,j)>crawler_width/2   -track_width)   |   (   pts_right(3,j)<crawler_width/2   &
pts_right(3,j)>crawler_width/2 -track_width)

x=pts_left(1,j)-(pts_left(1,j)-pts_right(1,j))*(pts_left(3,j)-z)/(pts_left(3,j)-pts_right(3,j));

y=pts_left(2,j)-(pts_left(2,j)-pts_right(2,j))*(pts_left(3,j)-z)/(pts_left(3,j)-pts_right(3,j));
               if isinshape(crawler_xy,[x;y]) ==1
                   interference=1;
                   break;
                end
          end
    end
    end

    if interference==1
         tuck_position(i)=tuck_position(i)+0.05;
    else
       break;
    end

end
end
return


%
function [in_out]=isinshape(shape,point)
   in_out=0;
   point=point(1:2,1);
   n=0 ;
```

```
  cross_y=[];
  for i= 1: size(shape,1)
        if strcmp(shape{i,1},'LINE')
              p1=shape{i,2};
              p2=shape{i,3};
              if     abs(p1(1)-p2(1))>eps     &     point(1)>=min(p1(1),p2(1))     &
point(1)<=max(p1(1),p2(1))
                    y=p1(2)-(p1(2)-p2(2))*(p1(1)-point(1))/(p1(1)-p2(1));
                    if n==0 | y~=cross_y(end)
                        n=n+1;
                        cross_y(n)=y;
                    end
              end
        else % arc

              p1=shape{i,2};
              p2=shape{i,3};
              ct=shape{i,4};
              rad=shape{i,5};
              if rad>abs(point(1)-ct(1))
                  y1=ct(2)+sqrt(rad*rad-(point(1)-ct(1))^2);
                  y2=ct(2)-sqrt(rad*rad-(point(1)-ct(1))^2);
                  a1=cart2pol(p1(1)-ct(1),p1(2)-ct(2));
                  a2=cart2pol(p2(1)-ct(1),p2(2)-ct(2));
                  a=cart2pol(point(1)-ct(1),y1-ct(2));
                  if     mod(a1-a+2*pi,2*pi)>=0     &     mod(a1-a+2*pi,2*pi)<=
mod(a1-a2+2*pi,2*pi)
                      if n==0 | y1~=cross_y(end)
                       n=n+1;
                       cross_y(end+1)=y1;
                    end
                  end
                  a=cart2pol(point(1)-ct(1),y2-ct(2));
                  if     mod(a1-a+2*pi,2*pi)>=0     &     mod(a1-a+2*pi,2*pi)<=
mod(a1-a2+2*pi,2*pi)
                     if n==0 | y2~=cross_y(end)
                         n=n+1;
                         cross_y(end+1)=y2;
                     end
                  end
              end
         end

         if n==2
            if (point(2)>min(cross_y(1),cross_y(2)) & point(2)<max(cross_y(1),cross_y(2)))
                in_out=1;
            end
            break;
        end
  end
```

```
return;
```

A.5 Trajectory generating program

%File Name: cutting_trajectory.m
%Use: generating the trajectories of the dipper tip or the heel.
%Description: with the start and end points, hoist and crowd speed, the program generates series of hoist and crowd length; then call the program "dipper_position" to obtain the tip and heel positions.
%Input: start and end points of the trajectory, hoist and crowd speeds, number of steps
%Output: trajectories coordinate, hoist and crowd length.

```
function
[x,y,lc,lh,alpha,v,dipper_angle,cutting_angle,xx,yy,t]=cutting_trajectory(start_point,end_point
,vh,vc,icount)
% retrieve the constant
shoveL_constant;
[jx1,jy1,lc1,lh1,alpha1]=handle_position(start_point(1),start_point(2),cutting_point);
[jx2,jy2,lc2,lh2,alpha2]=handle_position(end_point(1),end_point(2),cutting_point);
if nargin<3
    vh=2;
    vc=vh*abs(lc1-lc2)/abs(lh1-lh2);
    icount=ncount;
elseif nargin<4
    vc=vh*abs(lc1-lc2)/abs(lh1-lh2);
    icount=ncount;
elseif nargin<5
    icount=ncount;
end
T=max(abs(lh1-lh2)/vh,abs(lc1-lc2)/vc);
t=linspace(0,T,icount);

lc=min(repmat(lc2,1,icount),linspace(lc1,lc1+vc*T,icount));
lh=max(repmat(lh2,1,icount),linspace(lh1,lh1-vh*T,icount));

[x,y,alpha,beta]=dipper_position(lc,lh,cutting_point);
[xx,yy,alpha,beta]=dipper_position(lc,lh,dipper_heel);
[dipper_angle,r]=cart2pol(x-xx,y-yy);
v=0;
cutting_angle=0;
[v,cutting_angle,x1,y1]=dipper_velocity(lc,lh,vc,vh,cutting_point);
Return
```

A.6 Dipper motion velocity

%File Name: dipper_velocity.m
%Use: calculating dipper's linear velocity given the hoist and crowd speed.
%Description: this program uses the finite differential method to calculate the linear velocity of a point on the dipper. In a time tag, the change of hoist cable length and handle crowd length are constant due to both constant speeds, thus, the new dipper position can be determined using equation 3.9, 3.10, and 3.11; the dipper displacement can be obtained by calculating the position change; then the velocity can be determined using the dipper position change divided by the time tag.
%Input: hoist speed, crowd speed and the reference point
%Output: dipper velocity, direction, and x, y components.

```
function [v,angle,x,y]=dipper_velocity(lc,lh,vc,vh,local_point)
% retrieve the constant
shoveL_constant;
if nargin<5
   local_point=[2.868;0.385;1];
 else
   local_point=[local_point(1);local_point(2);1];
 end

 if size(vc,2)<size(lc,2)
    vc=[vc,repmat(vc(end),1,size(lc,2)-size(vc,2))];
    vh=[vh,repmat(vh(end),1,size(lh,2)-size(vh,2))];
 end

 pivot=[pivot_x;pivot_y];

 [jpx,jpy,alpha,beta]=dipper_position(lc,lh);
 for i=1:size(lc,2)
       trans_matrix=trans2D(jpx(i),jpy(i),alpha(i));
       point=trans_matrix*local_point;
       gama=alpha(i)+pi/2;
       contact_handle=pivot+[saddle_gear_radius*cos(gama);saddle_gear_radius*sin(gama)];
       joint_point=[jpx(i);jpy(i)];

       VC=[vc(i)*cos(alpha(i));vc(i)*sin(alpha(i))];
       VH=[vh(i)*cos(beta(i));vh(i)*cos(beta(i))];

       [v(i),angle(i)]=plane_point_velocity(contact_handle,VC,joint_point,VH,point);

       x(i)=point(1);
       y(i)=point(2);
 end
 return
```

A.7 Sample outputs of the Kinematic model

- Dipper kinematic simulation result

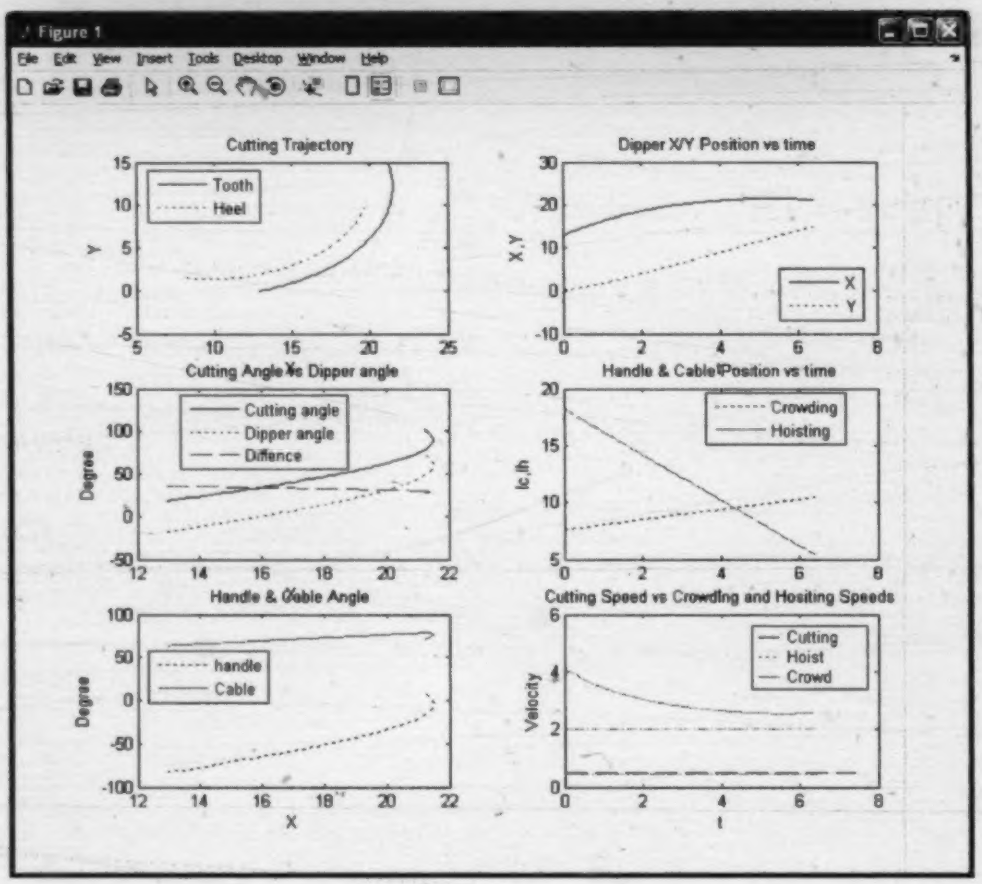

- Idealized digging trajectories and sequence

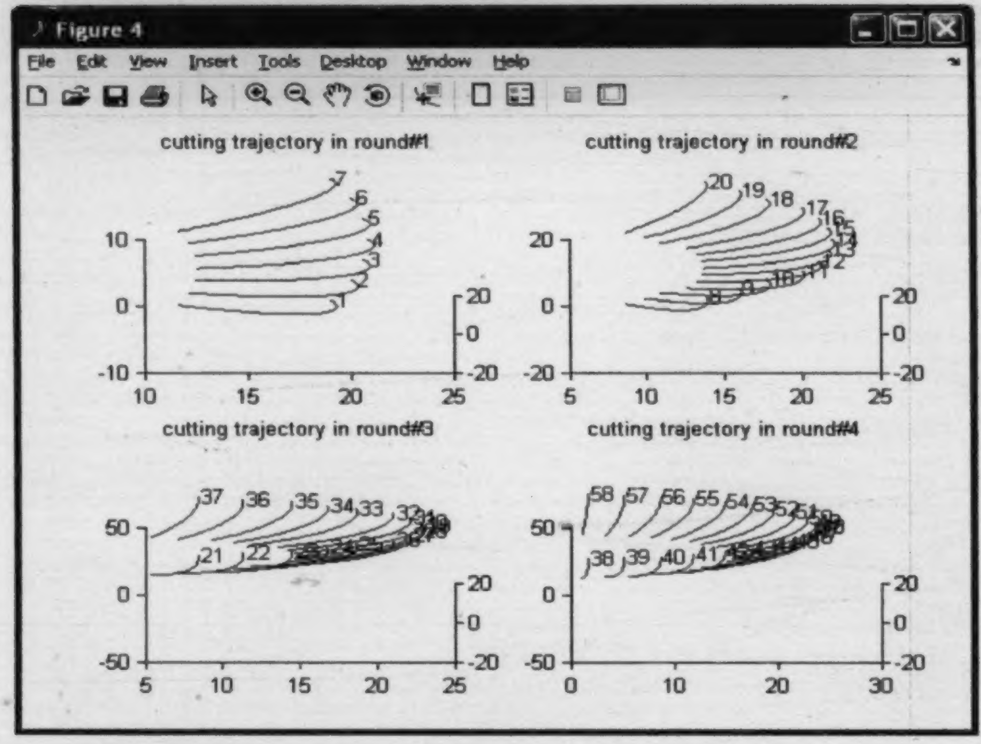
Figure 4
File Edit View Insert Tools Desktop Window Help
cutting trajectory in round#1
cutting trajectory in round#2
cutting trajectory in round#3
cutting trajectory in round#4
1
2
3
4
5
6
7
8
9
10
11
12
13
14
15
16
17
18
19
20
21
22
33
34
35
36
37
38
39
40
41
51
52
53
54
55
56
57
58
10
0
-10
10
15
20
25
20
0
-20
20
0
-20
5
10
15
20
25
50
0
-50
5
10
15
20
25
0
10
20
30

- Shovel cutting positions on the bearing floor and the bench top.

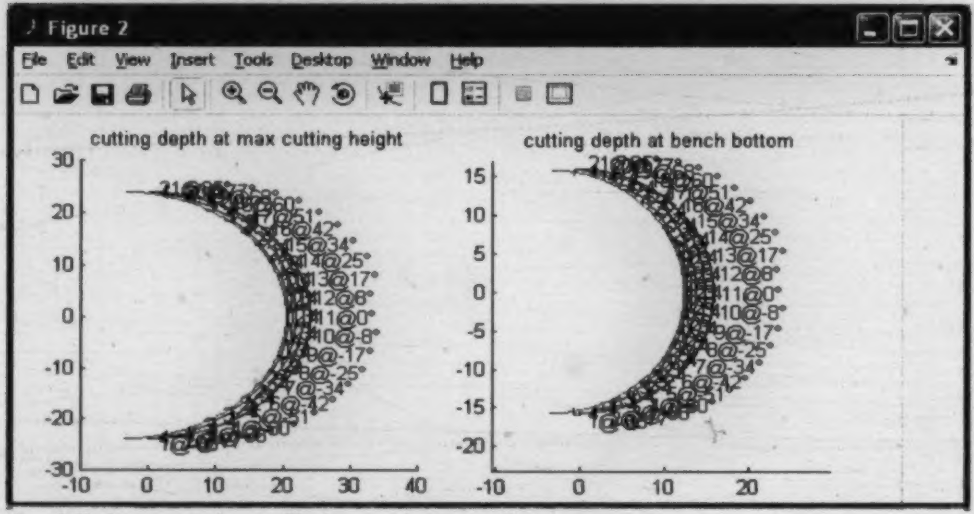

- Minimum tuck profile in a polar coordinate

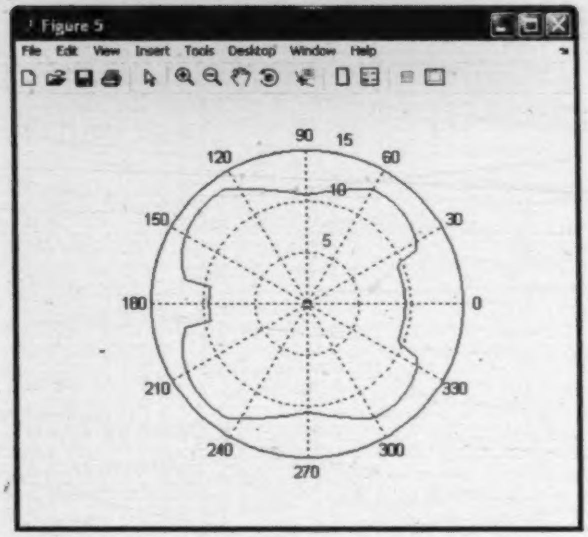
Figure 5
File
Edit
View
Insert
Tools
Desktop
Window
Help
90
15
120
60
10
150
30
5
180
0
210
330
240
300
270

Appendix B

Shovel Action Simulation Software

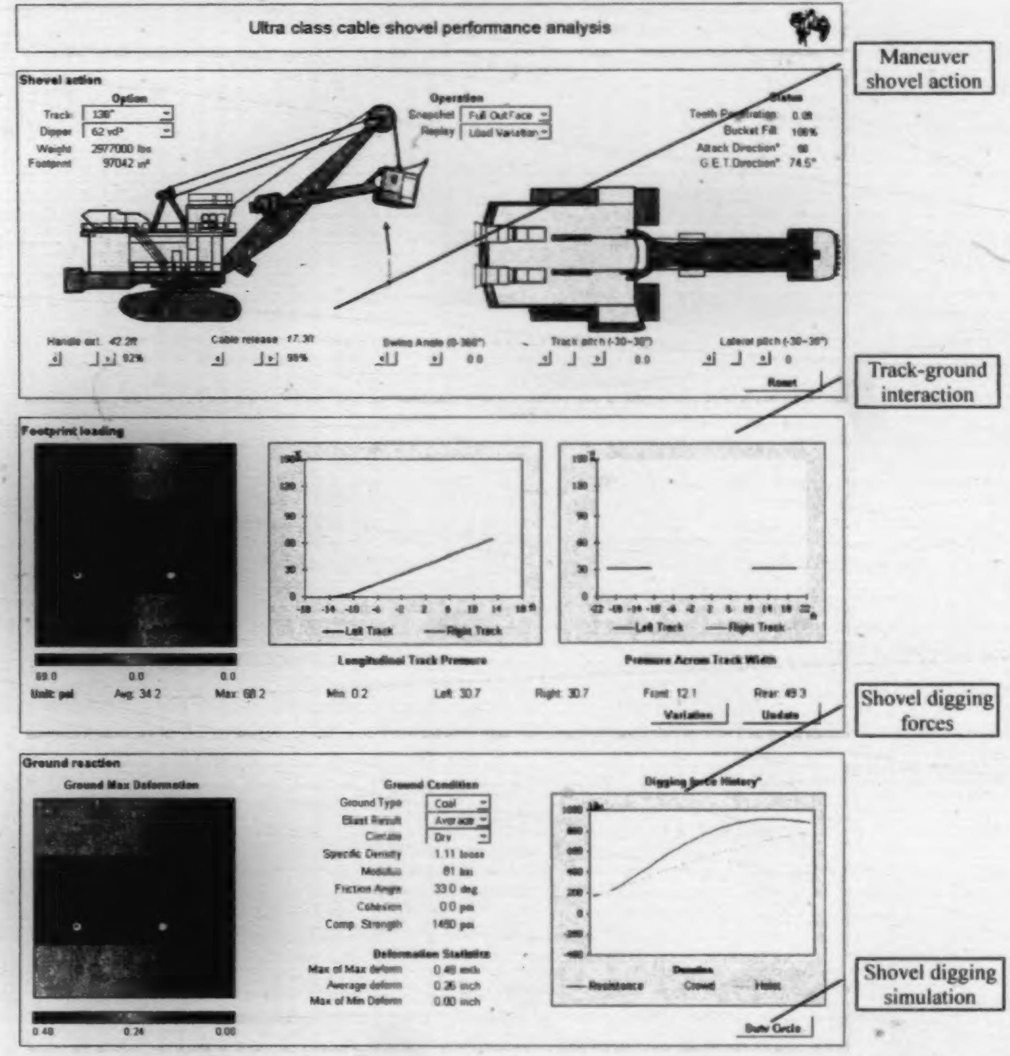
Ultra class cable shovel performance analysis

Shovel action

Option
Track: 138°
Dipper: 62 yd³
Weight: 2977000 lbs
Footprint: 97042 in²

Operation
Snapshot: Full Out Face
Replay: Load Variation

Status
Tooth Penetration: 0.0ft
Bucket Fill: 100%
Attack Direction°: 90
G.E.T.Direction°: 74.5°

Handle ext. 42.2ft 92%
Cable release 17.3ft 99%
Swing Angle (0-360°) 0.0
Track pitch (-30~30°) 0.0
Lateral pitch (-30~30°) 0

Footprint loading

Unit: psi Avg: 34.2 Max: 68.2 Min: 0.2 Left: 30.7 Right: 30.7 Front: 12.1 Rear: 49.3

Ground reaction

Ground Condition
Ground Type: Coal
Blast Result: Average
Climate: Dry
Specific Density: 1.11 loose
Modulus: 81 ksi
Friction Angle: 33.0 deg
Cohesion: 0.0 psi
Comp. Strength: 1450 psi

Deformation Statistics
Max of Max deform: 0.48 inch
Average deform: 0.26 inch
Max of Min Deform: 0.00 inch

- This software combines the Visual Basic for Application (VBA) programs and Excel spreadsheet formulas to run the shovel digging simulation. The kinematic functions were transplanted from MatLab to the VBA; the user friendly interface was established with VBA too. The dipper-ground interaction analytical model and free equilibrium model were established with the spreadsheet formulas.

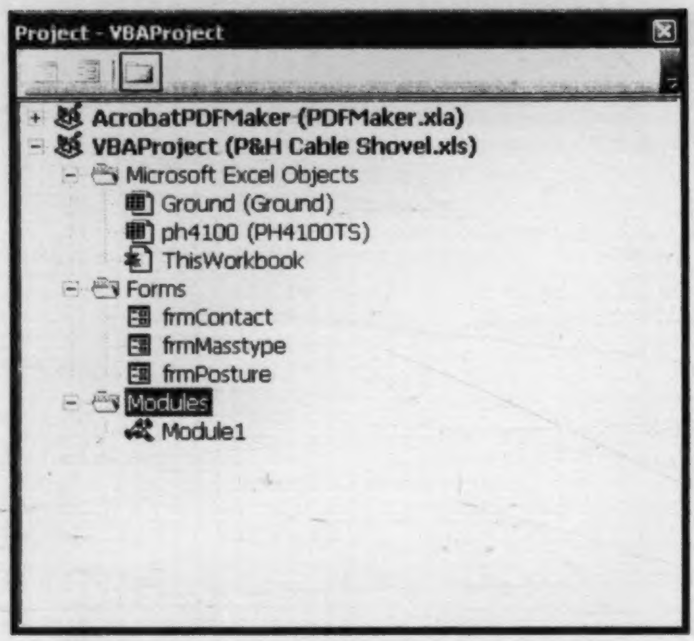

- Visual Basic for Application (VBA) project properties
    - Ground: ground material properties
    - PH4100: user interface sheet
    - Forms: interactive dialogue boxes
    - Modules: common used subroutines.

- Duty cycle simulation

Sub Name: Duty_cycle()

Use: run the digging simulation.

Description: this program uses methodology described in chapter 5 to run the digging simulation cycles. The formulas input in the spreadsheet were the same as those equations derived in chapter 5 so that there is no explicit expression of the equations in the program codes. The shovel animation the digging force plots were synchronized with the simulation progress.

```
Public Sub DutyCycle()
 '' On Error GoTo giveup:
   col = Me.Range("snapshot").Column
   row = Me.Range("snapshot").row
   'snapshots
   Call cmdReset_Click
   ''ActiveWindow.ScrollRow = 1
      k = 0
   choist1 = Me.Cells(row, col + 1)
   hextent1 = Me.Cells(row. col + 2)
   penetration1 = Me.Cells(row, col + 7)
   fillfactor1 = Me.Cells(row, col + 6) * 100
   attackdirection1 = Me.Cells(row, col + 5)
   choist2 = Me.Cells(row + 2, col + 1)
   hextent2 = Me.Cells(row + 2, col + 2)
   penetration2 = Me.Cells(row + 2, col + 7)
   fillfactor2 = Me.Cells(row + 2, col + 6) * 100
   attackdirection2 = Me.Cells(row + 2, col + 5)
   For i = 0 To 30
         cHoist = (choist2 - choist1) * i / 30 + choist1
         hExtent = (hextent2 - hextent1) * i / 30 + hextent1
         Call HandlePosition(hExtent, cHoist)
         Me.txtFillfactor = (fillfactor2 - fillfactor1) * i / 30 + fillfactor1
         Me.txtPenetration = (penetration2 - penetration1) * i / 30 + penetration1
         Me.txtAttack = (attackdirection2 - attackdirection1) * i / 30 + attackdirection1
         k = k + 1
         Me.Range(Me.Names("resihistory")).Cells(k, 1) = Me.Range(Me.Names("resistance"))
/ 1000 * 0.4536
         Me.Range(Me.Names("resihistory")).Cells(k,                    2)                =
Me.Range(Me.Names("crowdforce")) / 1000 * 0.4536
         Me.Range(Me.Names("resihistory")).Cells(k, 3) = Me.Range(Me.Names("hoistforce"))
/ 1000 * 0.4536
         DoEvents
   Next i
   For j = 3 To 8
         choist1 = Me.Cells(row + j, col + 1)
         hextent1 = Me.Cells(row + j, col + 2)
         sAngle1 = Me.Cells(row + j, col + 4)
         penetration1 = Me.Cells(row + j, col + 7)
         fillfactor1 = Me.Cells(row + j, col + 6) * 100
         attackdirection1 = Me.Cells(row + j, col + 5)
         choist2 = Me.Cells(row + j + 1, col + 1)
         hextent2 = Me.Cells(row + j + 1, col + 2)
         sAngle2 = Me.Cells(row + j + 1, col + 4)
         penetration2 = Me.Cells(row + j + 1, col + 7)
         fillfactor2 = Me.Cells(row + j + 1, col + 6) * 100
         attackdirection2 = Me.Cells(row + j + 1, col + 5)
         For i = 0 To 10
```

```
          cHoist = (choist2 - choist1) * i / 10 + choist1
          hExtent = (hextent2 - hextent1) * i / 10 + hextent1
          Call HandlePosition(hExtent, cHoist)
          SwingAngle = ((sAngle2 - sAngle1) * i / 10 + sAngle1) / 180 * 3.1415926

          Me.txtFillfactor = (fillfactor2 - fillfactor1) * i / 10 + fillfactor1
          Me.txtPenetration = (penetration2 - penetration1) * i / 10 + penetration1
          Me.txtAttack = (attackdirection2 - attackdirection1) * i / 10 + attackdirection1
          DoEvents
          Next i

   Next j

  "ActiveWindow.ScrollRow = 39
   Call Deformation

Giveup:
   Application.ScreenUpdating = True
End Sub

Public Sub Update()
     If BodyWidth = 0 Then Me.initialize
     Range(Me.Names("swingangle")) = sAngle
     Range(Me.Names("pitchangle")) = pAngle
     Range(Me.Names("lateralpitch")) = LateralPitchAngle
     Range(Me.Names("crawlercenterx")) = CrawlerCenterX
     Range(Me.Names("crawlercentery")) = CrawlerCenterY
     Range(Me.Names("bodycenterx")) = BodyCenterX
     Range(Me.Names("bodycentery")) = BodyCenterY
     Range(Me.Names("handlecenterx")) = HandleCenterX
     Range(Me.Names("handlecentery")) = HandleCenterY
     Range(Me.Names("dippercenterx")) = DipperCenterX
     Range(Me.Names("dippercentery")) = DipperCenterY
     Me.Range("payload") = Me.Range("bucketcapacity") * Ground.Range("density") *
1685.5 * Val(Me.Range(Me.Names("bucketfill"))) / 100

     "stickweight = Range(me.names("stickwieght"))
    "Refresh track range
     For i = 1 To Range(Me.Names("trackrange")).Columns.Count
          Range(Me.Names("trackrange")).Cells(2, i) =
Range(Me.Names("trackrange")).Cells(1, i)
     Next i
     "Validate track range
     Do While Range(Me.Names("px1z1")) < 0 And Range(Me.Names("px1z4")) < 0

        Range(Me.Names("trackrange")).Cells(2, 1) =
Range(Me.Names("trackrange")).Cells(2, 1) + 0.1
        If Range(Me.Names("trackrange")).Cells(2, 1) >=
Range(Me.Names("trackrange")).Cells(2, 2) Then
            MsgBox "The shovel can not stand at all under this condition !", vbOKOnly,
"Warning"
            Exit Sub
        End If
    Loop

    Do While Range(Me.Names("px2z1")) < 0 And Range(Me.Names("px2z4")) < 0
        Range(Me.Names("trackrange")).Cells(2, 2) =
Range(Me.Names("trackrange")).Cells(2, 2) - 0.1
        If Range(Me.Names("trackrange")).Cells(2, 2) <=
Range(Me.Names("trackrange")).Cells(2, 1) Then
            MsgBox "The shovel can not stand at all under this condition !", vbOKOnly,
"Warning"
            Exit Sub
        End If
    Loop

    Do While Range(Me.Names("px1z1")) < 0 And Range(Me.Names("px2z1")) < 0
        Range(Me.Names("trackrange")).Cells(2, 3) =
Range(Me.Names("trackrange")).Cells(2, 3) + 0.1
        If Range(Me.Names("trackrange")).Cells(2, 3) >=
Range(Me.Names("trackrange")).Cells(2, 4) Then
            Range(Me.Names("trackrange")).Cells(2, 5) =
Range(Me.Names("trackrange")).Cells(2, 5) + 0.1
            Range(Me.Names("trackrange")).Cells(2, 3) =
Range(Me.Names("trackrange")).Cells(2, 5)
            Range(Me.Names("trackrange")).Cells(2, 4) =
Range(Me.Names("trackrange")).Cells(2, 5)
        End If
        If Range(Me.Names("trackrange")).Cells(2, 5) >=
Range(Me.Names("trackrange")).Cells(2, 6) Then
            MsgBox "The shovel can not stand at all under this condition !", vbOKOnly,
"Warning"
            Exit Sub
        End If
    Loop

    Do While Range(Me.Names("px1z4")) < 0 And Range(Me.Names("px2z4")) < 0
        Range(Me.Names("trackrange")).Cells(2, 6) =
Range(Me.Names("trackrange")).Cells(2, 6) - 0.1
        If Range(Me.Names("trackrange")).Cells(2, 5) >=
Range(Me.Names("trackrange")).Cells(2, 6) Then

            Range(Me.Names("trackrange")).Cells(2, 4) =
Range(Me.Names("trackrange")).Cells(2, 4) - 0.1
            Range(Me.Names("trackrange")).Cells(2, 5) =
Range(Me.Names("trackrange")).Cells(2, 4)
            Range(Me.Names("trackrange")).Cells(2, 6) =
Range(Me.Names("trackrange")).Cells(2, 4)
        End If
        If Range(Me.Names("trackrange")).Cells(2, 3) >=
Range(Me.Names("trackrange")).Cells(2, 4) Then
            MsgBox "The shovel can not stand at all under this condition !", vbOKOnly,
"Warning"
            Exit Sub
          End If
      Loop

    Call GetTrackRange


    "savefile
    Dim filename As String
    filename = Environ("temp") & "\loadmap.bmp"

  trackspan = Range(Me.Names("trackspan"))
  tracklength = Range(Me.Names("tracklength"))
  maxload = Int(Range(Me.Names("maxload")) + 1)
  minload = Int(Range(Me.Names("minload")))

    ncounter = 0

If BMPInfo.biHeight = 0 Then Call buildBMPhead
  For intRow = 1 To BMPInfo.biHeight
        zz = (intRow / BMPInfo.biHeight) * trackspan - trackspan / 2
            For intColumn = 1 To BMPInfo.biWidth
                xx = (intColumn / BMPInfo.biWidth) * tracklength - tracklength / 2
                pp = pxz(xx, zz)
                pb = Int((pp - minload) / (maxload - minload) * 255)
                If pb < 0 Then pb = 0: If pb > 255 Then pb = 255
                pdata(intColumn - 1, intRow - 1) = pb
                ldata(intColumn - 1, intRow - 1) = pp
                ncounter = ncounter + 1
                DoEvents
          Next intColumn
        Next intRow

    Call SaveMap(Me.optColorLoad.Value, filename)

    Me.loadmap.Picture = LoadPicture(filename)
    Me.lblmaxload = Format(maxload, "0.0")
    Me.lblminload = Format(minload, "0.0")
    Me.lblmiddleload = Format((minload + middleload) / 2, "0.0")

End Sub
```

Appendix C

Dominion 450/500 Shovel and Dipper Specifications

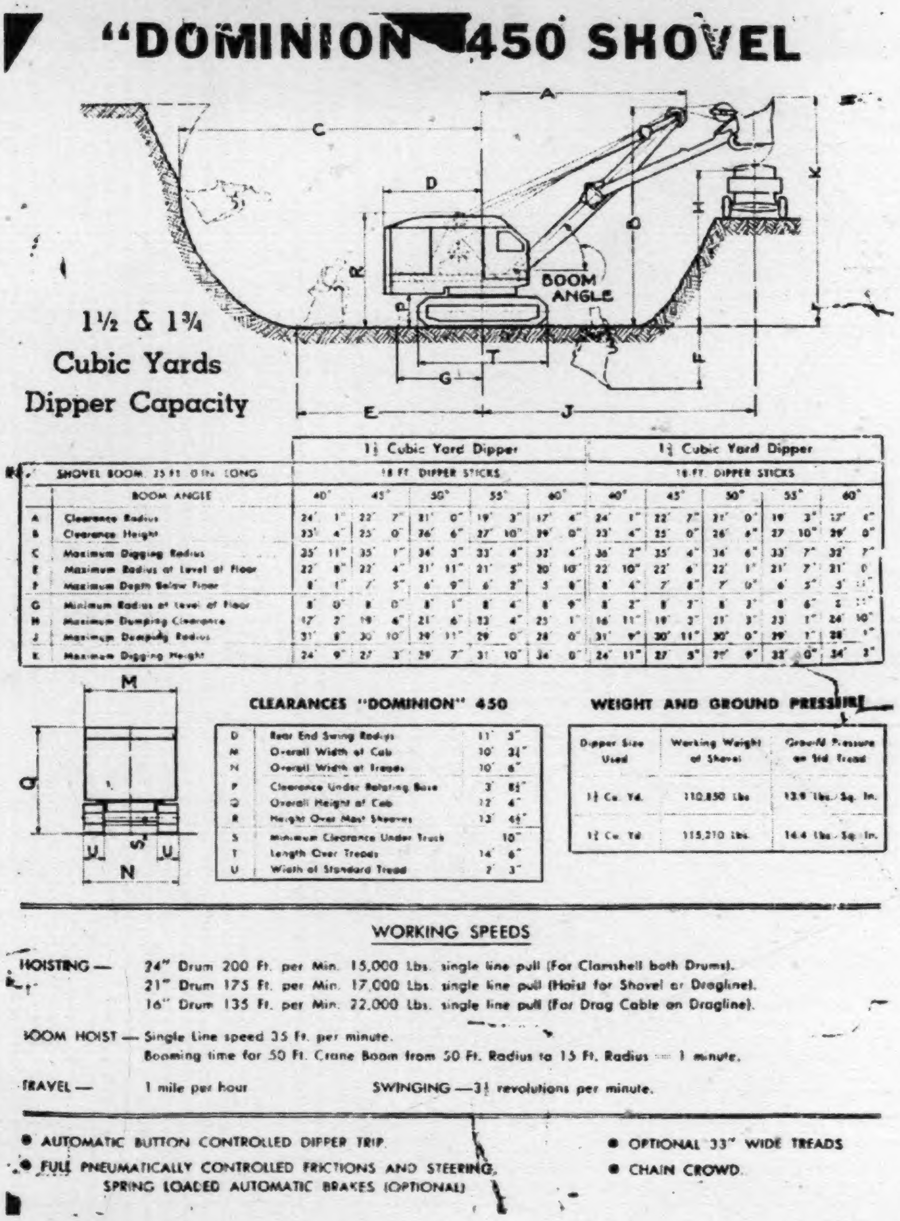

C
A
D
B
H
K
R
P
BOOM ANGLE
T
G
F
E
J
M
Q
U
S
U
N

"DOMINION" 450 SHOVEL

1½ & 1¾
Cubic Yards
Dipper Capacity

	SHOVEL BOOM 25 FT. 0 IN. LONG	1½ Cubic Yard Dipper					1¾ Cubic Yard Dipper				
		18 FT. DIPPER STICKS					18 FT. DIPPER STICKS				
	BOOM ANGLE	40°	45°	50°	55°	60°	40°	45°	50°	55°	60°
A	Clearance Radius	24' 1"	22' 7"	21' 0"	19' 3"	17' 4"	24' 1"	22' 7"	21' 0"	19' 3"	17' 6"
B	Clearance Height	23' 4"	25' 0"	26' 6"	27' 10"	29' 0"	23' 4"	25' 0"	26' 6"	27 10"	29' 0"
C	Maximum Digging Radius	35' 11"	35' 1"	34' 3"	33' 4"	32' 4"	36' 2"	35' 4"	34' 6"	33' 7"	32' 7"
E	Maximum Radius at Level of Floor	22' 8"	22' 4"	21' 11"	21' 5"	20' 10"	22' 10"	22' 6"	22' 1"	21' 7"	21' 0"
F	Maximum Depth Below Floor	8' 1"	7' 5"	6' 9"	6' 2"	5' 8"	8' 4"	7' 8"	7' 0"	6' 5"	5' [illegible]
G	Minimum Radius at Level of Floor	8' 0"	8' 0"	8' 1"	8' 4"	8' 9"	8' 2"	8' 2"	8' 3"	8' 6"	8 [illegible]
H	Maximum Dumping Clearance	17' 2"	19' 6"	21' 6"	23' 4"	25' 1"	16' 11"	19' 3"	21' 3"	23' 1"	24' 10"
J	Maximum Dumping Radius	31' 8"	30' 10"	29' 11"	29' 0"	28' 0"	31' 9"	30' 11"	30' 0"	29' 1"	28' 1"
K	Maximum Digging Height	24' 9"	27' 3"	29' 7"	31' 10"	34' 0"	24' 11"	27' 5"	29' 9"	32' 0"	34' 2"

CLEARANCES "DOMINION" 450

D	Rear End Swing Radius	11' 5"
M	Overall Width of Cab	10' 3½"
N	Overall Width of Treads	10' 6"
P	Clearance Under Rotating Base	3' 8½"
Q	Overall Height of Cab	12' 4"
R	Height Over Mast Sheaves	12' 4½"
S	Minimum Clearance Under Truck	10"
T	Length Over Treads	14' 6"
U	Width of Standard Tread	2' 3"

WEIGHT AND GROUND PRESSURE

Dipper Size Used	Working Weight of Shovel	Ground Pressure on Std. Tread
1½ Cu. Yd.	110,850 Lbs.	13.9 Lbs./Sq. In.
1¾ Cu. Yd.	115,210 Lbs.	14.4 Lbs./Sq. In.

WORKING SPEEDS

HOISTING — 24" Drum 200 Ft. per Min. 15,000 Lbs. single line pull (For Clamshell both Drums).
21" Drum 175 Ft. per Min. 17,000 Lbs. single line pull (Hoist for Shovel or Dragline).
16" Drum 135 Ft. per Min. 22,000 Lbs. single line pull (For Drag Cable on Dragline).

BOOM HOIST — Single Line speed 35 Ft. per minute.
Booming time for 50 Ft. Crane Boom from 50 Ft. Radius to 15 Ft. Radius = 1 minute.

TRAVEL — 1 mile per hour SWINGING — 3½ revolutions per minute.

- AUTOMATIC BUTTON CONTROLLED DIPPER TRIP.
- FULL PNEUMATICALLY CONTROLLED FRICTIONS AND STEERING, SPRING LOADED AUTOMATIC BRAKES (OPTIONAL)
- OPTIONAL 33" WIDE TREADS
- CHAIN CROWD.

* The Dominion 450 and 500 shovels share the same infrastructure except for a bigger engine on the 500.

11-11-U

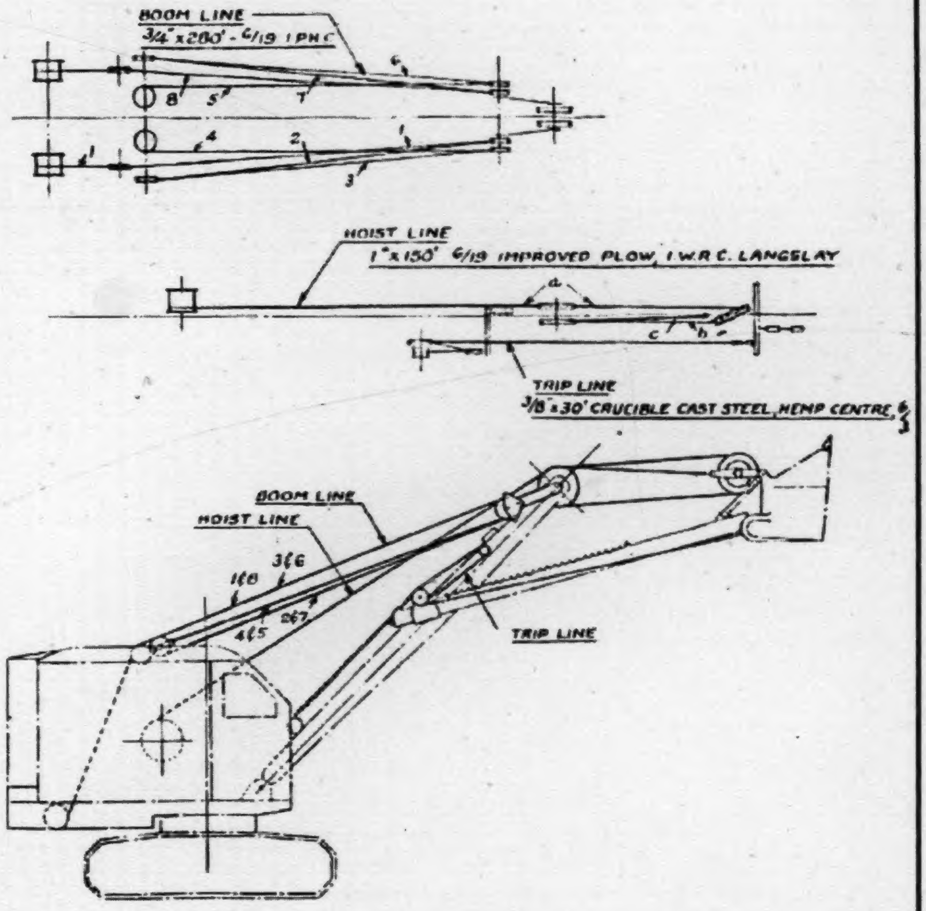
BOOM LINE
3/4" x 280' - 6/19 I.P.H.C.
1
2
3
4
5
6
7
8
HOIST LINE
1" x 150' 6/19 IMPROVED PLOW, I.W.R.C. LANGSLAY
a
b
c
TRIP LINE
3/8" x 30' CRUCIBLE CAST STEEL, HEMP CENTRE, 6/3
BOOM LINE
HOIST LINE
1 & 8
3 & 6
2 & 7
4 & 5
TRIP LINE

DR JMG	TR JMG	DOMINION ENGINEERING WORKS LIMITED MONTREAL POWER CRANE AND SHOVEL DIVISION	SCALE 1 FT.
CK C.M Nov. 2/53			
PASS	DATE OCT 29-53	CHAIN CROWD SHOVEL REEVING K-450-K-550 MACHINES	DATA SHEET G/R-11-11

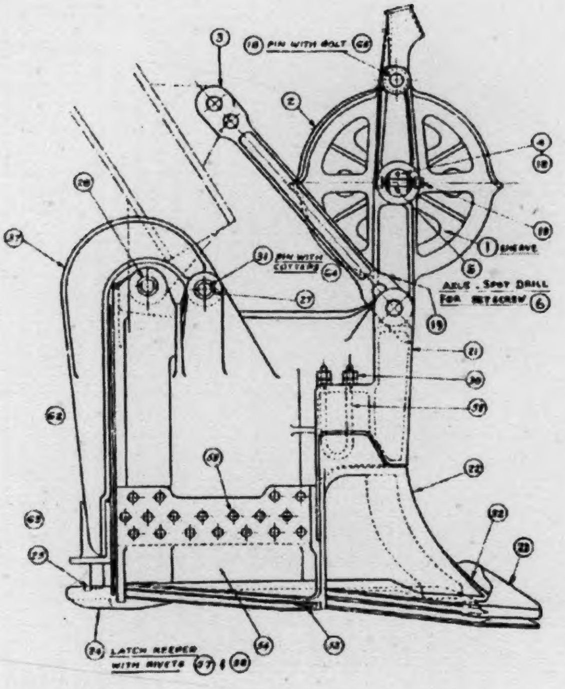

18 PIN WITH BOLT 68
1 SHEAVE
AXLE . SPOT DRILL
FOR SETSCREW 6
31 PIN WITH
COTTERS 64
24 LATCH KEEPER
WITH RIVETS 37 & 38

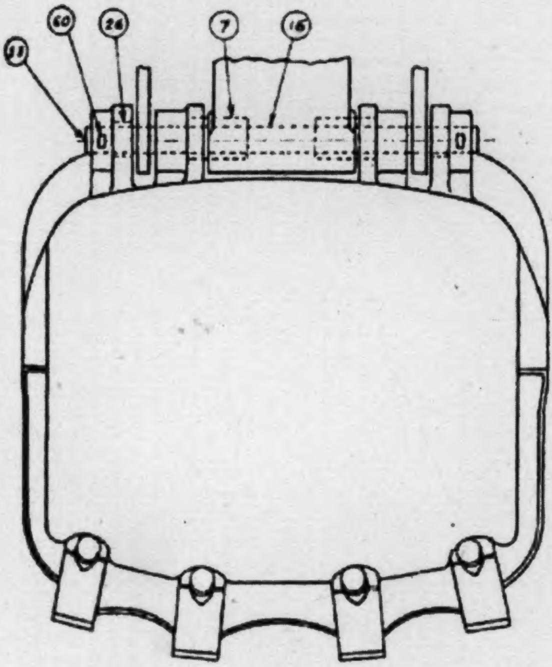

Appendix D

1/20th Prototype Dipper and Door Specifications

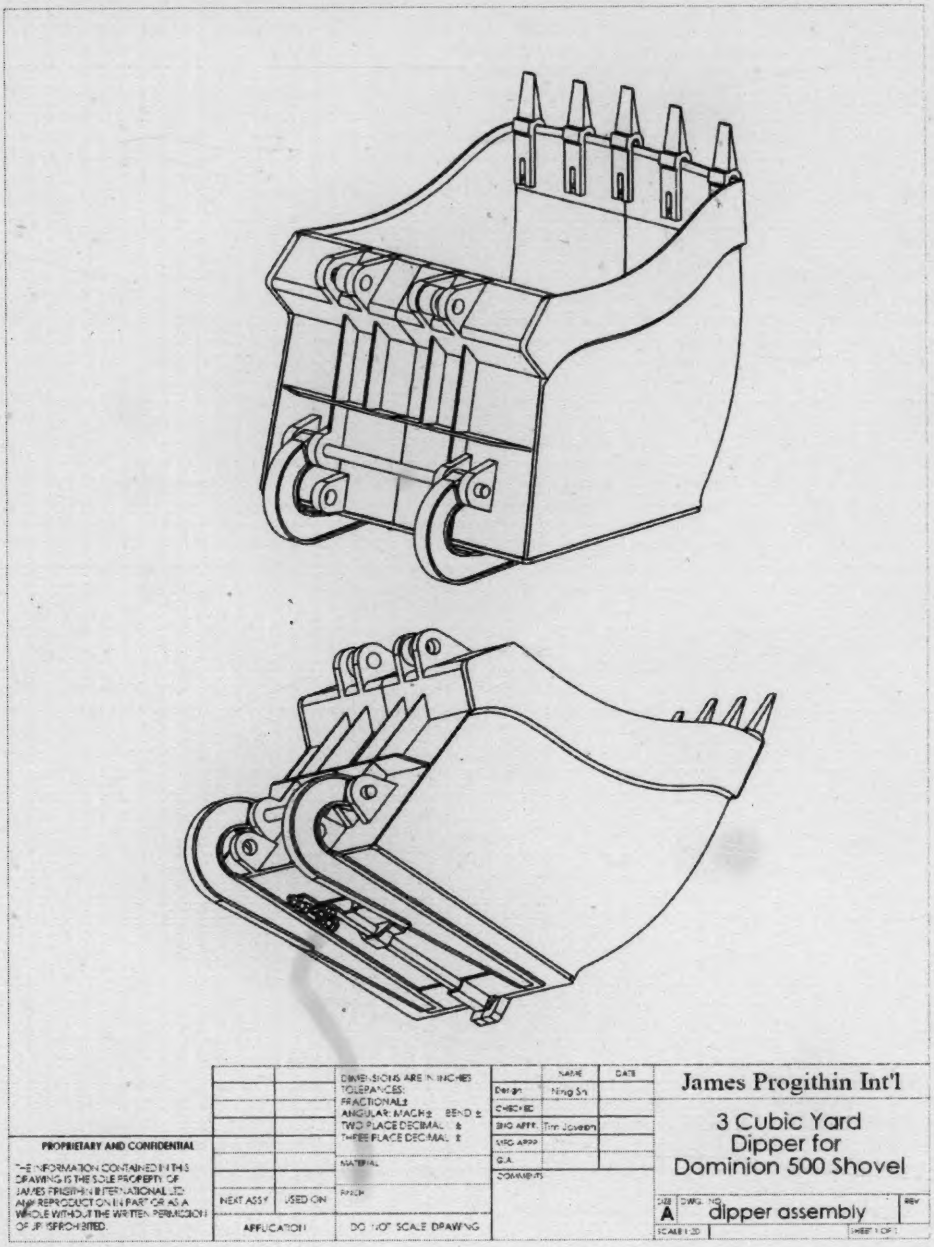

Dipper Parts List

#	Description	ACAD File	Fabrication	Qty
1	Dipper Assembly	dipper 11.DWG	-	1
2	Top (Back) wall	backwall.DWG	Cutting	1
3	Side walls	sidewalls.DWG	Cutting	2
4	Side lips	sidelips.DWG	Cutting	2
5	Front lip	frontlip.DWG	Cutting	1
6	Teeth (including adapters)	tooth.DWG	From market	5
7	Bottom (Front) wall	frontwall.DWG	Cutting	1
8	Back Casing	backcasing.DWG	Cutting	1
9	Brace Lug Bushing	brace_lug_busing.DWG	Cutting+Drilling	4
10	Brace Block	brace_block.DWG	Machining	2
11	Door Hinge Bushing	door_hinge_bushing.DWG	Cutting+Drilling	4
12	Handle Lug Bushing	handle_pin_bushing.DWG	Cutting+Drilling	2
13	Back Reinforcement Frame	backFrames.DWG	Cutting	5
14	Back Arrangement	back_arrangement.DWG	-	1

Door Parts

#	Description	ACAD File	Fabrication	Qty
1	Assembly	door.DWG	-	1
2	Latch	latch.DWG	Cutting+Grinding	1
3	Latch Lever	latch lever.DWG	Cutting	1
4	Latch Bracket	latch bracket.DWG	Cutting+Bending	1
5	Adjusting Block	adjusting block.dwg	Machining	1
6	Bottom Plate	door plate.DWG	Cutting	1
7	Door Lug	door lug.DWG	Cutting+Drilling	4
8	Arm Frame (Inside)	door arm Frame1.DWG	Cutting+Bending	2
9	Arm	door arm.DWG	Cutting	2
10	Arm Frame (Outside)	door arm Frame2.DWG	Cutting+Bending	2
11	Latch Guide 1	latch guide 1.DWG	Cutting+Welding	1
12	Latch Guide 2	latch guide 2.DWG	Cutting+Welding	1
13	Adjusting Bolt and Nuts 10"x Dia 0.94"	-	-	1.3
14	Lever Bolt and Nut 3"x Dia 0.94"	-	-	1
15	Lever Bolt and Nut 3"x Dia 0.94"	-	-	1
16	Chain Shack	-	-	1
17	Door Arm Assembly	Door Arm Assembly.DWG	-	1

* The "cutting profile.dwg" includes all steel sheets' profile being cut.

1 Dipper
2 Top (Back) wall
3 Side walls
4 Side lips
5 Front lip
6 Teeth (including adapters)
7 Bottom (Front) wall
8 Back Casing
9 Brace Lug Bushing
10 Brace Block
11 Door Hinge Bushing
12 Handle Lug Bushing
13 Back Reinforcement Frame
14 Back Arrangement

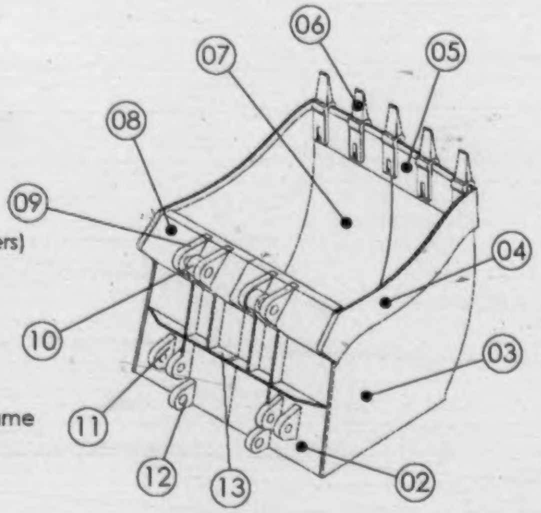

1 Door
2 Latch
3 Latch Lever
4 Latch Bracket
5 Adjusting Block
6 Bottom Plate
7 Door Lug
8 Arm Frame (Inside)
9 Arm
10 Arm Frame (Outside)
11 Latch Guide 1
12 Latch Guide 2
13 Adjusting Bolt and Nuts
14 Lever Bolt and Nut
15 Lever Bolt and Nut
16 Chain Shack

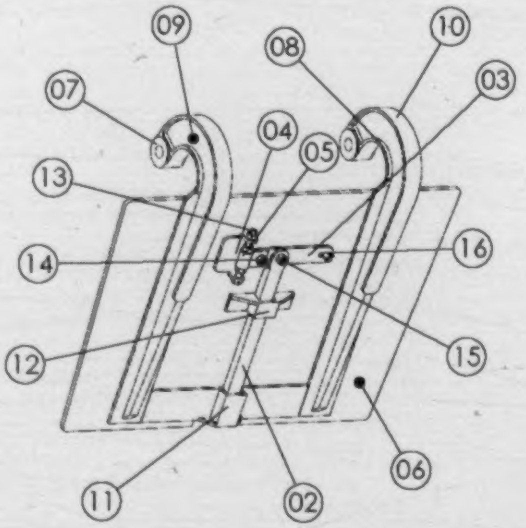

PROPRIETARY AND CONFIDENTIAL
THE INFORMATION CONTAINED IN THIS DRAWING IS THE SOLE PROPERTY OF JAMES PROGITHIN INTERNATIONAL LTD ANY REPRODUCTION IN PART OR AS A WHOLE WITHOUT THE WRITTEN PERMISSION OF JP IS PROHIBITED

NEXT ASSY
USED ON
APPLICATION

DIMENSIONS ARE IN INCHES
TOLERANCES:
FRACTIONAL ±
ANGULAR: MACH ± BEND ±
TWO PLACE DECIMAL ±
THREE PLACE DECIMAL ±
MATERIAL
FINISH
DO NOT SCALE DRAWING

	NAME	DATE
Design	Ying Jin	
CHECKED		
ENG APPR	Tim Joseph	
MFG APPR		
Q.A.		

COMMENTS:

James Progithin Int'l

Dipper Assembly
3 cubic yard

SIZE A
DWG NO dipper&door
REV
SCALE 1:5
SHEET 1 OF

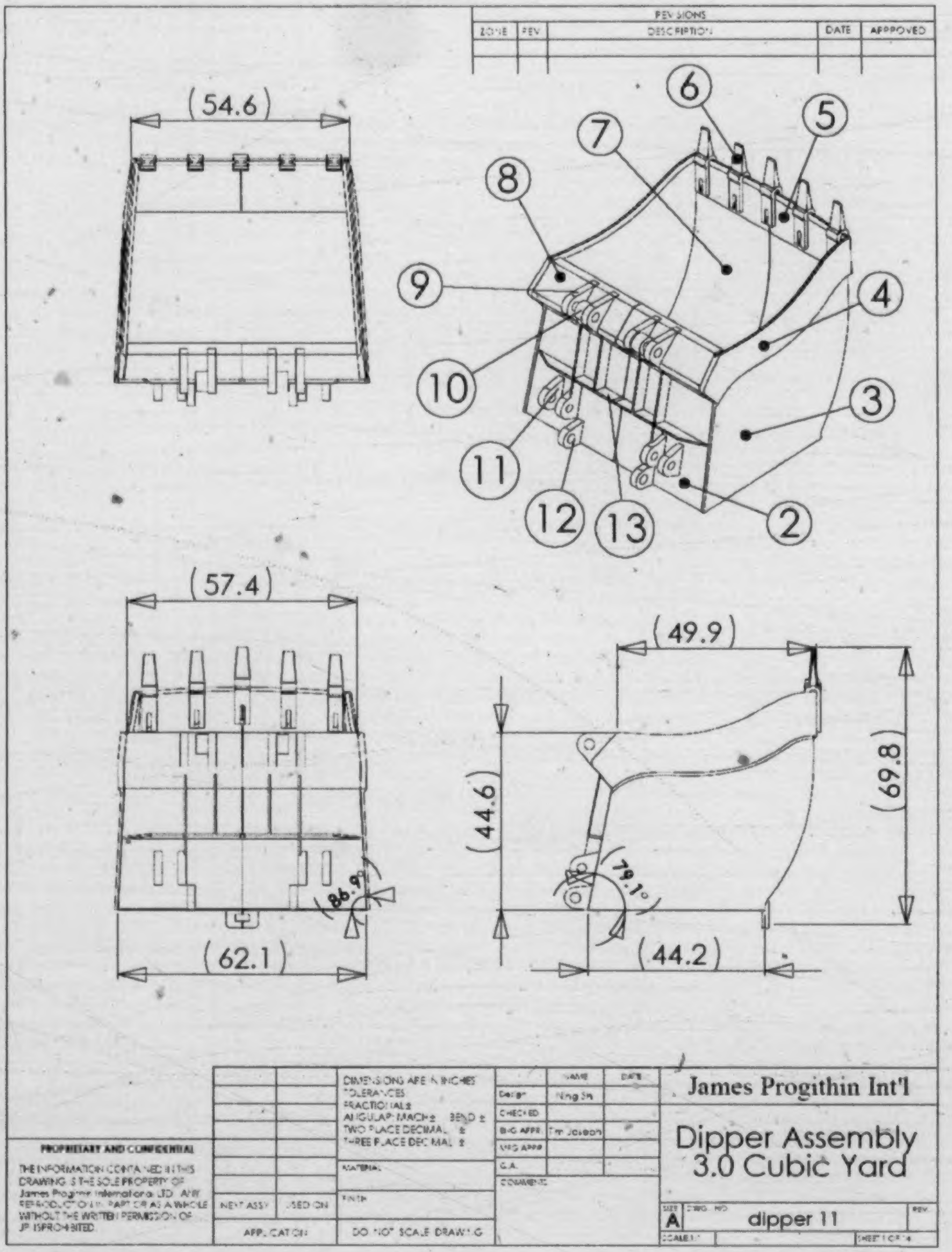

PROPRIETARY AND CONFIDENTIAL

THE INFORMATION CONTAINED IN THIS DRAWING IS THE SOLE PROPERTY OF James Progithin International LTD. ANY REPRODUCTION IN PART OR AS A WHOLE WITHOUT THE WRITTEN PERMISSION OF JP IS PROHIBITED.

NEXT ASSY	USED ON
APPLICATION	

DIMENSIONS ARE IN INCHES
TOLERANCES:
FRACTIONAL ±
ANGULAR: MACH ± BEND ±
TWO PLACE DECIMAL ±
THREE PLACE DECIMAL ±

MATERIAL

FINISH

DO NOT SCALE DRAWING

	NAME	DATE
Design	Ning Sh	
CHECKED		
ENG APPR.	Tim Joseon	
MFG APPR.		
Q.A.		

COMMENTS:

James Progithin Int'l

Dipper Assembly
3.0 Cubic Yard

SIZE A
DWG. NO. dipper 11
REV.
SCALE 1:
SHEET 1 OF 14

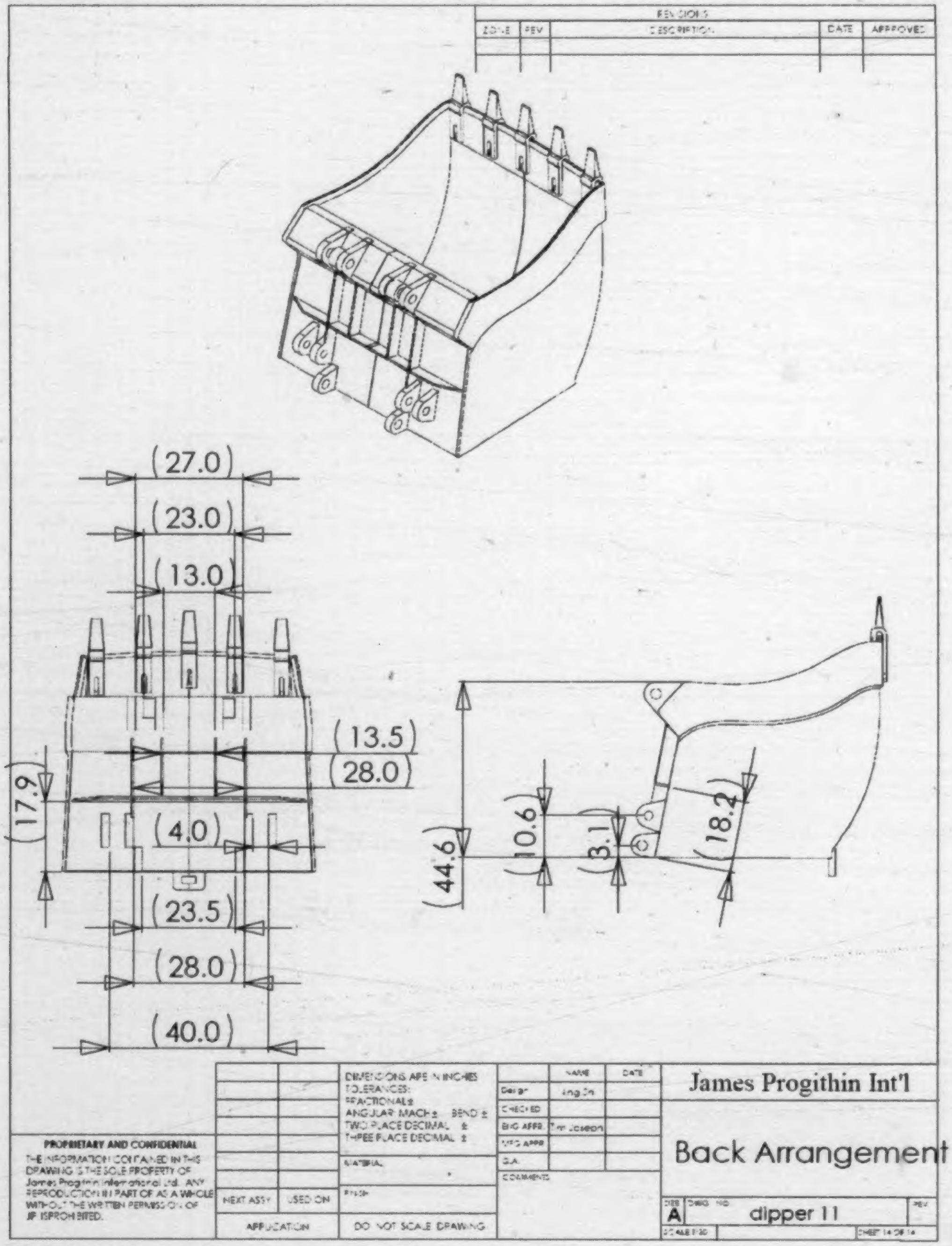
REVISIONS
ZONE
REV
DESCRIPTION
DATE
APPROVED
(27.0)
(23.0)
(13.0)
(13.5)
(28.0)
(17.9)
(4.0)
(23.5)
(28.0)
(40.0)
(44.6)
(10.6)
(3.1)
(18.2)
DIMENSIONS ARE IN INCHES
TOLERANCES:
FRACTIONAL±
ANGULAR: MACH± BEND ±
TWO PLACE DECIMAL ±
THREE PLACE DECIMAL ±
MATERIAL
FINISH
NEXT ASSY
USED ON
APPLICATION
DO NOT SCALE DRAWING
NAME
DATE
Design
Ang Sn
CHECKED
ENG APPR.
Tim Joseph
MFG APPR.
Q.A.
COMMENTS:
PROPRIETARY AND CONFIDENTIAL
THE INFORMATION CONTAINED IN THIS DRAWING IS THE SOLE PROPERTY OF James Progithin International Ltd. ANY REPRODUCTION IN PART OR AS A WHOLE WITHOUT THE WRITTEN PERMISSION OF JP IS PROHIBITED.
James Progithin Int'l
Back Arrangement
SIZE
A
DWG. NO.
dipper 11
REV
SCALE 1:30
SHEET 14 OF 14

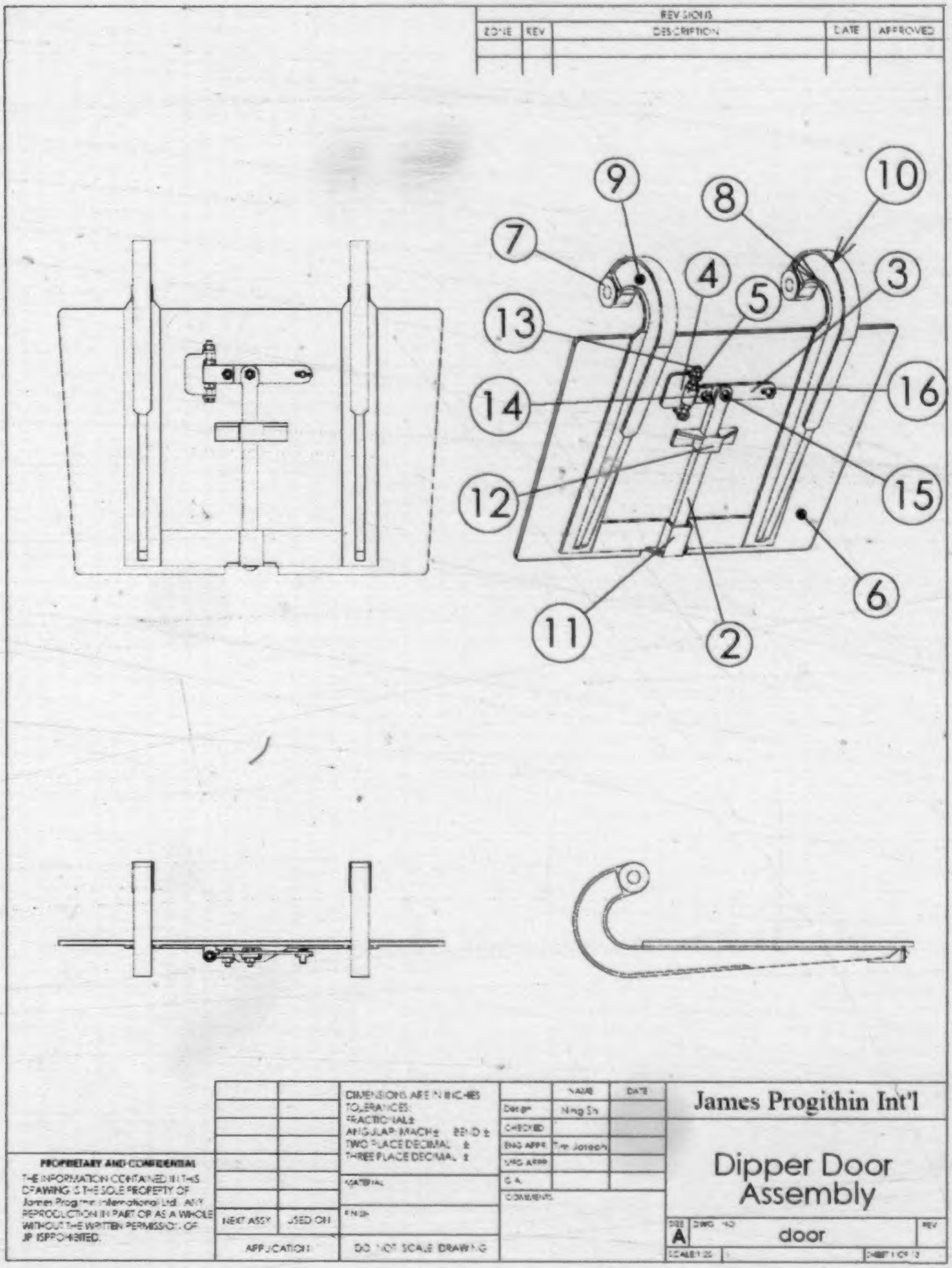REVISIONS
ZONE
REV
DESCRIPTION
DATE
APPROVED
9
8
10
7
4
5
3
13
16
14
12
15
6
11
2
DIMENSIONS ARE IN INCHES
TOLERANCES:
FRACTIONAL ±
ANGULAR: MACH ± BEND ±
TWO PLACE DECIMAL ±
THREE PLACE DECIMAL ±
MATERIAL
FINISH
NEXT ASSY
USED ON
APPLICATION
DO NOT SCALE DRAWING
NAME
DATE
Design
Ning Sh
CHECKED
ENG APPR.
Tim Joseph
MFG APPR.
Q.A.
COMMENTS:
James Progithin Int'l
Dipper Door Assembly
SIZE
A
DWG. NO.
door
REV
SCALE: 1:20
SHEET 1 OF 3
PROPRIETARY AND CONFIDENTIAL
THE INFORMATION CONTAINED IN THIS DRAWING IS THE SOLE PROPERTY OF James Progithin International Ltd. ANY REPRODUCTION IN PART OR AS A WHOLE WITHOUT THE WRITTEN PERMISSION OF JP IS PROHIBITED.

Appendix E

Hensley Tooth and Adaptor Specifications

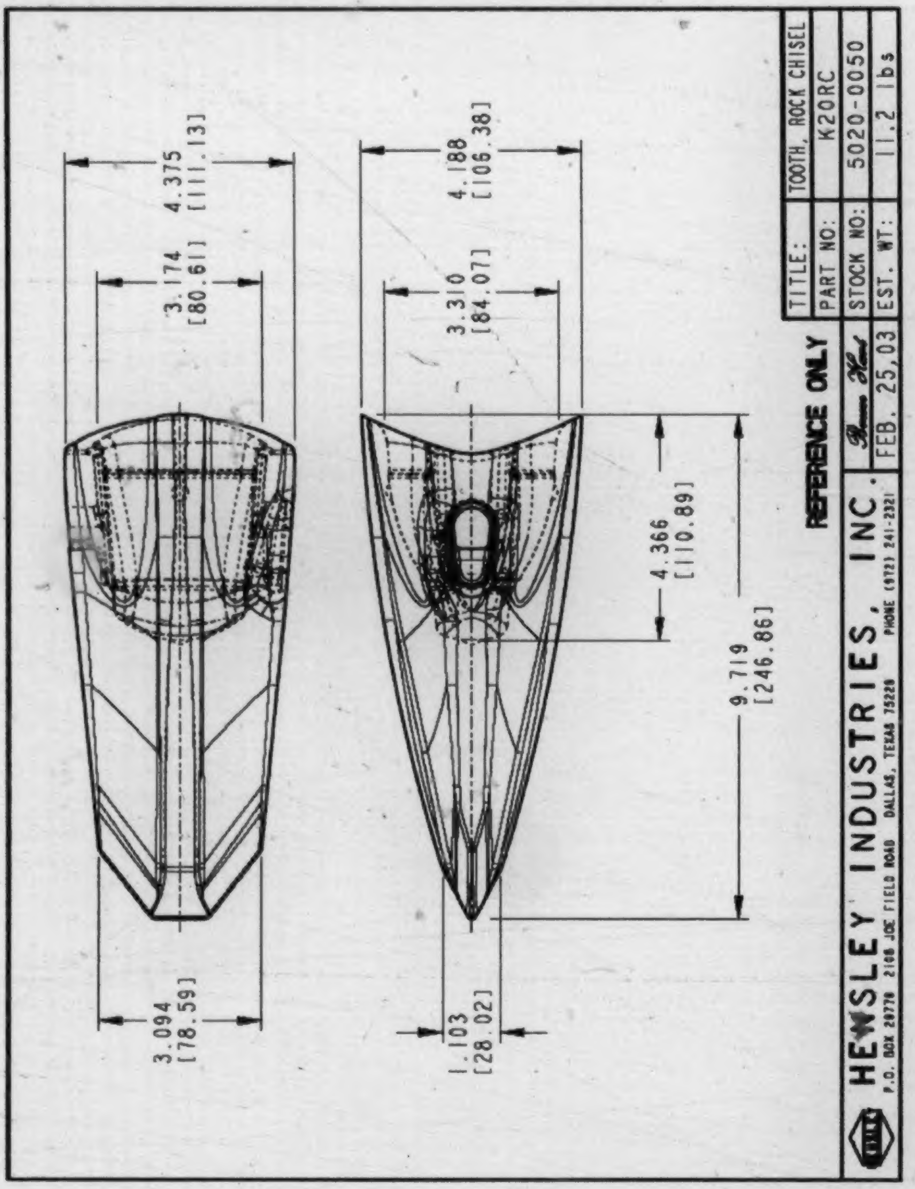

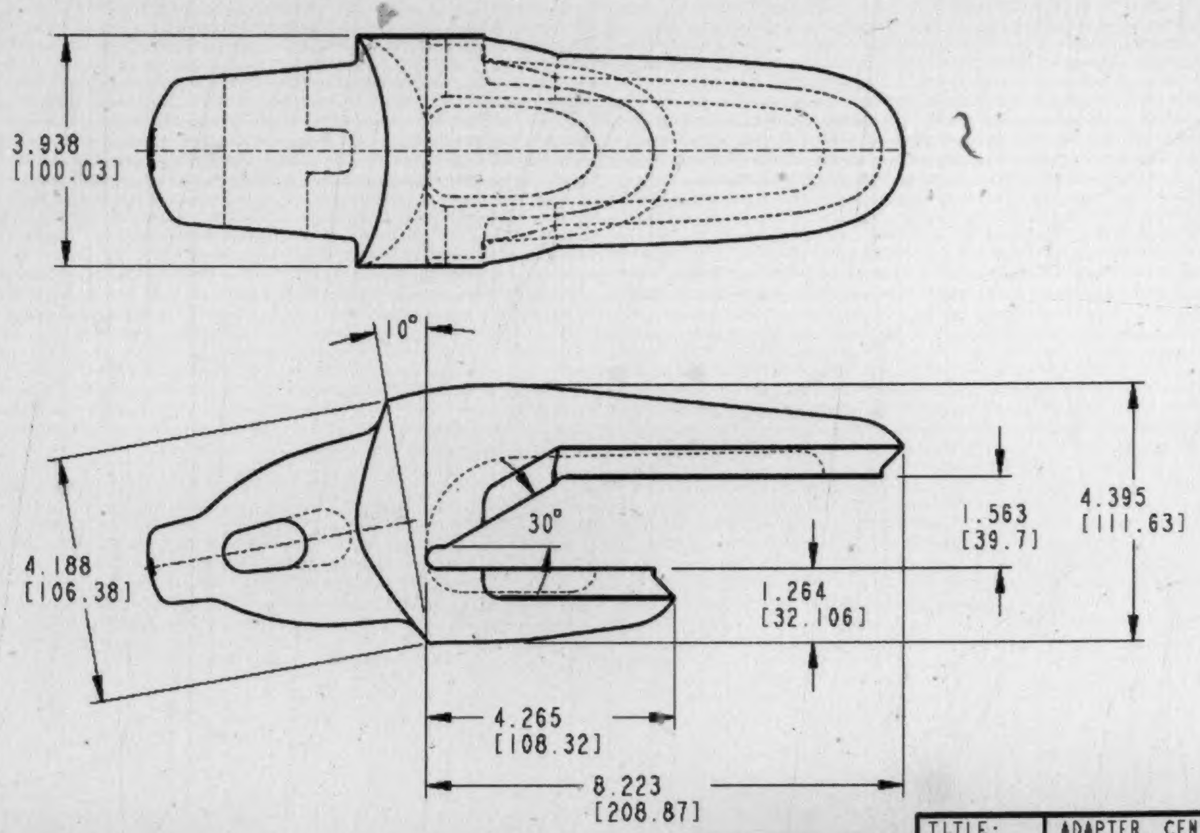

REFERENCE ONLY

HENSLEY INDUSTRIES, INC.
P.O. BOX 29779 2108 JOE FIELD ROAD DALLAS, TEXAS 75229 PHONE (972) 241-2321

FEB. 18,03

TITLE:	ADAPTER, CENTER
PART NO:	K1150-20
STOCK NO:	5020-1150
EST. WT:	17.8 lbs

Appendix F

New dipper Test Location

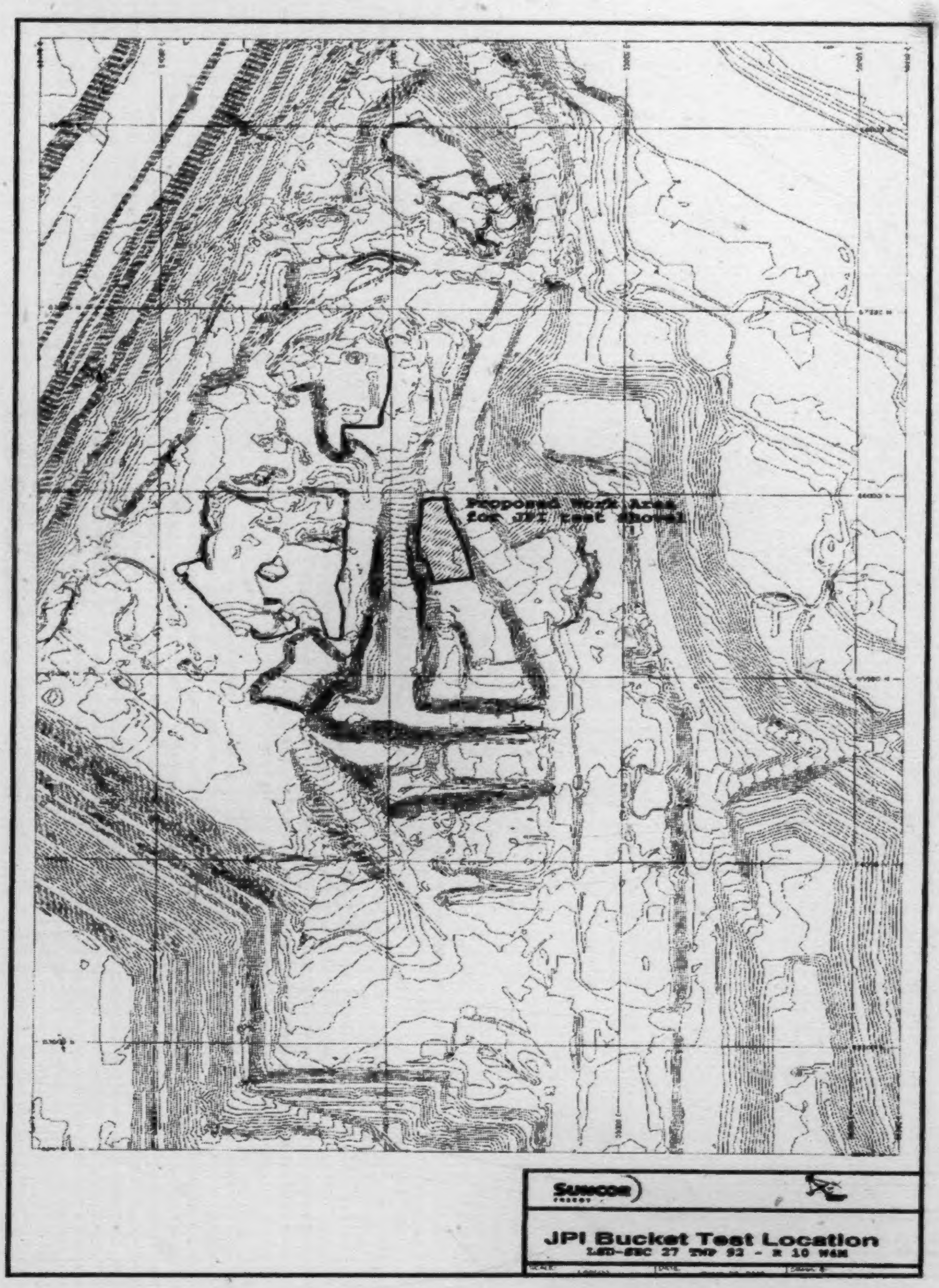

Appendix G

New dipper Project Field Test Visual Report

- Using original dipper

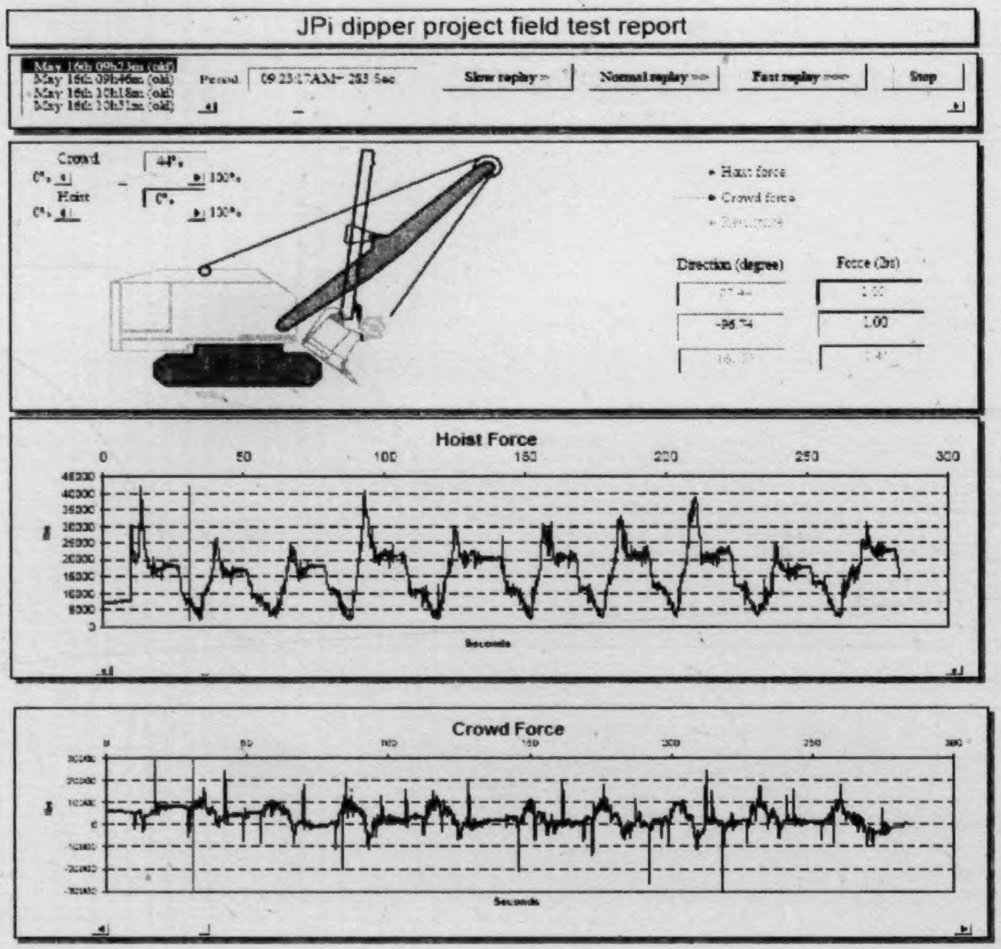

JPi dipper project field test report

May 16th 09h23m (old)
May 16th 09h46m (old)
May 16th 10h18m (old)
May 16th 10h51m (old)

Period: 09:23:17AM~ 283 Sec

Crowd: 44%

Hoist: 0%

Direction (degree) -96.74

Force (lbs) 1.00

- Using New dipper

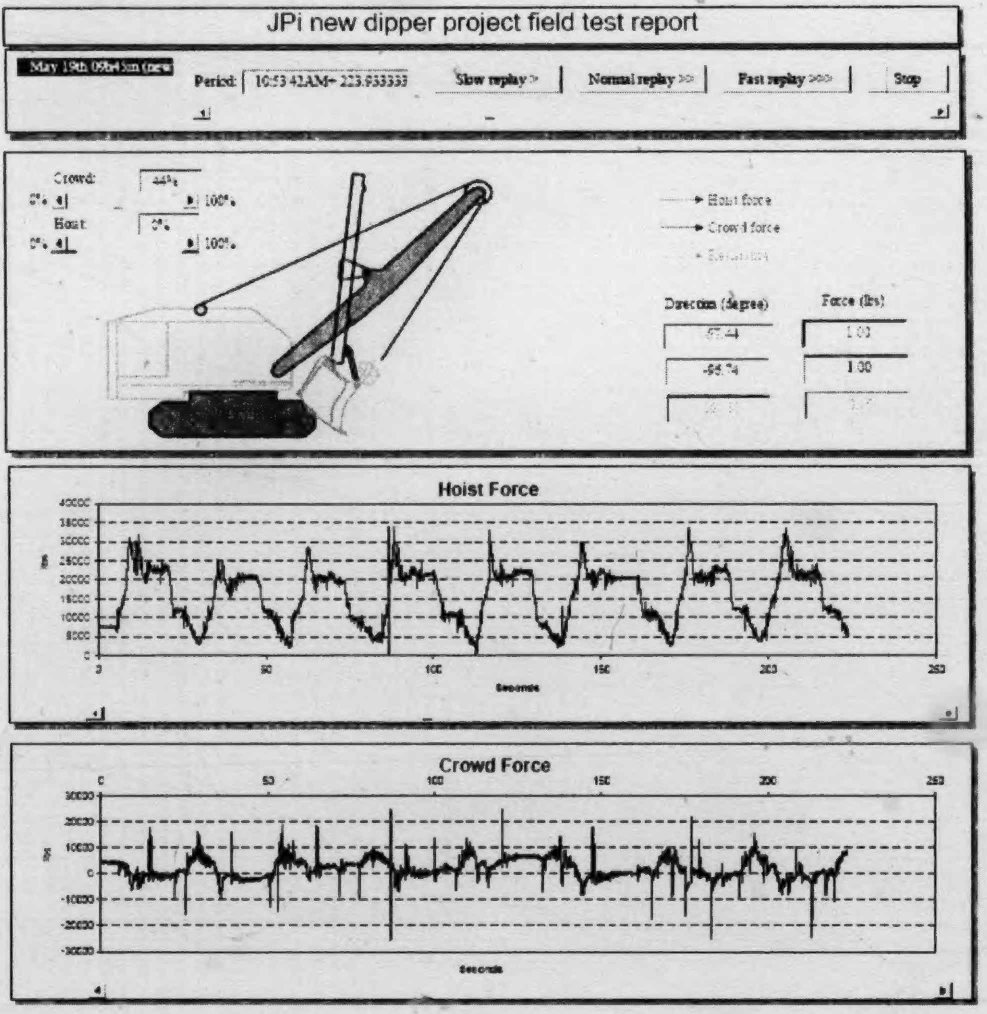

JPi new dipper project field test report

May 19th 09h45m (new

Period: 10:53:42AM~223.933333

Crowd: 44%

Hoist: 0%

Direction (degree)	Force (lbs)
-67.44	1.00
-95.74	1.00

Appendix H

JPi (2001) New Dipper Concept

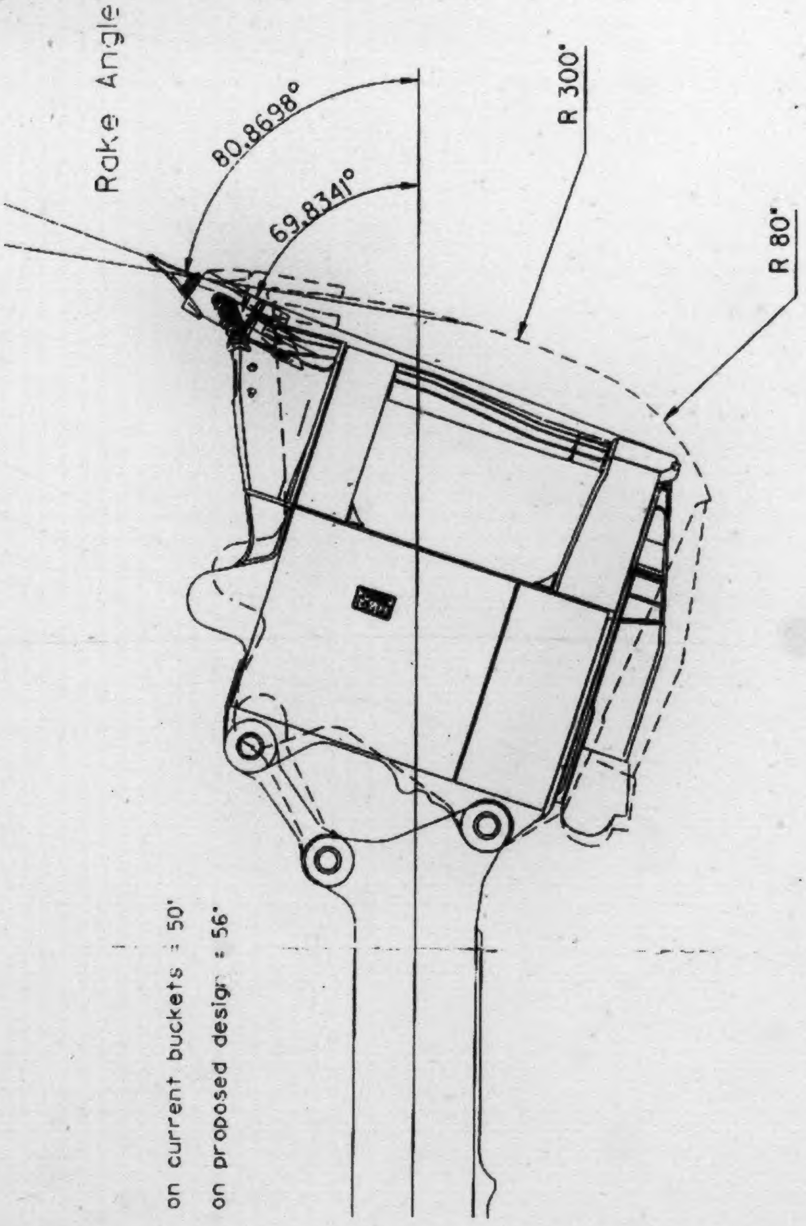

Appendix I

Visible Weakness of Current Dipper Designs

- High wear or damage in the heel area

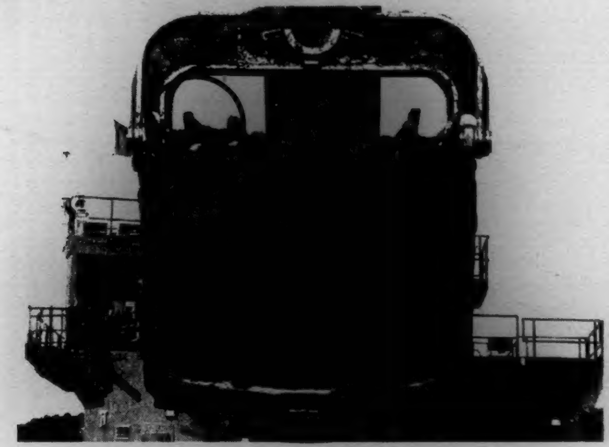

- High wear or damage in the heel area
- Teeth damages due to high attack angle

- The damage of the door close to heel area

- Refurbished heel protection band

- Refurbished latch keeper

Appendix J

P&H 4100 Hoist Motor Armature Current Record